ROLE OF THE INORGANIC MATTER IN AGGLOMERATION AND DEFLUIDISATION DURING THE CIRCULATING FLUID BED COMBUSTION OF LOW-RANK COALS

A THESIS SUBMITTED BY ALI REZA MANZOORI

FOR

THE DEGREE OF DOCTOR OF PHILOSOPHY

awarded 6.9.90

APRIL 1990

Department of Chemical Engineering

The University of Adelaide

Adelaide, S. A. 5001

Australia

DECLARATION

This thesis contains no material which has been accepted for the award of any other degree or diploma in any University and, to the best of author's knowledge and belief, the thesis contains no material previously published or written by another person, except where due reference is made in the text or where common knowledge is assumed.

The author consents to the thesis being made available for photocopying and loan if accepted for the award of the degree.

A R Manzoori

ACKNOWLEDGEMENT

The author wishes to express his sincere thanks to the Board and management of the Electricity Trust of South Australia (ETSA) for the opportunity to carry out this study. The author is particularly indebted to Dr M. Bosio, former Research Director of ETSA, for his assistance and continual encouragement throughout this project and is very grateful to Dr E.R. Lindner, Manager Technical Services of ETSA, for his valuable advice and personal encouragement.

The author also wishes to thank the staff of the ETSA Technical Services Department in particular Mr D.R. O'Keefe for his assistance in the construction and operation of the experimental apparatus, Mrs A Nuttall for preparation of samples for microscopic examination, Mr A. Kosminski for valuable discussions and Messrs R.G. Williams and J. Kapetas for their assistance in preparing this thesis. Mr F Myszka and staff members of Torrens Island and Northern Power Stations are thanked for the chemical analyses of coal and ash samples.

The assistance of the staffs of the workshop and the Electron Optical Centre of the University of Adelaide is acknowledged.

The author is especially grateful to Dr P.K. Agarwal, the project supervisor, and Professor J.B. Agnew, Dean of the Engineering Faculty of the University of Adelaide, for their constructive criticism, advice and continual encouragement.

The financial support of the State Energy Research Advisory Committee and the assistance of Lurgi GmbH of the Federal Republic of Germany are also acknowledged.

Finally I wish to thank my wife Sonia and my sons Anoosh and Amin for their support and encouragement which made this possible and for the innumerable sacrifices made by them through the course of this study.

CONTENTS

ABSTRACT

Sodium in low-rank coals is known to cause agglomeration and defluidisation in fluid bed combustors. However, its exact role is not fully understood. To make use of the potential of fluid bed combustion systems in utilising low-rank coals, particularly those with high contents of sodium and sulphur, the current study was undertaken. The main objective of the study is to elucidate the role of the inorganic matter in agglomeration and defluidisation under the conditions in circulating fluid bed combustion systems.

The experimental investigations were designed to study:

- the ash formation mechanism and its chemistry;
- the interaction of inert bed particles with ash in a multi-particle stirred fluid bed combustor;
- the mechanisms by which the bed particles agglomerate and defluidise.

A single particle furnace was used to investigate the ash formation mechanism and the ash chemistry during combustion of a single particle of coal under conditions relevant to fluid bed combustion. These experiments were carried out under reducing as well as oxidising environments for various residence times. Other variables examined were:

- furnace temperature (700°, 770° and 830°C);
- coal particle size (approximately 5.5, 7.0 and 9.0 mm);
- oxygen partial pressure; and
- sulphur dioxide partial pressure in the fluidising gas.

A coal sample of uniform composition containing low content of minerals and high contents of sulphur and sodium was used for these experiments. A portion of sodium in this coal is in the form of sodium chloride.

The experimental program included the study of the inorganic matter transformations; determination of the extent of vaporisation of volatile species; and characterisation of the ash formed on the char's surface.

The results of single particle experiments indicated that, under fluid bed combustion conditions, most of the species formed from the organically bound sodium and from sodium chloride remain in the char. These species form low melting eutectics with each other and with other compounds resulting in the formation of a molten ash matrix on the char surface.

A fluid bed combustion system was used to study the behaviour of the inorganic matter under conditions simulating those in circulating fluid bed combustors. The variables investigated were:

- operating time of up to 24 hours;
- bed temperature of 700°, 750°, 800° and 850°C;
- coal quality (various proportion of the organically bound elements, sodium chloride and mineral inclusions);
- bed particle size distribution;
- bed material; and
- excess oxygen in flue gas.

From these experiments, it was concluded that the molten ash on the char's surface deposits on the surface of bed particles. The rate of deposition of ash on the bed particles is a function of the amount and the mode of occurrence of the inorganic matter in coal. Chemical and microscopic examination of the bed material indicated that the ash coating on the bed particles is slightly enriched in those species which have lower melting point.

The ash deposited on the bed particles renders them capable of sintering (agglomerating) together and/or increasing the minimum fluidisation velocity. Microscopic examination of the agglomerates indicated that agglomeration is caused by sintering of the coating deposited on the bed particles. Agglomeration occurs at bed temperatures above the initial sintering temperature of the ash coating which is significantly lower than the initial deformation temperature determined by the ASTM ash fusion test.

Simultaneous thermogravimetric and differential thermal analyses suggested that sintering of the bed particles occurs due to the presence of a molten phase in their ash coating. Using a combination of analytical techniques (chemical analysis; electron microprobe analysis; and X-ray diffraction analysis), the compounds and eutectics responsible for the formation

of agglomerates were identified. From the results of single particle experiments, the exact role of the inorganic matter, particularly Na, S, Ca and Mg, in the agglomeration and defluidisation mechanisms was elucidated.

The fluid bed combustion experiments also indicated that the sintering propensity of the bed particles increases with temperature and proportion of the molten phase in their coating. The presence of mineral inclusions in the coal is likely to reduce the sintering propensity of the bed particles by altering the characteristics of the ash coating.

Having established the mechanism of sintering of the bed particles, the Frenkel sintering theory (Frenkel, 1945) was applied to derive expressions for agglomeration and defluidisation in terms of operating variables as well as physical properties of the ash coating. These expressions are expected to form the basis for the development of agglomeration and defluidisation models.

LIST OF TABLES

LIST OF FIGURES

Chapter 1

INTRODUCTION AND OBJECTIVE

1.1 INTRODUCTION

Over the past few years, considerable research and development work has been directed towards the utilisation of coals for power generation using fluid bed combustion (FBC) systems. The well known and established "bubbling" FBC system is characterised by fluidising velocities of about 1-2 m/s which are sufficiently low to maintain a well defined bed with high solids density. In-bed heat transfer surfaces are provided to extract heat from the bed and keep it at temperatures of about 800° to 900°C. These operating temperatures reduce production of nitrogen oxides and favour sulphur capture by limestone or dolomite added to the bed. This characteristic is, in fact, the main impetus for the development of FBC boilers as they can meet most of the latest NO_X and SO_X emission limits at reasonable costs.

Although bubbling fluid bed combustion boilers have met with success for small to medium industrial applications, none of the large commercial bubbling FBC plants in operation are completely trouble free as they often experience erosion/corrosion of the in-bed tubes and have sluggish dynamic response. In order to offset the limitations inherent in these systems, the newer circulating fluid bed combustion (CFBC) technology has been developed in the

past few years. CFBC operates at higher fluidisation velocities, typically about 6-8 m/s, and recirculates a large inventory of solid material which enhances the heat transfer and improves the combustion and sulphur capture efficiencies. It can also maintain a more uniform combustion temperature well below that of the conventional pulverised coal (pc) combustion systems. This technology now dominates the market for large FBC boiler plants and has the potential to replace the conventional pc fired systems.

The FBC process can be considered as being composed of two different subprocesses (Hajicek et al., 1985): a) fluidisation of solids, in which the solid particles are fluidised by an upward flow of a gas, and b) combustion, in which coal particles are burned in the presence of oxygen to produce heat. In utilising fluid bed reactors as combustors, one has to consider the impact of the inorganic matter in coal on the performance of such systems. Coals are complex material and contain inorganic species in numerous forms. The inorganic matter in high-rank coals is mostly in the form of fine micro-size crystallites of minerals such as clays, quartz, carbonates and pyrites embedded in the coal matrix. These minerals are released from the coal matrix in the form of ash when the coal is burned in the FBC system. The ash from high-rank coals is mostly refractory and imposes minimal impact on the design of the FBC systems.

In low-rank coals, however, along with the above minerals, there are also a number of inorganic elements, mostly alkaline in nature, bound to the inorganic matter. The transformations undergone by the organically bound inorganic elements during combustion of low-rank coals are complex. Therefore, it is difficult to determine the influence of the inorganic matter on the design and operation of FBC systems.

In pc fired systems, the main undesirable effects of the inorganic matter in low-rank coals are fouling, slagging and high temperature corrosion. Consequently, the behaviour of the inorganic matter in these systems has received considerable research attention; the literature has been recently reviewed by Lindner (1988). However, most of this knowledge is not directly applicable to FBC systems due to the significant difference in the two technologies.

Despite difficulties, low-rank coals are finding increased use for power generation. In the United States up to 1970, the utilisation of low-rank coals was less than 1-2 % of the total annual coal production. By 1980, the production of brown coals accounted for approximately 24% of the total national production (Energy Resources Co. ,1980) and it has been continually increasing not only in the United States but also in other countries.

The ever more stringent environmental regulations and the cost of their implementation in pc fired plants have resulted in an increasing demand for CFBC systems. CFBC has the potential to alleviate the operational problems of pc fired systems using low-rank coals and to utilise effectively the alkaline constituents of these coals to capture sulphur. However, the effects of the inorganic matter in low-rank coals on the performance of CFBC systems have not been fully investigated. Most of the efforts, so far, have been directed towards the development of appropriate hardware and assessing the capability of the system in reducing the emission of NO_X and SO_X resulting from combustion of high-rank coals.

The research work carried out to date on FBC of low-rank coals has indicated that sodium in these coals could have a detrimental effect on the operation of FBC systems by causing the formation of agglomerates and defluidising the bed. The mechanisms of agglomeration and defluidisation are extremely complex. Despite some research efforts made in recent years to determine the effect of sodium and operating parameters on the formation of agglomerates (Goblirsch et al., 1983), the exact role of the inorganic matter and the mechanism of agglomerate formation are not fully understood. In addition, the reasons for the onset of defluidisation experienced during FBC of high-sodium coals are not yet known. To make use of the potential of CFBC system in utilising low-rank coals, particularly those with high contents of sodium and sulphur, it is necessary to elucidate the behaviour of the inorganic matter during CFBC and to determine the mechanisms involved in agglomeration and defluidisation.

1.2 STUDY OBJECTIVE

The overall objective of this study was to elucidate the mechanisms involved in agglomeration and defluidisation, and the role of the inorganic matter in these mechanisms during CFBC of high-sulphur, high-sodium low-rank coals.

Chapter 2

LITERATURE REVIEW

2.1 INTRODUCTION

In FBC systems, agglomeration and defluidisation occur due to the formation of molten or semi-molten (sticky) ash. The characteristics of the ash formed are governed by the mode of occurrence of the inorganic matter and its physico-chemical transformations during fluid bed combustion.

Although the transformation of the inorganic matter in pc combustion has received considerable research attention, very few investigations have been carried out covering this subject in FBC. However, the literature dealing with pc combustion indicates that most of the work has been carried out in crucibles cover a wide range of temperatures including the temperatures found in FBC. Hence, this literature, reviewed in this chapter, does provide an indication of the inorganic matter transformation occurring in FBC systems. This review also identifies the research work which should be carried out in simulated FBC systems in order to develop a quantitative understanding of these transformations.

This chapter also reviews the literature related to agglomeration and defluidisation phenomena in fluid bed systems. These phenomena have been predominantly considered in context of slagging fluid bed gasifiers and fluid bed systems used for the reduction of iron

ore concentrates to metallic iron. There are very few papers dealing with these subjects in relation to fluid bed combustion. This is so because low-rank coals, which have the potential to cause agglomeration, have been considered for utilisation in fluid bed combustion systems only recently.

2.2 INORGANIC MATTER IN COAL

2.2.1 Definitions and Classification

Coal is a heterogeneous mixture of complex organic and inorganic species. For this study, all the species in coal other than elemental carbon and those consisting of organically bound carbon, hydrogen, oxygen and nitrogen are defined as "inorganic matter".

The organic species in coal originate from plant tissues. The inorganic matter in coal originates from a wide range of sources which can be reasonably grouped as follows (Wall et al., 1979):

(a) Elements absorbed by the plant tissues during their growth. These elements are predominantly calcium, magnesium, potassium, sodium, phosphorus with a number of trace elements including silicon, aluminium, manganese, rare earths and some radioactive elements;

(b) Elements intimately bonded with the coal originating from water with which the plant tissues came in contact during deposition and coalification;

(c) Fine discrete particles of sedimentary materials deposited with the plant material and distributed through the coal matrix at varying concentrations. These minerals are predominantly clays and quartz;

(d) Band of sedimentary materials, predominantly clays and quartz, laid down periodically above the plant remains producing "partings" or "dirt bands" which vary in thickness from, say, 1 mm upwards;

(e) Minerals, mainly carbonates and sulphides, which have deposited in fractures, cleats and joints by percolating solutions during the later stages of coalification;

(f) Fragments of roof and floor material which are unavoidably included with the coal while mining;

(g) Certain inorganic compounds such as sodium chloride and sodium sulphate which can be present in the coal's inherent water in the form of free ions.

A number of classifications have been used in the literature to differentiate the forms of the inorganic matter in coal. For this study the inorganic matter in coal is divided into the following two categories:

- "Inorganics" which include the atomically dispersed organically bound inorganic elements in groups (a) and (b) above:

  "Inorganics" = Na, Ca, Mg, K, P, S, Al, Cl

- "Minerals"- material from groups (c), (d), (e) and (f) which occur as discrete particles in the coal forming a relatively heterogeneous mixture, and those in the inherent water (group g) which, upon drying the coal, crystallise as fine particles within the coal matrix:

  "Minerals" = Quartz, clays, carbonates, sulphates, pyrites, and dissolved salts

Henceforth, the words "inorganic matter", "inorganics" and "minerals" will be used in accordance with the above definitions.

2.2.2 Occurence and Nature of the Inorganic Matter

The mode of occurrence and nature of the inorganic matter in coal depends on the degree of coalification (Bryers and Walchuk, 1984), the original plant material and the deposition and coalification environment. At the early stages of coalification, the coal structure contains numerous functional groups which participate in ion exchange and chelation processes resulting in retention of a significant amount of inorganic elements (inorganics) in the coal matrix. For this reason, in low-rank coals, which are at the early stages of coalification, the inorganics form a significant proportion of the inorganic matter. The characteristics and the structure of low-rank coals have been the subject of numerous studies (Durie and Swaine, 1971; Bryers and Walchuk, 1984; Kube et al., 1984; Brockway and Chalmers, 1986; Miller and Given, 1977).

As coalification proceeds the nature of the inorganic matter in coal changes. The number of active sites reduces and a higher proportion of extraneous minerals will be introduced into the coal seam. The reasons for these changes are explained by Fowkes (1978). At the later stages of coalification, that is in high-rank bituminous coals, the active sites practically vanish and the minerals are the only inorganic constituents in coal. The nature and distribution of the major inorganics are discussed in the following:

Alkali elements (sodium, calcium, magnesium and potassium):

In low-rank coals, a significant proportion of the alkaline elements can be bonded to the oxygen containing groups of the coal matrix. By water and acid leaching of Yallourn brown coal, Durie (1961) concluded that these elements in this coal were bonded to the coal matrix via carboxylic acid groups. Phenolic groups in the coal may also exchange their hydrogen with the alkaline elements. However, Murray (1968) suggested that the carboxylic groups are more likely to do this due to their greater acidity than phenolic groups. By acid leaching the coal, Murray demonstrated that the carboxylic acid content in the leachate solution corresponded approximately to the cations extracted from the coal. As the alkaline elements are attached to the active sites in the coal, the proportion of these elements reduces with increasing coal rank.

Sodium can be present in coal as free ions in association with sulphate and/or chloride ions in the coal's inherent water. The presence of water-soluble sodium in brown coals and bituminous coals have been reported by numerous investigators: Edgecombe (1956); Daybell and Pringle (1958); Saunders (1980); Caswell (1981); Gluskoter and Ruch (1976); Neavel et al. (1977); Murray (1968), Allan (1981a, 1981b); and Readett (1983, 1984). By leaching and pressure-dewatering of the South Australian brown coals, Readett et al. (1988) found that the water-soluble sodium can be weakly bonded to the coal's surface.

Sodium, calcium and magnesium can also be part of the minerals in coal. Sodium containing clay minerals such as plagioclase (sodium calcium aluminium silicate) have been identified by Kemezys and Taylor (1964); and Karner et al. (1986). A summary of the related literature is given by Raask (1985). The proportion of sodium present in this form is very small for high sodium coals. Hale (1980) suggested that this could be due to conversion of sodium containing minerals to soluble salt. Calcium and magnesium can also be present in the coal as sulphates and/or oxides.

Since most of the sodium in high-sodium coals is bound to the organic matter or is present as free ion in the coal's inherent moisture, it is evenly distributed in the carbonaceous matter on a micro-scale. The sodium in the inherent moisture can vary within the seam depending on the salinity of the aquifers associated with the coal. By scanning electron microscopy Sondreal et al. (1977) demonstrated that the organically bound inorganics in North Dakota and Montana lignites have a relatively uniform concentration.

Unlike sodium, potassium in coal does not tend to increase with decreasing coal rank (Hale, 1980) and its concentration in coal ash rarely exceeds four percent. It can attach to the coal matrix in the same manner as sodium.

Aluminium:

Aluminium is mostly present in coal as part of discrete minerals. However, it can also be present as an acid extractable form evenly distributed in the coal matrix (Lisner and Gobel, 1965; Murray, 1968, 1970, 1971a, 1971b; Murray and Bonafede, 1972; Kube et al., 1984). Therefore it is also considered as part of the inorganics in this study. The exact form of aluminium bound to the organic matter has not been determined with certainty. Murray and Bonafede (1972); Murray (1968,1970, 1971a, 1971b); Kiss and King (1979) proposed that the acid extractable aluminium in the Latrobe Valley brown coal is in the form of hydrated aluminium oxide but it can also exist as a complex cation attached to the carboxylic groups.

Sulphur:

Sulphur can be found in coal in three forms: organically bound sulphur, inorganic sulphides and inorganic sulphates. Sulphur is bound to the organic structure in forms which are still conjectural. However, the functional groups containing sulphur which have been identified include thiolic, thiophenolic, aliphatic, sulphide, aryl sulphide and thiophene (Attar, 1980). The distribution of the organically bound sulphur on a micro-scale is expected to be relatively even. Inorganic sulphides are pyrite and marcasite in the form of discrete minerals. The inorganic sulphates (such as calcium sulphate) generally form only a minor portion of the sulphur in coal.

Chlorine:

The nature of chlorine in coal has been the subject of numerous studies. By leaching studies on British coals, Edgecombe (1956) and Daybell (1967) found that chlorine in these coals is organically bound in a water extractable form. A literature review carried out by Hodges et al. (1983) indicated that chlorine is attached to the organic structure in forms

which remain uncertain. The presence of chloride in a South Australian brown coal in the form of free ion has been identified by Readett and Quast (1988). A series of water leaching tests carried out on the same coal by Readett et al. (1983, 1984); and Allan (1981a, 1981b) showed that a stoichiometric equivalent quantity of sodium was extracted, indicating that sodium and chloride ions originated from sodium chloride which is dissolved in the coal's inherent moisture. From studies of a few coal fields in USA, Gluskoter and Rees (1964) established that the amount of chlorine in coal is mainly determined by the salinity of the aquifers associated with the coal.

Minerals in Coal

A large number of minerals have been identified in coal, but only a small number of these minerals occur in appreciable quantities. A comprehensive list of minerals in coal has been compiled from the literature by Warne (1983a). The minerals commonly found in coal are:

kaolinite
illite
montmorillonite } clays
quartz
calcite
siderite
dolomite
pyrite.

Clays are the most common followed by quartz, carbonates and sulphides. The type and distribution of minerals in coal are influenced by depositional and post-depositional environment and, consequently, they vary within the individual coal seams. The minerals, generally, have an uneven distribution on a micro-scale and are prone to marked lateral and vertical variations.

Due to the almost general presence of quartz and clay minerals in coal, silicon and aluminium are the dominant inorganic elements in high-rank coals. In low-rank coal with higher concentration of alkali elements, silicon and aluminium often constitute less than 50% of the inorganic elements in coal. In many coals, quartz and clays occur in bands and large particles which can be easily separated by physical methods. In some low-rank coals, these minerals can exist in small particles down to 1 micron in size and consequently they are considered as inherent minerals (Sondreal et al., 1977; Fowkes, 1978; Readett and Quast, 1986).

Iron is mostly present as iron sulphide (FeS_2). Of the two forms of iron sulphide, pyrite and marcasite, the former is by far the most common. The iron content of a coal can be quite variable within a coal field and on a micro-scale depending on the distribution of the parent mineral.

2.3 TRANSFORMATION OF THE INORGANIC MATTER

2.3.1 Background

In FBC the coal particles with a top size of about 5 mm are fed into a fluid bed which is maintained at constant temperature. The coal particles at first undergo drying and devolatilisation followed by ignition and combustion of volatiles and the residual char. The processes of devolatilisation and combustion in FBC are relatively slow. The heating rate of the coal particles in fluid bed combustors is significantly less than that in pc fired systems. Consequently, the behaviour of the inorganic matter in FBC may differ substantially from that observed during pc combustion.

The literature on pc combustion indicates that as the coal particles are dried, devolatilised and combusted, the inorganic matter undergoes both chemical and physical transformations:

1. Chemical transformations: Thermal decomposition, reaction between the species in the inorganic matter, reaction with char, and reactions with gaseous species in the furnace.

2. Physical transformations: Crystallisation, fusion, coalescence and vaporisation.

The literature covering these transformations is reviewed in order to give an indication of the behaviour of the inorganic matter in FBC systems. Subjects specific to fluid bed processes (that is, agglomeration and defluidisation) are reviewed separately in Section 2.4.

Henceforth, the definition of "inorganic matter" given in Subsection 2.2.1 is extended to include the inorganic species which are the product of the transformations undergone by the inorganic matter in coal.

2.3.2 Chemical Transformation

Decomposition of the Inorganics

Thermal decomposition of the coal's functional groups containing the inorganic elements begins with the devolatilisation of the organic matter. The work carried out by Morgan and Jenkins (1984) on rapid pyrolysis of American brown coals, and by Schafer (1979) and Murray (1982) employing a fixed bed reactor with slow heating rates indicated that carboxylic groups decompose very early during devolatilisation. Murray (1972) reported that the decomposition of the carboxylic groups in Victorian brown coals began below 400°C and was completed at about 600°C. As a result of decomposition of the carboxylic groups, active inorganic species are formed.

By pyrolysing specially prepared single cation coal samples made from Victorian brown coals, Murray and Ledger (1982) found that the decomposition products of metal carboxylates were:

- sodium carbonate at all temperatures up to 800°C;
- calcium and magnesium carbonate at low temperatures;
- calcium and magnesium oxides at 800°C and 900°C respectively;
- iron was mainly present as magnetite at 600°C but it reduced to α-iron at higher temperatures.

By burning samples of synthetic char incorporating Na-Ca-Mg-Al acetates in crucibles, Domezitis (1985) found that alumina phases were formed at 1000° to 1150°C. However, in the presence of SO_2 or sulphur in the char, sodium and calcium formed sulphates, and Al and Mg formed the spinel $MgAl_2O_4$.

A significant proportion of sulphur is bonded to the coal's organic structure. The organically bound sulphur is intimately distributed in the coal matrix (Subsection 2.2.2) and can react with other species when released from the coal structure. By pyrolysing a Montana lignite, Suuberg et al. (1978) found that the release of sulphur started at 400°C; and at 1000°C about 30% of the original sulphur was retained. The mode of occurrence of the sulphur in this coal was not reported. Solomon and Kersten (1977) reported that about 40% of the organically

bound sulphur is removed at temperatures below 900°C. Further evidence on the release and retention of the organically bound sulphur, measured at temperatures higher than 900°C, are given by Lester et al. (1982); Halstead and Raask (1969); Atogi et al. (1986).

The literature indicates that the organically bound sulphur and the alkali elements attached to the functional groups are liberated from the coal matrix in the same temperature range and hence have the potential to react. Under the reducing conditions prevailing inside the char while burning, sulphides are likely to be formed. The sulphides then oxidise to sulphates once they get exposed on the char surface. Lyon and Freund (1980) found that calcium sulphide is formed from the reaction of sulphur with calcium under fuel rich conditions. Although the gas phase reactions of sulphur oxides with the alkaline compounds have received considerable research attention, there is limited information in the literature on the reaction of sulphur with the alkali elements inside the coal particles.

The occurrence and transformations of the organically bound chlorine is yet conjectural. Work carried out by Edgecombe (1956); Daybell and Pringle (1958); and Gibb (1983) indicated that chlorine was released from British bituminous coals at 200°-250°C for an extended period of 16 to 24 hours. It was suggested that a proportion of the chlorine may be organically bound, however, the evidence given is not very conclusive.

Decomposition and Oxidation of the Minerals

The general effects of heating minerals have been investigated by numerous researchers (O'Gorman and Walker, 1973; Mitchell and Gluskoter, 1976; Jenkins and Walker, 1978). These effects are illustrated in Figure 2.1 and are described as follows:

Dehydration of some minerals begins at temperatures below 350°C. Illite and montmorillonite dehydrate to aluminium silicates. At temperatures higher than 350°C, decomposition of the minerals begins with the formation of carbon dioxide and sulphur oxides. The decomposition products of the minerals commonly found in coals when heated to 1000°C are listed in Table 2.1 (Warne, 1983b): they are oxides of Al, Ca, Mg, Fe, and Mn together with aluminium silicates. Under reducing conditions, pyrites decompose to iron sulphide and sulphur. All that is known on the decomposition products of the minerals at temperatures up to 1000°C is applicable to FBC.

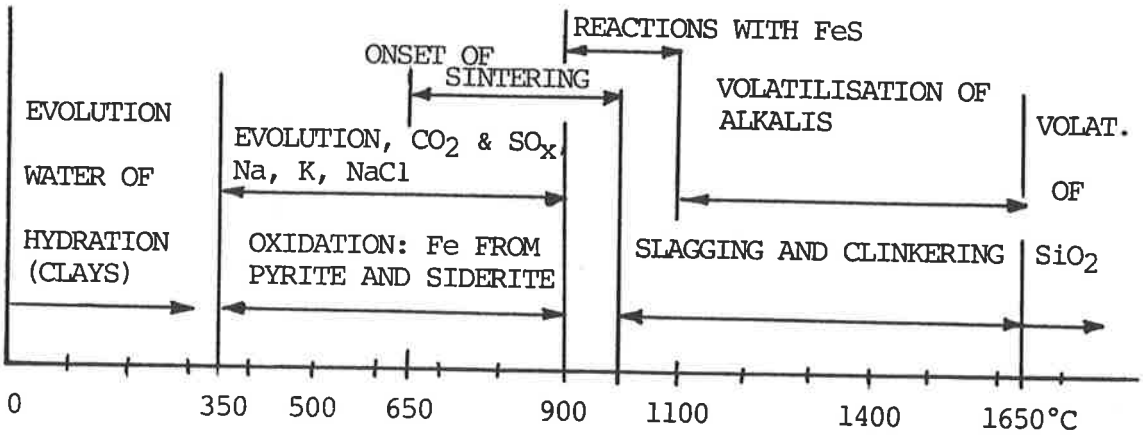

Figure 2.1: General Effects of Heating the Mineral Matter (Source: Warne, 1983b)

Table 2.1: ***The Decomposition Products of Minerals Commonly Found in Coals When Heated up to 1000°C. Listed in order of Increasing Initial Decomposition Temperature. (Source: Warne, 1983b).***

Mineral	Decomposition Products
illite	Al silicates + H_2O
siderite	$FeO + CO_2$; then Fe_2O_3 (and Fe_3O_4?);(+MnO_3?)
pyrite/marcasite	$FeO + SO_2$; then Fe_2O_3 (and Fe_3O_4?)
kaolinite	aluminates + Al silicates (mullite);(+SiO_2?)+H_2O
montmorillonite	Al silicates +H_2O
ankerite	Fe_2O_3 (and Fe_3O_4?) + MgO +CaO + CO_2 (MnO_3?)
dolomite	MgO + CaO + CO_2
calcite	CaO + CO_2
quartz	no decomposition
feldspar	no decomposition

At 1200°C, gypsum decomposes to lime (CaO) and anhydrite ($CaSO_4$), and kaolinite decomposes to mullite ($2SiO_2.3Al_2O_3$) and corundum (Al_2O_3), (Padia, 1976). Quartz does not decompose even at higher temperatures.

Interactions of the Inorganic Matter

The species formed from the organically bound elements are more reactive than minerals (Falcone and Schobert, 1986). For reactions to take place inside the coal particles, the reactants must be intimately distributed in the coal matrix. In coals, the inorganics and part of the minerals (groups c and g in Subsection 2.2.1) are finely distributed. Hence, the species formed from their transformations can establish the required contact for reactions to take place.

The vaporisation and melting of the species inside the coal particle are expected to enhance their reactions with other species. Pure sodium chloride melts at about 800°C and has a relatively high vapour pressure at this temperature (Jackson, 1963). On the basis of heat and mass transfer calculations, Halstead and Raask (1969) found that sodium chloride vaporises almost instantaneously in a pc flame. However, work carried out by Daybell and Pringle (1958); Brinsmead and Kear (1956); and Boow (1972) indicated that mechanisms other than straightforward volatilisation of sodium chloride are involved particularly when coal particles are subjected to low to medium temperatures that is up to 1000°C.

Daybell and Pringle found that sodium chloride undergoes decomposition at slow heating rate and at temperatures as low as 200°C. By pelletising a mixture of sodium chloride and carbon, and burning the samples at temperatures up to 1000°C, Brinsmead and Kear (1956) found that a significant proportion of sodium was retained in the char. They concluded that mechanisms other than direct physical vaporisation were involved. The addition of kaolin increased the retention of sodium. Similar experiments carried out by Boow (1972) confirmed that sodium chloride reacts with kaolin. The reaction of sodium species with kaolin produces nepheline which has a higher melting point relative to that of sodium salts.

The reaction of the organically bound sodium and calcium with kaolin was investigated by Falcone and Schobert (1986) for a temperature range between 750° to 1000°C at a low heating rate. They concluded that the organically bound sodium and calcium react with kaolin to form complex aluminium silicates.

The reactions of sodium chloride vapour have been studied by Halstead and Raask (1969). From equilibrium calculations, they concluded that sodium chloride vapour can hydrolyse to sodium hydroxide. However, the calculation shows that the extent of hydrolysis of sodium chloride is small at temperatures below 1000°C.

Of greater importance are the reactions of vaporised sodium species with sulphur oxides and with silica; the products of these reactions are sodium sulphate and sodium silicates respectively (Halstead and Raask, 1969). The mechanisms of these reactions are reviewed by Lindner (1988). The formation of sodium sulphate can cause fouling of heat transfer surfaces, and glassy sodium silicate can cause agglomeration and defluidisation in fluid bed combustors.

2.3.3 Physical Transformations

Crystallisation of Soluble Salts

With the vaporisation of the inherent moisture in coal, which occurs below 200°C, sodium chloride and other water soluble salts such as sodium sulphate crystallise within the coal particles. Although not confirmed, it is likely that these crystals are in the form of fine particles distributed through the coal matrix. No attempts have been made in the literature to determine the distribution of these crystals in the dried coal particles.

Fusion and Sintering

With the exclusion of the sodium compounds, the individual components of the inorganic matter have relatively high melting points in their pure state. However, in combination, they form solid solutions (eutectics) with melting points less than those of the individual compounds.

Pure sodium carbonate and sodium sulphate melt at about 851°C and 884°C respectively (Dean, 1985). These compounds are likely to be formed as a result of transformations of the organically bound sodium (Subsection 2.3.1). A mixture of these compounds forms a solid solution with a melting point of 844°C. Moreover, some brown coals contain sodium chloride which melts at about 800°C. Mixtures of sodium chloride and other sodium compounds form solid solutions with very low melting points:

- a mixture of sodium chloride and sodium carbonate forms a eutectic at 633°C;

- a mixture of sodium chloride and sodium sulphate forms a eutectic at 623°C;
- a three component system of these sodium compounds forms a eutectic at 612°C.

Similarly, inorganic species formed from transformations of other organically bound inorganic elements can form low melting eutectics. Pure calcium sulphate and magnesium sulphate melt at about 1300°C and 1185°C respectively; high enough to remain solid in FBC. However, a mixture of calcium sulphate and sodium sulphate forms a eutectic at about 900°C, and a mixture of magnesium sulphate and sodium sulphate melts at about 670°C.

Furthermore, sodium compounds can form solid solutions with silica with melting points as low as 800°C. These melting points are well within the temperature ranges found in FBC systems. Phase diagrams of sodium compounds are given in Figure 2.2.

The onset of sintering of the oxides derived from the decomposition of the minerals may begin at temperatures as low as 650°C, Figure 2.1. However, Mitchell and Gluskoter (1976) found that the extent of interactions between the oxides is not significant below 900°C. The oxides initially present in the coal and those formed as a result of decomposition of the minerals can be divided into two groups:

- acidic oxides, for example SiO_2 and Al_2O_3, derived from the quartz and clay minerals;
- basic oxides, for example Na_2O, K_2O, CaO, MgO, FeO, derived from other minerals in coal.

The former two oxides are termed acidic due to the affinity of their metal ions for the negative oxide ion O_2^-. The basic oxides are donors of oxide ions. As a result of reaction between acidic and basic oxides, low temperature eutectics can be formed. The fused material found in most fly ash particles obtained from pc fired systems is the result of such interactions. By conducting simulated pc combustion, Padia (1976) found that acidic and basic oxides react to form relatively low melting eutectic of calcium, aluminium silicates, for example gehlenite ($CaOSiO_2Al_2O_3$). The proportion of glass phases was found to decrease with decreasing combustion temperature.

a) Na_2SO_4–$CaSO_4$

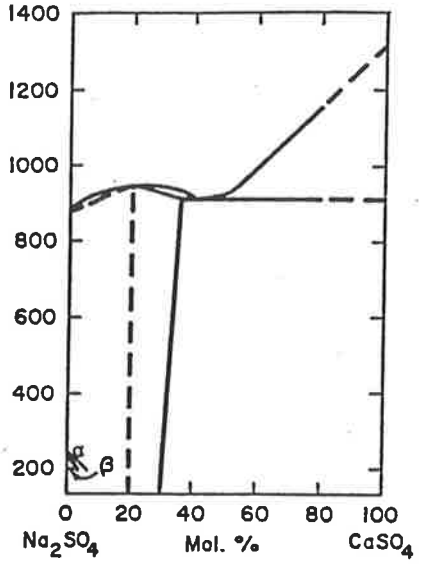

b) $NaCl$–Na_2CO_3

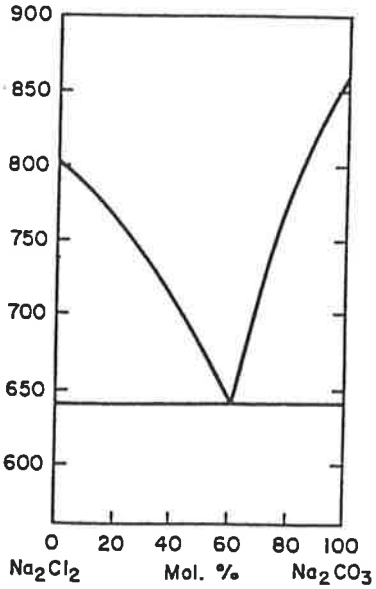

c) $NaCl$–Na_2SO_4

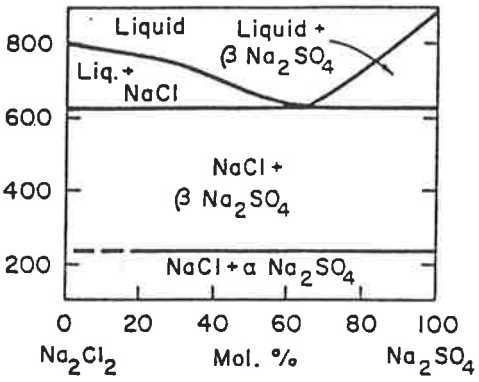

d) Na_2SO_4–$MgSO_4$

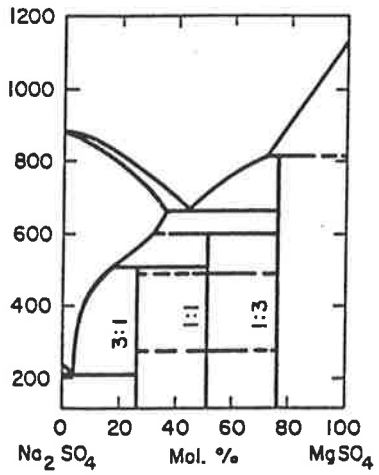

e) $NaCl$–$CaSO_4$

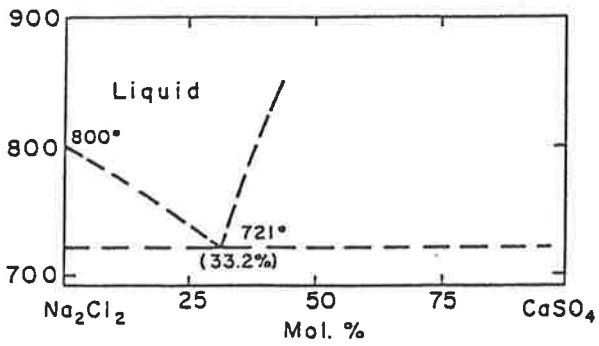

Figure 2.2: Phase Diagrams Showing the Sodium Eutectics
(Source: Levin et al., 1979)

f) Na_2O–SiO_2

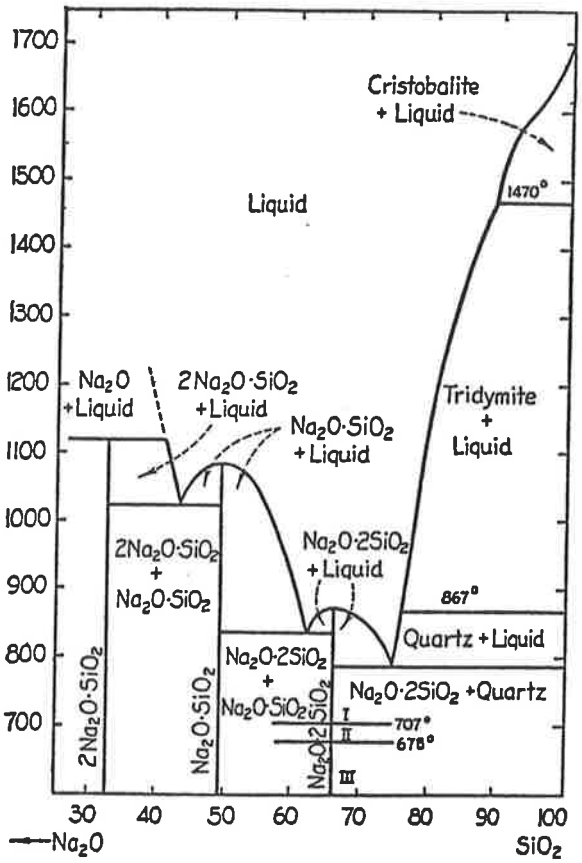

g) $NaCl$–Na_2CO_3–Na_2SO_4

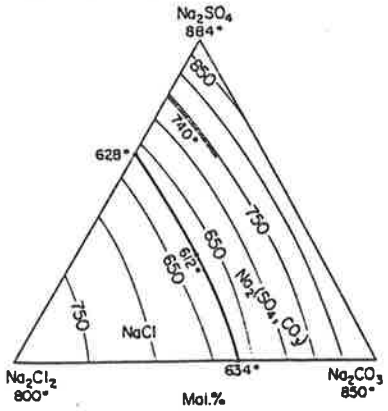

Figure 2.2: Phase Diagrams Showing the Sodium Eutectics (Cont'd.).

The clays containing iron and potassium, illite and biotite, form a glassy phase at 950°C and 1000°C respectively; pyrite can melt at 600°C under reducing conditions (Bryers and Walchuk, 1984). Under oxidising conditions, the fusion of pyrite begins at 830°C (Moza, 1981).

Vaporisation of Minerals

As mentioned in Section 2.3.2, with the exclusion of sodium silicates, sodium compounds have relatively high vapour pressure (Jackson, 1963). Part of sodium chloride which does not take part in reactions with other compounds can vaporise under conditions found in FBC. Work carried out by Brinsmead and Kear (1956) on the transformations of sodium chloride indicated that the extent of vaporisation of sodium chloride increases with temperature.

At temperatures above 1300°C, volatile species SiO, Mg and Ca are formed from the interaction of the refractory oxides SiO_2, MgO, and CaO with the char (Padia, 1977; Neville, 1982; Quann, 1982). These species contribute to the formation of sub-micron fly ash in the furnace gases. However, under the conditions found in FBC, they are not likely to be formed.

Coalescence

During the combustion process, and depending on the combustion conditions, a fraction of the inorganic matter is lost to the gas phase by vaporisation. The remaining inorganic matter is distributed within the char particles.

By examination of char obtained from pc combustion at different stages of char burnout (Shibaoka and Ramsden, 1977; Quann and Sarofim, 1986) it has been shown that the inorganic matter becomes exposed as the surface of the char recedes while burning. As combustion proceeds, the exposed inorganic matter is drawn together. Molten phases either coalesce or sinter while solid particles may agglomerate with the molten phase. The unfused particles may also be lost to the gas phase. The sintering of solid particles which are drawn together may occur due to interaction between the inorganic matter and formation of low melting eutectics. The mechanism by which the molten and solid particles are retained on the char's surface is not well understood.

By microscopic examination of ashes obtained from the Ignifluid gasification process, Yerushalmi et al. (1976) found small glassy beads on the surface of char particles and

concluded that the beads may have oozed out from micro-cracks. However, there is not enough evidence to support this suggestion. The presence of beads could be the result of coalescence of the inorganic matter on the char surface.

2.4 AGGLOMERATION AND DEFLUIDISATION

2.4.1 Agglomeration Mechanism

Agglomeration has received appreciable research attention as it is an important aspect of fluid bed gasification processes. The bed inventory of fluid bed gasifiers (FBG) consists mostly of carbon, typically about 80%, and ash. Due the to the slow rate of gasification reactions, gasifiers have to operate at high temperatures, often higher than the melting point of ash, in order to attain high carbon conversion. Under these circumstances, the bed particles may undergo agglomeration which, if not controlled, could result in the formation of ash clinkers with consequent plant shutdown.

A mechanism for agglomeration in FBG was postulated by Yerushalmi et al. (1976) following the discovery of the so-called "Godel phenomenon". Godel (1966) discovered that if a FBG is operated at high fluidisation velocity, it is possible to operate the gasifier at temperatures substantially higher than the melting point of ash. The higher fluidisation velocity allows for small agglomerates to form and grow to a size sufficient to be segregated and removed from the gasifier without causing the bed to defluidise. This discovery formed the basis of the Ignifluid process which is described by Squires (1972); Yerushalmi et al. (1976); and Gluckman et al. (1976). Yerushalmi et al. (1976) suggested that the following four steps occur in the agglomeration process in fluid bed gasifiers:

1) In the first stage, small molten beads appear on the surface of the coal particles undergoing gasification.

2) In the second stage, the molten beads grow on the surface of char particles either by further consumption of char or by capturing molten ash beads from other particles during collision.

3) In the third stage, the beads, as they grow eventually separate from the char surface due to the high interfacial tension between the molten material and the char.

4) In the final stage, the molten beads remain sticky at the gasifier operating temperature and continue to grow either by coalescence with other agglomerates or with other beads.

Because of the high interfacial tension between the molten material and char, the agglomerates formed in FBG contain only a minimal amount of organic matter. This has been confirmed by the results obtained from a number of gasification processes developed based on agglomeration (Merry et al., 1975).

In fluid bed combustors, the bed inventory consists mostly of inert material. High carbon burn-out is achievable at relatively lower temperatures due to the faster rate of combustion reactions compared to those of gasification. Consequently, agglomeration in fluid bed combustors has received less attention except in cases where the temperature of the fluid bed has been deliberately increased to form agglomerates (Goldberger, 1967) or where brown coals are used (Goblirsch et al., 1983; Atakul and Ekinci, 1989).

Goldberger (1967) applied the Godel phenomenon to remove the ash generated in a fluid bed combustor in order to use the gas in a gas turbine. It was postulated that by operating the combustor at sufficiently high temperatures, fly ash may form agglomerates which remain in the bed and subsequently grow to sizes that can be segregated from the bed. The continuous operation of the combustor is ensured by employing a high fluidisation velocity. Bench scale and pilot plant tests were carried out using either crushed ash agglomerates or quartz sand as the initial bed inventory. When sand was used, it was quickly coated with molten ash and behaved as crushed ash agglomerate. In both cases, it was observed that agglomeration was a direct consequence of stickiness of the bed particles caused either by melting of bed particles at a certain temperature level or by deposition of a molten layer on the surface of inert particles. The mechanism of agglomeration was considered to be the same for both cases.

By burning a high-sodium lignite in a fluid bed combustor, Goblirsch et al. (1983) discovered that agglomerates were formed at relatively low temperatures. They suggested that agglomeration occurred due to formation of fine-grained sulphated ash from the inorganics in coal:

- The ash initially accumulated on the bed particles and reacted on the surface;
- Then, the ash trapped additional sulphated ash formed by combustion;

- Finally, the bed particles coated by molten phases adhered together and formed bed agglomerates.

When limestone was used as bed material, the agglomeration process was suggested to begin with the calcination of the limestone and subsequent formation of similar coating which, again, resulted in formation of bed agglomerates. Limestone grains were observed to disintegrate extensively and become mixed with the coating material. Due to the lack of information on the transformations of the inorganic matter during FBC, the mechanisms involved in the formation of the molten ash and its interactions with the bed material could not be explained.

While it appears that agglomeration occurs due to formation of molten phases, the literature indicates that the actual phenomena for agglomeration are not well understood.

2.4.2 Operational Effects

The effect of the operational parameters on agglomeration in fluid bed systems has received considerable research attention. Godel's discovery in using the fluidisation velocity to control the extent of agglomeration led to the development of high temperature gasification processes. In order to establish the optimum operating conditions for these gasifiers, numerous experiments have been carried out to determine the effect of temperature, fluidisation velocity, coal and bed particle sizes as well as design parameters on the extent of agglomeration and segregation of the agglomerates from the fluid bed gasifiers.

By gasifying coke in the U-Gas gasification process under various conditions, Patel (1977) investigated the effect of a number of variables on agglomeration. The analysis of the results was carried out by Sandstrom et al. (1979). The results indicated that the size of the agglomerates was sensitive to feed size, bed temperature, and fluidisation velocity. When operating the bed at the minimum temperature required to produce agglomerates, the average size of agglomerates appeared to be related to the feed size. At higher temperatures, larger agglomerates with different characteristics were formed. At the minimum temperature required to form agglomerates, small ash particles adhered to the surface of agglomerates. At higher temperatures, agglomerates were denser indicating that a significant amount of melting had occurred. In certain experiments, fluidisation velocities up to 7 times the minimum fluidisation velocity had to be used to control the size of the agglomerates. In a similar type

of gasifier, Jacquier et al. (1960) also found that the size of the agglomerates formed increased with increasing temperature. Gas velocities as high as 20 times the minimum fluidisation velocity were used to control the formation of agglomerates.

The fluid bed combustion experiments carried out by Goldberger (1967), using American Pittsburg No 8 coal, also indicated that the extent of agglomeration increased dramatically with increasing temperature. Below 1040°C, the sand particles in the bed received a continuous coating of molten ash. At temperatures above 1080°C, the ash coatings were sticky enough to cause agglomeration of bed particles. Again, the fluidisation velocity was a key variable in maintaining stable fluidisation after the initiation of agglomerate formation. As the temperature increased, higher fluidisation velocity was required to maintain the bed under stable conditions. Furthermore, increasing the bed depth had the same effect as increasing the temperature.

By conducting a series of fluid bed combustion tests on a North Dakota high sodium brown coal, Goblirsch et al. (1980) found that severe agglomeration occurred at higher bed temperatures. Other variables investigated included limestone addition and ash recycle. The extent of agglomeration decreased with the addition of limestone and it increased with the ash recycle. The effect of other operating variables on agglomeration was not reported.

A simple method was developed by Stallmann and Neavel (1980) to determine the effect of temperature on ash agglomeration. Samples of coal less than 100 mesh were ashed at low temperature using a 3% oxygen stream to prevent excessive particle temperatures. The ash produced was screened to ensure that its top size remained below 100 mesh. These samples were then heated at various temperatures in a platinum crucible in a reducing environment. After cooling, the samples were screened to determine the weight percentage retained on a 100 mesh screen. It was suggested that the percentage retained on 100 mesh screen represented agglomerates formed by fusion. The results confirmed that the extent of agglomeration increases with increasing temperature. However, it should be noted that the percentage of ash retained on 100 mesh screen can not represent all the agglomerates formed during the heating process as, depending on the initial size of the ash particles, formation of smaller agglomerates is also possible.

Stallmann and Neavel (1980) also found that agglomeration begins at temperatures several hundred degrees less than the initial deformation temperature of the coal ash measured by standard methods. This temperature is referred to as the "initial sintering temperature" which

will be discussed later in this thesis. The micrographs of the agglomerates presented by Stallmann and Neavel (1980) indicated that at temperatures slightly above the initial sintering temperature, the ash particles were sintered together and neither melting nor substantial softening had taken place. At higher temperatures, the agglomerates had a molten morphology indicating that substantial softening had occurred.

2.4.3 Agglomeration Tendencies

The work described earlier was mainly concerned in defining the temperatures and velocities at which the fluid bed gasifiers and combustors can operate effectively. Also, it indicated the effect of these parameters on the agglomeration process. Due to the complexity of fluid bed combustion and gasification processes, the quantitative study of the effects of fluidisation velocity and temperature on agglomeration should be carried out in systems where these variables can be maintained independently. This section reviews a number of studies conducted in such systems in order to provide a more detailed knowledge of the mechanism of agglomeration.

A number of experiments have been carried out in fluid bed systems for the production of iron from iron ore concentrates. Reduction of iron ore results in a production of metallic iron which has a relatively low softening point. The agglomerating tendencies of the iron ore particles after reduction to metallic iron have been used as a means of segregating and removing the product from the fluid bed reactor. The fundamental feature of this process is the mechanism which gives the adhesive properties to the particles and, at the same time, permits stabilisation of the fluid bed. The cause of the stickiness of the iron ore particles is the formation of an iron phase on their surface. The basic concepts of this process could be applicable to fluid bed gasifiers and combustors operating with agglomerating bed particles.

Langston and Stephens (1960) examined the agglomeration tendencies of iron ore particles during reduction in a fluid bed system. They postulated that the agglomeration tendency of the particles when they collide is directly proportional to the adhesive force and area of contact and inversely proportional to their momentum.

This explains the trends observed during gasification and combustion experiments described earlier. Increasing the temperature increases the plasticity or adhesive characteristics of the particles and, consequently, their agglomeration tendency. The larger contact area per unit mass and the lower momentum of smaller particles increase their agglomeration tendency. The higher the fluidisation velocity, the higher the particle momentum, hence a lesser agglomeration tendency.

Langston and Stephens (1960) carried out two sets of experiments in support of their theory. In the first experiment with coarse bed particles, fluidisation could be maintained at temperatures as high as 870°C. However, with fine bed particles in the second experiment, the bed defluidised at 760°C. They concluded that the coarse particles, having a greater mass and thus greater momentum, could tolerate a greater adhesive force (or higher temperature) without causing defluidisation of the bed.

The agglomerating tendency of polyethylene spheres in fluid bed system was investigated by Huang et al. (1982) and the results are reviewed by Matulevicius and Golan (1984). By operating the bed at the melting point of polyethelene, a molten layer was formed on the spheres. The thickness of the molten layer and the extent of agglomeration increased with increasing temperature. It was suggested that the adhesive force defined is also a direct function of the thickness of the molten layer. However, the increase in agglomeration could also be due to changes in the physical characteristics of the coating caused by the higher temperatures. The results also indicated that small particles agglomerate at lower temperatures. This could be due to two reasons:

. the small particles heat up and melt faster than larger particles; and

. the small particles have lower momentum.

Additionally, it was found that the extent of sintering between particles increased with time and temperature.

2.4.4 Defluidisation

Numerous cases have been reported in the literature where fluid beds operating with sticky bed materials defluidised under certain operating conditions. This stickiness may be an inherent property of the bed material becoming effective at some temperature level, or it may be due to a molten layer otherwise formed on the surface of the bed particles. The conditions

causing the defluidisation of the bed may depend in a complex way on many variables, that is: particle size, temperature, fluidisation velocity, bed geometry, characteristics of the coatings, amongst others. The principles governing defluidisation phenomenon are not well understood. Godel's discovery only indicates that defluidisation of the bed can be prevented by increasing the gas velocity. In some of the experiments described earlier, gas velocities up to 20 times the minimum fluidisation velocity were required to maintain the bed under stable condition.

Langston and Stephens (1960) suggested that the principles applicable to agglomeration also apply to defluidisation. Based on the equation proposed for agglomeration (Subsection 2.4.3) they concluded that because of the large surface area to mass ratio of the particles, the bed tends to agglomerate into a single mass and defluidise. Other work reported in the previous subsections also suggests that the tendency to defluidise increases with increasing adhesive force and decreasing momentum. For this reason, defluidisation is often regarded as the extreme case of agglomeration.

Gransden et al. (1970) measured the degree of fluidisation in the iron bed reduction process using a fluidisation meter which consisted of a silica rod capable of measuring the forces exerted by the fluid bed. The reduction of iron ore was carried out at various temperatures. The signals representing the degree of fluidisation transmitted by the meter were recorded as a function of time (Figure 2.3). Below 710°C, no change in the fluidisation behaviour was observed. At 710°C, a molten iron phase was formed which resulted in a gradual decrease in the fluidisation tendency. At 740°C, a rapid reduction in the degree of fluidisation occurred at the point of the formation of the iron phase followed by a slower rate of decline for the remaining period of the reduction process. At 840°C, the rapid drop in the degree of fluidisation continued until the bed completely defluidised. The bed could be re-fluidised, however, when the velocity was increased immediately.

The increase in the rate of decline of the degree of fluidisation with temperature appears to be due to the enhancement of the stickiness of the bed particles with temperature. The reason for the decline in the degree of fluidisation is likely to be due to either or a combination of the following reasons:

- formation of agglomerates;

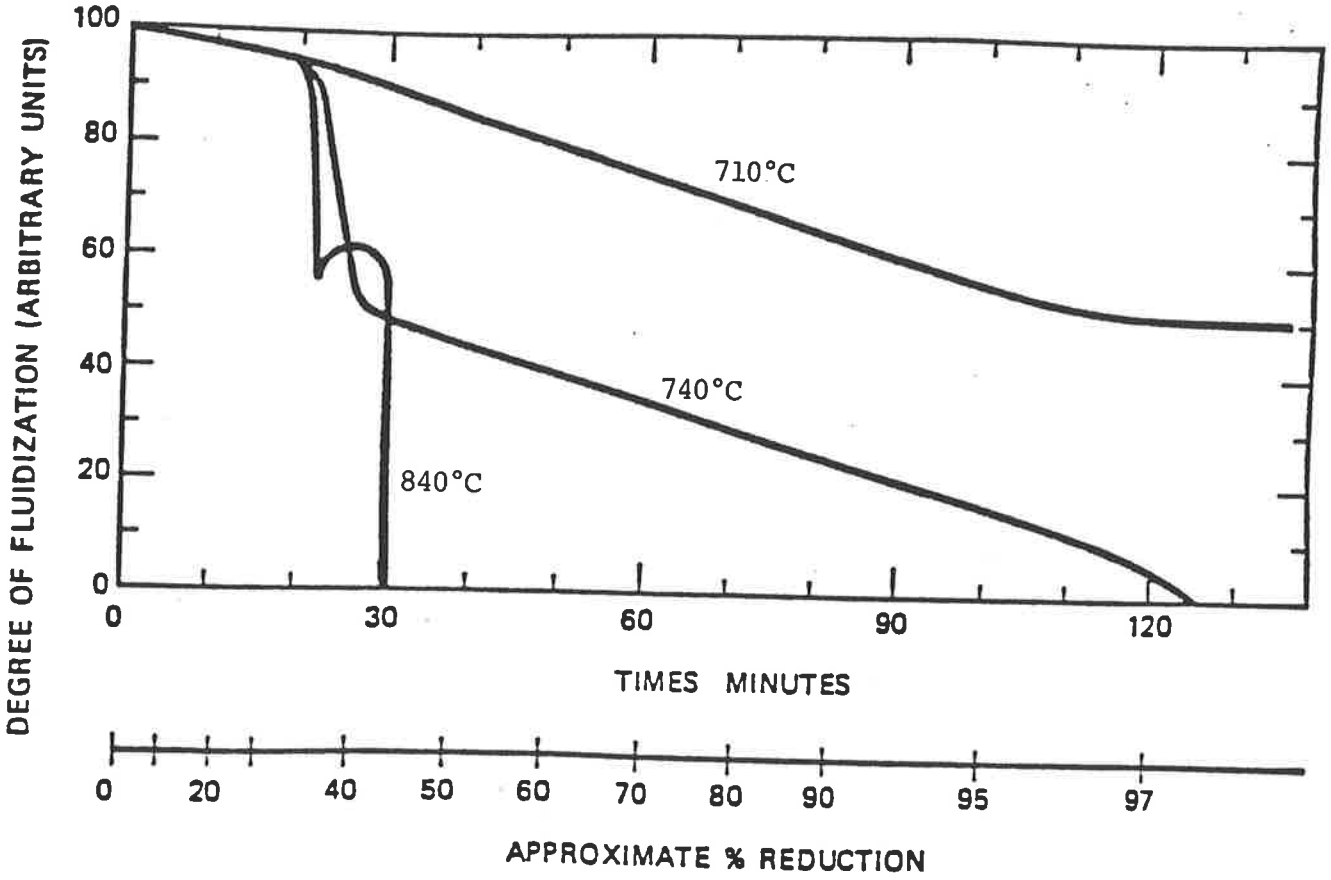

Figure 2.3: Relation Between the Degree of Fluidisation and the Percentage Reduction for Ore Reduced at Different Temperatures. (Source: Matulevicius and Golan, 1984)

- interaction of sticky bed particles in the combustor without necessarily forming agglomerates. This interaction may introduce a new variable into the equation of gravity, drag and buoyancy which defines the characteristics of a fluid bed.

If the latter is the main mechanism, then, agglomeration and clinker formation could occur after the bed has defluidised.

The exact mechanism of defluidisation is not yet known. However, work carried out by Gluckman et al. (1976); and Basu (1982) indicates that the defluidisation of beds of sticky particles is a well-ordered phenomenon obeying precise rules. At low temperatures, there is a minimum fluidisation velocity above which the bed is highly fluidised. This velocity is determined by the balance between gravity, drag force and buoyancy. As the temperature is increased, a limit is reached at which the gas velocity must be increased beyond the theoretical minimum fluidisation velocity for non-sticky particles in order to maintain a stable fluid bed. The temperature at which this occurred was identified as the initial sintering temperature (T_S) of the bed material, and it was defined as the temperature of contraction of a sample of a material as it is heated progressively in a dilatometer.

Above this temperature, the true minimum fluidisation velocity had a linear relationship with temperature, Figure 2.4. Gluckman and his collaborators noted that the slopes of the curves for beds containing various sticky materials (that is copper particles, poly-propylene beads or glass particles) were different. Basu (1982) modified the expression for the minimum fluidisation velocity by including a force term due to the interaction of bed particles in addition to those due to buoyancy and drag. By assuming a linear relationship between the sintering force and temperature, he found that the experimental results agree with the theoretical predictions. Basu's findings suggest that the principles governing defluidisation may be different from those of agglomeration even though both are caused by the stickiness of the bed particles.

Using a laboratory scale fluid bed combustion system Atakul and Ekinci (1989) examined the agglomeration and defluidisation tendencies of three Turkish lignites. They found that the degree of fluidisation of the bed declined after about 3 to 20 minutes. The temperature at which this occurred depended on the type of lignite, particle size, fluidisation velocity and

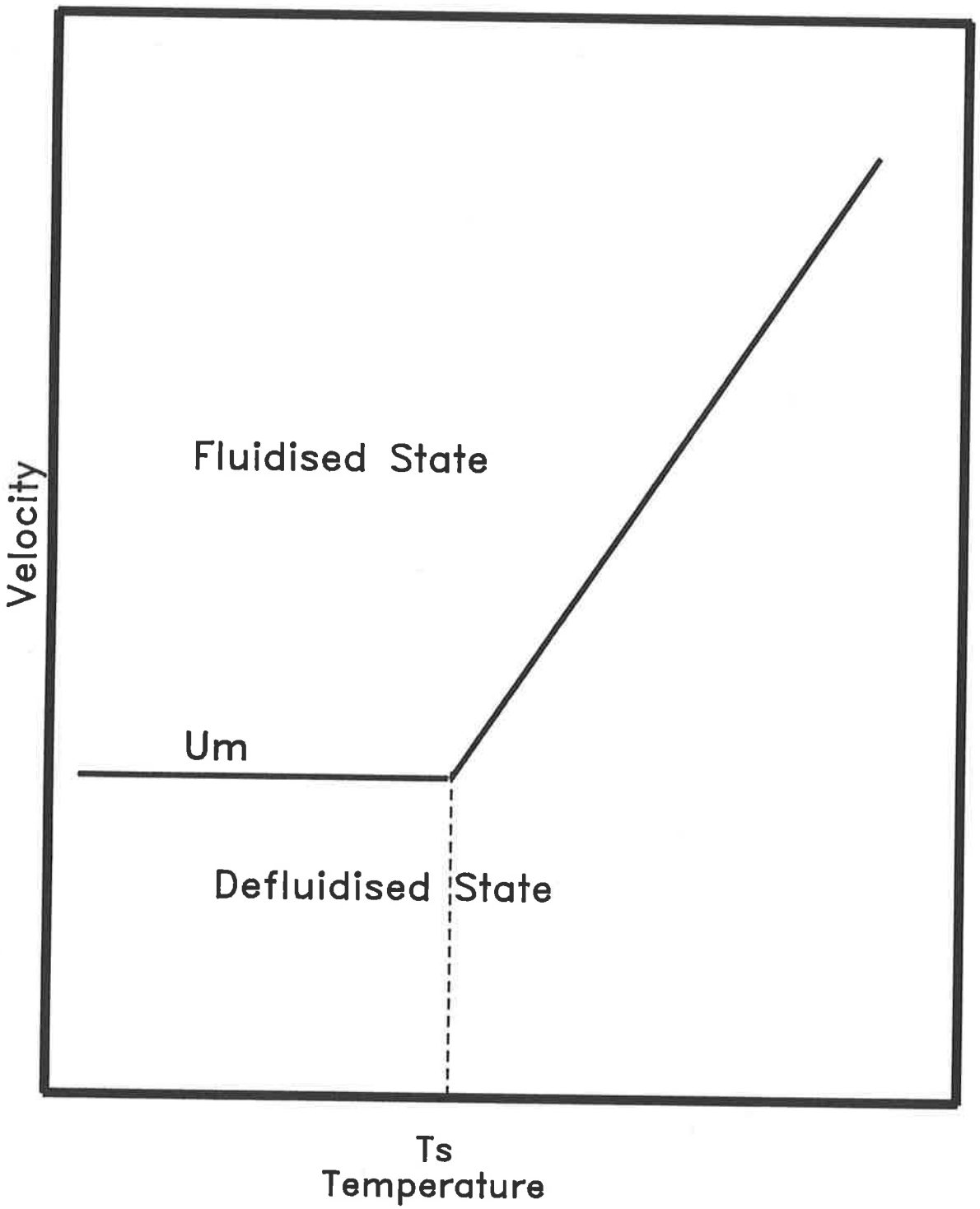

Figure 2.4: High Temperature Regimes of Fluidised Bed Operation

dynamic bed height. This work confirms that agglomeration and defluidisation are affected by the same variables, that is, adhesive force, momentum, particle size. Atakul and Ekinci, however, did not elaborate on the principles governing the defluidisation phenomenon.

2.4.5 Mathematical Modelling

The literature reviewed indicate that models which can describe agglomeration and defluidisation are not fully developed because of:

- the lack of complete understanding of the mechanisms of agglomeration and defluidisation processes; and
- the complexity of the interactions which occur between the bed particles in a fluid bed system.

The models for agglomeration which have been reported in the literature can be divided in three categories:

- prediction of minimum temperature required for agglomeration;
- empirical models; and
- mechanistic models.

The details of these models are described by Matulevicius and Golan (1984). In the first category, which is more applicable to ash agglomeration in fluid bed gasifiers, the temperature of the coal particles is determined using the gasification models. If the computed temperature is below an arbitrary minimum temperature assumed to be required for agglomeration then the agglomeration would not take place (Rehmat and Saxena, 1980). The model, relying on this assumption, does not describe the agglomeration process and has limited application.

In the second category, the probability of collision between particles of two different sizes in a fluid bed system is calculated from the population of these particles. A constant, representing the fraction of collisions that are effective for agglomeration, is used to calculate the rate of agglomeration. This constant, which has to be determined empirically, is a function of bed temperature, fluidising velocity, particle size and other physical characteristics such as binding force, surface forces (Matulevicius and Golan, 1984).

A mechanistic approach (the third category) has been used by Jen and Tsao (1980) to determine the agglomeration rate of particles in a high temperature cyclone. In this model, the forces of attraction and repulsion during collision between two particles are evaluated. Then, the criteria for the formation of agglomerates is applied to each collision involving two particles. Due to the reasons mentioned earlier, the mechanistic models are not yet fully developed.

Work reported in the literature on modelling of the defluidisation process is even more limited. By introducing a function for the sintering force into the Ergun equation (Ergun, 1952), Basu (1980) derived an equation for the true minimum fluidisation velocity. Although he could not define the sintering force in terms of measurable parameters, he suggested a linear relationship between the sintering force and temperature based on the experimental results.

2.5 SUMMARY AND CONCLUSION

The mode of occurrence of the inorganic matter can be summarised as follows:

- Coal is a heterogeneous mixture of complex organic and inorganic matter. The latter is either in the form of minerals scattered in the coal matrix or as elements attached to the organic structure (inorganics). The distribution of the inorganics in coal, on a micro-scale, is even, whereas the minerals are predominantly present in the coal as discrete particles distributed unevenly.

- A significant proportion of the inorganic matter in low-rank coals is in the form of organically bound inorganic elements. The active sites in these coals (functional groups) can readily retain the alkali elements such as sodium, calcium and magnesium. In coals with high sodium content, most of the sodium is organically bound or is present as free ions in the inherent moisture.

- Chlorine is present in the coal in forms which are still conjectural. In low-rank coals, chlorine can occur as free ions in the inherent moisture. In bituminous coals, chlorine appears to be organically bound.

- Sulphur is predominantly present as sulphides and/or organically bound. It can also occur as sulphates in the form of discrete minerals or as sulphate ion in the inherent water.

- Aluminium can be present as an organically bound element but in most cases it is present in the form of minerals. Clays are the most commonly found aluminium minerals in coal. Silicon is only present in minerals. The principal silicon containing minerals are quartz and clays. In most coals, quartz and clays exist in bands and large particles. In some low-rank coals, these minerals occur as super-fine particles (down to 1 micron) evenly distributed in the coal matrix.

- The distribution of minerals in coal is generally uneven. The most commonly minerals found in coal are clays, quartz, carbonates and sulphides.

During combustion, the coal particles are heated, dried, devolatilised and the remaining char is burnt. During these stages, the inorganic matter in coal undergoes physical transformations (crystallisation, fusion, vaporisation and coalescence) and chemical transformations (thermal decomposition, reaction between the species in the inorganic matter, reaction with char, and reactions with gaseous species in the furnace). The transformations undergone by the inorganic matter can be summarised as follows:

- The inherent moisture in coal evaporates as the coal particles are heated. The evaporation is complete when the particle temperature reaches 200°C. Sodium chloride and other salts dissolved in the inherent water crystallise within the coal particles. The crystals are likely to be finely distributed in the coal matrix.

- At temperatures between 400° and 900°C, the coal devolatilises releasing the organic volatiles. During pyrolysis, the functional groups containing the inorganics decompose resulting in the formation, inside the coal particles, of reactive inorganic species. Some of these species are volatile (i.e. those from Na, S, and Cl) and may be released into the gas phase. Those species remaining in the coal are finely distributed in the coal matrix. Sodium carbonate, calcium oxide, magnesium oxide, alkali sulphides, iron oxide and alumina phases may be formed.

- Sodium chloride melts at about 800°C and has a significant vapour pressure at temperatures found in FBC. At these temperatures, however, it reacts with other compounds inside and/or at the char's surface resulting in a disproportionate release of sodium and chlorine. Direct vaporisation of sodium chloride increases with increasing temperature.

- The vaporised alkali species can react with sulphur, silica and clay to form sulphates, silicates and aluminium silicates. The formation of sodium sulphate contributes to the fouling of heat transfer surfaces in pc fired systems.

- The minerals undergo dehydration below 350°C. At higher temperatures, they decompose to mainly oxides and silicates. Above 900°C, significant reactions can occur between the acidic and basic oxides with the resultant formation of low melting eutectics.

- Sodium chloride and the species formed from the alkali elements can form solid solutions with melting temperatures often below those found in FBC systems. Sodium oxide and silica can form a eutectic at 800°C.

- During char burnout, the inorganic matter becomes exposed. As combustion proceeds, the char surface recedes and the inorganic matter is drawn together. The molten phases either sinter or coalesce while the solid particles:

  + agglomerate with the molten phase; or

  + escape into the combustion chamber.

  Sintering and coalescence occur due to the formation of low melting eutectics when the particles are drawn together as a result of the receding char surface.

In pc combustion, the coalescence and sintering of the inorganic matter continue until char burnout is completed. By conducting laboratory scale pc combustion experiments, Padia (1976) showed that 3-5 particles can form from a pc particle. In fluid bed gasifiers, the collision between char particles covered in molten ash could result in formation of large ash agglomerates. In FBC systems where there is an inventory of inert material, the collisions are likely to occur between the burning char particles and the inert material. These collisions could remove the molten phases from the surface of burning char particles. The unfused ash particles and small ash agglomerates are collected downstream of the process as fly ash.

The exact role of the inorganic matter and the mechanisms involved in agglomeration are not well understood. However, the prime factors in causing agglomeration are:

- agglomeration occurs due to the stickiness of the bed particles (fly ash and inert material). The stickiness may be an inherent property of the bed particles coming into effect at some temperature level, or it may be due to a molten phase deposited upon the inert bed particles. For particles to agglomerate, the bed temperature must exceed the sintering temperature of the bed material or its coatings. This temperature, determined by dilatometer, is substantially lower than the ash fusion temperature.

- sticky bed particles collide and, depending on their characteristics and the operating conditions, a bond is formed between the particles either by surface diffusion or viscous flow. The strengthening of the bond occurs with time and temperature. Agglomerates formed at lower temperatures are sintered, whereas, those formed at higher temperatures experience a significant amount of coalescence.

- agglomeration increases with increasing temperature, thickness of the coatings, and larger coal feed size. Higher fluidisation velocities and larger particles reduce the amount of agglomeration. Other variables affecting the extent of agglomeration include bed height and system geometry.

Defluidisation of a fluid bed combustor can occur at velocities significantly higher than the theoretical minimum fluidisation velocity for non-sticky particles. By operating fluid bed systems containing sticky bed particles at high velocities, it is possible to maintain the bed under stable conditions while forming agglomerates in the bed at a controlled rate. The variables affecting the defluidisation are the same as those for agglomeration. It is, therefore, suggested by most researchers that defluidisation is the result of agglomeration of the bed materials. Other evidence suggests that defluidisation is governed by separate rules from those for agglomeration.

Models which can describe agglomeration and defluidisation processes are not yet fully developed. In order to develop such models, an understanding of the mechanisms of these processes is required.

The formation of molten phases in FBC is the result of physico-chemical transformations undergone by the inorganic matter. There is little qualitative information available concerning these transformations in FBC systems. The role of sodium in enhancing agglomeration and defluidisation has not been explained.

Based on the results of literature review, a schematic diagram is developed (Figure 2.5) which illustrates the transformations of the inorganic matter during FBC of coals and the formation of ash and bed agglomerates. This diagram is expected to assist in determining the areas in which research has to be carried out in order to ascertain an understanding of the processes involved in agglomeration and defluidisation. The areas of particular importance, which are investigated in this thesis, are:

- quantitative assessment of the extent of vaporisation of the volatile species;
- characterisation of the inorganic matter formed on the char surface;
- interaction of the inert bed particles with the inorganic matter and its effect on the fate of the inorganic matter;
- collision of inert particles resulting in the formation of agglomerates and/or defluidisation.

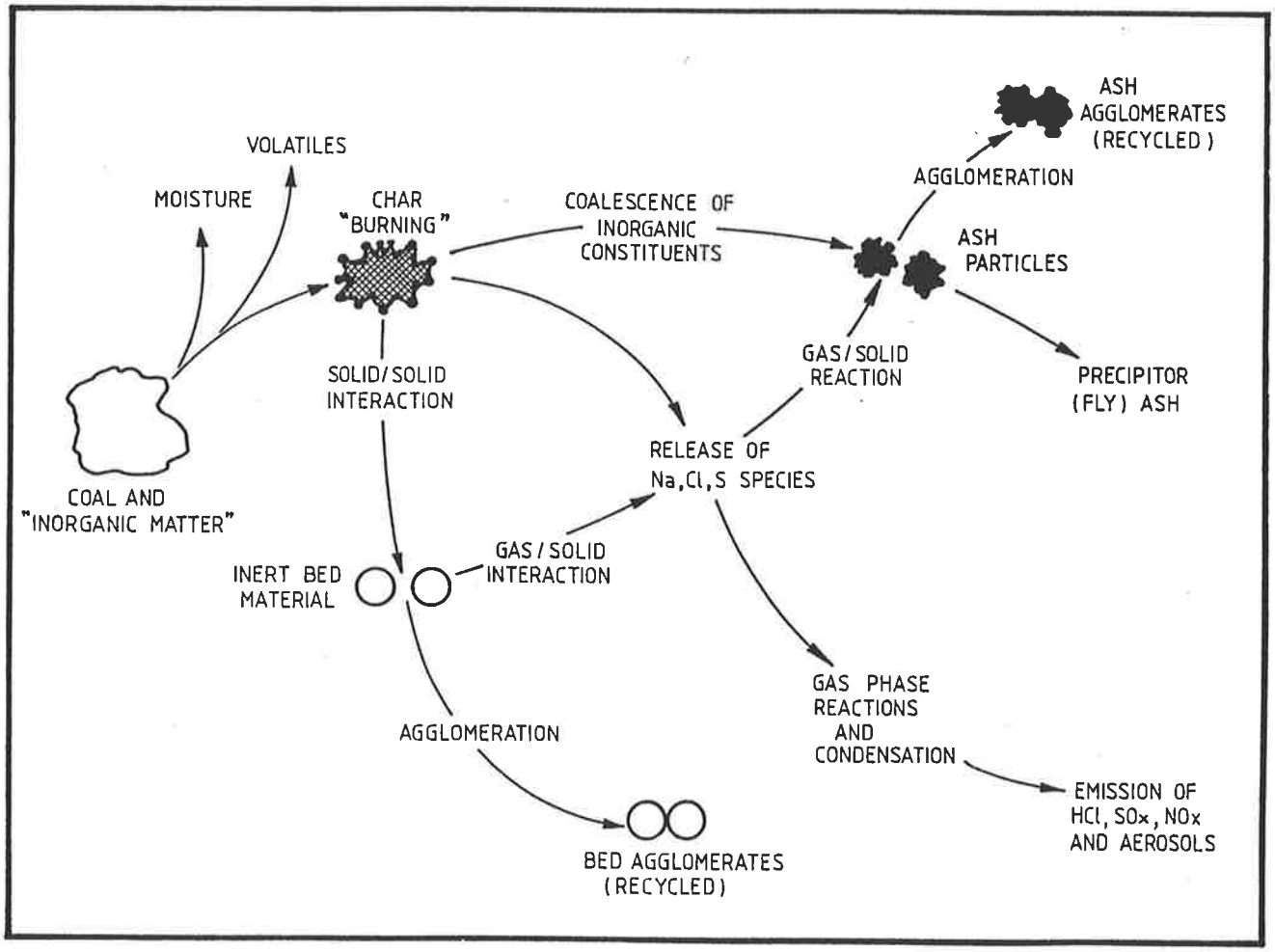

Figure 2.5: Schematic of the Transformation of the Inorganic Matter in Circulating Fluid Bed Combustors

Chapter 3

EXPERIMENTAL

3.1 INTRODUCTION AND OBJECTIVES

The behaviour of the inorganic matter during combustion of low-rank coals has been investigated by a number of researchers (Chapter 2). Irrespective of the utilisation process, the inorganic matter in low-rank coals undergoes complex physico-chemical transformations and forms inorganic species which can cause a variety of operational problems through mechanisms which are not yet completely understood. For example, fluid bed combustion of certain low-rank coals causes ash and bed agglomeration under certain operating conditions. The exact roles of sodium and other inorganic matter and the mechanisms by which they participate in the formation of agglomerates are not fully known.

In accordance with the program proposed in Chapter 2, the first stage of the experimental program was designed with the following objectives:

- to determine the physico-chemical transformations experienced by the inorganic matter under conditions relevant to FBC;
- to quantify the extent of vaporisation of the inorganic matter;

- to elucidate the ash formation mechanism, ash chemistry and its morphology.

This stage of the investigation was carried out using an existing single particle furnace (SPF) at the University of Adelaide.

The literature reviewed, Subsection 2.5, indicated that agglomeration occurs due to stickiness of bed particles; the stickiness may be an inherent property of the bed particles coming into effect at some temperature level, or it may be due to a molten phase deposited on the inert bed particles. Consequently, the results of the single particle experiments (to be reported in Chapter 4) formed a basis for the hypothesis that, in circulating fluid bed combustors (CFBC), bed agglomerates are formed by the following mechanisms:

- collision of bed particles with burning char particles covered in molten ash in the stirred environment of CFBC;
- transfer of molten ash from the surface of burning char particles to the bed particles, which consequently become sticky; and
- formation of agglomerates as a result of collision of sticky bed particles with each other.

In order to investigate the validity of the above hypothesis, a fluid bed combustion system (FBCS) was designed and fabricated to carry out the experiments and to determine the phenomenological trends. The system was designed with the following requirements:

- it had to simulate the hydrodynamics of a circulating fluid bed combustor in which solid particles are well mixed;
- the particle bed had to be observed at all times;
- the formation of agglomerates and the bed defluidisation had to be detected easily;
- the temperatures and the differential pressure across the bed had to be accurately measured and recorded;
- the distributor had to be designed to allow for the discharge of the bed inventory so that tests could be performed one after another and the bed material examined for selected sets of conditions.

The experimental program, conducted using this equipment, was planned with the following objectives:

- to investigate the mechanism of deposition of molten material on the bed particles and the exact role of the inorganic matter in this mechanism;
- to determine the rate of deposition of the molten material on the bed particles as a function of operating time, coal quality, combustion temperature, excess air, bed material and bed particle size distribution;
- to investigate the mechanisms of bed agglomeration and defluidisation and their dependence on operating time, coal quality, furnace temperature, bed material and bed particle size.

The description of the experimental apparatus and the analytical techniques employed are given in this chapter. The results of the experiments are given in Chapters 4, 5 and 6. For the investigation, a South Australian brown coal from the Lochiel deposit with high contents of sodium and sulphur was used.

3.2 SINGLE PARTICLE APPARATUS

A schematic diagram showing the single particle furnace (SPF) is given in Figure 3.1. It consists of an electrical furnace enclosed inside a refractory brick insulation which houses 12 silicon carbide electric heating rods having a total heat output of up to 8 kW. Air or nitrogen, preheated in the electrical furnace to the required temperature, enters a glass cylinder of 20 mm ID located above the electrical furnace and fluidises an introduced single particle of coal. A butterfly valve controls the flow of the fluidising gas in order to retain the single particle in the glass furnace during the test. The char particle (from now on referred to as "product particle") is withdrawn from the furnace at various residence times using nitrogen as a carrier gas. The product particle so withdrawn is then collected and quenched in a dry ice container for examination. The detailed description of the SPF and its operating procedure is given by Wildegger-Gaissmaier (1989).

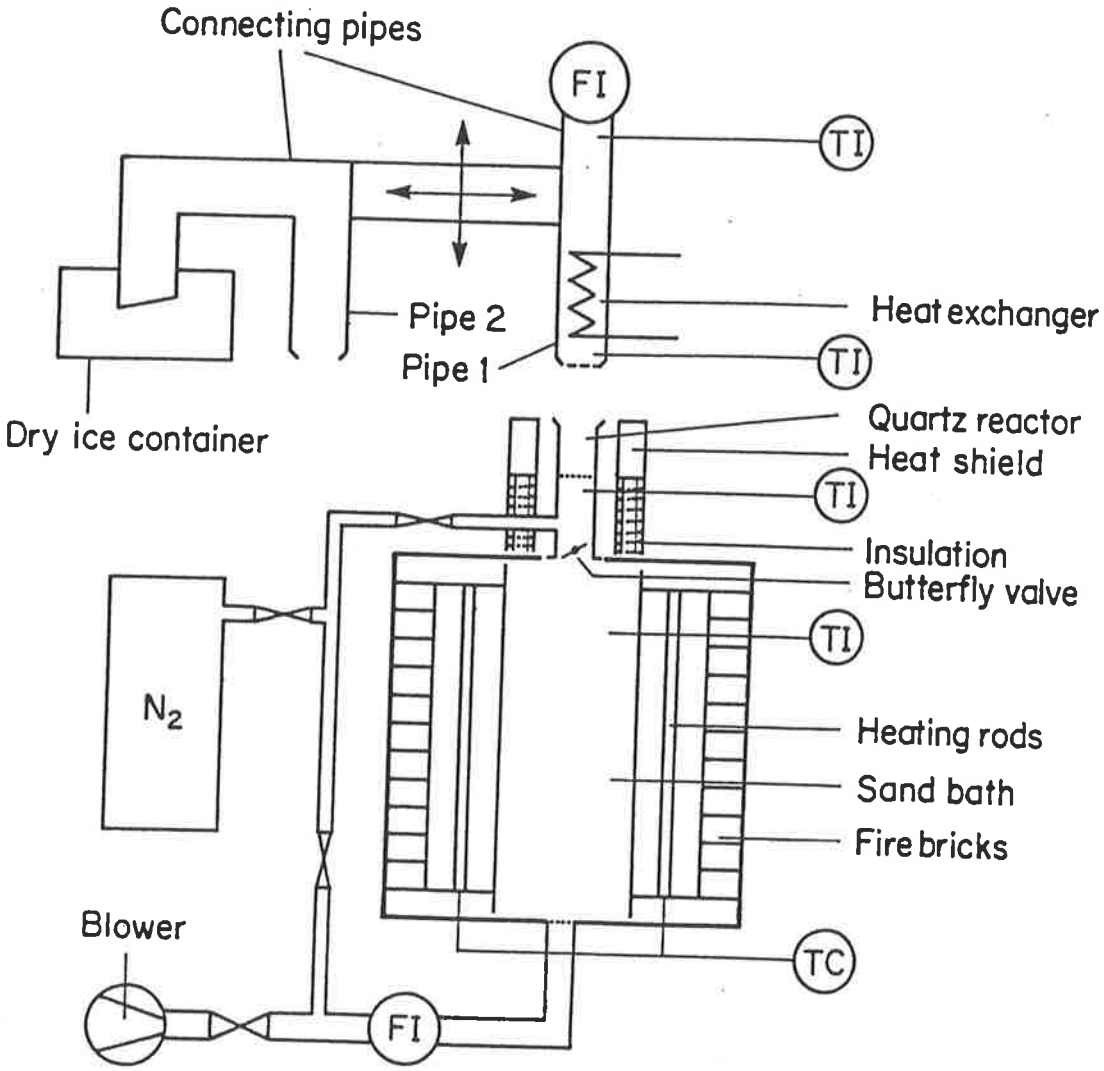

Figure 3.1: Schematic Diagram Showing the Single Particle Furnace
(Source: Wildegger - Gaismaier, 1989)

3.3 FLUID BED COMBUSTION SYSTEM

3.3.1 Description

Fluid Bed Combustion System

A schematic diagram and a photograph showing the fluid bed combustion system (FBCS), designed and fabricated for this project, are given in Figures 3.2 and 3.3. The basis for designing the FBCS is discussed in Subsection 3.3.2. The FBCS consists of a cylindrical furnace, 77 mm ID, with a conical distributor. Due to high gas velocities, the particles at the narrow end of the distributor acquire considerable momentum and are spouted to the cylindrical part of the furnace. As they move upwards, the particles lose their momentum as a result of the increasing cross-sectional area and lower gas velocities. The FBCS design and operating parameters are selected so that the particles then recirculate back, along the wall, into the base of the conical distributor. The section of the combustor in which the recirculation of particles take place is referred to as "combustion zone", Figure 3.2.

Such recirculation will ensure that light coal particles mix with the heavier bed particles as is the case in CFBC. With this design, the stratification of bed particles and isolated combustion of coal particles, which is a characteristic of bubbling fluid bed systems, is avoided. Additionally, the confinement of the combustion zone in a section of the combustor eliminates the requirement of an external recirculation loop. The features of the FBCS are:

- the bed can be observed at all times through a glass viewing port installed at the top of the furnace and a mirror overlooking the bed;
- the temperature and the differential pressure across the bed can be measured accurately; and
- the formation of agglomerates and the defluidisation of the bed can be detected promptly.

Air dried coal, ground and sieved to a size range between 2.0 and 3.35 mm, is fed continuously into the combustion zone via a water cooled screw feeder. The cooling is provided to avoid devolatilisation of the coal in the feeder line. The screw feeder is driven

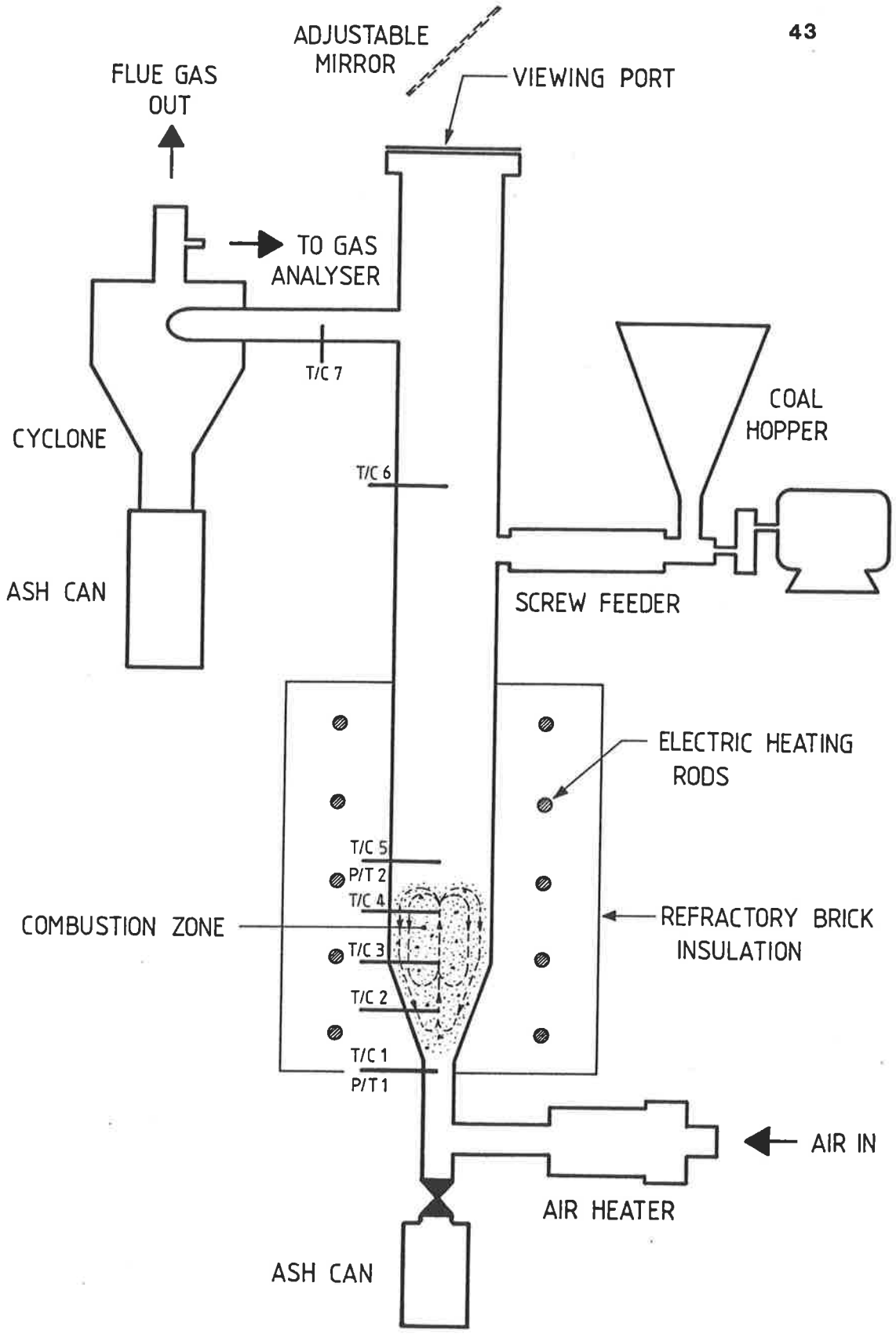

Figure 3.2: Schematic Diagram of the Fluid Bed Combustion System

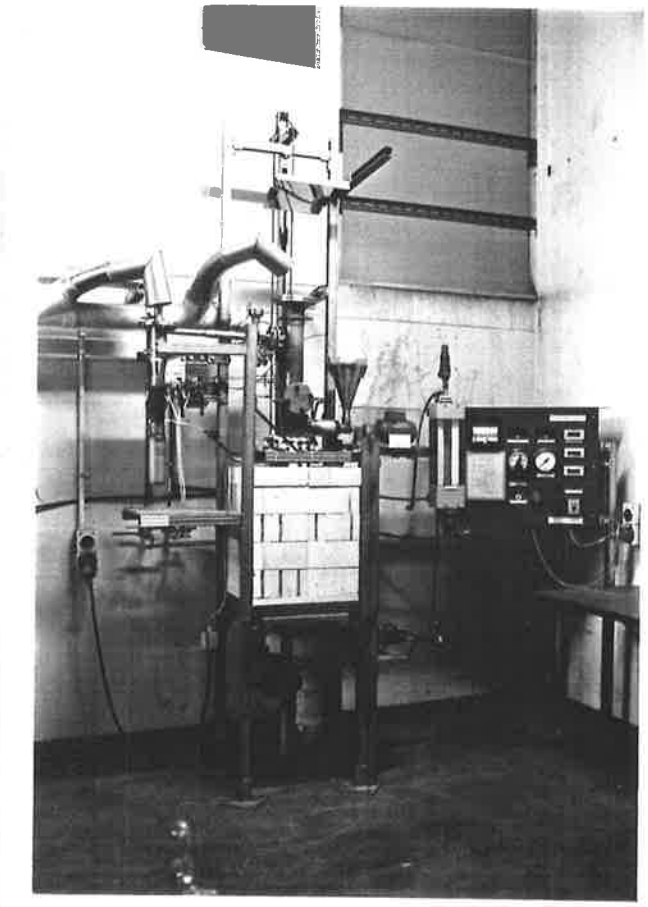

Figure 3.3: Photograph of the Fluid Bed Combustion System

by a variable speed DC motor through a double reduction gearbox providing feed rate control of between 100 to 700 g/h of coal. A hopper positioned above the feeder holds 700 g of coal.

The feeding point is positioned above the bed to avoid fluctuation in the coal feed rate due to pressure excursions within the bed as a result of bed turbulence. Hence, after enering the furnace, the coal particles have to settle into the combustion zone at the conical bottom of the furnace. For this reason, the minimum size of the coal particles is dictated by the fluidisation velocity in the cylindrical part of the furnace. Also, the top size of the coal particles is limited by the ability of the small screw feeder to handle large particles. Therefore, the size range of the coal samples selected for the combustion experiments was 2.0 to 3.35 mm.

Combustion air is introduced to the base of the combustor after passing through a 5 kW electric heater. The heater, equipped with a controller, lifts the temperature of the incoming air from ambient to any selected temperature up to 700°C. The combustion air is supplied by a compressor at a pressure of 700 kPa, then regulated to 200 kPa to ensure a uniform supply. The air flow is controlled through a rotameter to a set value between 40 to 280 litres per minute before entering the air heater. Provisions have been made to dilute the air with other gases supplied from cylinders. Hence, the system can be used for pyrolysis and gasification experiments as well.

The ash-laden flue gas leaving the combustor enters into a cyclone in which fly ash particles down to micron size are removed. The cyclone ash can be sampled on-line using an ash can attached to its underside. Flue gas is exhausted from the top of the cyclone into the gas extraction system where some gas is directed to the gas analysis system to monitor excess oxygen and carbon monoxide levels. A pressure vent situated at the top of the combustor allows safe venting of any sudden increase in combustion gas pressure.

At the base of the combustor, a sealed ash can collects any material which is too heavy to be fluidised. An isolating valve above the ash can allows this material to be extracted for examination whenever desired during an experiment. At the completion of a test, the bed material is automatically discharged into the ash can by simply shutting the supply air. This allows the tests to be carried out one after another.

The lower part of the combustor is enclosed inside a refractory brick insulation which houses 9 silicon carbide electric heating rods having a total heat output of up to 14.5 kW. The heating rods are installed to provide supplementary heat during the combustion experiments, if required.

The front elevation of the combustion system showing the furnace and the control panel is given in Figure 3.4. The furnace is suspended via a pulley and a counter-weight arrangement. The differential expansion is accommodated by allowing the brackets attached to the furnace to slide in a vertical frame. The diagrams showing the detailed design of the furnace, screw feeder and its spindle are given in Figures 3.5, 3.6 and 3.7 respectively.

Data Acquisition and Measurements

The data acquisition and display wiring diagram is shown in Figure 3.8. Process temperatures are measured at 7 points using 'K' type (chromel-alumel) thermocouples suitable for temperature between 0°C and 1300°C. All thermocouples are connected via two switch banks to a 240 V powered digital display giving a read-out in degrees Celsius. The position of the thermocouples are shown in Figure 3.4.

Differential pressure is measured across the bed in the combustion zone by a diaphragm sensor-transmitter. The resultant 4-20 mA signal is sent to a process monitor where it is displayed as a value between 0 Pa and 1000 Pa. The process monitor also provides a regulated 24 V, DC power supply, to the pressure transmitter.

A programmable six point chart recorder is connected to four thermocouples (T/C 1 to T/C 4) and the differential pressure transmitter.

Process Control and Power

The power and control wiring diagram is shown in Figure 3.9. The rate at which coal enters the combustor is set by the feeder speed control potentiometer. Single phase power is rectified and supplied to the DC feeder motor via a double pole single throw isolating switch mounted on the control panel next to the speed control potentiometer.

Temperature of the incoming combustion air is set by the air temperature control potentiometer. This changes the power (two phase) supplied to the 5 kW element and it is installed on the control panel. An isolating switch is also mounted on the control panel next to the air temperature control potentiometer.

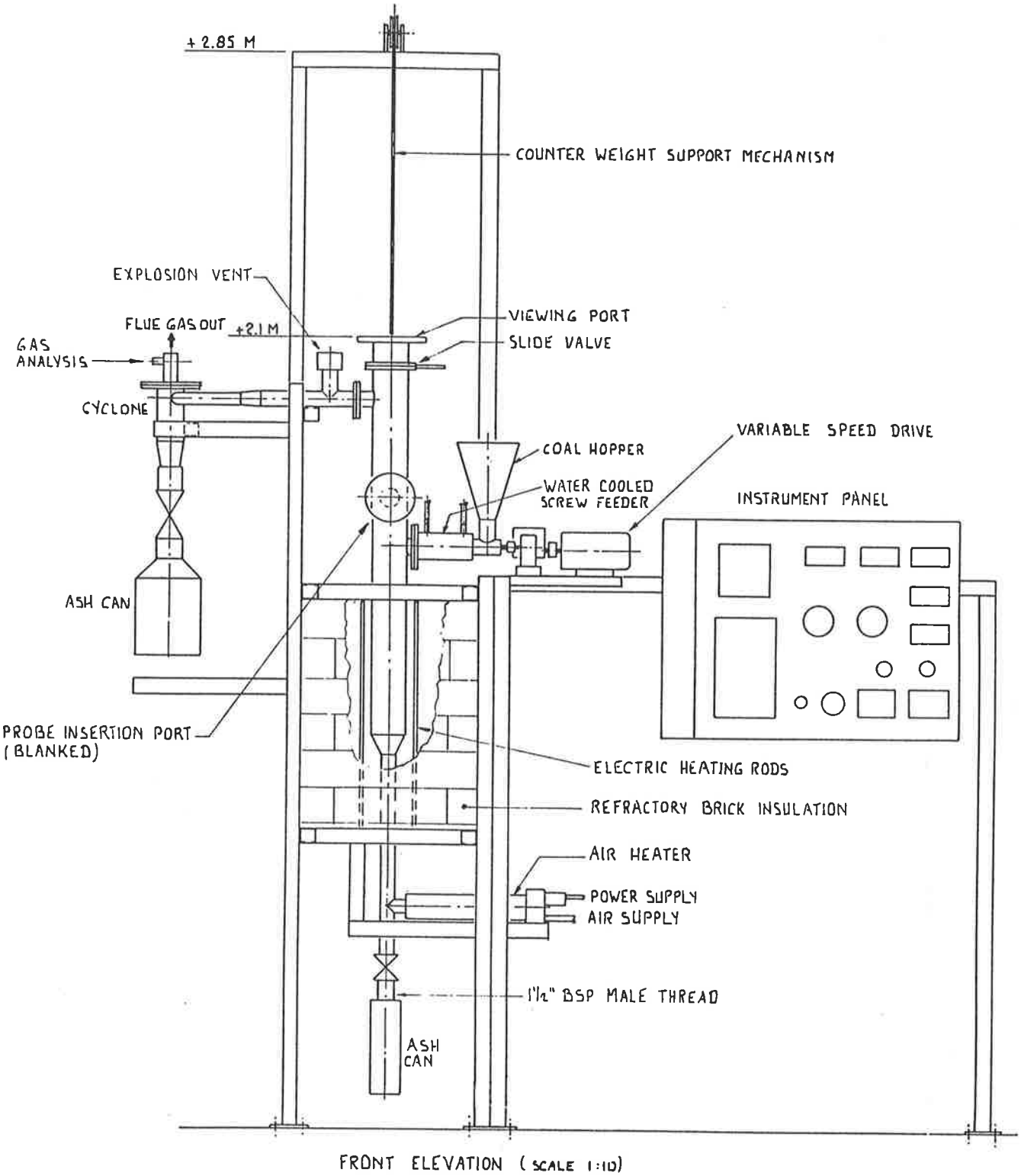

Figure 3.4: Front Elevation of the Fluid Bed Combustion System

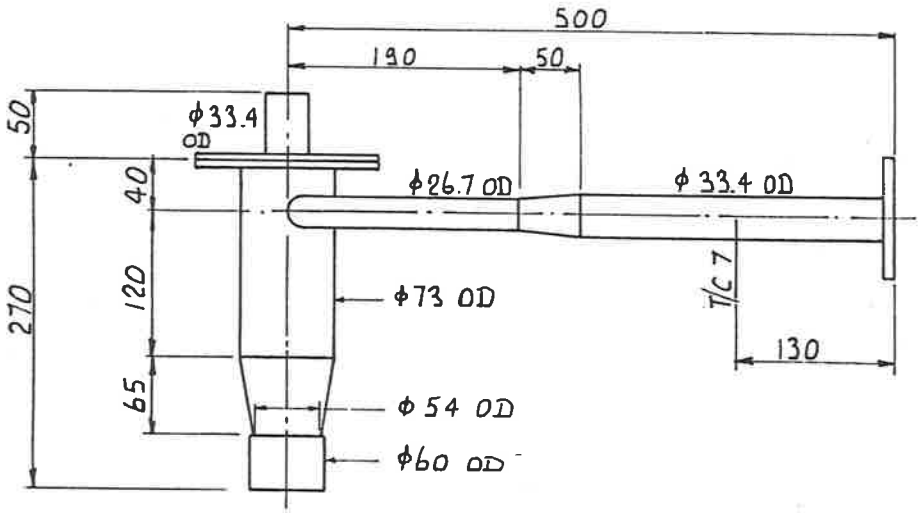

CYCLONE DETAIL (SC. 1:5)

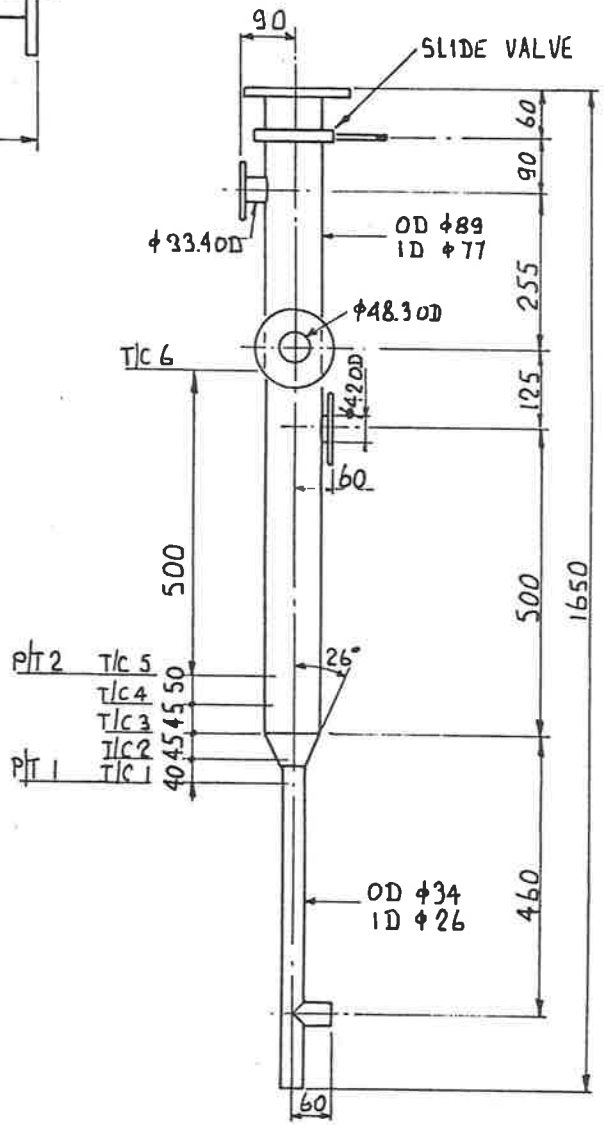

COMBUSTOR DETAIL (SC.1:10)

Figure 3.5: Fluid Bed Combustion System Combustor and Cyclone Details

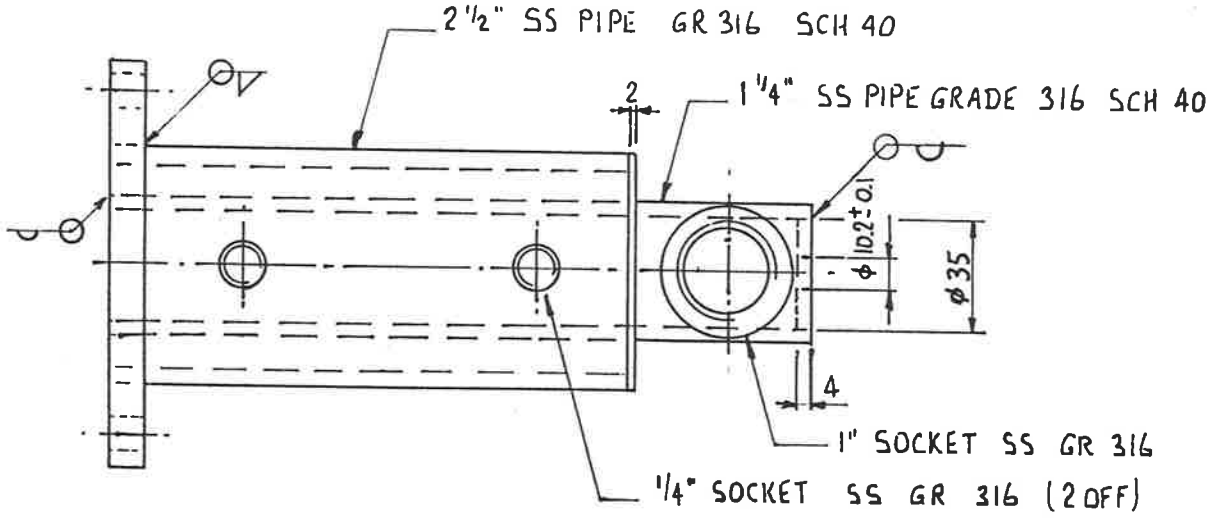

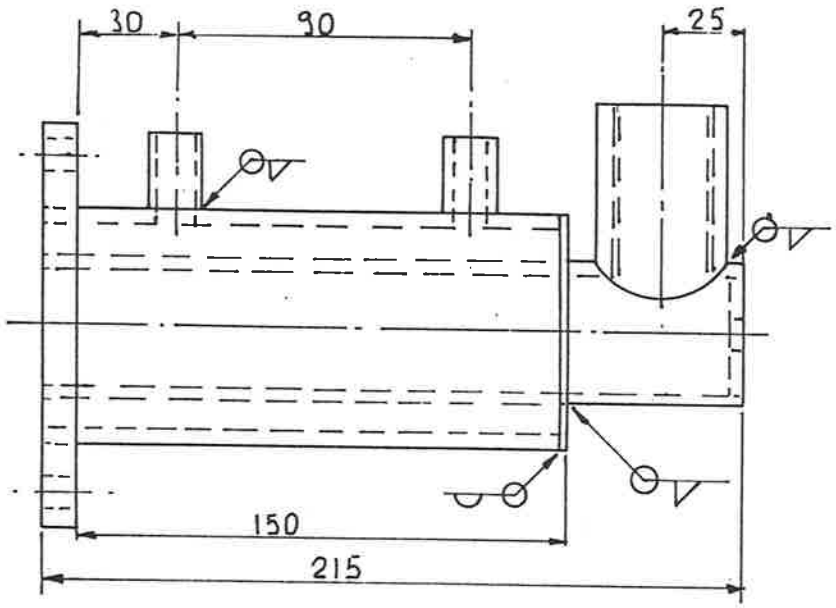

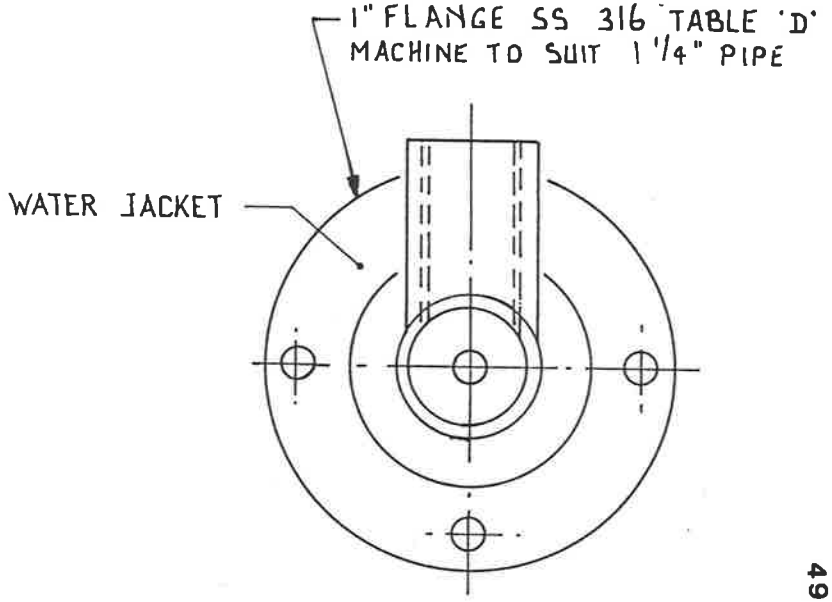

Figure 3.6: Fluid Bed Combustion System Screw Feeder Details

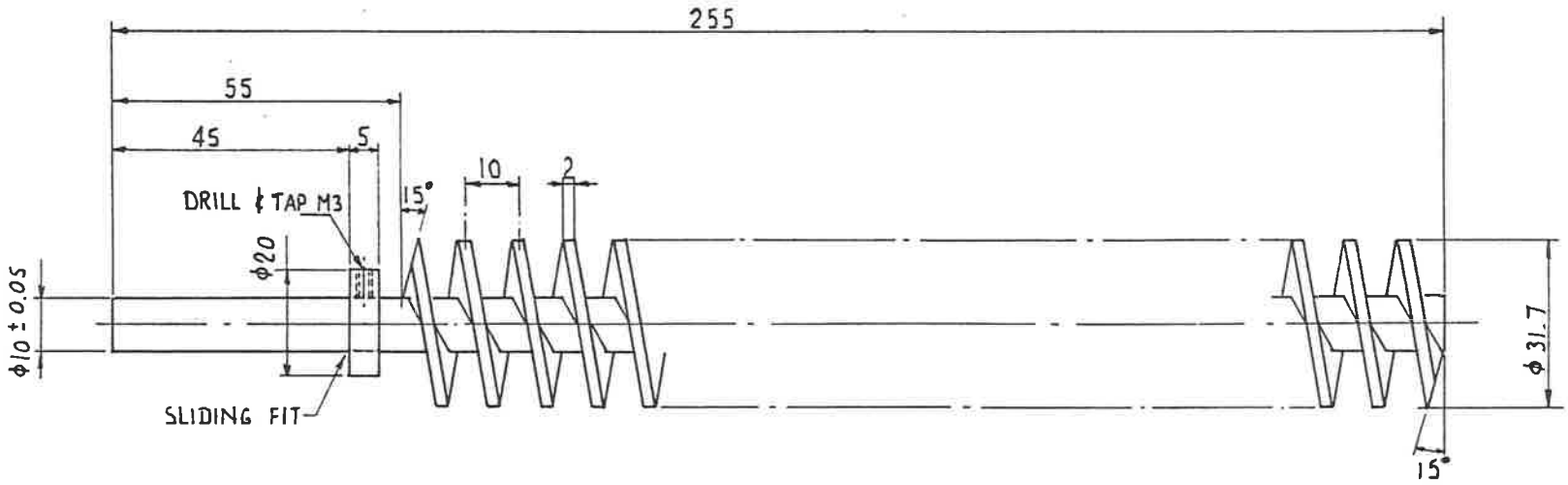

MATERIAL : SS STEEL GR 316

Figure 3.7: Fluid Bed Combustion System
Screw Feeder Spindle Details

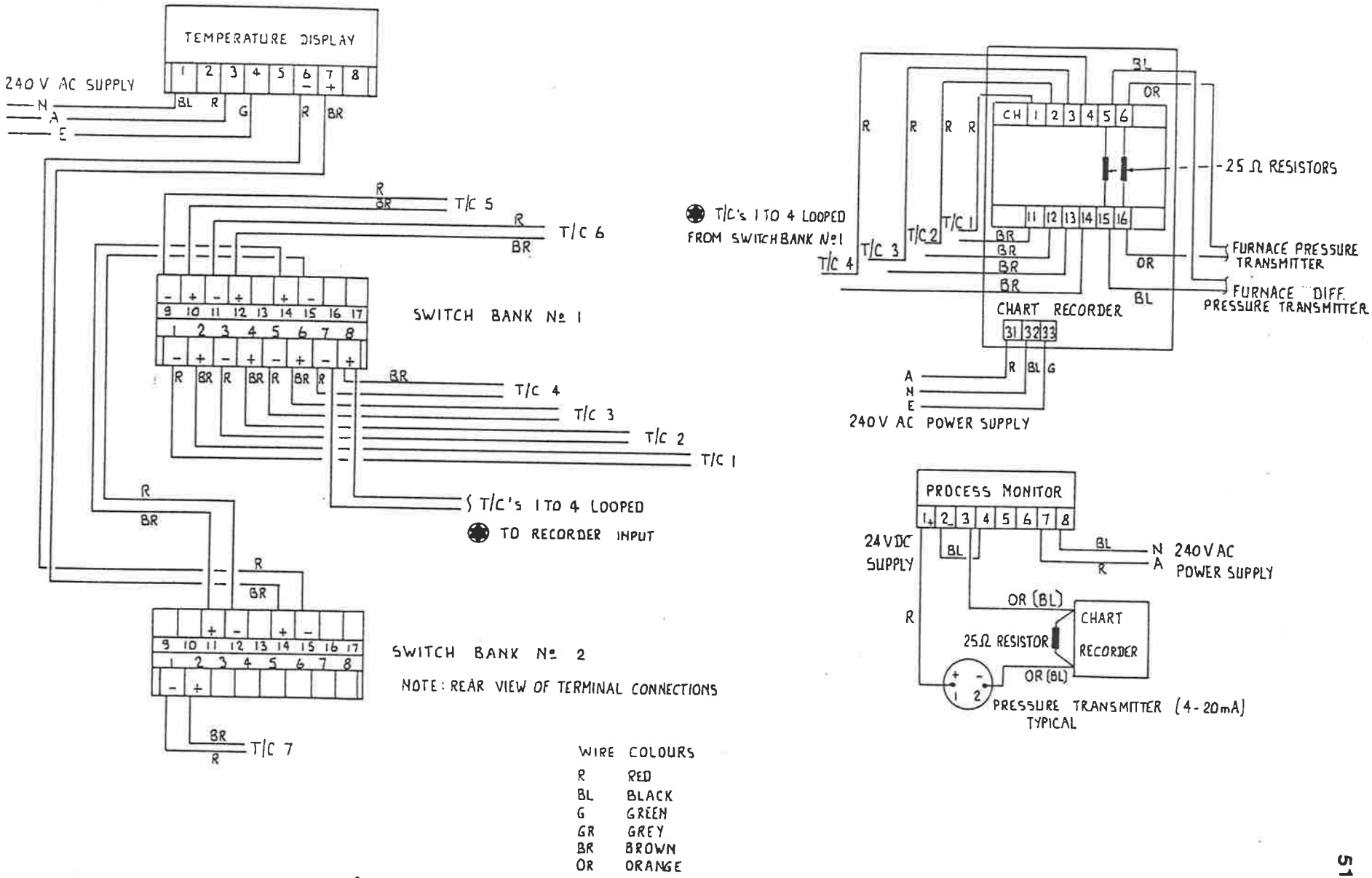

WIRE COLOURS

R	RED
BL	BLACK
G	GREEN
GR	GREY
BR	BROWN
OR	ORANGE

Figure 3.8: Fluid Bed Combustion System Data Acquisition and Display Wiring Diagram

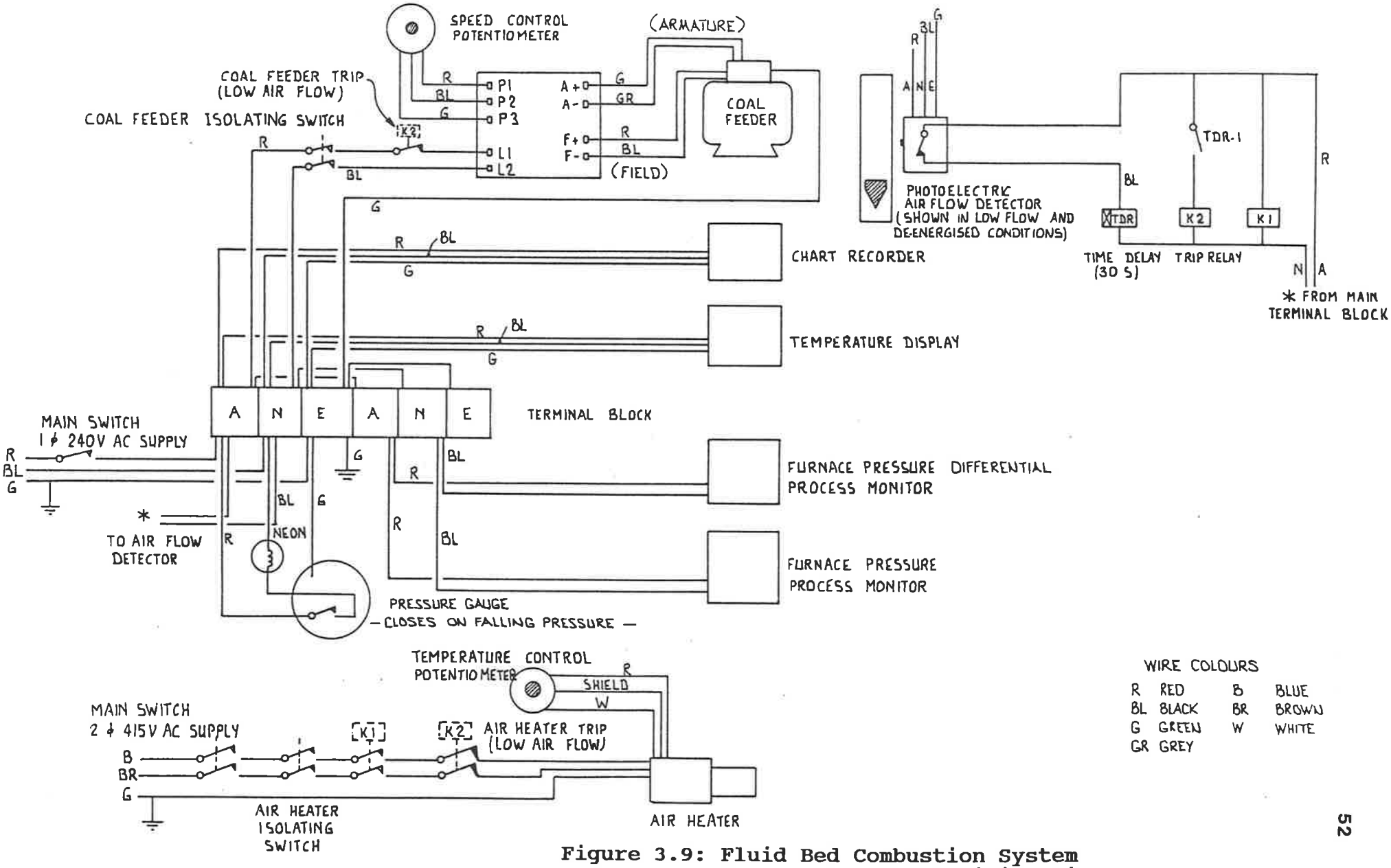

Figure 3.9: Fluid Bed Combustion System Power and Control Wiring Diagram

The flow of the incoming combustion air is controlled by a pressure regulator and a needle valve with the flow being indicated and measured by a rotameter.

The heating rods, in three groups of three in series, are star connected to the secondary side of a three phase variable (auto) transformer.

Alarms and Protections

To alarm the operator of sudden changes in the operating conditions, the system is equipped with a number of alarm systems:

- the temperature digital display unit has a high and a low alarm setting. This provides a visual indication via two light-emitting diodes (LED) and a remote signalling facility via two integral relays with voltage free contacts. Similarly, each channel of the chart recorder can be programmed with the alarm setting;
- the supply air pressure is 700 kPa. Should this drop to 550 kPa an alarm light is illuminated on the control panel. As the process working air pressure is 200 kPa, this gives the operator ample time to rectify the problem;
- in case there is a significant variation in the combustion air flow rate, for example due to compressor failure, a photo-electric transceiver unit senses the rotameter float at its alarm point. Should this happen, a trip timer relay is activated. The timer can be set for up to 30 seconds and if the rotameter float does not return above the alarm point before this time has elapsed, then both the air heater and the coal feeder will trip.

The air heater is also provided with an integral high temperature cut-out to protect the element.

In designing a fluid bed reactor as a combustor, the fluid bed combustion process has to be considered as being composed of two different subprocesses with inter-related design parameters: a) fluidisation of solids, in which the solid particles are fluidised by an upward flow of a gas, and b) the combustion process, in which coal particles are burned in the presence of oxygen to produce heat.

The fluid bed combustion process has to be designed in such a way that the requirements for combustion of coal and fluidisation of solids are met co-currently. Additionally, the heat released by the combustion of the coal has to be removed from the combustion zone to

maintain the system in thermal balance. Gaseous combustion products are used as the fluidisation agent for the coal particles, coal ash particles, initial bed material and also sorbents and ballast material which are often injected into the combustor.

3.3.2 Design Method

In designing the FBCS described in the previous section, a fluidisation velocity of 1 to 2 meters per second in the cylindrical part of the furnace was considered to be adequate to allow solids to return to the combustion zone shown in Figure 3.2. Given the diameter of the cylindrical part of the furnace, the flue gas flow rate and coal throughput were calculated for various levels of excess air (Appendix A). Based on these results, the diameter of the narrow end of the conical distributor was selected (26 mm ID) in order to obtain an average fluidisation velocity of 5 to 10 m/s in the combustion zone. The height of the conical distributor was selected to ensure satisfactory recirculation of solids within the combustion zone.

The air heater duty and the minimum fluidisation velocity were then calculated. The details of the calculations are given in Appendix A.

3.3.3 Pre-Commissioning Studies

Cold model

A cold model of the lower part of the furnace was fabricated from a transparent acrylic pipe ("Perspex") in order to evaluate the fluidisation behaviour of the bed material and of the coal particles in the furnace. The cold model was used to optimise:

- the fluidisation velocity;
- the size distribution of the coal and bed particles;
- the quantity of the bed material for optimum recirculation.

The fluidisation velocities employed were the same as those under hot condition. Larger quantities of air are required for the cold model in order to simulate the velocities attained during combustion. The same rotameter was used but the aluminium float was replaced with a stainless steel float in order to measure the larger flow of air.

Bed materials of various size distribution (0.71 to 1.73 mm) were fluidised in the cold model using air as the fluidisation agent. The expansion, elutriation and recirculation of the material were investigated as a function of the air flow and bed inventory. The results indicated that a minimum gas velocity of 1.0 to 2 m/s in the cylindrical part of the furnace (77 mm ID) and a corresponding velocity of about 9.0 to 18 m/s at the narrow end of the conical distributor (26 mm ID) were adequate to fluidise and recirculate a bed of solid particles in the so-called combustion zone of the furnace.

Tests with bed inventories of up to 200 g demonstrated satisfactory recirculation of solid particles. For larger bed inventories the downwards flow of the bed particles around the conical wall became sluggish. Higher fluidisation velocities improved the recirculation of solid particles and resulted in higher bed expansion towards the cylindrical part of the furnace. Observation of bed expansion versus fluidisation velocity ensured the correct selection of the position of the thermocouples and pressure tappings. The bed inventory was weighed after each fluidisation test to determine whether elutriation of bed particles occurred at the velocities considered.

Coal particles of various size distribution were added to the cold model and their fluidisation/mixing characteristics with the bed particles were observed. Coal particles larger than 1.0 mm in diameter could be uniformly mixed and fluidised with the bed particles. Tests carried out on coal particles up to 5.0 mm diameter indicated satisfactory fluidisation/mixing in the combustion zone.

Screw feeder

The top size of coal particles which can be used in a laboratory scale fluid bed combustor such as FBCS is limited by the small size of the screw feeder. At ambient temperature and with no fluidising air, coal particles of different moisture content and various size distribution were fed into the furnace through the screw feeder and the output was collected at the bottom of the combustor in the ash can. The coal collected at regular intervals was weighed and sieved to establish:

- the top size of the coal particles that the screw feeder can handle without causing interruption in flow or breakage of coal particles;
- the effect of coal drying on the breakage of coal particles;
- the characteristic curve for the screw feeder.

Feeding of coal particles greater than 3.35 mm in diameter resulted in an interrupted flow and the formation of a significant amount of fines. The interruption was caused by the bridging of large coal particles in the neck of the coal hopper. The size of the hopper outlet (neck) is small given the small size of the laboratory scale screw feeder.

The breakage of coal particles, for wet and air-dried coals, was determined by size analysis of the coals collected in the ash can. The results, given in Appendix A, indicated that breakage of coal particles in the screw feeder and formation of fines could be minimised by air drying the coal. The air dried samples of Lochiel coal appeared to have greater hardness and more resistance towards breakage. Hence, it was decided to air dry the coal (to about 20% moisture) prior to combustion in the furnace. The characteristic curve of the screw feeder is also given in Appendix A.

Air heater

The air heater was tested and was found to be very responsive to changes in set temperature. It delivered air up to 670°C (30°C less than the set temperature due to losses) at the base of the conical section of the furnace.

3.3.4 Operation

Trial runs were carried out to determine the optimum conditions for the operation of the FBCS. The furnace was heated first with hot air supplied by the electric air heater and then by feeding coal. The maximum temperature of hot air supplied by the air heater was sufficient for igniting the coal. During the trial runs all the equipment and instrumentation operated as expected. In the combustion zone the mixing of the coal particles with the inert bed material was good. The temperature of the combustor could be accurately controlled at the set point without an appreciable excursion. The maximum temperature of the combustor was found to be in the combustion zone (T/C 3 and T/C 4) where the coal was burning. Thermocouples T/C 3 and T/C 4 were nearly at the same temperature indicating a good fluidisation in the combustion zone. At steady conditions the fluid bed appeared to contain a constant concentration of carbon.

In a CFB combustor, to maintain a desired temperature within the constraints imposed by a fixed range of fluidisation velocities and a realistic O_2 concentration in the flue gas, one has to balance the heat input by the coal and the combustion air with:

- the heat transfer to the installed heat exchanger(s); and
- the heat losses from the walls of the combustor and from the flue gas and fly ash exiting the combustor.

In a large-scale CFBC facility, the heat balance is readily controlled by installing heat exchangers in the system. In a small system without heat exchangers (such as FBCS), the combustion temperature has to be maintained by operating the furnace under flexible excess O_2 levels to control the heat balance.

At thermal balance conditions with a combustion zone temperature of 850°C (the maximum envisaged for the combustion experiments), the FBCS had to operate at excess O_2 concentration in the flue gas of about 16%. This level is higher than in a full scale plant. Attempts were made to reduce the excess O_2 levels by:

- reducing the combustion air temperature and, at the same time, increasing the coal feed rate;
- reducing the combustion air flow and operating at lower fluidisation velocities.

These attempts, made singly or in combination and within the constraints of combustor set temperature and minimum fluidisation velocity, could not achieve excess O_2 levels lower than about 12%. It was, therefore, decided to carry out the experiments with an excess O_2 level of about 16% which provides a greater flexibility in operating the furnace. Separate experiments were carried out to investigate the effect of excess O_2 in flue gas.

During the shut-down procedure, which takes about 15 minutes, it was important to maintain the fluidisation velocity while the combustor temperature was high, because the momentum of the bed particles which is determined by the fluidisation velocity has a significant effect on the extent of agglomerate formation. For this reason, the combustion air flow rate was increased to compensate for its temperature reduction. The bed material was discharged into the ash can when the furnace temperature reached 100°C.

3.4 EXPERIMENTAL PROGRAMS AND PROCEDURES

3.4.1 Ash Formation Studies

Particles of coal of 5.5 to 9.0 mm diameter were carbonised and burned in the single particle furnace (SPF) for various residence times and temperatures. The variables explored are given in Table 3.1. The experiments were carried out at furnace temperatures of 700°, 770° and 830°C which represented the range of operating temperatures normally used for fluid bed combustion of brown coals. Tests could not be performed at higher temperatures due to the limitations of the SPF. The combustion air in certain experiments was diluted with nitrogen to investigate the effect of oxygen partial pressure on the transformations of the inorganic matter. Because of its design and function, the SPF operates with a large amount of gas (air or nitrogen) which sweeps away the combustion products from around the coal particles. For this reason, sulphur dioxide (SO_2) was added to the fluidising air in certain tests to investigate the possible reaction between SO_2 and the ash constituents on the char's surface.

In order to examine quantitatively the transformations experienced by the inorganic matter, it was important to select a coal sample of uniform inorganic composition. A large lump of Lochiel brown coal was collected from a particular zone of the deposit where, due to the small amount of mineral inclusions, the coal has a relatively uniform inorganic composition. Spherical coal particles were carved from this lump of coal.

The product particles withdrawn from the furnace were weighed and leached with demineralised water and then with hydrochloric acid. The residues (acid insolubles) were ashed and then analysed for the inorganic content (procedures are given in Section 3.5.1). The extent of the vaporisation of sodium chloride and of the species formed from the organically bound inorganic elements was determined by the difference between the amount of the inorganic elements in the raw coal and those in the product particles. The changes in the amount of the inorganic elements distributed between the leachate solutions and the residues gave an indication of certain inorganic transformations. The details of the experimental results are given in Chapter 4.

Table 3.1: ***Experimental Variables, Single Particle Experiments***

Type of Experiment	Particle Size,mm	Furnace Temp. °C	Fluid. Gas	Residence Time,seconds
combustion	5.5	700	air	10,20,30,40
"	7.5	"	"	10,20,30,40,50
"	9.0	"	"	20,30,40,50,60,70
"	7.5	770	"	10,20,30,35,40
"	"	830	"	10,20,30,35,40
carbonis.	"	700	N_2	10,20,30,40,60,90,120
"	"	770	"	10,30,60,90,120
"	"	830	"	10,30,60,90,120
combustion	"	700	air+N_2	10,30,50,90,120
"	"	"	air+SO_2	10,30,60,120

In order to characterise the ash formed during combustion, duplicate samples of the product particles were obtained for microscopic examinations. The details of the analytical methods employed are given in Section 3.5. The analytical procedure carried out on the product particles is presented schematically in Figure 3.10.

3.4.2 Ash/Bed Material Interactions

The combustion experiments carried out in the fluid bed combustion system (FBCS) were designed to investigate the interaction of ash and bed particles and the resultant effect on the fate of the inorganic matter under the conditions relevant to the CFBC of brown coals. The following variables: coal quality, combustion temperature, excess oxygen, bed material, size distribution of the initial charge and operating time were investigated (see Table 3.2).

Two samples of high-sodium, high-sulphur coal were collected from the Lochiel deposit in South Australia. Sample 1 was a mixed coal from different zones of the deposit and had an inorganic matter which consisted mostly of minerals in the form of inclusions and partings (Subsection 2.2.1). Sample 2, selected from a particular zone of the deposit, had an inorganic matter which consisted predominantly of organically bound inorganic elements. Both samples contained sodium chloride as dissolved salt in the coal's inherent moisture. Sample 2, which is similar to the low-mineral sample employed for the SPF experiments, was used to investigate the behaviour of the inorganics in coal without the interference from the minerals initially present in the coal. Experiments were also carried out with water-leached, acid-leached and added-sodium chloride samples of the low-mineral coal.

The experiments were carried out with an initial charge of 100 g of bed inventory. Each test was stopped every three hours to remove the bed material from the furnace for weighing, sieving and sampling. Then the bed material was returned to the furnace for the subsequent three hour runs. Samples of bed material and cyclone ash collected at the end of each run were analysed using different combinations of the following analytical techniques (described in Section 3.5):

- chemical methods;
- electron microprobe analysis;

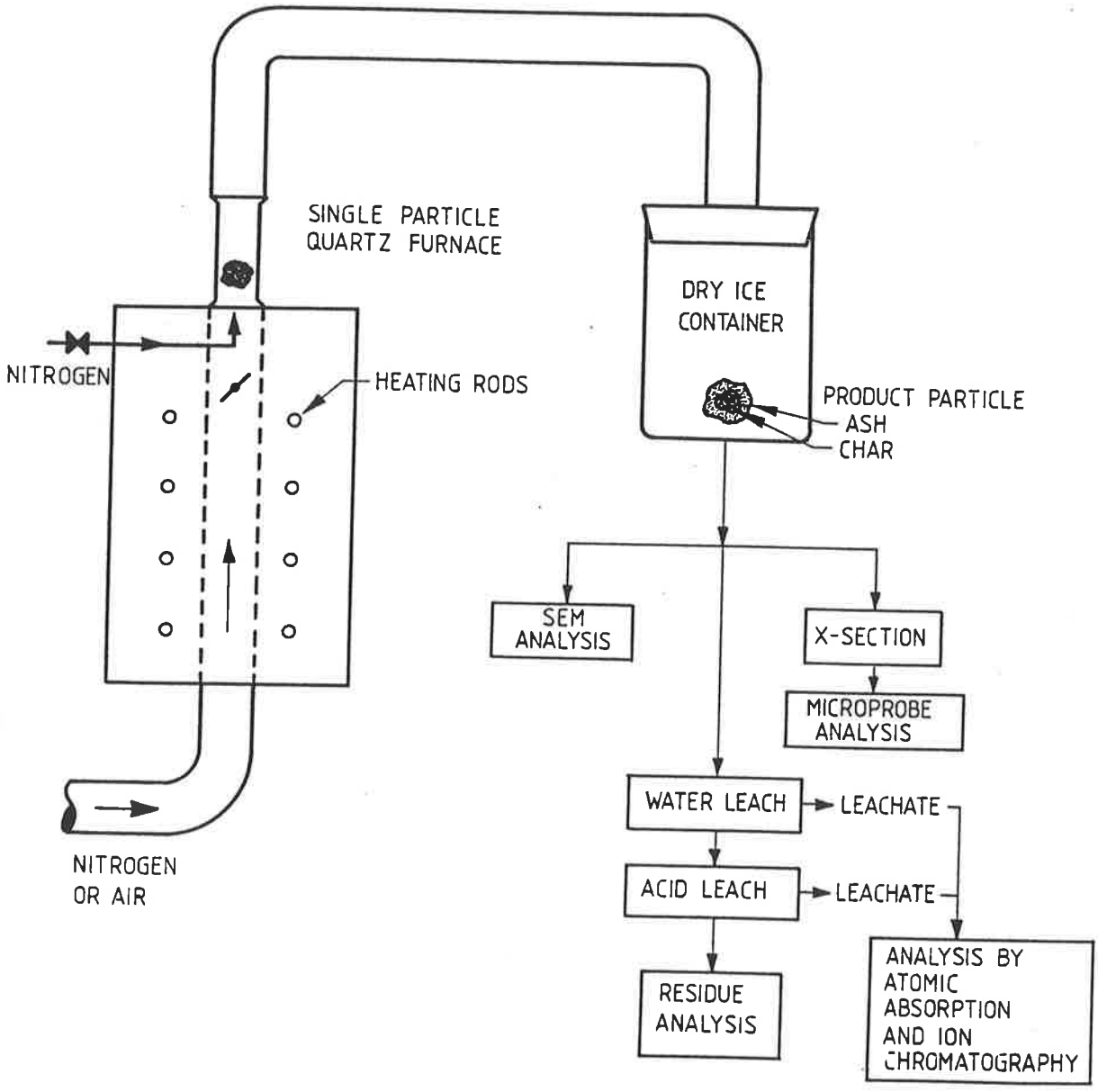

Figure 3.10: Schematic Diagram Showing the Single Particle Furnace and the Analytical Methods Employed.

Run No	Coal Sample	Furnace Temp. °C	% Excess O_2	Bed Material	Particle Size,mm	Run hr
1	high-mineral	850	16	sand	0.85 to 1.0	24
2	low-mineral	"	"	"	"	3.5*
3	"	800	"	"	"	9
4	water-leached	"	"	"	"	10.5
5	acid-leached	"	"	"	"	9
6	NaCl-added, 1	"	"	"	"	9
7	NaCl-added, 2	"	"	"	"	0.5*
8	low-mineral	750	"	"	"	12
9	"	700	"	"	"	12
10	"	800	"	"	0.71 to 0.85	9
11	"	"	"	dolomite	0.85 to 1.0	12
12	"	"	12	sand	"	3
13	"	"	5	"	"	3

* Aborted due to defluidisation of the bed

Table 3.2: ***Experimental Variables, Fluid Bed Combustion Experiments.***

- scanning Electron microscopy;
- x-ray diffraction analysis;
- thermomechanical analysis;
- differential thermal analysis;
- thermogravimetric analysis.

Due to the variables involved in the fluid bed combustion process, it is important to carry out the experiments under the same conditions with only one variable changed at a time. In case other variables are changed as a consequence, the procedures resulting in the least impact on the other variables should be adopted. For example, to compare the effect of varying the coal quality, it is necessary to burn the same amount of carbonaceous matter per unit time. During the FBCS experiments, the rate of combustion of carbonaceous matter was controlled by setting the combustion air flow rate at a fixed level (140 L/min at ambient conditions) and by adjusting the coal feed rate to attain a fixed level of excess O_2 in the flue gases (16%). The combustor temperature was then controlled at the desired level by adjusting the combustion air heater outlet temperature. By this method, the fluidisation velocity in the combustion zone can be maintained while changing other variables.

Similarly, to explore the effect of varying combustor temperature the same control procedure was employed.

To investigate the effect of excess O_2, two experiments were carried out on the same coal. In one experiment the excess O_2 was lowered to the minimum for the system (Section 3.3.4) to give 12% excess O_2. This experiment, conducted over 3 hours, gave an indication of the effect of oxygen partial pressure on the chemical composition of ash and that of bed material. In the second experiment, nitrogen was used together with air to achieve an excess O_2 level in flue gas of only 5% while maintaining the same fluidisation velocity and the same coal feed rate as in the experiment with 16% O_2 in flue gas. The combustor temperature was controlled at the desired level by setting the combustion air temperature. This experiment lasted for only three hours as it was difficult to control all the variables at the same time. The results of the experimental investigation are given in Chapter 5.

The procedures used to prepare the treated coals from the air-dried, low-mineral, Lochiel coal samples (1.0 to 3.35 mm) are given as follows:

1- Water-soluble inorganics were removed from a five kilogram coal sample by leaching it with dimineralised water. Leaching was carried out with a continuous flow of water. The solution was analysed at regular intervals for chlorine, when its concentration approached zero, leaching was stopped and the product coal was air dried.

2- Another five kilogram sample of coal was leached with dilute (1.0 N) hyrochloric acid for partial removal of the ion exchangeable inorganics. The coal remained in the acid for a few hours and was stirred and sampled periodically. After leaching, the acid was decanted off and the coal was washed with demineralised water and then air dried.

3- Sodium chloride (laboratory grade) was added to two coal samples of five kilogram each using two solutions of different concentrations. The coal samples remained in the salt solutions for a few hours and were stirred and sampled periodically. The excess solutions were then decanted off and the coals were washed with demineralised water and air dried.

3.4.3 Agglomeration and Defluidisation

The bed material periodically removed from the furnace was subjected to sieve analysis and the polished samples of the bed particles in each fraction were examined using the electron microprobe. The examination revealed that only a small proportion of the bed material (less than 1%) consisted of fly ash and ash agglomerates which were present in a size range much less than that of the initial charge and hence could be separated from the bed material as fines. The remainder of the bed inventory consisted of individual bed particles coated with ash and, in most circumstances, bed agglomerates.

A criterion was established to separate the bed agglomerates from the bed inventory. Microscopic examination indicated that the individual bed particles, having an initial top size of 1 mm, grew to a size which was always less than 1.4 mm at the completion of the runs. Therefore, a 1.4 mm sieve was used to separate the agglomerates from the individual bed particles. A proportion of the agglomerates which had linear shape was found to pass the 1.4 mm sieve. However, microscopic examination indicated that their proportion relative to the total amount of agglomerates was negligible.

The mass fraction of the bed material retained on 1.4 mm sieve gave the percent by mass of the bed particles which had agglomerated. The effect of the variables, given in Table 3.1, on the extent of agglomeration was investigated.

The onset of defluidisation was detected by monitoring the bed pressure drop and the bed temperature profile: a sudden change in these measurements indicated the onset of defluidisation. This was then confirmed by visual observation of the bed through the viewing port installed on the top of the furnace (Figure 3.2). A typical graph showing the pressure drop through the bed and the furnace temperature at various positions in the bed (thermocouples T/C1 to T/C4) before and after defluidisation is given in Figure 3.11.

3.5 ANALYTICAL METHODS

3.5.1 Coal and Solid Products Analyses

The coal samples were analysed according to the following Australian Standard methods:

Moisture	AS 2434.1 - 1981
Ash	AS 1038.3 - 1979
Volatile Matter	AS 2434.2 - 1983
Sulphur	AS 1038.6 - 1971 (Eschka)
Chlorine	AS 1038.8 - 1980 (Eschka)

For chlorine concentration less than 0.05%, the sample was leached with water, the leachate was then acidified in order to precipitate the interfering tannins before analysing for chlorine using:

Chlorine ASTM D512 - 67 Method C (Mercuric Thiocyanate)

The analysis of the ash constituents (Fe_2O_3, Al_2O_3, SiO_2, MgO, CaO, K_2O, Na_2O) in coal and other materials was carried out according to the following Australian Standard method:

Ash constituents AS 1038.14.1 - 1981

SO_3 was separately analysed using the following British Standard method:

SO_3 British STD 1016.14 - 1963

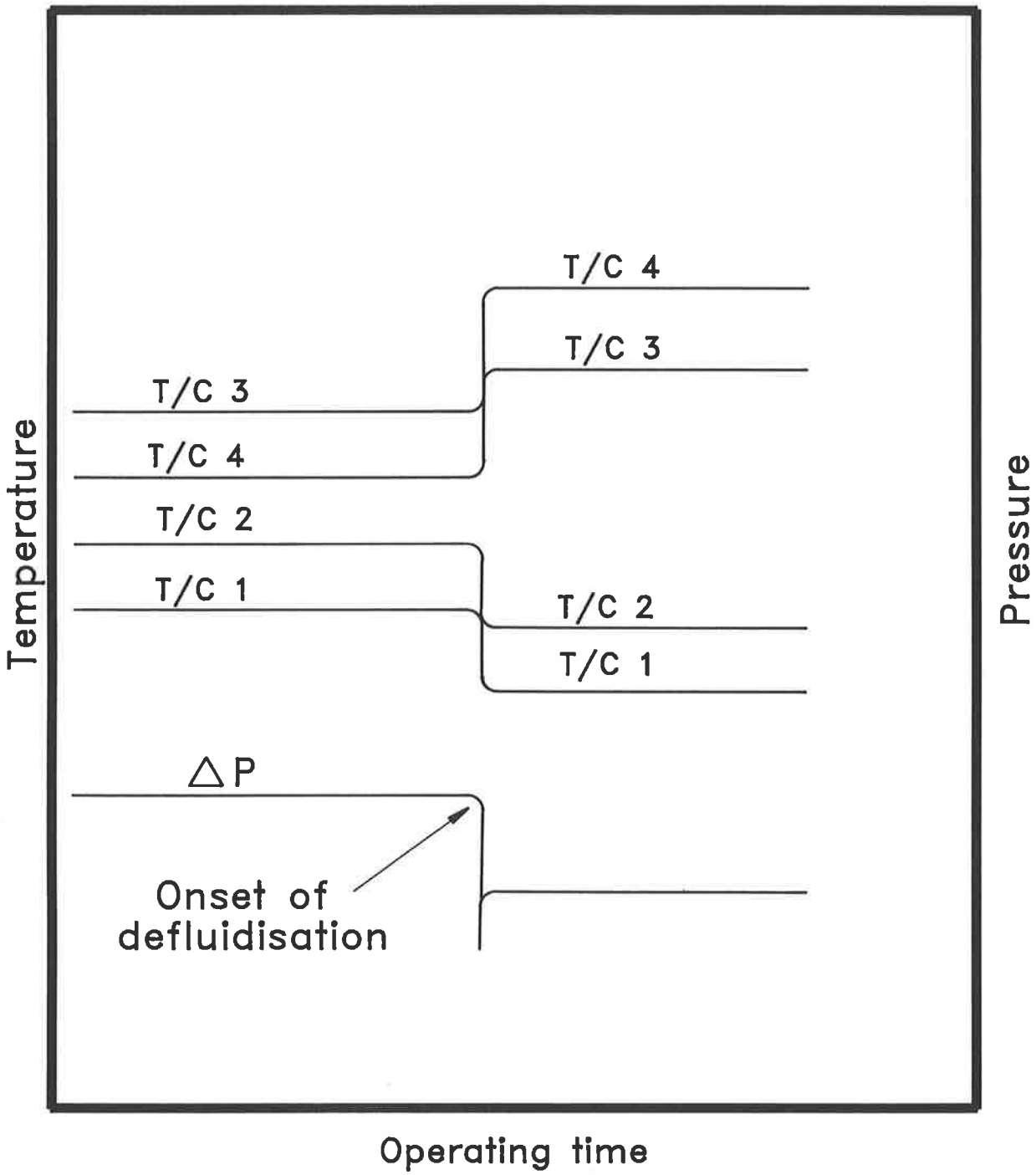

Figure 3.11: Typical Graph Showing the Onset of Defluidisation

The following extraction methods were used to determine the mode of occurrence of the inorganic matter in coal as well as in solid products:

A- **Water-soluble fraction of coal and solid products:** One gram of sample was boiled with 100 mL of demineralised water for 0.5 hour. The demineralised water used had a pH of about 6.0. The solution was filtered through a No 42 filter paper into a 200 mL volumetric flask. The filter paper was washed several times with demineralised water and the solution in the flask was made up to the mark. This solution was then analysed for:

- Fe, Al, Ca, Mg, Na, K using Atomic Absorption Spectroscopy
- SiO_2 using ASTM D859 - 68 Method B
- Chloride using ASTM D512 - 67 Method C

B- **Water-insoluble/acid-soluble fraction of coal and solid products:** The filter paper and residue from step (A) above was boiled in 100 mL demineralised water and 5 mL of concentrated hydrochloric acid for 0.5 hour. The solution was filtered through a No 42 filter paper into a 200 mL flask. The filter paper was washed several times with demineralised water and the solution in the flask was made up to the mark. This solution was then analysed for:

- Fe, Al, Ca, Mg, Na, K using Atomic Absorption Spectroscopy
- SiO_2 using ASTM D859 - 68 Method B

C- **Acid-insoluble (residue) of coal and solid products:** The filter paper and residue from the step above (B) was ashed and then analysed for:

- Fe, Al, Ca, Mg, Na, K, Ti, SiO_2 using AS 1038.14.1 - 1981

The distribution of the inorganic matter in coal and in solid products was determined by analysing the polished cross-section of samples using an electron microprobe. The technique and the instrument employed are described in the following section.

3.5.2 Electron Microscopy

Electron Microprobe

Samples of raw coal, product particles (from SPF) and bed material (from FBCS) were mounted in an epoxy block and then the surface of the block was ground, polished and coated with carbon. An automated JOEL 733 Superprobe, electron microprobe analyser (EMA) with KEVEX 7000 series energy dispersive X-ray analysis (EDAX) system was used. The analysis conditions employed were 15 kV accelerating voltage and 5 nA electron beam current. The data were collected on-line using PIBS style software.

The electron microprobe analyses were carried out to determine the composition and the distribution of the inorganic matter in the ash samples, product particles and bed material. The analyses provided direct evidence of the transformations of the inorganic matter and of the physico-chemical processes experienced by the bed material in the fluid bed combustor.

Scanning Electron Microscope

The surface of partially oxidised product particles from the SPF combustion experiments and that of bed particles from the FBCS experiments were examined in detail by scanning electron microscopy (SEM). A Phillips SEM 505 equipped with a lanthanum hexaboride emitter and a Tracon Northern type 5500 EDAX was used. The accelerating voltage and the current of the electron beam used were 20 kV and 5 nA respectively. Samples were mounted on aluminium stubs and then coated with either carbon or gold-palladium mixture.

The SEM was operated in the secondary electron imaging mode to determine the morphology of the ash formed on the surface of the SPF product particles and of the FBCS bed particles. A qualitative analysis of the ash and the bed particles was also carried out using the EDAX system.

3.5.3 X-Ray Diffraction Analysis

Samples of product particles from the SPF, and bed material and cyclone ashes obtained from the FBCS combustion experiments were analysed using X-ray diffraction (XRD) in order to identify the principal species formed from the transformations of the inorganic matter. The

analyses were carried out to gain an insight into the ash formation chemistry and to explain the low melting characteristics of the ash formed. The method is not quantitative unless considerable calibration is carried out.

The analyses were carried out by the Commonwealth Scientific and Industrial Research Organisation (CSIRO), Division of Soils. Sub-samples of the bulk materials were finely ground by hand and pressed into aluminium holders. XRD patterns of the samples were recorded with a Phillips PW 1800 microprocessor-controlled diffractometer using Co K radiation, variable divergence slit and a graphite monochromator. The data were logged to permanent files on an IBM PC-XT (Self 1988) and were subsequently analysed using a software package developed by Raven and Self (1988).

In addition to the above samples, bed materials were obtained from tests carried out on Lochiel coal using a 300 kg/h CFBC pilot plant owned and operated by Lurgi GmbH in Frankfurt, Federal Republic of Germany. These samples were analysed by X-ray diffraction (XRD) in order to validate the results obtained from the bench scale experiments. XRD patterns of samples were recorded by Lurgi GmbH using a Siemens D 5000 powder diffractometer. The instrument is equipped with an automatic aperture diaphragm, a secondary monochromator and a scintillometer. The Cu tube was operated at 40 kV and 30 mA. The measurements were taken on the rotating sample using the step scan mode (step intervals: 0.05°, measuring time: 4 seconds).

3.5.4 Thermomechanical Analysis

The initial sintering temperatures (or the onset of sintering) of the bed material were determined by thermomechanical analyses. The change in the dimension of the samples under a specified load was measured by a Mettler TMA 40 analytical system.

3.5.5 Differential Thermal and Thermogravimetric Analysis

Simultaneous differential thermal and thermogravimetric analyses were carried out on bed particles from the FBCS experiments using a Rigaku TG-DTA infra-red heating apparatus (Thermoflex 8100 series). Samples of approximately 10 mg were heated in Pt crucibles at a

rate of 10°C per minute under static air and, in selected samples, under flowing nitrogen atmosphere from ambient to 1000°C. One of the samples was heated to 1200°C. The analyses were carried out by CSIRO, Division of Soils.

Chapter 4

ASH FORMATION STUDIES

4.1 INTRODUCTION

In accordance with the objectives of this study (Section 1.2) the transformations of the inorganic matter and the ash formation mechanism were investigated under conditions relevant to fluid bed combustion.

The physico-chemical transformations of the inorganics and the minerals have been the subject of numerous investigations (Section 2.3), however they have been carried out under conditions differing considerably from those in FBC systems. In order to obtain more realistic information about the transformations of the inorganic matter during FBC, investigations were carried out using the single particle furnace (SPF), described in Section 3.2, operating under conditions relevant to FBC.

The process of ash formation during the combustion of brown coals begins with the physico-chemical transformations of the coal's inorganic matter in the reducing environment prevailing inside the char particles. In order to elucidate some of these transformations, the first series of experiments were carried out in an atmosphere of nitrogen.

In the second series, the combustion experiments were carried out to monitor and characterise the formation of ash and to determine the extent of vaporisation of the inorganic matter using the analytical techniques described in Section 3.5.

For the quantitative assessment of the transformations undergone by the inorganic matter, single coal particles of known composition had to be used. This was achieved by selecting a coal sample of uniform inorganic composition from a particular zone of the Lochiel coal deposit where the coal has a low mineral content. The experimental programs and procedures have been described in Section 3.4.

4.2 RAW COAL CHARACTERISATION

The lump of coal collected from the Lochiel trial pit was analysed using chemical methods. The results of the analyses are given in Table 4.1. From these it is apparent that Lochiel coal is characterised by high moisture, high sulphur, high sodium and high chlorine. The inorganic matter in this lump of coal is predominantly soluble in water and/or acid; only a minute quantity of acid-insoluble minerals is present. Henceforth, this lump of coal is referred to as "low-mineral" sample.

About 28 percent of the sodium in the low-mineral sample is acid soluble; the rest is water soluble. The acid-soluble sodium is organically bound (inorganics). The water-soluble sodium is either weakly bonded to the coal's surface or is present in the inherent water as free ions (Readett and Quast, 1988).

Chlorine is 100% water soluble in the low-mineral sample. The water-soluble chlorine can be present in coal as free ions in association with cations such as sodium and calcium and/or in an organic form (Subsection 2.2.2). The fact that the Lochiel coal deposit is in contact with saline ground water suggests that a significant part of the chlorine in this coal, and hence in the low-mineral sample, is present as free ions in association with sodium. The chloride and sodium ions are likely to combine and form sodium chloride crystals after the evaporation of the inherent moisture.

The results of the chemical analysis, given in Table 4.1, indicate that sodium is the major water soluble cation present in the low-mineral sample and exists in excess of the

Table 4.1: ***Bulk sample analysis.***

Proximate Analysis:	
moisture %	62.69
ash %	3.59
volatiles %	18.21
f.c. %	15.51

Inorganics %db	Water-Soluble	Acid-Soluble	Acid-Insoluble
Na	0.65	0.93	0.003
Ca	0.007	1.33	0.027
Mg	0.001	0.92	0.015
K	0.012	0.02	-
Fe	<0.002	0.005	0.012
Al	<0.005	0.36	0.031
Si	0.002	0.004	0.046
Cl	0.60	0.60	-
S	<0.50	<0.05	-

Ash Analysis % (Australian Standard)	
Fe_2O_3	0.21
Al_2O_3	8.35
SiO_2	1.50
MgO	17.48
CaO	21.50
K_2O	0.22
Na_2O	11.95
TiO_2	0.08
SO_3	38.71

Eschka Method	
Total Cl %db	0.6
Total S %db	3.4

stoichiometric amount required to bind with the chloride ions. Other cations such as calcium and potassium, which could combine with the chlorine ions, are not present in the water soluble form in significant quantities.

Calcium and magnesium in the low-mineral sample are soluble in acid. As no evidence of mineral carbonate inclusions was found, it is suggested that these elements are predominantly organically bound. Aluminium is mostly soluble in acid and is inferred to be mostly organically bound. Silicon and iron are present in small quantities in acid-insoluble forms. Potassium is also present in small quantities and is soluble in water and acid. Most of the sulphur in this sample is part of the organic structure being mostly acid insoluble.

Examination of the back-scattered images of the polished cross-section of a few samples of dried coal by the electron microprobe showed the presence of a number of discrete mineral inclusions within the coal matrix (Figure 4.1). These mineral inclusions, along with the carbonaceous matter of the coal samples, were analysed by the electron microprobe. The analyses indicated that the discrete minerals are mostly silica and clay with some calcium sulphate and pyrites. Sodium chloride crystals were not detected in the coal matrix suggesting that these crystals are intimately distributed in the coal matrix as sub-micron particles. For the carbonaceous matter, the X-ray analysis showed that sodium, calcium, magnesium, aluminium, sulphur and chlorine are intimately dispersed in the coal matrix and have a relatively even distribution. Silicon was also found to be intimately dispersed in the carbonaceous matter as super-fine particles, but its concentration was variable. A typical microprobe analysis of the inorganic matter dispersed in the carbonaceous matter is given in Table 4.2.

To ensure that the composition of the low-mineral coal sample is uniform to the point that the particles extracted from it for the SPF experiments are also of the same composition, three coal particles of 7.5 mm diameter (samples A, B and C) were carved from the low-mineral sample and then analysed for the inorganic elements using the extraction technique. The results of the analysis of the leachate solutions, Table 4.3, indicated that the composition of the inorganics in the small particles are the same as those in the bulk sample.

Table 4.2: ***Typical Microprobe Analysis of the Inorganic Matter Intimately Dispersed in Char of the Low-Mineral Coal Sample.***

P_2O_5	0.20%
SiO_2	5.69%
Al_2O_3	7.43%
MgO	11.63%
CaO	6.22%
Na_2O	13.91%
SO_3	46.73%
Cl	8.19%

Table 4.3: ***Chemical Analysis by Extraction Methods of Three Single Particles (A,B and C) Carved from the Low-Mineral Coal Sample (Bulk).***

Coal Samples	A		B		C		Bulk	
	WS	AS	WS	AS	WS	AS	WS	AS
Na %db	0.62	0.91	0.63	0.91	0.68	0.93	0.65	0.93
Ca "	-	1.32	-	1.32	-	1.34	-	1.33
Mg "	-	0.92	-	0.90	-	0.91	-	0.92
K "	-	0.02	-	0.02	-	0.02	-	0.02
Fe "	-	-	-	-	-	-	-	-
Al "	-	0.39	-	0.35	-	0.36	-	0.36
Si "	-	-	-	-	-	-	-	-
Cl "	0.60	0.60	0.58	0.58	0.62	0.62	0.60	0.60
S "	-	-	-	-	-	-	-	-

WS = Water-soluble dash line (-) = <0.01 %db

AS = Acid-soluble

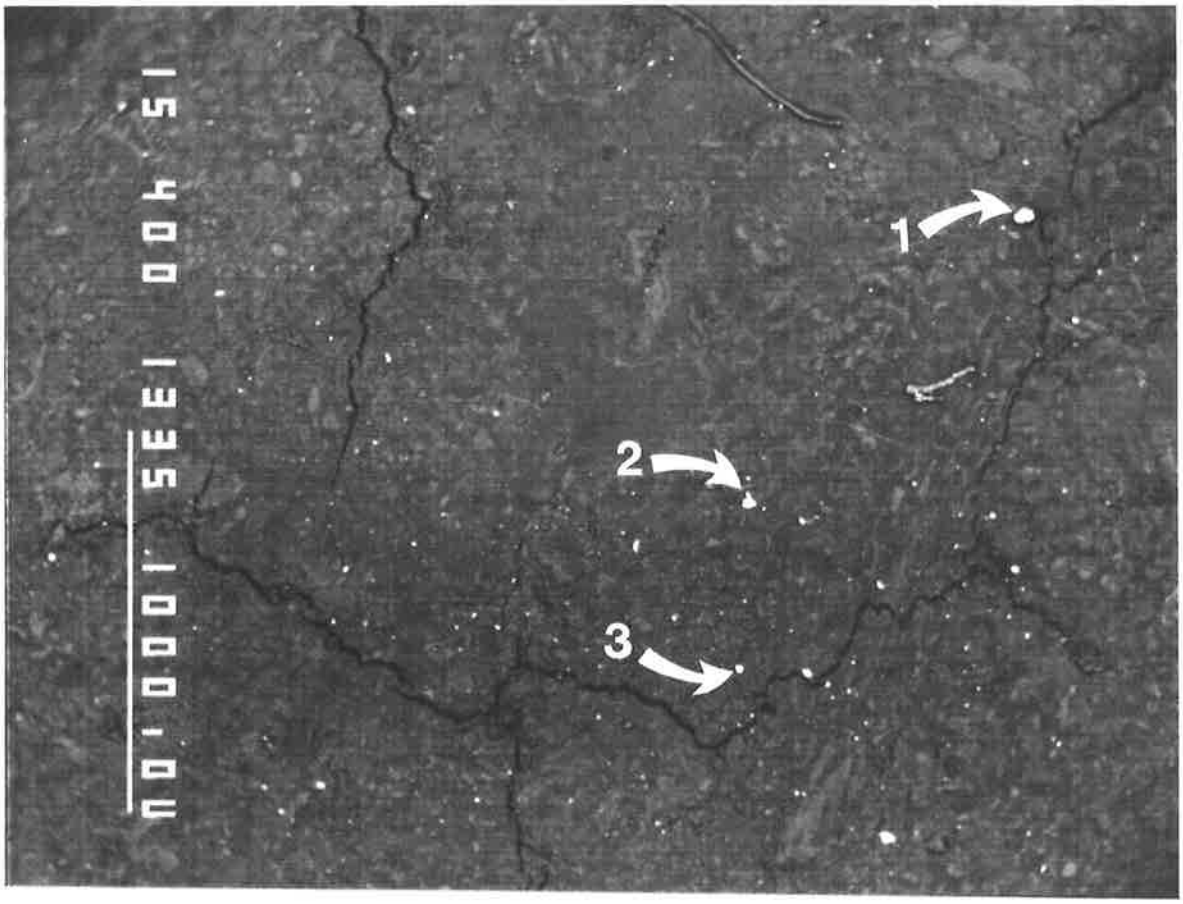

Positions Analysed:	Na_2O	CaO	MgO	SO_3	Al_2O_3	SiO_2	K_2O	FeO	Cl
1	2.3	-	1.2	1.4	0.8	1.2	-	91.3	0.8
2	1.0	-	0.4	-	19.0	65.7	13.7	-	-
3	-	-	-	-	-	99.9	-	-	-

Figure 4.1: **Back-scattered Electron Image of the Low-Mineral Coal Sample** - EDAX analyses of selected minerals are presented. 1 mm bar is shown on the left.

4.3 TRANSFORMATIONS OF THE INORGANIC MATTER DURING CARBONISATION

The spherical coal particles of 7.5 mm diameter required for the carbonisation experiments in the SPF experiments were extracted from the low-mineral sample. The experiments tests were carried out at three different temperatures: 700°, 770°, and 830°C. The product particles were withdrawn from the furnace after various residence times. The particles so withdrawn were weighed and leached with demineralised water and then with hydrochloric acid. The leachate solutions and the residues (acid insoluble) were analysed for the inorganic content.

Given the amount of the inorganic elements present in the raw coal sample and by calculating from the analysis those in the product particles, the percent losses of the inorganic elements during carbonisation were estimated.

The results of the chemical analyses indicated that the distribution of the inorganic elements between the leachate solutions and the residue changes with residence time. This was used as an indication of the chemical transformation undergone by the inorganic matter during carbonisation. The raw data on the chemical analysis and their recalculations are given in Appendix B.

Vaporisation of Volatile Species

The loss of the inorganic matter from a coal/char particle during carbonisation could be attributed to:

- vaporisation of volatile inorganic species;
- dissociation/chemical reaction of inorganic species that results in the formation of gaseous inorganic compounds;
- char fragmentation.

The mass balance carried out on Ca and Mg indicated that the amounts of these elements in the product particles did not change with residence time. It is considered that the organically bound calcium and magnesium transform into refractory compounds, and that the fragmentation of char is insignificant during carbonisation.

Similar calculation on sodium and chlorine, however, indicated that these elements were partially lost during carbonisation (Figure 4.2). The loss of sodium was significantly less than the stoichiometric equivalent of chlorine. The disproportionate release of sodium and chlorine suggests that mechanisms other than straightforward vaporisation of sodium chloride are involved.

The literature reviewed indicated the complexity of the release of sodium chloride during combustion. The work carried out by Brinsmead and Kear (1956) showed that sodium chloride can react with compounds such as water, silica and clay in the coal. As a result of these reactions, sodium chloride dissociates into sodium compounds and hydrochloric acid.

Small amount of sub-micron silica (and/or clay) inclusions in the low-mineral coal sample which are intimately distributed in the coal (Section 4.2) can react readily with sodium chloride which is also intimately distributed within the coal matrix. These reactions could partly account for the disproportionate release of sodium and chlorine. The loss of sodium from the samples is considered to be due to a combination of sodium chloride vaporisation and formation of gaseous species from the transformations of the organically bound sodium.

The vaporisation of the species formed from the organically bound sodium and of sodium chloride has been investigated by Murray and Ledger (1982) using Victorian brown coals. They found that only a small amount of the organically bound sodium was lost during carbonisation. However, when both halite (NaCl) and the organically bound sodium were present, the halite sodium was lost at just above 600°C. Considering Murray and Ledger's findings, it can be suggested that the small amount of sodium loss experienced during carbonisation of low-mineral sample is primarily due to sodium chloride vaporisation.

The vaporisation of sulphur species from the particle could not be determined due to the limitation of the chemical method in analysing small quantities of sulphur in a single particle.

Chemical Transformations of the Inorganic Matter

The distribution of sodium between the leachate solutions and the residue as a function of residence time and temperature is given in Figure 4.3.

At 700°C most of the organically bound sodium is transformed into water-soluble form(s). At higher temperatures (i.e. 770° and 830°C) it appears that the transformation of the organically bound sodium to water-soluble sodium occurs to a lesser extent. This is in accordance with the findings of Murray and Ledger (1982).

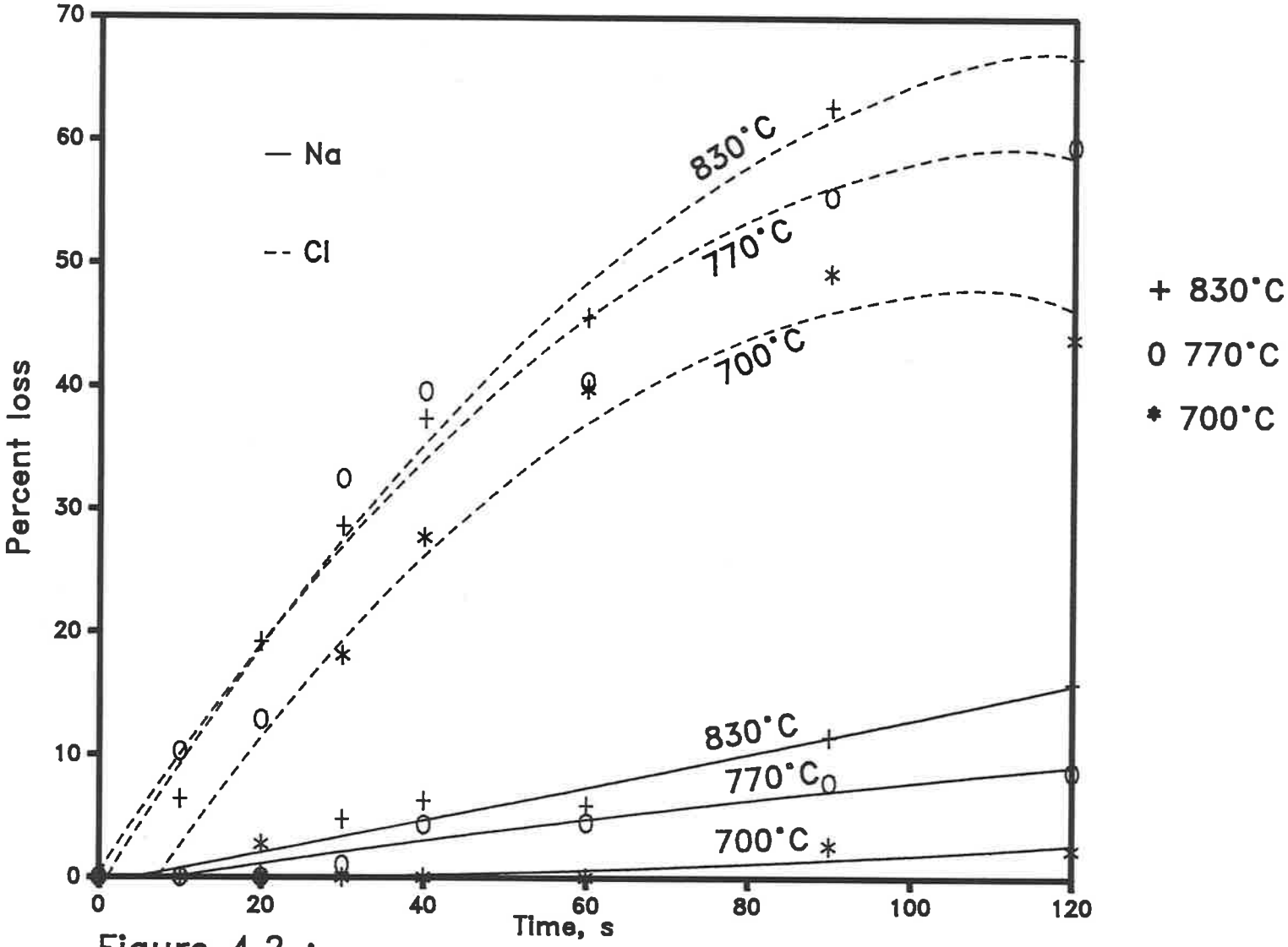

Figure 4.2 :
Sodium and chlorine loss during carbonisation

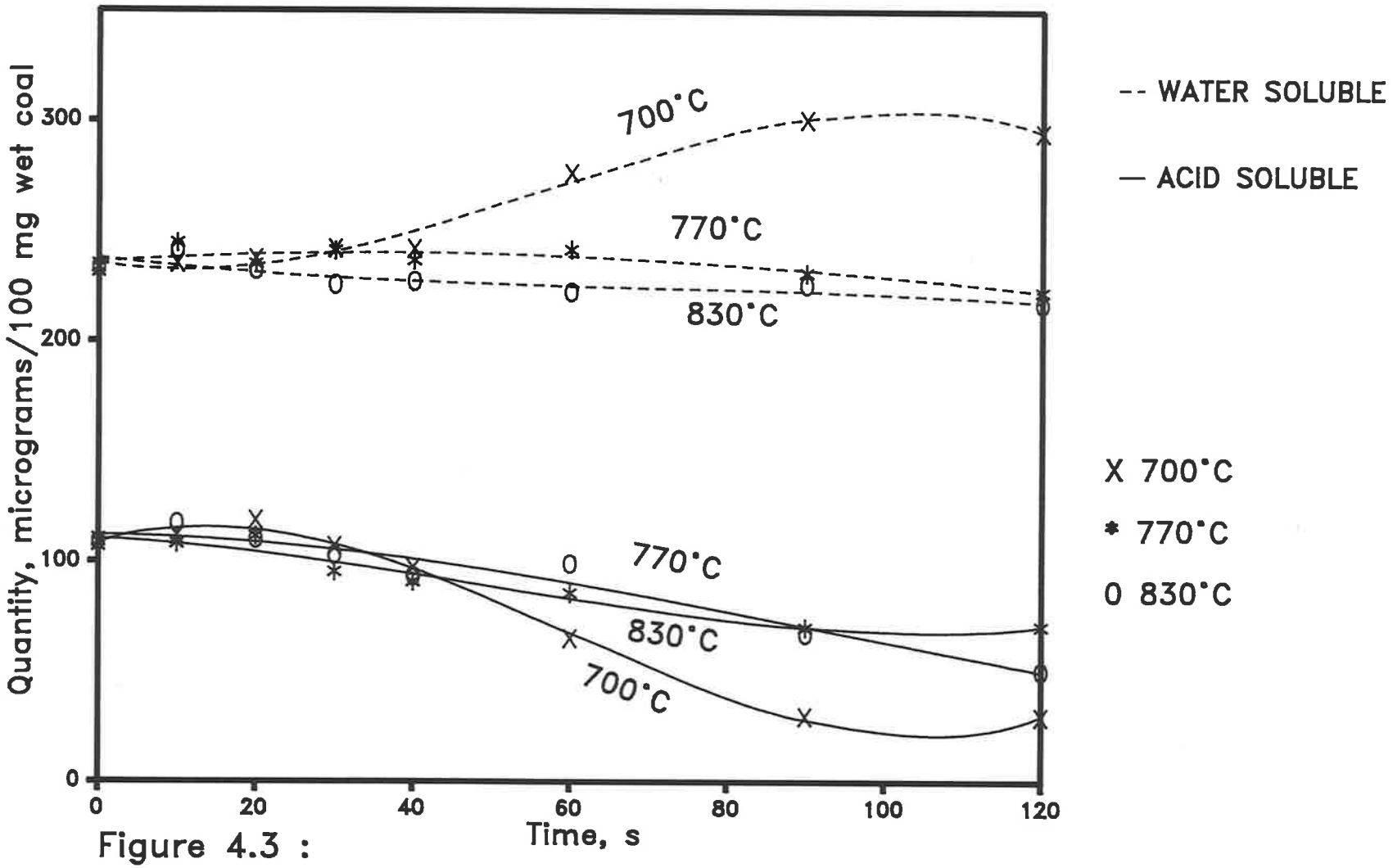

Figure 4.3 :

Sodium transformations under carbonisation conditions

Calcium and magnesium which were initially present in the low-mineral coal in acid-soluble forms became acid-insoluble. The distribution of calcium and magnesium between the leachate solutions and the residue as a function of residence time and temperature is given in Figures 4.4 and 4.5 respectively. Aluminium could not be analysed due to the limitation of the atomic absorption in analysing small quantities of aluminium leached from a single particle of coal.

The above transformations commenced after about 30 to 40 seconds in the furnace. At this stage the product particles had lost about 50% of their original weight. This indicates that the transformations of the inorganics began before all the moisture in the coal (about 62%) was evaporated. Devolatilisation is likely to begin near the surface of the coal particles while their centre is still drying. Part of the total weight loss of coal particles is due to devolatilisation of the organic matter.

A small proportion of sulphur in the coal, which is acid insoluble, became water soluble.

Characterisation of the Inorganic Species Formed

While they give an indication of the transformations undergone by the inorganics, the above results do not assist in predicting the chemical composition of the species formed as a result of these transformations. In an attempt to predict the chemical composition of the species formed, equilibrium thermodynamic calculations were carried out using the computer program CHEMIX, which is based on Gibbs free energy minimisation and is part of the CSIRO-SGTE Thermodata system (Turnbull and Wadsley, 1985 and 1987). The calculations indicate that, under reducing conditions with Na, Ca, Mg, Al and large amount of sulphur present, the following species are likely to be formed (note: c=condensed, g=gas phase):

- at 700°C: Na_2CO_3, CaS, Al_2O_3, MgO all in condensed phase;
- at 800°C: the same species as at 700°C plus Na_2S(c); and minute quantity of NaOH(g);
- at 900°C: Na_2S(c), CaS(c), Al_2O_3(c), MgO(c) and significant amount of NaOH(g), that is about 7%.

This calculation is of little assistance because, due to intrinsic as well as data base limitations, it could not predict the formation of water insoluble sodium compounds nor the formation

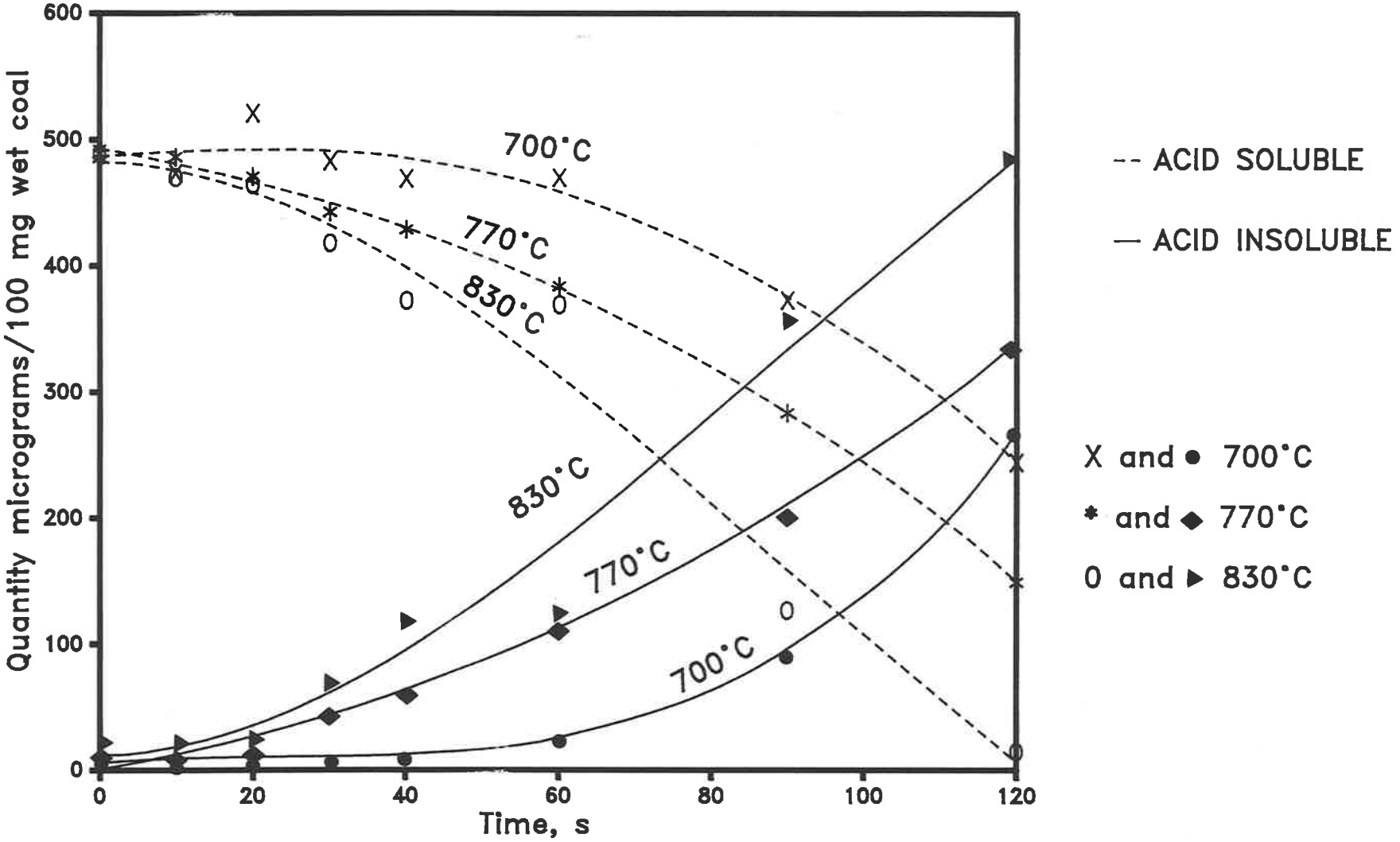

Figure 4.4:
Calcium transformation from acid soluble to acid insoluble during carbonisation

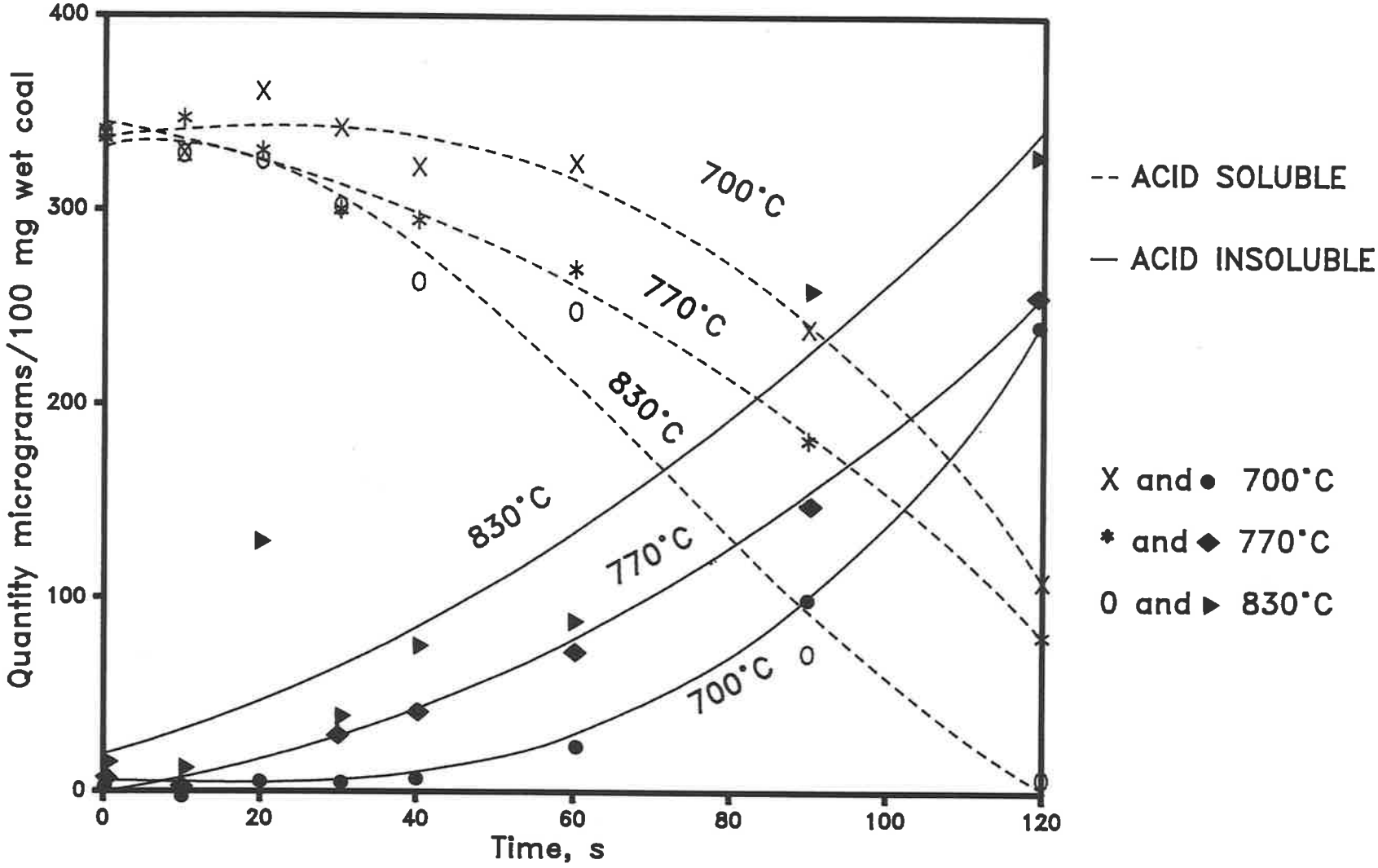

Figure 4.5:
Magnesium transformation from acid soluble to acid insoluble during carbonisation

of acid-insoluble Ca, Mg and Al compounds. It appears that, in the presence of sulphur, complex compounds are likely to be formed from the transformations of certain organically bound inorganic elements.

XRD analysis was also used to determine the chemical composition of the species formed as a result of transformation of the inorganics and sodium chloride during carbonisation. The main phases identified included organic carbon, sodium chloride, calcium sulphide and magnesium oxide (periclase). Some of the diffraction lines could not be assigned, at the present state of knowledge, to minerals or compounds. The results confirm that complex compounds are likely to be formed from the decomposition of the organically bound Na, Ca, Mg, Al and sulphur in a reducing environment. Further work has to be carried out to investigate the nature of the acid-insoluble compounds formed from the organically bound Ca, Mg and Al.

4.4 TRANSFORMATIONS OF THE INORGANIC MATTER DURING COMBUSTION

Combustion tests were carried out on single particles of coal (5.5, 7.0 and 9.0mm diameter) at temperatures of 700°, 770° and 800°C. Depending on the particles size and the combustion temperature, residence times up to 60 seconds were used during which an estimated char burn-out up to about 80% was achieved. The product particles withdrawn from the furnace after various residence times were analysed by chemical methods and by electron microscopy. Similar methods to those described for the carbonisation tests were employed to determine the loss of the inorganic elements and the changes in their distribution between the leachate solutions and the residue (Subsection 3.5.1). The raw data on the chemical analysis and their recalculations are given in Appendix B.

Vaporisation of Volatile Species

In addition to the mechanism described in Section 4.3, the loss of the inorganic matter from a coal particle during combustion can be attributed to the formation of ash and its segregation from the product particle. Hence, the total loss of the inorganic matter from a coal particle during combustion is due to:

a) vaporisation of volatile inorganic species;

b) dissociation/chemical reaction of inorganic species that results in the formation of gaseous inorganic compounds;

c) char fragmentation;

d) segregation of ash from the char particles.

The percent loss of Na, Cl, Ca and Mg for various coal particle sizes and furnace temperatures are given in Figures 4.6 to 4.10.

The species formed from the organically bound Ca and Mg are likely to be refractory under the conditions of the experiments. Hence the loss of these elements is considered to be due to the mechanisms (c) and (d) above. The vaporisation of the volatile species sodium and chlorine can, therefore, be estimated from their relative loss with respect to the loss of calcium and magnesium.

The results indicate that the percent loss of chlorine remains significantly higher than that of sodium. The disproportionate release of sodium and chlorine suggests that vaporisation of sodium chloride does not occur to a significant extent even at higher particle temperatures under oxidising conditions. It appears that most of the sodium chloride reacts within the char particles or at the char's surface to form solid sodium species and gaseous hydrochloric acid (Halstead and Raask, 1969).

The results also indicate that, for a given residence time, the percent loss of Na and Cl increases with increasing temperature and with decreasing initial coal particle size. This is because the rate of heat-up of the coal particles increases with furnace temperature and the bulk of the smaller coal particles is heated faster than the larger particles. The role of Na, Cl and S species in the ash formation process is reported later in this section.

Chemical Transformations of the Inorganic Matter

The chemical transformations undergone by the inorganic matter during combustion are more complex than those which occur during carbonisation. Inside the coal particles the transformations occur under the prevailing reducing environment. The species so formed undergo further transformations when they become exposed to high oxygen partial pressure on the char's surface (Section 2.3). Consequently, the inorganic matter in the product particle, withdrawn from the furnace under combustion condition, consists of two sets of species:

- those formed under the prevailing reducing environment inside the char particle; and

- those having undergone further transformations on the char surface.

The acid and water solubilities of the two sets of species are considered to be different. Hence, depending on their proportion in the product particle, the distribution of the inorganic elements between the leachates and the residue may vary markedly. For this reason, it is not possible to give an indication of the extent of transformations of the inorganic matter under combustion conditions using the extraction method.

Determination of the Inorganic Species Formed Under Combustion

As mentioned earlier, the product particles withdrawn from the furnace during combustion contain inorganic species formed under both oxidising and reducing environments. In order to characterise a fully oxidised ash, a sample of the low-mineral coal was ashed in a crucible at 600°C and then analysed for the inorganic matter by XRD. The main phases identified were anhydrite, quartz and periclase. The results also showed a diffraction pattern which corresponded to the shifted diffraction pattern of pure Na-Ca-sulphate suggesting that this compound is likely to have foreign elements such as Mg substituted in its crystalline structure.

Equilibrium thermodynamic calculations were also carried out for oxidising conditions. The details of the package used are given in Section 4.3. The results indicate that sodium and calcium can form sulphates whereas magnesium and aluminium can form combinations of MgO, Al_2O_3 and the spinel Al_2MgO_4. Sodium can also form gaseous NaOH and atomic Na. These results appear to be in accordance with the findings of Domezitis (1985) who reported that, when the organically bound Na, Ca, Mg, Al and S are present, complex alumina phases as well as sulphates could form under oxidising conditions. Again, due to intrinsic and data base limitations, the equilibrium thermodynamic calculations cannot predict the formation of complex compounds.

The results of electron microscopic examination of the ash formed on the surface of char particles are given in the following section.

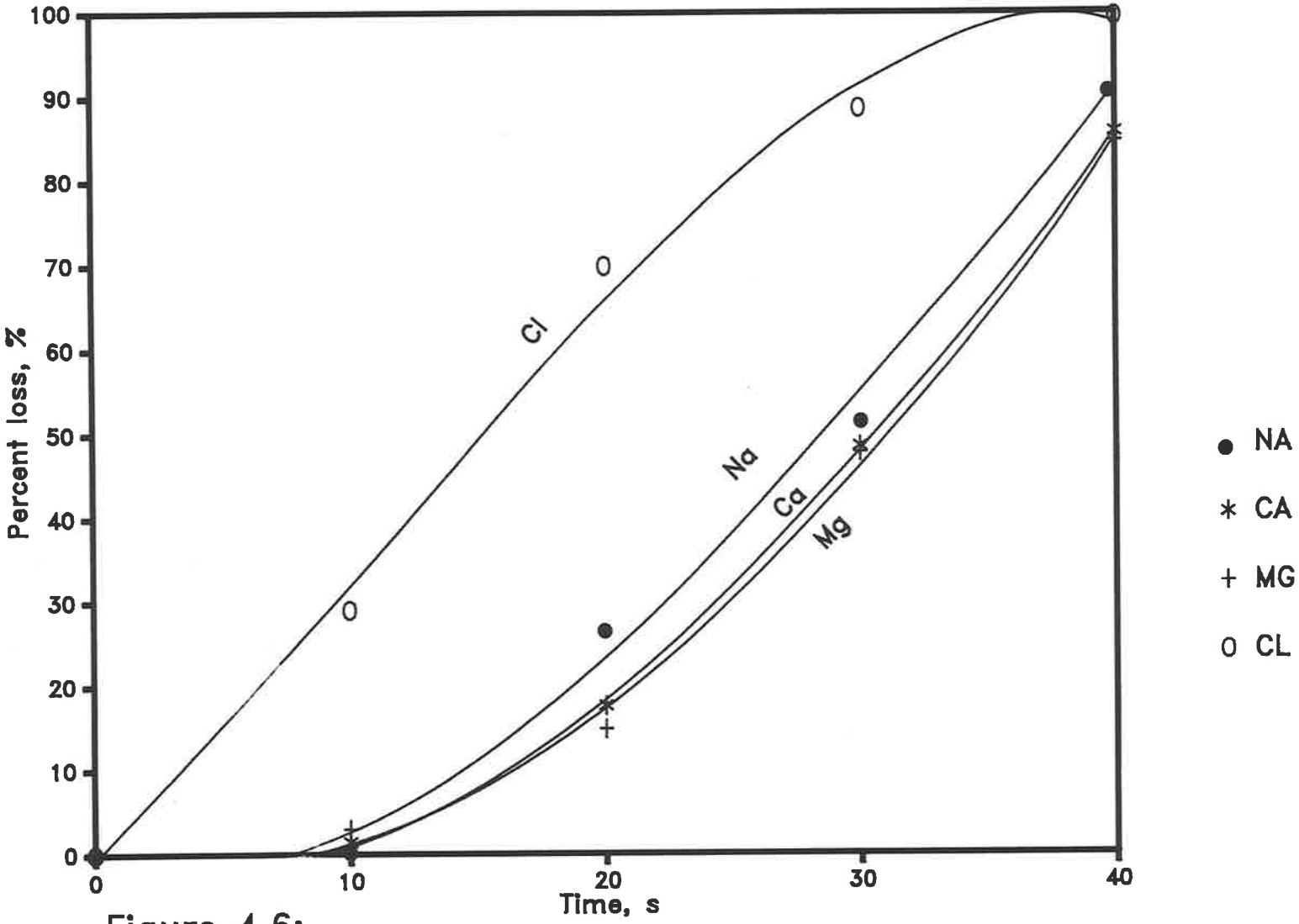

Figure 4.6:

Loss of inorganic matter during combustion –
initial particle size 5.5 mm, furnace temperature 700°C

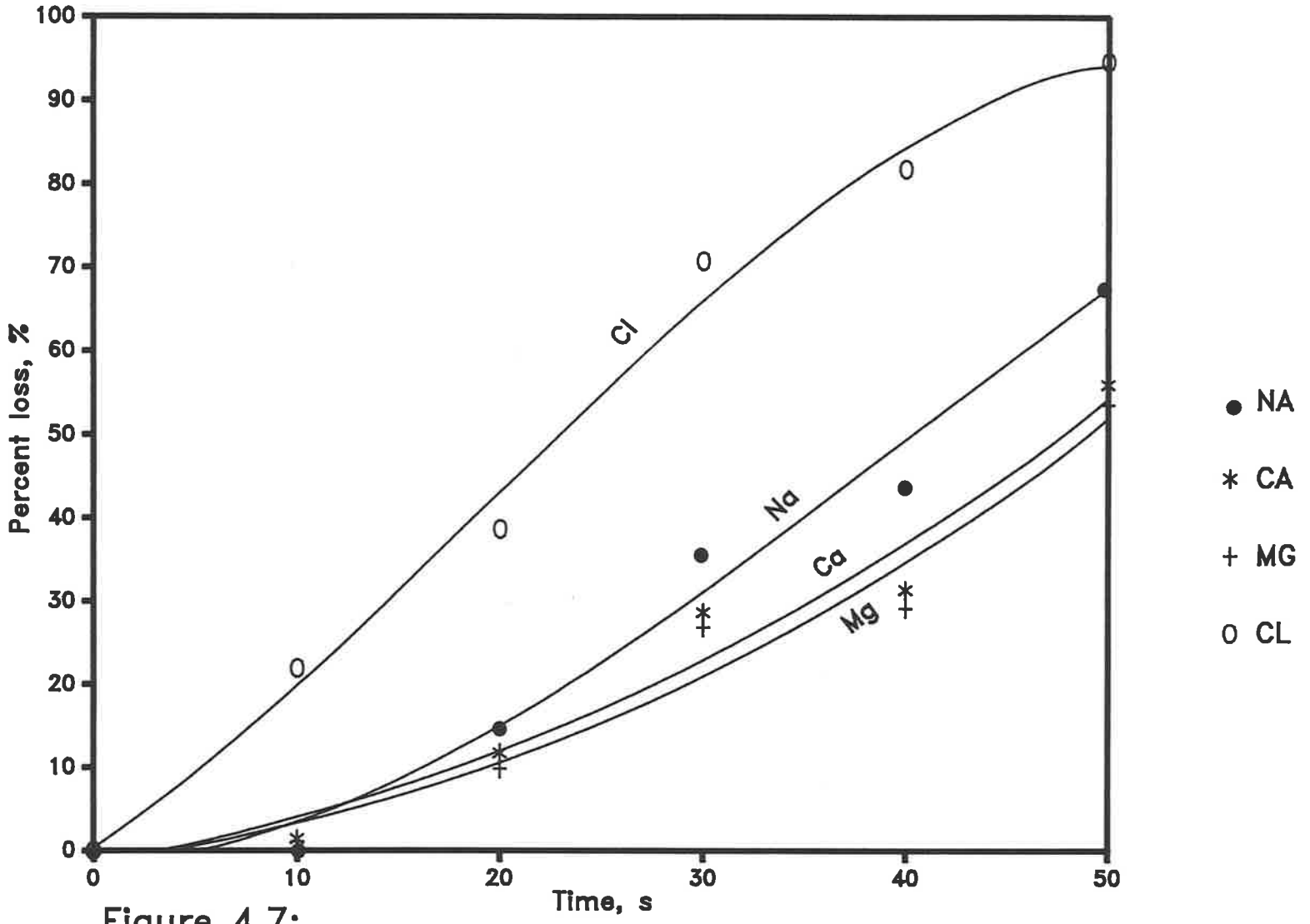

Figure 4.7:

Loss of inorganic matter during combustion –
initial particle size 7.5 mm, furnace temperature 700°C

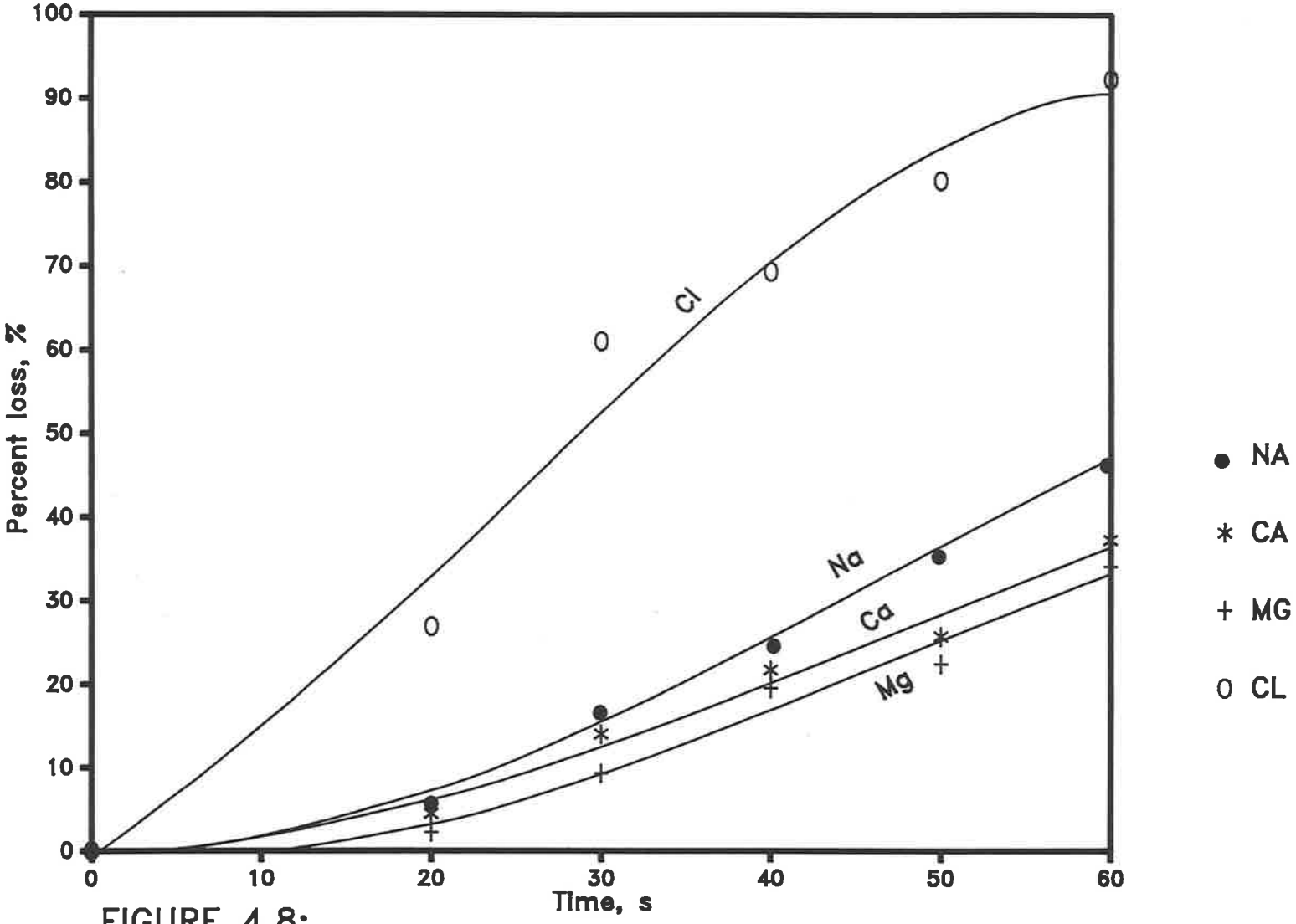

FIGURE 4.8:

Loss of inorganic matter during combustion –
initial particle size 9.0 mm, furnace temperature 700°C

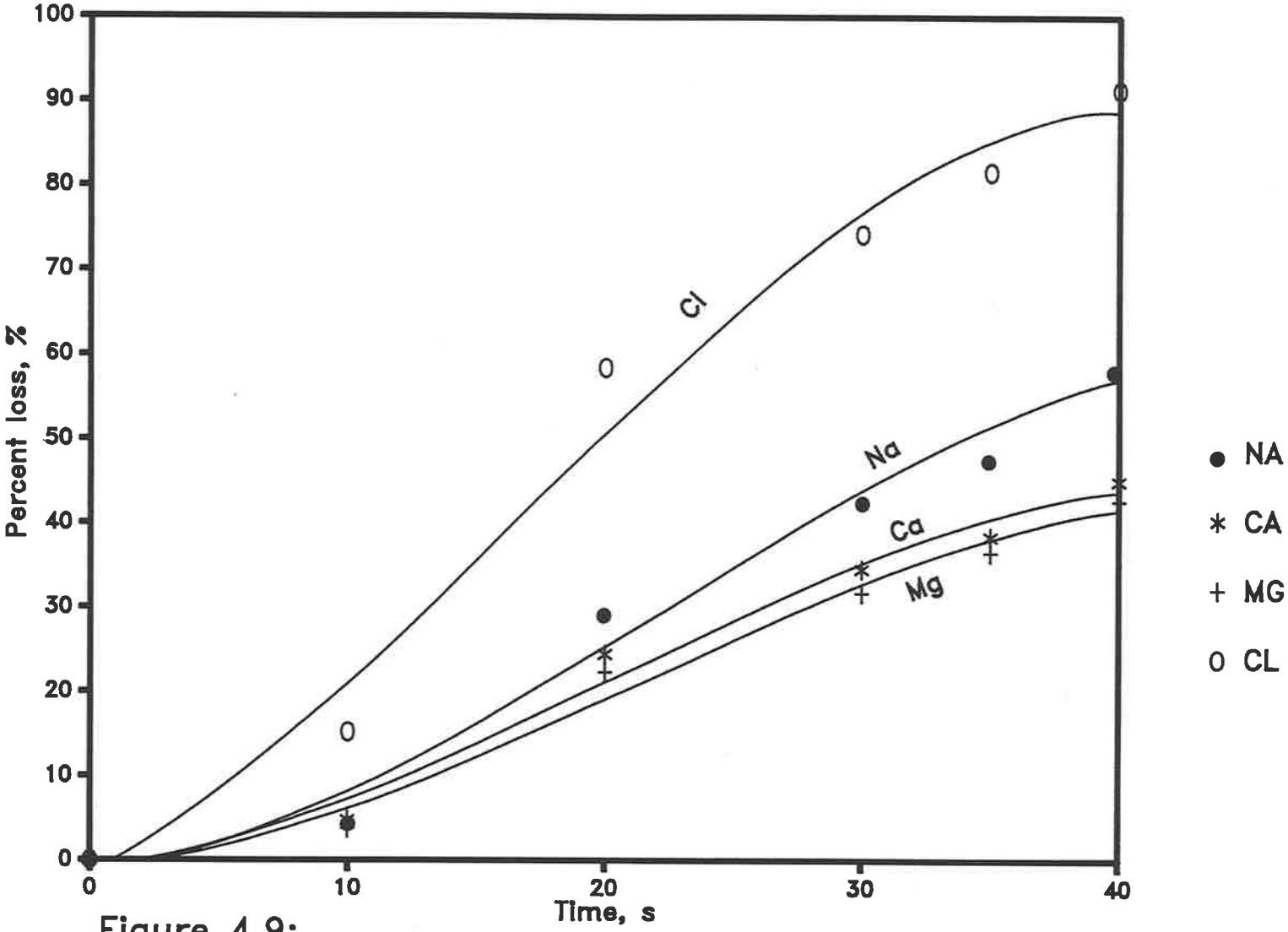

Figure 4.9:

Loss of inorganic matter during combustion –
initial particle size 7.5 mm, furnace temperature 770°C

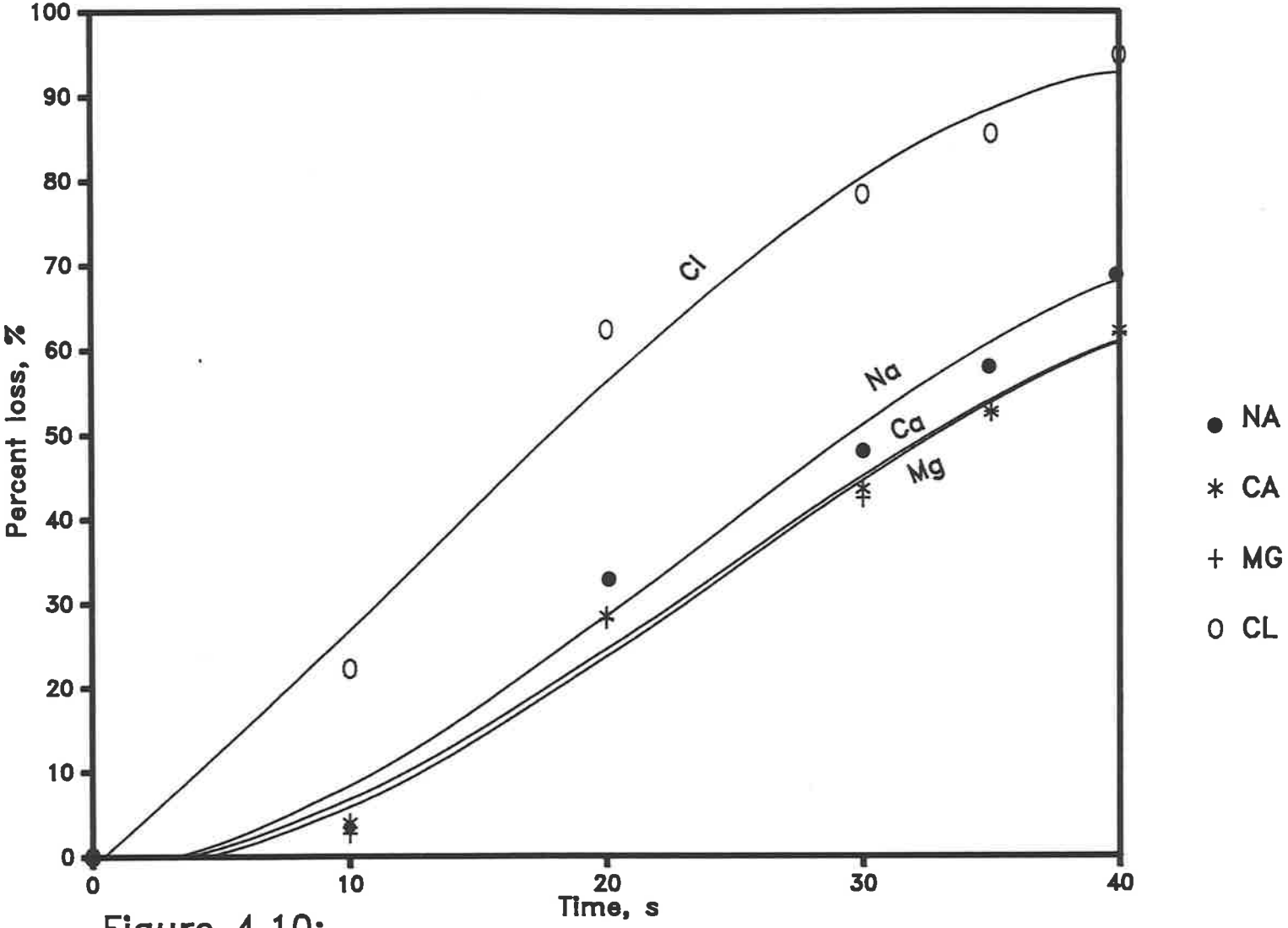

Figure 4.10:

Loss of inorganic matter during combustion –
initial particle size 7.5 mm, furnace temperature 830°C

4.5 ASH CHARACTERISATION

Electron microprobe was used to study the formation of ash and its subsequent physi-co-chemical transformations. Back-scattered electron image of the polished cross-section of the product particles, withdrawn from the furnace after various residence times, were examined. Quantitative analysis of the ash formed on the char's surface was carried out using the energy dispersive x-ray analysis (EDAX) system.

The morphology of the ash formed on the char's surface was examined by scanning electron microscopy (SEM) using the secondary electron image. Qualitative analysis of the ash was carried out by the EDAX system.

Electron Microprobe Examination

Examination of the back-scattered electron image of the product particles at the early stages of combustion indicated that the inorganic matter on the char's surface is drawn together as a result of the receding char surface. The back-scattered electron image of a polished cross-section of a char particle after 38% total weight loss (based on the initial wet coal of 62% moisture) is shown in Figure 4.11. The formation of ash on the char's surface, shown as a bright band around the char particle, is evident. EDAX analyses of the char and the ash indicate that the char near the surface of the product particle contains significant amount of S, Na, Cl, Ca, Mg and Al and traces of K and Si. Compared to the analysis of the char, the ash formed on the char surface (positions 1 and 2) is slightly depleted in S and contains only a minute quantity of Cl. The content of Si in the ash is also less than that in the char.

It appears that, at this stage of combustion, a proportion of S in the char near the surface of the product particle is free to be released into the gas phase. The remaining S in the char is likely to be present as intimately dispersed inorganic species formed during the trans-formations of the inorganic matter (Section 4.3). As the char's surface recedes, these species coalesce and form a sulphated ash on the char surface. The results suggest that sodium chloride either evaporates from the char's surface or/and reacts with other compounds including those in the ash. The sodium species formed as a result of sodium chloride reactions on the char's surface are likely to participate in the ash formation process. Some of the sub-micron mineral inclusions containing silicon, which are intimately distributed in the coal matrix, are retained in the ash.

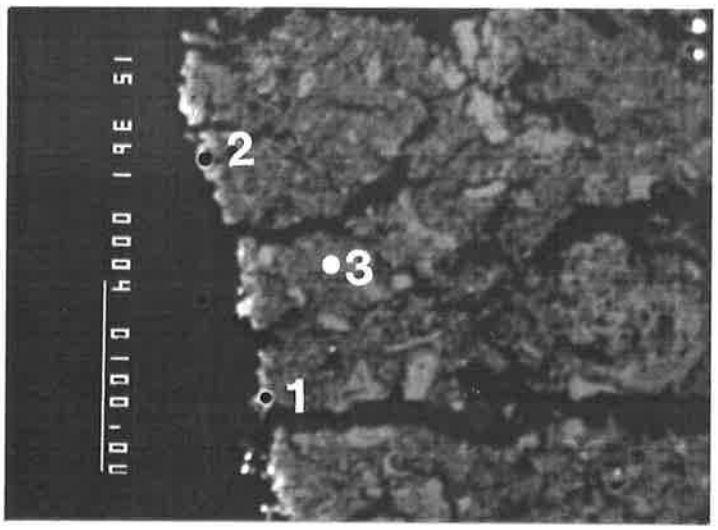

Positions Analysed:	Na_2O	CaO	MgO	SO_3	Al_2O_3	SiO_2	K_2O	P_2O5	Cl
1	11.2	17.8	14.2	49.9	6.5	-	0.1	-	0.3
2	9.7	18.5	13.0	52.5	6.0	0.1	-	-	0.2
3(char)	11.6	7.4	6.9	60.7	3.5	0.7	0.3	-	8.9

Figure 4.11: Back-scattered Electron Image of a Polished Cross-Section of a Char Particle After 38% Total Weight Loss - EDAX analyses at selected positions are presented. Bright band on the char surface shows the formation of ash. 100 μm bar is shown on the left.

The spot analysis of the ash by the electron microprobe represents a volume of about 1 cubic micron. Therefore, the results of the spot analysis, given in Figure 4.11, indicate that the inorganic species formed are mixed together on a micro-scale. Calcium and sodium could be present as sulphates, whereas magnesium, aluminium and the excess calcium could be present as oxides and/or alumina phases in a multi-component system. The minute quantities of chlorine and silicon could exist as sodium chloride and silica respectively.

As char burn-out proceeds, the ash further develops on the char's surface. Figure 4.12 shows the back-scattered electron image of a polished cross-section of a product particle after a total weight loss of 89%. Due to the simultaneous processes of drying, devolatilisation and char burn-out, the exact calculation of char burn-out from weight loss is not possible. However, the extent of burn-out at this stage is estimated to be about 40% of the total char.

EDAX analyses given in Figure 4.12 indicate that, compared with the results in Figure 4.11, the char near the char-ash interface is slightly depleted in Cl and S. However, the ash composition at this stage remains unchanged. That is, it contains varying concentrations of Na, Ca, Mg, Al and S and no Cl. Some of the analyses show traces of potassium and phosphorus.

As char burn-out proceeds further in the SPF, the inorganic matter on the char's surface develops into an ash matrix. Figure 4.13 shows the back-scattered electron image of a polished cross-section of a char particle after 95% total weight loss (about 80% char burn-out). The ash matrix, shown at low magnification, has a thickness of a few hundred microns. The breakage of the ash matrix, evident at some locations, is likely to be due to rapid quenching during discharge of the product particle from the furnace and its subsequent impact with the dry ice container.

Figure 4.14 gives the back-scattered electron image of a polished cross-section of the same particle, having 95% total weight loss and an estimated 80% char burnout, at higher magnification. EDAX analyses indicate that the composition of the char (grey area in the micrograph) is similar to that in the previous samples which were subjected to lower burn-out, except for a significant reduction in Cl concentration. The freshly formed ash around the char fragments, positions 2 and 3, contains high amount of sulphur and sodium. Position 3 appears to contain pure sodium sulphate. Further from the char-ash interface, point 4, the

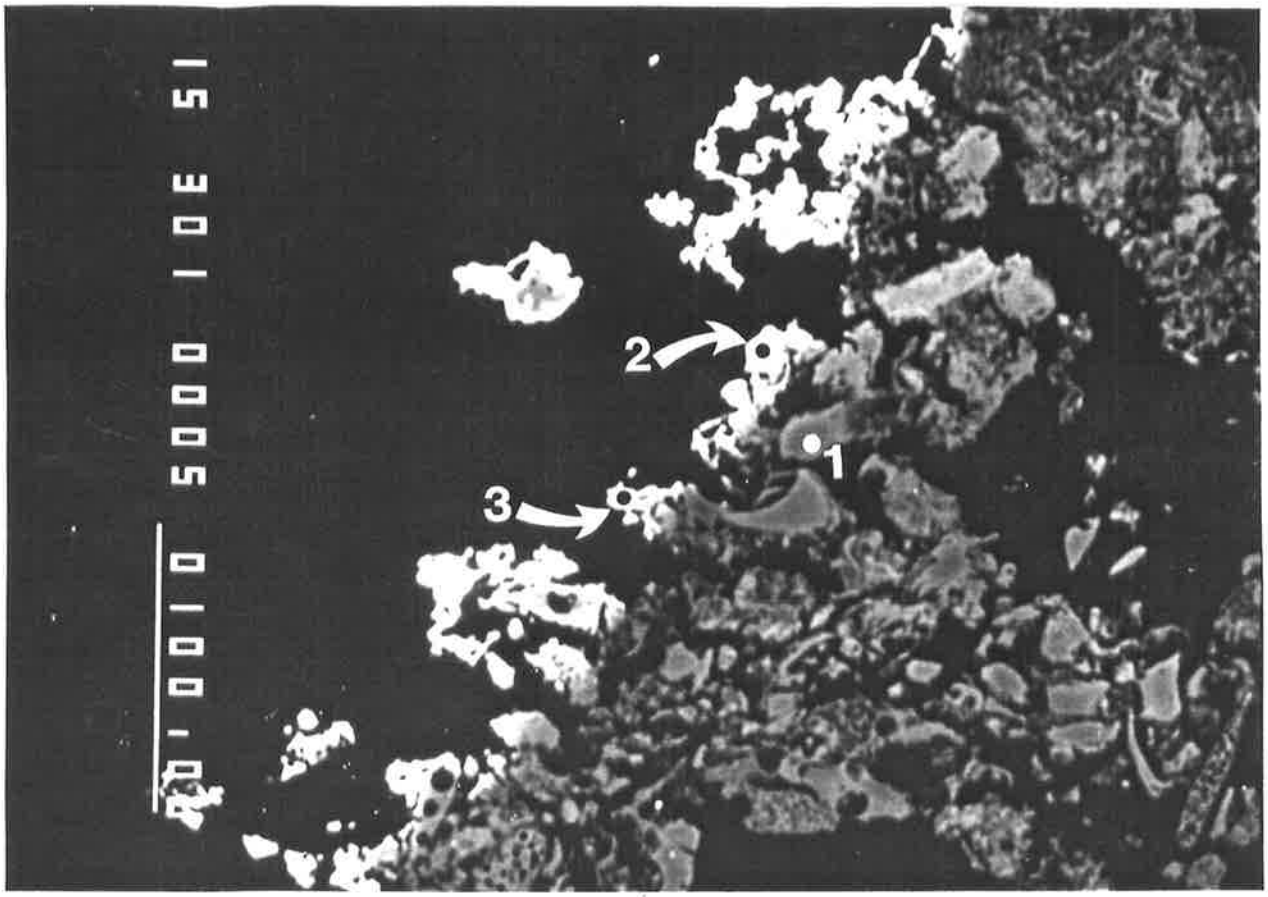

Positions Analysed:	Na_2O	CaO	MgO	SO_3	Al_2O_3	SiO_2	K_2O	P_2O_5	Cl
1(char)	12.7	12.8	10.6	52.0	5.3	1.1	-	0.4	5.1
2	10.3	18.7	15.0	49.1	6.3	0.1	0.1	-	0.4
3	15.2	20.4	10.6	48.2	5.2	-	-	-	0.3

Figure 4.12: Back-scattered Electron Image of a Polished Cross-Section of a Char Particle After 89% Total Weight Loss (About 50% Char Burn-out) - EDAX analyses at selected positions are presented. Bright band on the char surface shows the formation of ash. 100μm bar is shown on the left.

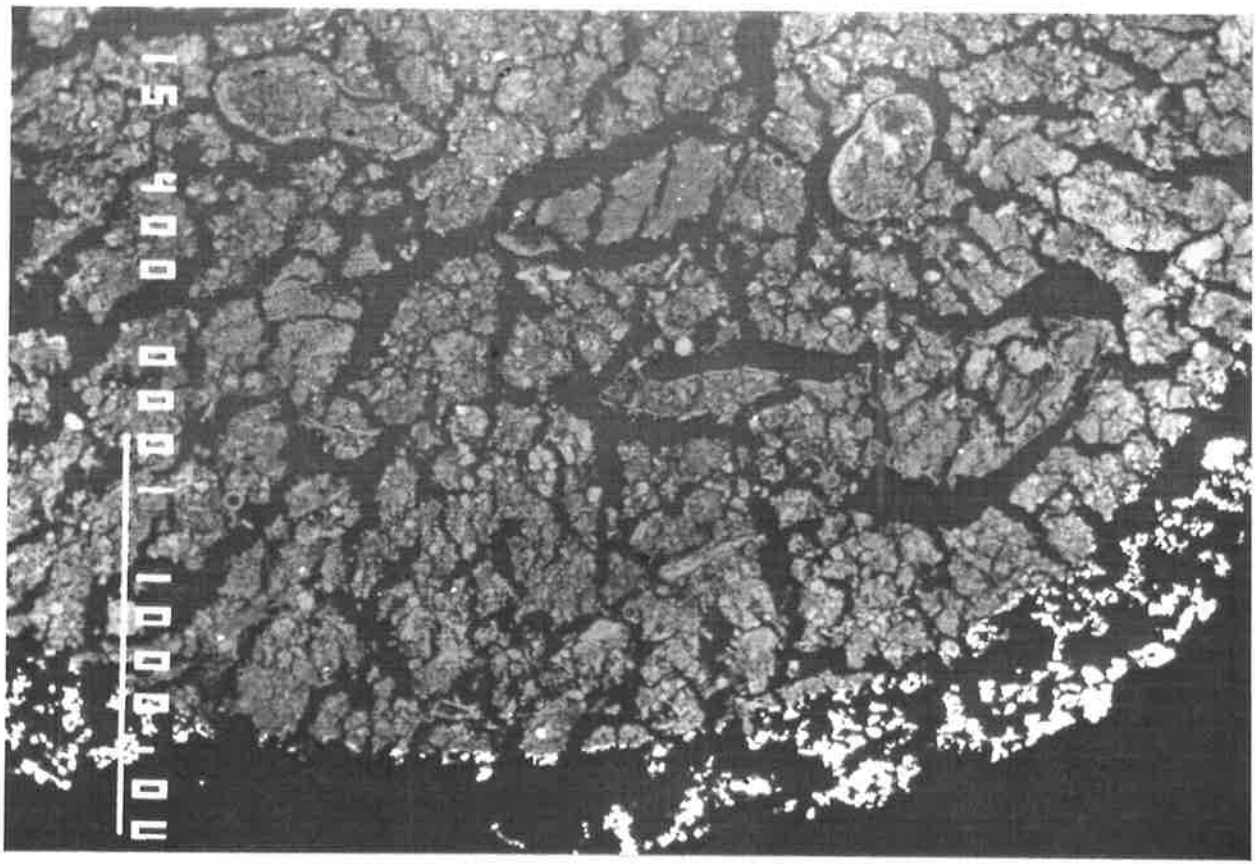

Figure 4.13: **Back-scattered Electron Image of a Polished Cross-Section of a Char Particle After 95% Total Weight Loss (About 80% Char Burn-out) at High Magnification** - Bright band around the char shows the porous ash matrix. 1000 μm bar is shown on the left.

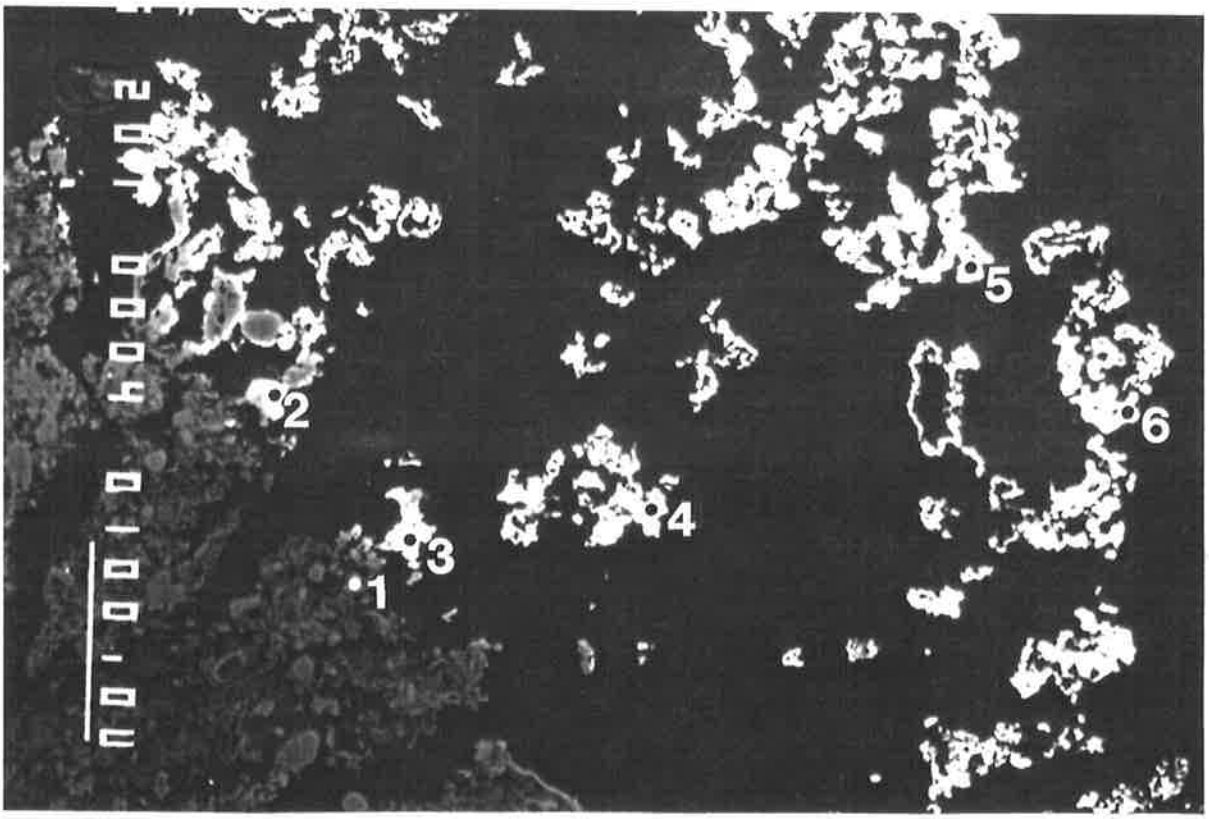

Positions Analysed:	Na_2O	CaO	MgO	SO_3	Al_2O_3	SiO_2	K_2O	P_2O_5	Cl
1(char)	13.71	12.8	14.6	46.0	7.4	1.0	-	0.6	3.8
2	14.4	10.1	4.1	68.6	2.0	-	0.2	-	0.6
3	30.1	0.4	-	68.6	-	-	0.3	-	0.4
4	5.5	24.8	15.2	47.5	6.6	-	0.2	-	0.3
5	4.3	62.0	10.6	15.7	7.0	0.1	0.1	-	0.3
6	3.9	57.7	2.0	9.4	2.8	23.3	0.1	-	0.2

Figure 4.14: Back-scattered Electron Image of a Polished Cross-Section of a Char Particle After 95% Total Weight Loss (About 80% Char Burn-out) at High Magnification - EDAX analyses at selected positions are presented. Bright area shows the porous ash matrix. 100 μm bar is shown on the left.

ash is depleted in sulphur and sodium. At the surface of the ash layer, position 5, the depletion of these elements is more pronounced and the ash is highly enriched in calcium. Position 6 shows the presence of a silica inclusion retained by the ash.

The reasons for the depletion of sulphur and sodium in the ash matrix could be the result of vaporisation of sodium sulphate and/or its chemical transformations. Equilibrium calculations, indicate that the formation of gaseous sodium species is favored with increasing temperature. The gradual decrease of sulphur and sodium from the char-ash interface towards the outer surface of the ash matrix suggests that these transformations are time dependent. The material on the char-ash interface is freshly formed and those on the outer surface of the ash matrix has been subjected to furnace conditions for longest time. It also appears that, after its formation, the ash becomes more consolidated with time; the surface of the ash matrix shows the highest consolidation (coalescence) of the inorganic matter.

It should be noted that, unlike the conditions in the SPF, the vigorous environment in the FBCS is likely to cause the separation of the ash from the char surface immediately after its formation. Due to the shorter retention time of the ash on the char's surface, the vaporisation of Na and S compound(s) would not take place to the same extent as in the SPF. This was confirmed during the experiments carried out in the FBCS as discussed in Chapter 5.

Similar results were obtained for various combustion temperatures employed. Figure 4.15 shows the back-scattered electron images and the EDAX analyses of char particles having nearly the same char burn-out (about 80%) but originating from coal particles subjected to different temperatures. The depletion of Na and S towards the surface of the ash matrix is again evident. The analyses of the ash matrix formed under various furnace temperatures are similar.

In order to investigate the effect of oxygen partial pressure on the characteristics of the ash formed, combustion experiments were carried out with diluted air (about 5% O_2). It was observed that, under these conditions, the particles burn at a slower rate. Back-scattered electron image of a polished cross-section of a char particle burnt in a diluted air is given in Figure 4.16. Only a thin layer of sulphated ash (100 micron maximum) remains attached to the char's surface even after a char burn-out of about 80%. It appears that, as the particle temperature is lower with diluted air, the binding force between the inorganic matter is weaker resulting in the release of ash to the gas phase once the ash reaches a certain thickness. Due to the shorter retention time of the inorganic matter (as formed ash) on the char's

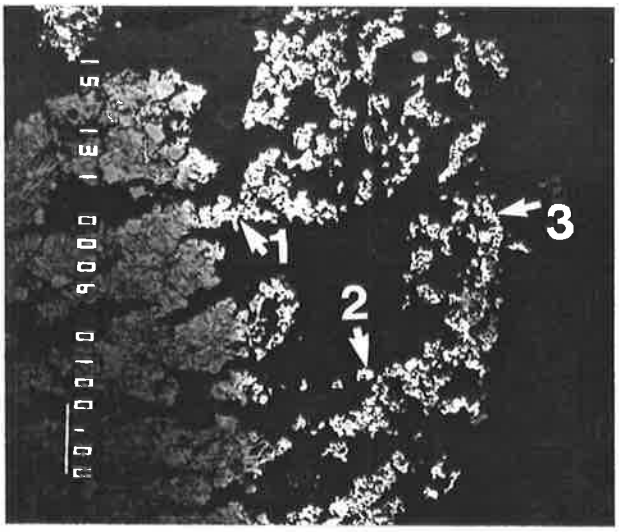

Figure 4.15a: (FT=770 °C)

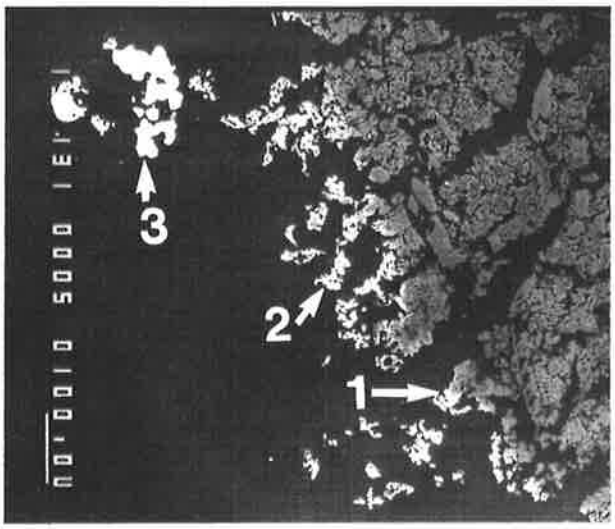

Figure 4.15b: (FT=830 °C)

Positions Analysed:	Na_2O	CaO	MgO	SO_3	Al_2O_3	SiO_2	K_2O	P_2O_5	Cl
1 Fig 4.15a	14.0	15.1	12.0	50.0	7.6	0.8	0.1	-	0.4
2 "	2.6	30.9	23.4	26.3	16.4	-	-	-	0.1
3 "	1.4	36.4	47.2	0.3	13.8	-	-	0.2	0.1
1 Fig 4.15b	12.0	13.8	11.2	55.9	6.6	-	0.2	-	0.3
2 "	2.8	28.7	17.3	40.0	10.7	0.2	-	-	0.3
3 "	0.3	53.5	34.9	-	10.9	-	-	-	-

Figure 4.15: Back-scattered Electron Images of Polished Cross-Sections of Char Particles Having the Same Char Burn-out (about 80%), Effect of Furnace Temperature(FT) - EDAX analyses at selected positions are presented. Bright areas shows the porous ash matrix. 100 μm bar is shown on the left.

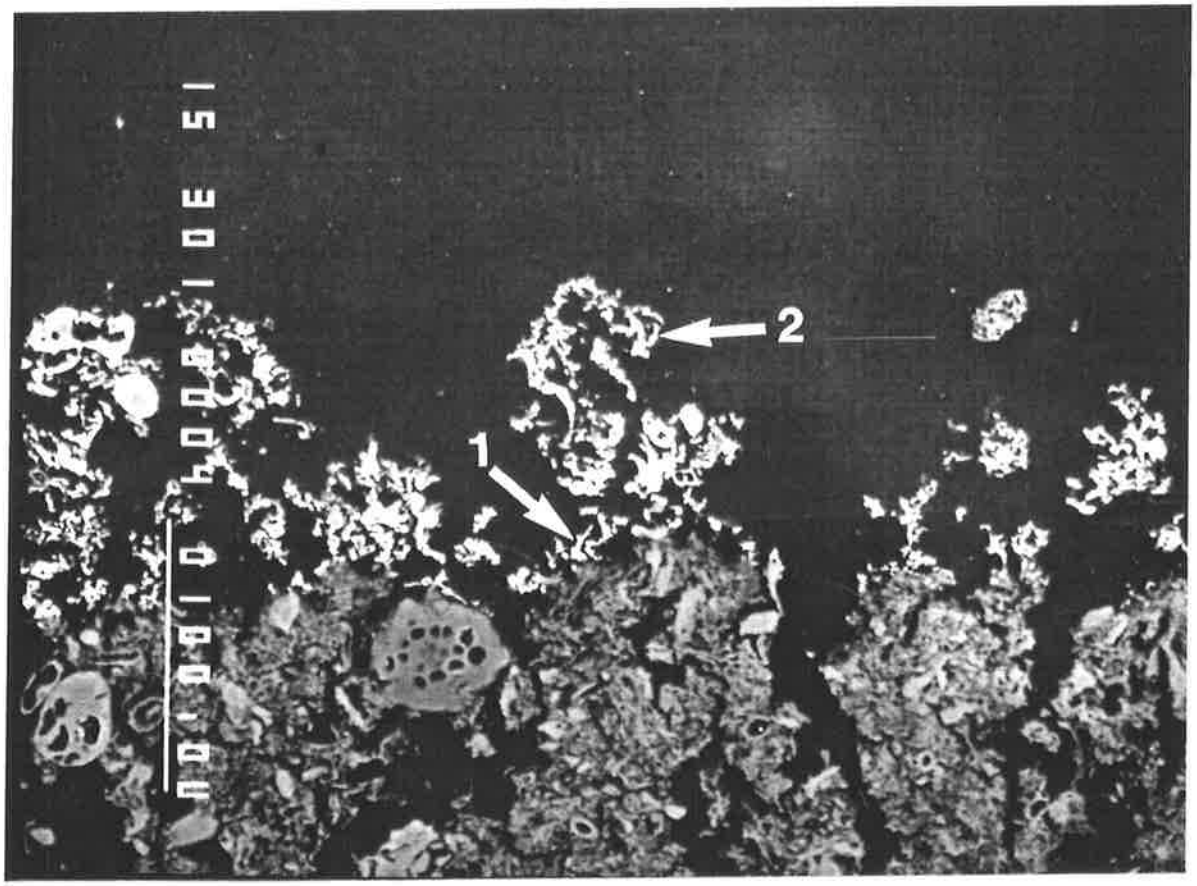

Positions Analysed:	Na_2O	CaO	MgO	SO_3	Al_2O_3	SiO_2	K_2O	P_2O_5	Cl
1	9.12	20.2	13.4	53.1	2.9	0.7	-	-	0.6
2	11.8	23.0	7.3	53.2	3.5	0.6	0.1	-	0.5

Figure 4.16: Back-scattered Electron Image of a Polished Cross-Section of a Char Particle After 91% Total Weight Loss (About 80% Char Burn-out), Effect of Excess O2 - EDAX analyses at selected positions are presented. Bright area shows a thin layer of ash. 100 μm bar is shown on the left.

surface and lower particle temperatures, depletion of sulphur and sodium does not occur. EDAX analyses indicate that the ash contains the same elements with similar proportions as the ash formed near the char surface in other experiments.

Because of its design and function, the SPF operates with a large amount of gas which sweeps away the combustion products from around the coal particles. In order to investigate the effect of SO_2 in the gas phase on the characteristics of the ash formed on the char's surface, SO_2 was added to the fluidising gas (diluted air with 5% O_2). The concentration of SO_2 in the fluidising gas was adjusted to around 2000 ppm by volume. The back-scattered electron image and the EDAX analysis, given in Figure 4.17, indicate that the ash contains the same elements with similar proportions as those formed near the char surface in other experiments.

Scanning Electron Microscopy

Scanning electron microscopy was used to examine the morphology of the ash formed on the char's surface. The results are presented in the form of micrographs (secondary electron image) and spectra showing the morphology and qualitative analysis of the ash formed at various stages of combustion.

The surface of a product particle having 49% total weight loss is shown in Figure 4.18. Although the total weight loss suggests that moisture is still present in the product particle, it appears from Figure 4.18 that the surface of the product particle has already experienced char burn-out to a certain extent. The bright areas show the formation of a sintered, sponge-like ash covering part of the char's surface. The qualitative analysis of the char (position 1) indicates the presence of sulphur, calcium, sodium, aluminium and small amount of magnesium. The analysis of ash (position 2) indicates that the sulphur in the ash is lower than that of the char adjacent to it.

The surface of another product particle having 74% total weight loss is given in Figure 4.19. The extent of burn-out can not be calculated as the total weight loss suggests that volatiles are still present in the product particle. The micrograph, however, shows the presence on the char's surface of a sponge-like ash. EDAX analyses indicate that the ash is highly sulphated and it contains varying concentrations of Ca, Mg and Al. Due to its low atomic number, low concentrations of sodium can not be detected.

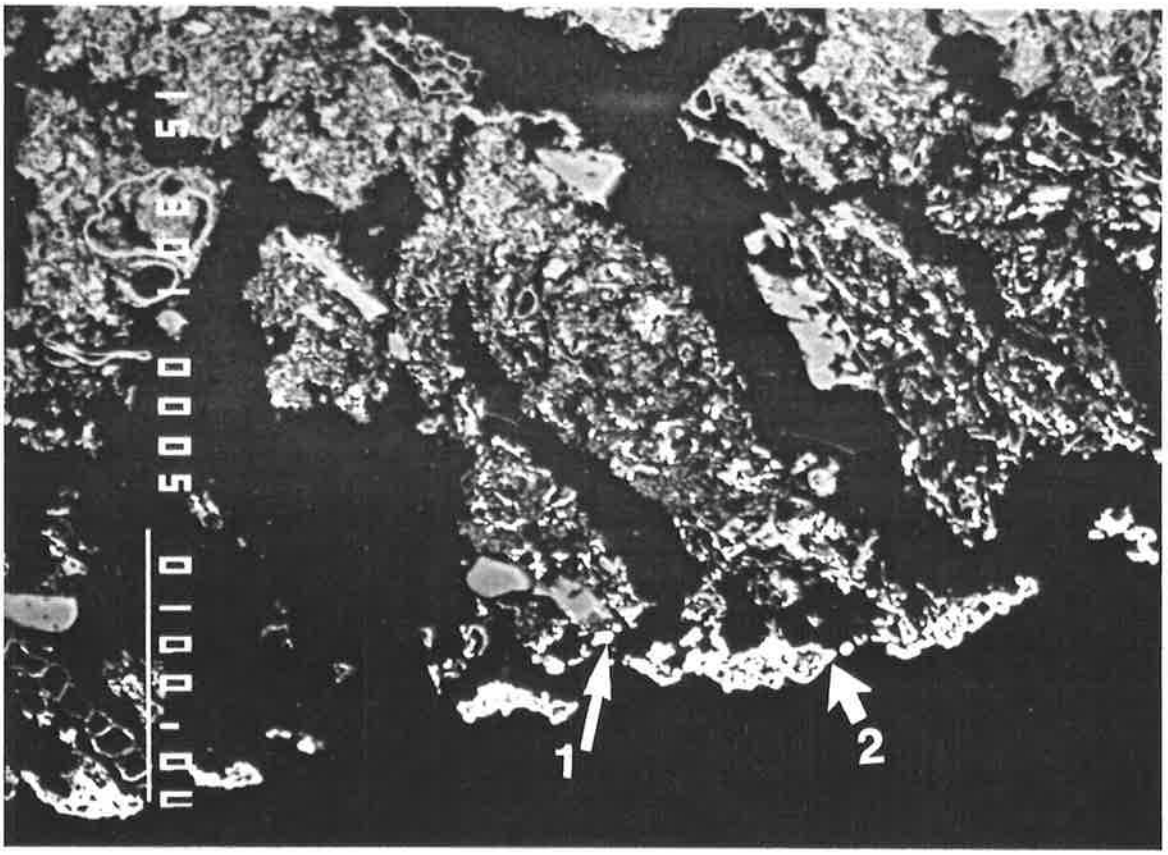

Positions Analysed:	Na_2O	CaO	MgO	SO_3	Al_2O_3	SiO_2	K_2O	P_2O_5	Cl
1	9.9	14.1	16.3	49.9	8.8	0.6	-	-	0.3
2	8.2	17.6	7.5	67.2	2.6	0.1	-	-	0.3

Figure 4.17: Back-scattered Electron Image of a Polished Cross-Section of a Char Particle After 91% Total Weight Loss (About 80% Char Burn-out), Effect of SO2 in Flue Gas - EDAX analyses at selected positions are presented. Bright area shows a thin layer of ash. 100 µm bar is shown on the left.

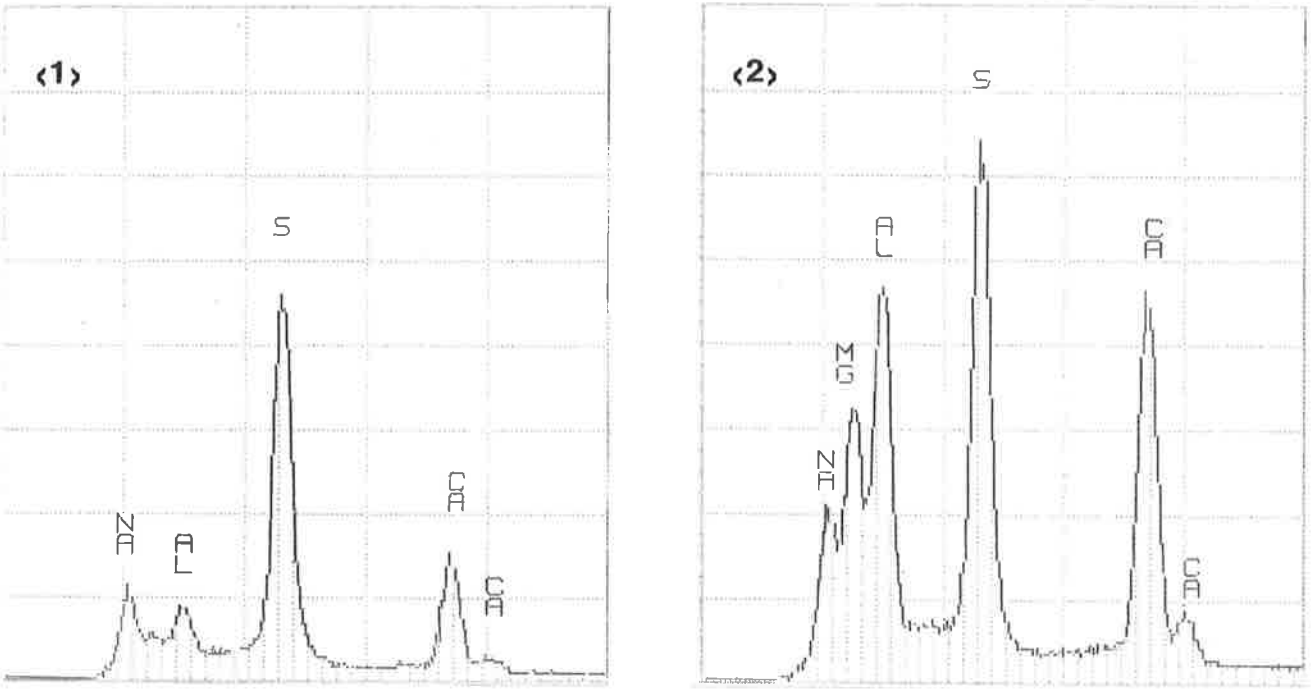

Figure 4.18: Secondary Electron Image of the surface of a Char Particle After 49% Total Weight Loss - EDAX spectra of selected positions are presented. Bright areas show the formation of ash on the char surface. 0.1 mm bar is shown at the bottom.

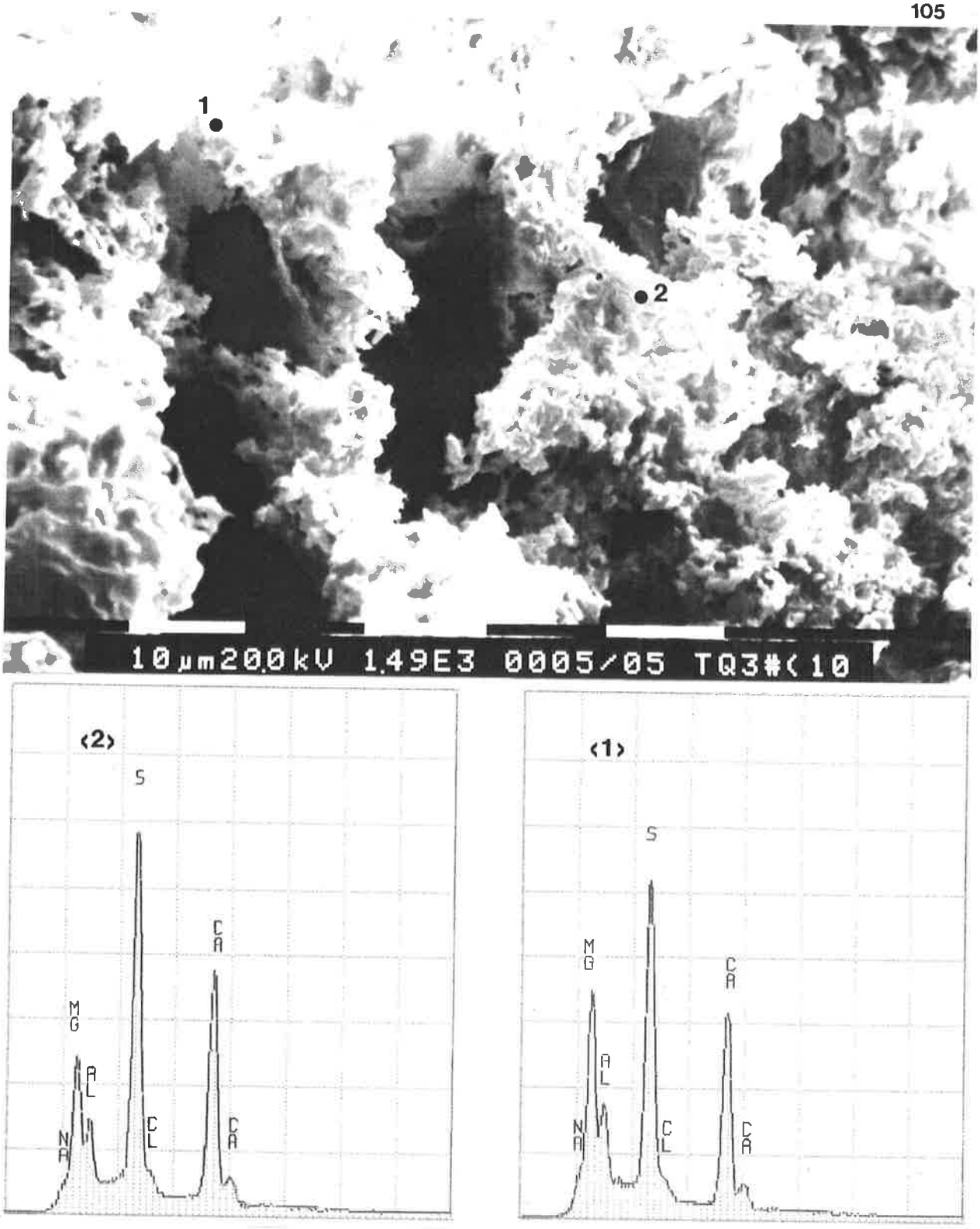

Figure 4.19: Secondary Electron Image of the surface of a Char Particle After 74% Total Weight Loss - EDAX spectra of selected positions are presented. The char surface is covered by a sponge-like ash. 10µm bar is shown at the bottom.

Figure 4.20 shows another location on the surface of the same particle which indicates that the formation of ash has further advanced. The morphology of the ash at this location appears to have changed to a less porous structure. The qualitative analysis carried out by EDAX indicates that the surface of the ash matrix is slightly depleted in sulphur.

The morphology and qualitative analyses of the ash formed on a product particle having 87% total weight loss (about 50% char burn-out) is given in Figure 4.21. The ash appears to consist of a molten matrix in which solid particles, rich in Ca, Mg and Al, are embedded. The molten matrix which contains mostly Ca is likely to be the product of transformation of the sulphated compounds of Na and Ca formed initially on the char's surface. It appears that these sulphates undergo transformation as well as coalescence while attached to the char surface.

The progressive coalescence of ash, once it is formed, and the presence of the solid phase in the molten matrix is also shown in the micrographs of Figure 4.22. The freshly formed ash near the char-ash interface has a sponge-like morphology, whereas, on the surface of the ash matrix it has a molten morphology.

Figure 4.23 shows the surface of the ash matrix on another product particle having 94% total weight loss (estimated 80% char burn-out). Through a wide fissure in this sample the char forming the internal part of the product particle (position 1) can be examined. EDAX analyses indicate that the woody char in Position 1 has high concentrations of sulphur and sodium. Position 2 shows a sintered sponge-like ash with lower content of sulphur compared to that in the char. Position 3 shows the surface of the ash matrix with a molten texture. The concentrations of sulphur and sodium in the molten ash is small. SEM analyses confirmed the results of microprobe analysis carried out on the cross-sections of the product particles.

Microscopic examinations as well as chemical analyses indicate that, within the range tested, the nature of the transformations undergone by the inorganic matter is not significantly affected by the furnace temperature nor by the initial coal particle size. Therefore, it is inferred that the coal particles burnt under various conditions may experience nearly the same temperature. This is possible as, under the FBC conditions, the temperature of the burning char particles is likely to exceed that of the furnace by a few hundred degrees. Thus the changes in the furnace temperature and in the initial coal particle size, in the range

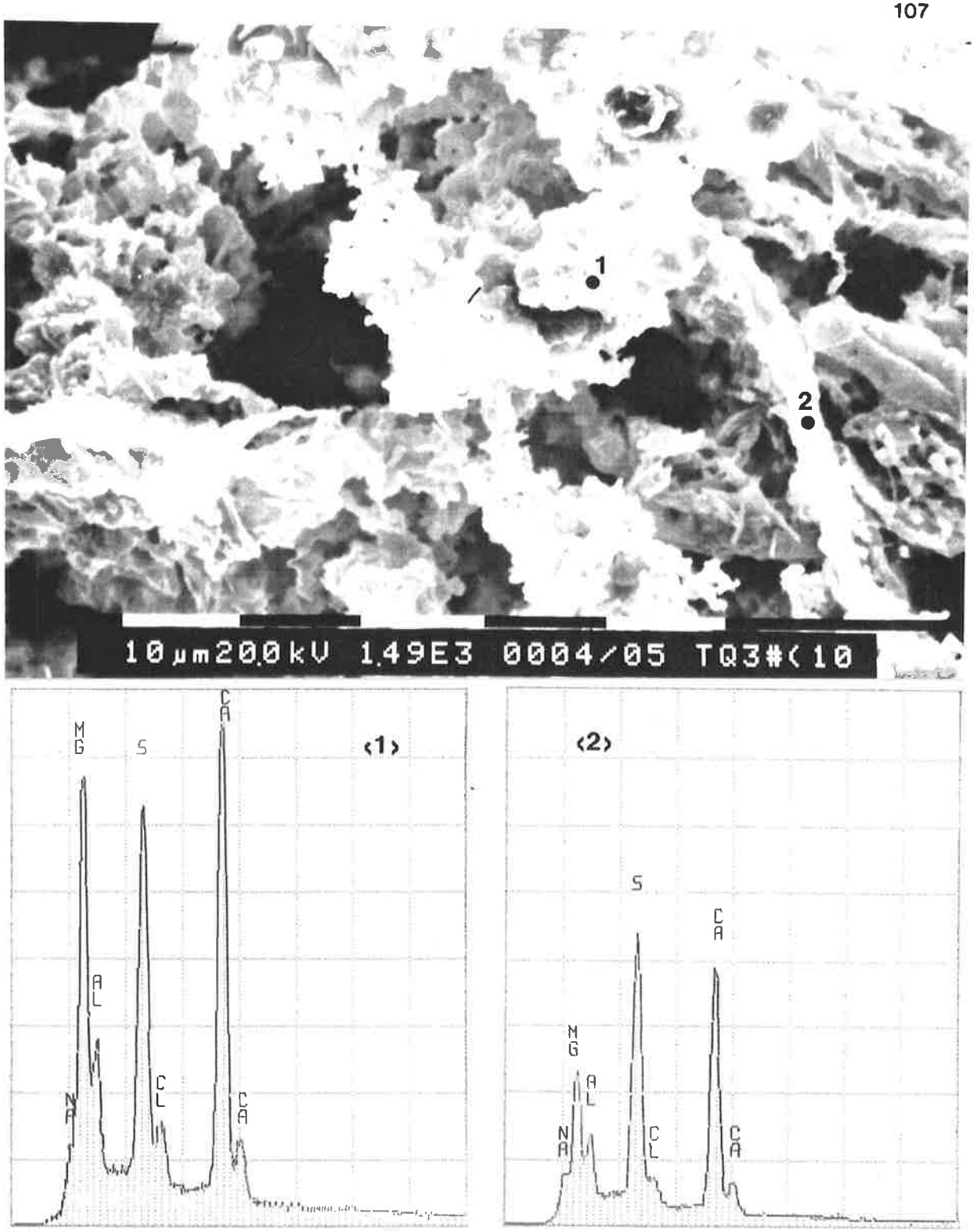

Figure 4.20: Secondary Electron Image of the surface of a Char Particle After 74% Total Weight Loss, Coalescence of Ash - EDAX spectra of selected positions are presented. The char surface is covered by ash. The surface of the ash is semi-molten. 10 µm bar is shown at the bottom.

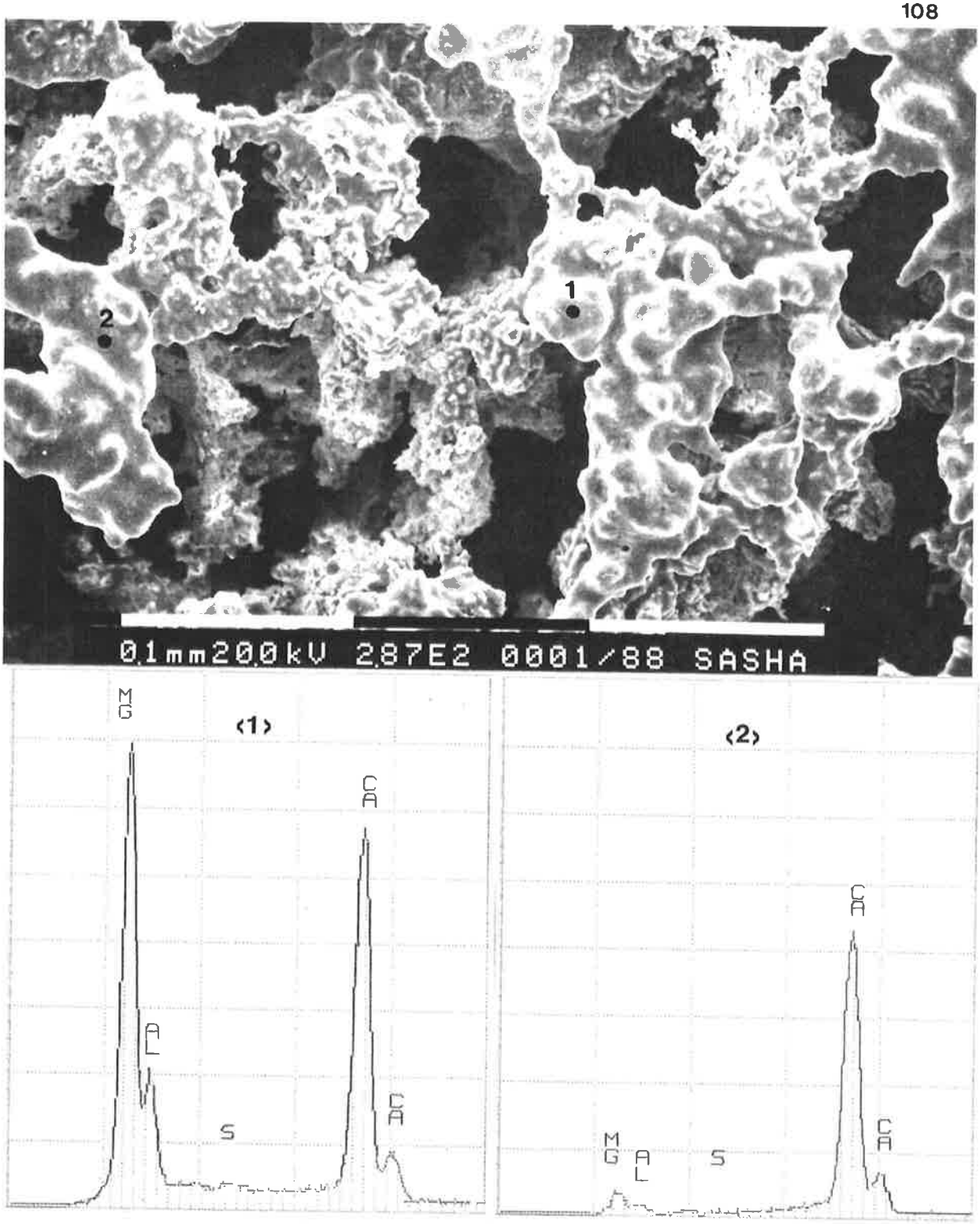

Figure 4.21: Secondary Electron Image of the surface of a Char Particle After 87% Total Weight Loss (about 50% char-burn-out) - EDAX spectra of selected positions are presented. The char surface is covered by ash. The surface of the ash is molten. Below the molten surface, the ash is sponge-like. 0.1 mm bar is shown at the bottom.

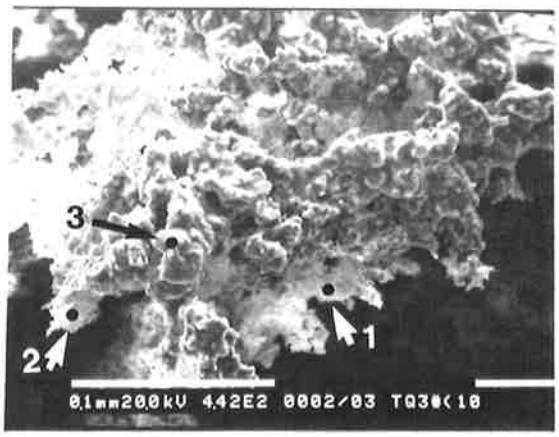

Figure 4.22 a:
Magnification x 442

1: S, Ca, Mg, Al, (Na)
2: Ca, (Mg, Al, S)
3: Ca, Mg, Al

Figure 4.22 b:
Magnification x 442

1: S, Ca, Mg, Al, (Na)
2: Ca
3: Ca, Mg, Al (S)

Figure 4.22: Secondary Electron Images of the surface of Char Particles After 87% Total Weight Loss (about 50% char-burn-out) Showing the Morphology of the Ash Matrix - Major and minor (in bracket) elements detected by EDAX at positions shown are presented. The surface of the ash matrix is molten. Below the molten surface, the ash is sponge-like. 0.1 mm bars are shown at the bottom.

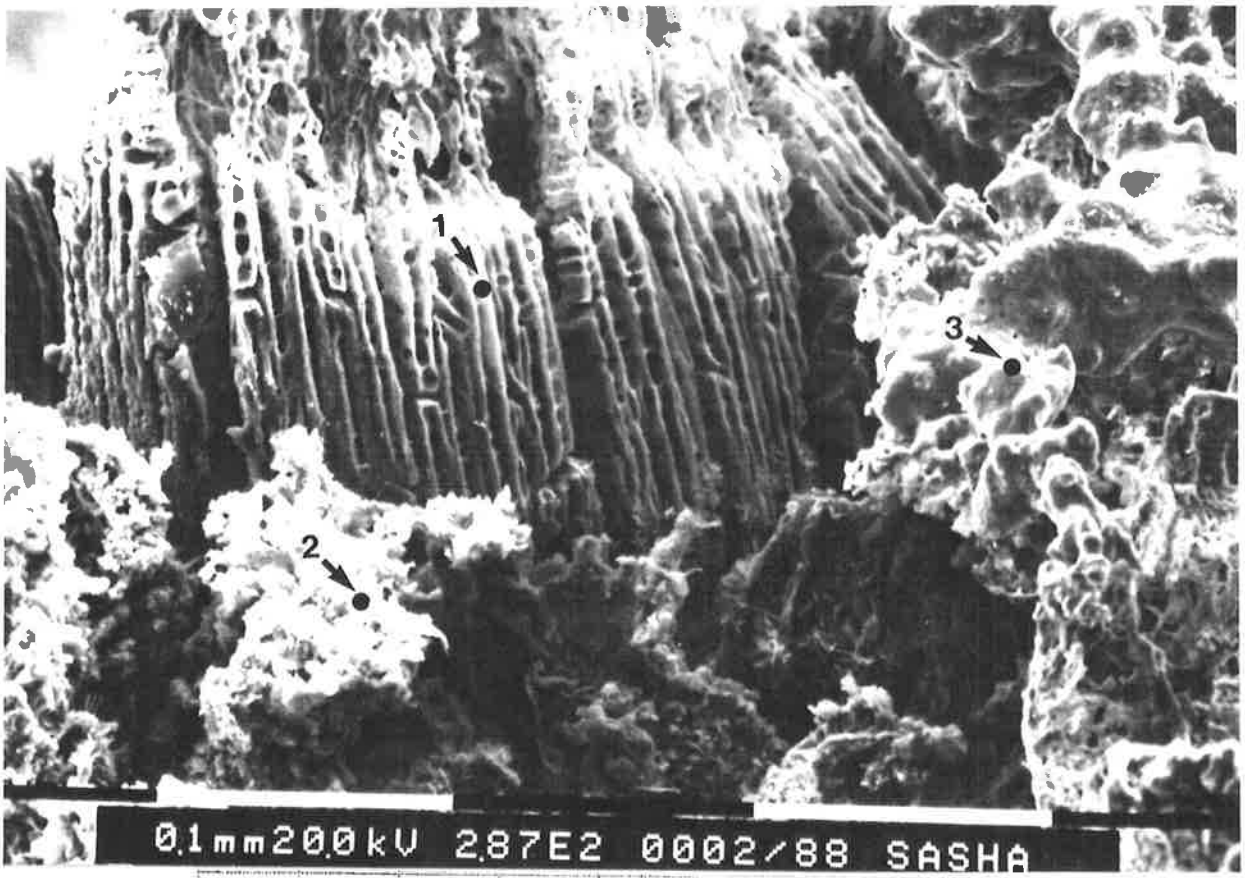

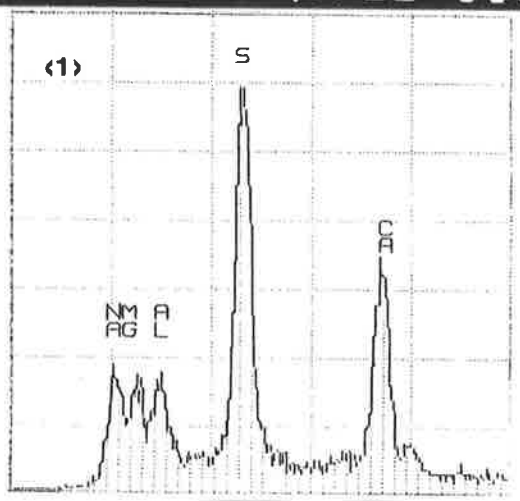

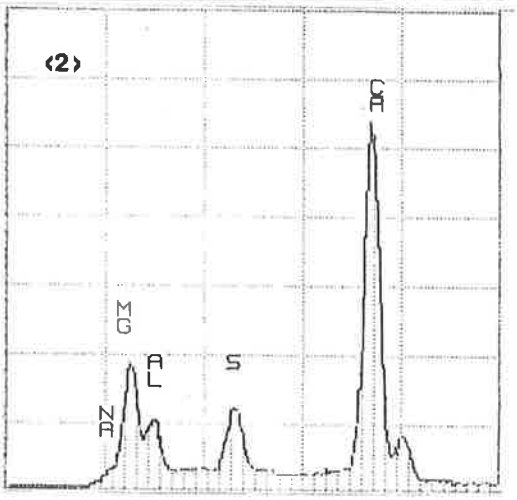

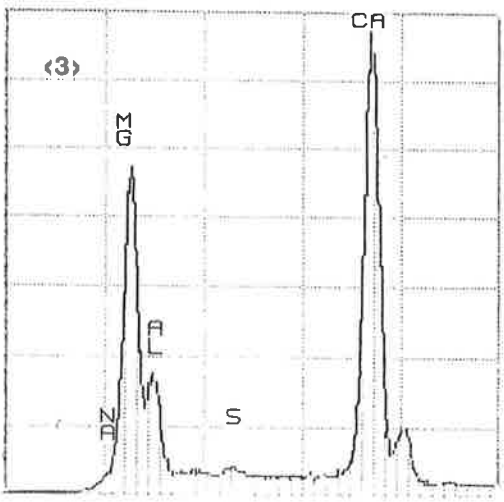

Figure 4.23:
Secondary Electron Image of the surface of a Char Particle After 94% Total Weight Loss (about 80% char-burn-out) - EDAX spectra of selected positions in the char(1), sintered ash (2) and molten ash (3) are presented. 0.1 mm bar is shown at the bottom.

investigated, may not be large enough to have a marked effect on the char particle temperature. The effect of furnace temperature on the inorganic matter behaviour was also investigated in the fluid bed combustion system (FBCS); the results are given in Chapter 5.

4.6 SUMMARY AND CONCLUSIONS

The physico-chemical transformations experienced by the inorganic matter during combustion of the low-mineral coal sample, with high content of sodium and sulphur, under conditions relevant to FBC are schematically shown in Figure 4.24 and are summarised as follows:

- The decomposition of the functional groups containing the inorganic elements results in the formation of intimately distributed and complex inorganic species within the coal matrix. Most of these species are refractory; those formed from sodium, chlorine and sulphur may be volatile;
- The extent of vaporisation of the sodium species including sodium chloride was found to be small. Most of the species formed from the organically bound sodium remain in the char and are likely to participate in the ash formation mechanism on the char's surface.
- Chlorine is released disproportionately to sodium suggesting that sodium chloride reacts with other compounds inside the char and/or on the char's surface. Sodium species formed as a result of these reactions can also participate in the ash formation mechanism.
- The presence of organic sulphur and sodium in low-rank coals results in a formation of a molten ash matrix on the char's surface. The ash matrix retains some of the solid species formed during the transformations of the organically bound elements such as Ca, Mg and Al as well as some of the mineral inclusions in the coal including sub-micron silica particles which are intimately distributed in the coal matrix. Although the molten phase is likely to include sodium species formed from NaCl transformations, it contains only minute quantities of Cl compounds.

- Due to the intimate distribution of the inorganics and sodium chloride in the coal, complex compounds and solid solutions are likely to form. The XRD analyses of product particles and ash suggest that complex compounds are formed. The formation of a molten phase is due to the formation of low melting eutectics such as Na-Ca-sulphate in which some of the Na and Ca may be displaced by other elements. Aluminates and oxides, formed from Al, Ca and Mg, appear to be in solid state at the prevailing char particle temperature.
- In the SPF, where there is no collision with other particles, the ash matrix remains attached to the char's surface and grows in thickness. Some of the species in the ash matrix undergo further transformations with time resulting in a decrease of sodium and sulphur concentration towards the outer surface of the ash matrix. The morphology of the surface of the ash matrix indicates partial fusion of the inorganic matter.

The results obtained are expected to be of significance in explaining the formation of binding material responsible for the agglomeration of bed particles in fluid bed combustors. The results obtained using the SPF will be discussed again in conjunction with the results obtained from the FBCS, Chapters 5 and 6.

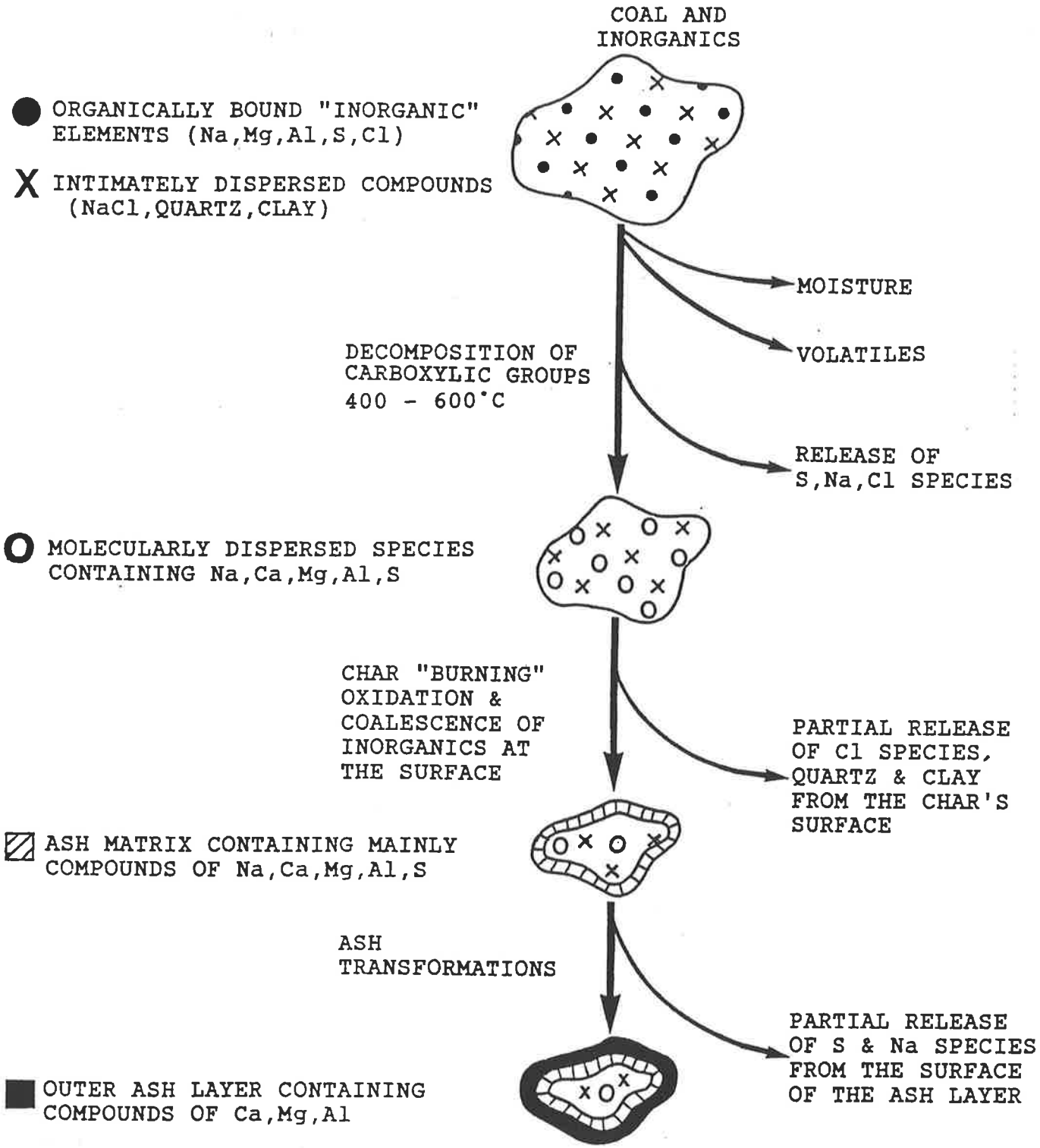

Figure 4.24: Schematic of the Transformations of the Inorganic Matter During Fluid Bed Combustion Of Low-Rank Coals.

Chapter 5

ASH/BED MATERIAL INTERACTIONS

5.1 INTRODUCTION

Combustion experiments carried out in the single particle furnace (SPF), described in Chapter 4, showed that, under the conditions relevant to fluid bed combustion (FBC), the inorganic matter in low-rank coals forms molten ash on the char's surface. The results provide a basis for the hypothesis that, in circulating fluid bed combustors (CFBC), bed agglomerates are formed by the following mechanisms:

- collision of bed particles with burning char particles covered in molten ash in the stirred environment of CFBC;
- transfer of molten ash from the surface of burning char particles to the bed particles, which consequently become sticky; and
- formation of agglomerates as a result of collision of sticky bed particles with each other.

In order to investigate the validity of the above hypothesis, combustion experiments were carried out in the fluid bed combustion system (FBCS), described in Subsection 3.3.1, with the following specific objectives:

- to investigate the mechanism of deposition of molten material on the bed particles and the exact role of the inorganic matter in this mechanism;
- to determine the rate of deposition of the molten ash on the bed particles as a function of coal quality, combustion temperature, excess air, bed material and bed particle size distribution;
- to investigate the mechanisms of bed agglomeration and defluidisation and their dependence on coal quality, furnace temperature and operating time.

The results on first two of these objectives are described in this chapter. The final objective is covered in Chapter 6.

The bed material periodically removed from the furnace and the fly ash collected in the cyclone were analysed using the analytical techniques described in Section 3.5. The formation of molten ash on the bed particles (coating) and the characteristics of the coating were determined for a variety of operating conditions.

Two samples of coal were collected from the Lochiel deposit in South Australia for these experiments. The first sample, referred to as "high-mineral", was a mixed coal from different zones of the deposit and had an inorganic matter which consisted mostly of minerals in the form of inclusions and partings (Subsection 2.2.1). The second sample, referred to as "low-mineral", had an inorganic matter which consisted predominantly of organically bound inorganic elements. Both samples contained sodium chloride as dissolved salt in their inherent moisture. The second sample, which is similar to the low-mineral sample employed for the single particle experiments, was used to investigate the behaviour of the inorganics in coal without the interference from the minerals initially present in the coal. Experiments were also carried out with water-leached, acid-leached and added-sodium chloride samples of the "low-mineral" coal.

The details of the experimental procedure and the experimental program are given in Subsection 3.4.2. The variables investigated were: coal quality, bed temperature, excess oxygen, bed particle size distribution and bed material.

In order to validate the conclusions drawn from these experiments, samples of bed material obtained from large pilot plant tests carried out in the Lurgi CFBC facility in Frankfurt were examined by XRD and electron microscope. The results of these examinations are also presented in this chapter.

5.2 COATING AND PARTICLE GROWTH

During the combustion tests carried out in the FBCS, it was observed that the differential pressure across the bed increased gradually. Examination of the bed inventory removed from the furnace every 3 hours (Subsection 3.4.2) indicated an increase in mass and grain size of the initial charge with operating time. From the size analysis and microscopic examination of the bed material, it was concluded that the bed material contained only an insignificant amount of ash (less than 1%) as fly ash and ash agglomerates, Subsection 3.4.3. Hence, the increase in grain size and mass of the bed inventory was found to be due to the deposition of the inorganic matter on the bed particles.

The mean diameter of the bed particles was calculated from the size distribution of the bed material periodically removed from the furnace. The size distribution of the bed material and the mean diameter of the bed particles for Run 1 are given in Figures 5.1 and 5.2 respectively. These figures illustrate that the bed particles undergo significant growth during the fluid bed combustion of high-sodium, high-sulphur low-rank coals.

It should be noted that the size distribution of the bed material, and hence the mean diameter of the bed particles, is influenced by the deposition of ash coating on the bed particles as well as the formation of agglomerates. Consequently, the mean diameter of the bed particles calculated from the size distribution of bed material can not give an accurate assessment of the rate of deposition of coating on the bed particles. This, however, can be obtained by plotting the percent increase in the mass of the initial bed inventory as a function of operating time. As mentioned earlier, only a small amount of ash, in the form of individual ash particles, is retained in the bed. These ash particles, being smaller than the size range of the initial charge, are separated before the bed inventory is weighed, Subsection 3.4.3. Hence, the increase in the mass of the initial charge is solely due to the formation of coating on the individual bed particles.

In order to study the effect of different operating variables on the rate of deposition of coating, the operating procedure described in Subsection 3.4.2 was employed. With the exclusion of Runs 11 and 12, the experiments were carried out using a constant combustion air flow rate. By controlling the excess oxygen at a constant level, approximately the same amount of carbonaceous matter (dry-ash-free coal) was fired in each run as illustrated in Table 5.1.

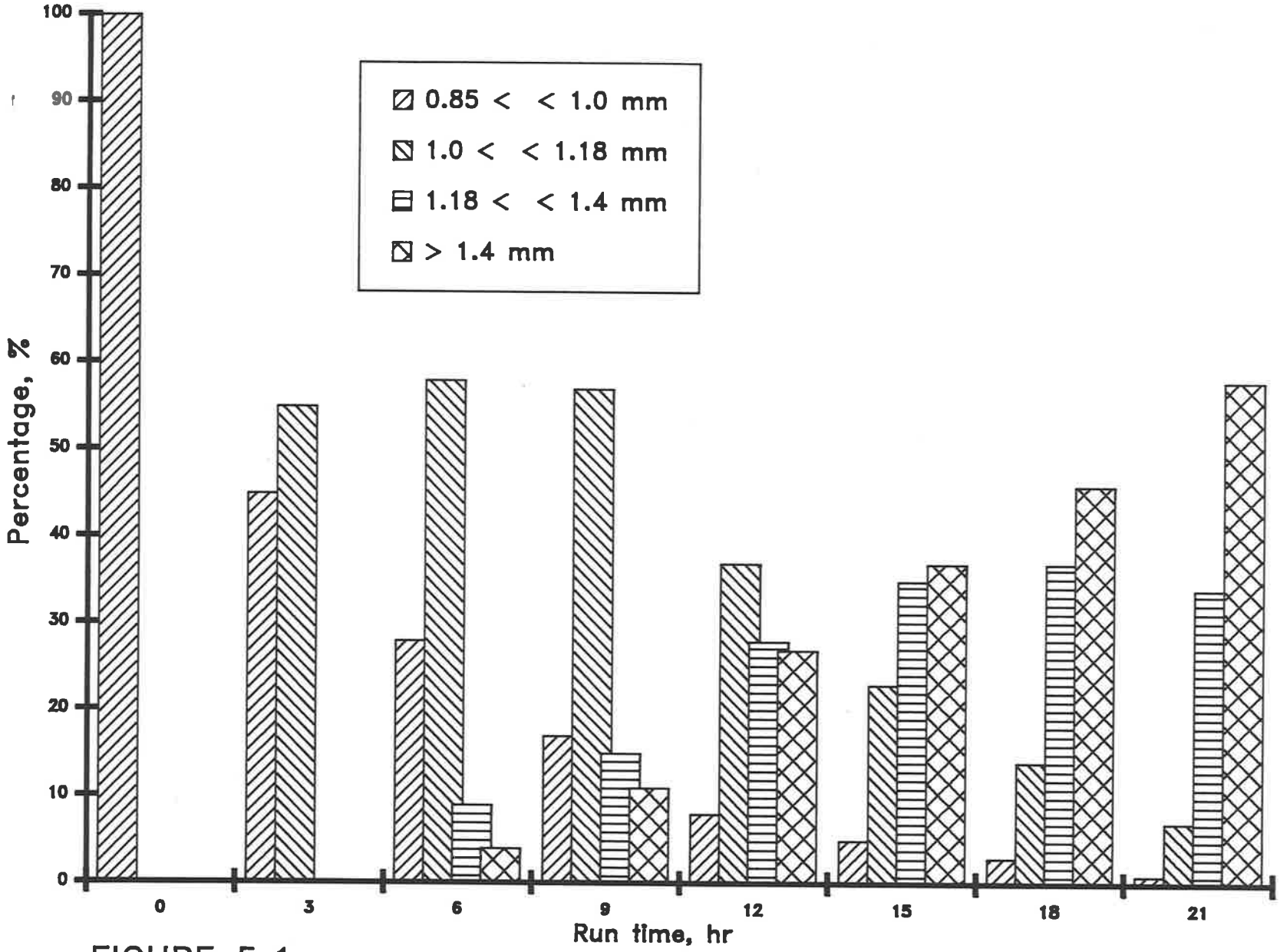

FIGURE 5.1 :

Graph of size distribution of bed material vs run time, Run 1

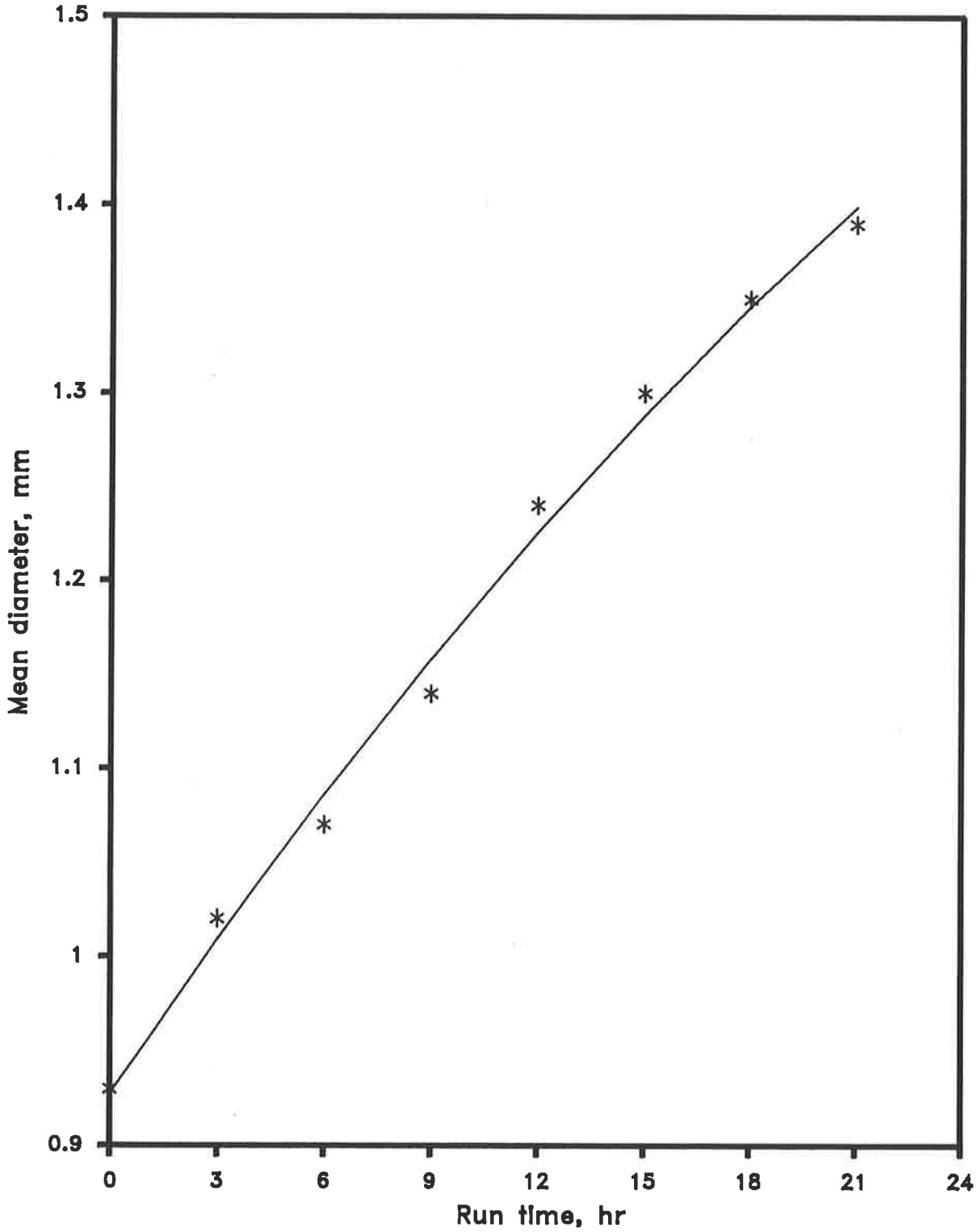

Figure 5.2:
Bed particle growth vs Run time, Run 1

Table 5.1: ***Operating Data.***

		Coal Input (as fired) g/h	Coal Input (daf) g/h	Air Flow Rate L/min	Air Temperature °C	Exess O_2 vol% (db)
Run	**1**	450	313	140	700	16
	2	479	308	"	"	"
	3	417	302	"	660	"
	4	426	317	"	"	"
	5	432	322	"	"	"
	6	438	305	"	"	"
	7	454	312	"	"	"
	8	569	302	"	630	"
	9	563	307	"	580	"
	10	548	295	"	660	"
	11	445	310	"	"	"
	12	451	312	"*	"	5
	13	571	403	125	"	12

* combustion air diluted with nitrogen

daf = dry-ash-free basis

db = dry-basis

The experiments carried out in the FBCS indicated that the rate of deposition of the coating on the bed particles, given in Table 5.2, does not change with operating time. Part of the inorganic matter which did not deposit on the bed particles finished as:

- fly ash which was collected in the cyclone;
- furnace wall deposits;
- gaseous species such as SO_2, HCl and NaCl;
- sub-micron particles escaping the cyclone.

The distribution of the inorganic matter is given in Table 5.2.

Effect of Coal Quality

The first two runs, described in Subsection 3.4.2, were conducted with the high and low-mineral coal samples at furnace temperature of 850°C. Sand particles of a narrow size range (0.85 to 1.0 mm) were used as the initial charge for the bed inventory. The chemical analyses of the coal samples are given in Tables 5.3 to 5.4; a graphical illustration of the ash compositions is given in Figure 5.3.

On a dry-basis, the high-mineral coal sample contains a larger proportion of sodium (Table 5.3). However, the percentage of sodium in the ash is nearly the same for both coals (Table 5.4).

The high-mineral coal sample contains significant amount of minerals (quartz and clays) whereas the inorganic matter in the low-mineral sample consists predominantly of organically bound sodium, sulphur, calcium, magnesium, and aluminium. Due to the larger proportion of Ca in the low-mineral coal sample, more sulphur is retained in the ash of this coal. The content of chlorine (on a dry-basis) in the low-mineral coal sample is slightly higher.

Run 1 was carried out with the high-mineral coal sample at 850°C and over a period of 24 hours during which the bed particles continued to grow due to the deposition of the ash coating. Run 2, however, carried out with the low-mineral coal sample at the same temperature as Run 1, was aborted after 3.5 hours of operation due to defluidisation of the bed.

Table 5.2: ***Distribution of the Inorganic Matter.***

	Input with Coal	Coated on Bed Particles		Cyclone Ash		Balance*	
Run	**g/h**	**g/h**	**%**	**g/h**	**%**	**g/h**	**%**
1	48.8	4.7	9.6	34.1	69.9	10.0	20.5
2	34.7	11.5	33.1	16.5	47.5	6.7	19.4
3	33.7	10.3	30.6	16.0	47.5	7.4	21.9
4	27.6	4.3	15.6	17.3	62.7	6.0	21.7
5	26.5	2.7	10.2	17.7	66.8	6.1	23.0
6	31.6	11.7	37.0	14.0	44.3	5.9	18.7
7	36.2	23.3	64.3	6.2	17.1	6.7	18.5
8	33.2	8.0	24.1	18.2	54.8	7.0	21.0
9	36.8	7.3	19.8	23.8	64.7	5.7	15.5
10	33.1	10.7	32.3	16.8	50.7	5.6	16.9
11	34.8	10.3**	29.6	23.6	67.9	0.9	2.5

* gaseous species, furnace wall deposits and sub-micron particles

** at the later stages of operation

Table 5.3: ***Chemical Analyses by Extraction Method of the Inorganic Matter in Coal.***

Coal Sample	Low-Mineral			High-Mineral		
	WS	**AS**	**AI**	**WS**	**AS**	**AI**
Na %db	0.58	0.92	-	0.79	1.07	-
Ca "	-	1.14	-	-	0.76	-
Mg "	-	0.83	0.01	-	0.70	0.01
K "	-	0.01	-	-	0.02	-
Fe "	-	0.02	0.08	-	0.24	0.08
Al "	-	0.33	0.04	-	0.61	0.90
Si "	-	-	0.19	-	0.17	1.97
Cl "	0.57	0.57	-	0.49	0.49	-
S "	-	-	3.40	-	-	3.20

WS = Water-soluble
AS = Acid-soluble
AI = Acid-insoluble (residue)
dash line (-) = less than 0.01% db

Table 5.4: ***Ash Analyses (Australian Standard Method).***

Sample	Low-Mineral	High-Mineral
Fe_2O_3	4.26	2.60
Al_2O_3	7.93	17.18
SiO_2	4.04	30.93
MgO	13.80	9.09
CaO	16.95	8.59
K_2O	0.30	0.42
Na_2O	11.53	10.30
TiO2	0.10	0.71
SO_3	38.55	18.55

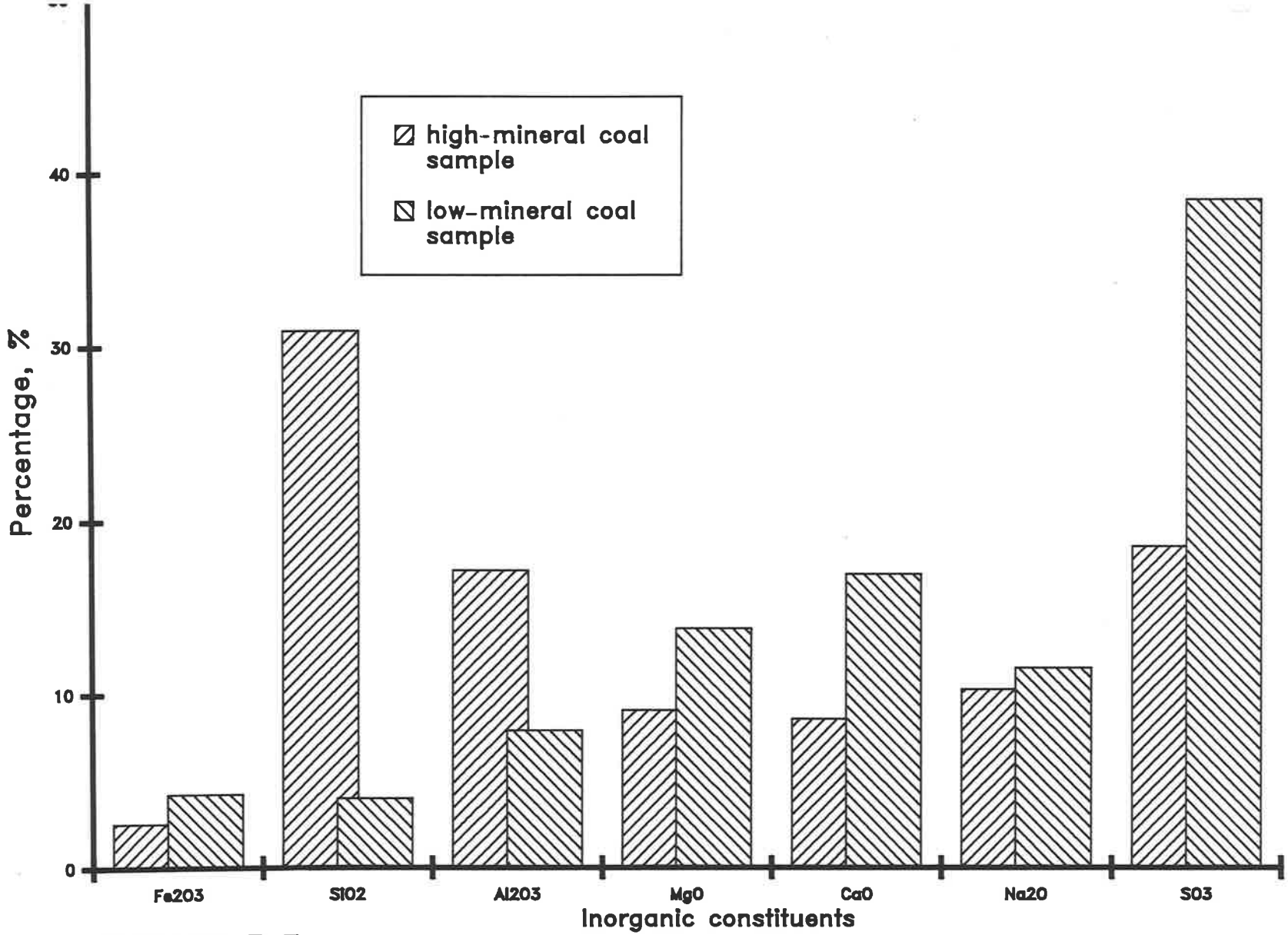

FIGURE 5.3 :

Diagrammatic representation of the ash composition

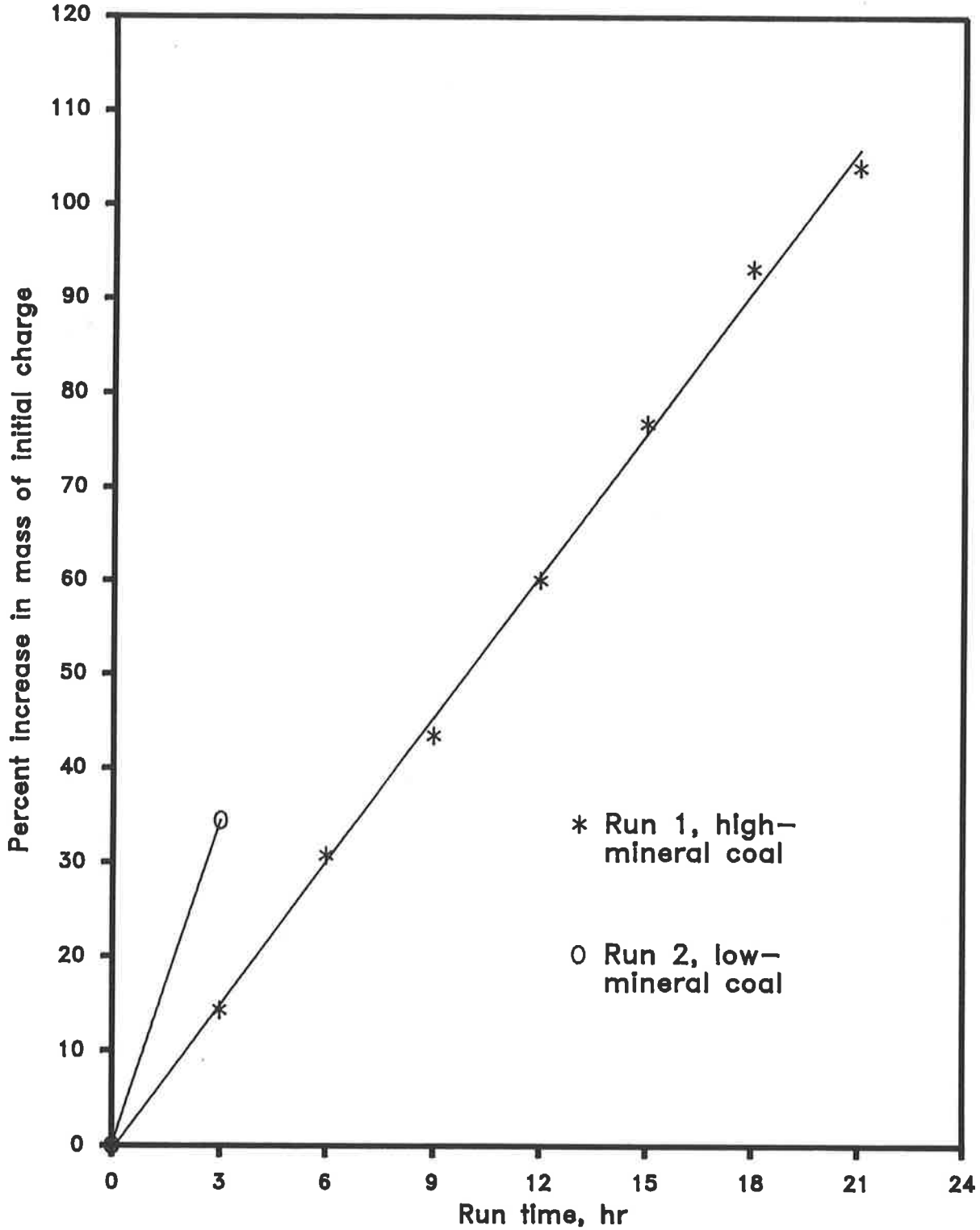

Figure 5.4:
Deposition of coating on the bed particles, furnace temperature 850°C

Although only one sample was collected from Run 2, the results presented in Table 5.2 and Figure 5.4 indicate that the rate of deposition of the coating on the bed particles is markedly higher when the low-mineral coal sample is burnt. It appears that the deposition rate of the coating is governed not only by the coal sodium content (Goblirsch et al., 1980; Atakul and Ekinci, 1989), but also by the mode of occurrence of other inorganic matter. Chemical and microscopic examination of the coating, given in Subsection 5.5, illustrates the role of the minerals in the formation of the coating and on the characteristics of the coating.

Sodium is reported to be a major inorganic element contributing to the formation of agglomerates in fluid bed combustors (Goblirsch, et al., 1980). Sodium can be present in the coal in numerous forms. In the South Australian low-rank coals, three major forms of sodium have been identified (Subsection 2.2.2). In order to investigate the role of various forms of sodium in the formation of the coating, similar experiments were carried out with water-leached, acid-leached and two added-sodium chloride samples of the low-mineral coal (Runs 4 to 7). Run 3, using the same coal sample as Run 2, was conducted at furnace temperature of 800°C to avoid defluidisation of the bed. Other runs, investigating the effect of coal quality, were also conducted at 800°C. The conditions of the runs and the procedures used for the preparation of the coal samples are described in Subsection 3.4.2.

The results of sodium and chlorine analyses of treated coal samples and those of untreated sample are given in Table 5.5.

Water leaching of the coal sample removed all the chlorine and most of the water soluble sodium (that is, sodium associated with chloride and sodium which is weakly bonded to the organic matter). The sodium removed corresponded to about 56% of the total sodium. The inorganic matter remaining in the water-leached coal sample consists predominantly of the organically bound inorganic elements (inorganics).

Acid leaching of the coal sample removed all the chlorine and about 80% of the total sodium including all the water-soluble and part of the acid-soluble organically bound sodium. Portions of other inorganics (that is, calcium, magnesium and aluminium) were also extracted.

Treating the coal sample with sodium chloride solutions of two different concentrations (that is, batch 1 and 2) increased the amount of NaCl in the coal by about 50% and 110%

Table 5.5: ***Sodium and Chlorine Analyses (%db) (low-mineral coal).***

Coal Samples	Na	Cl
Untreated coal	0.89	0.57
Water-leached	0.35	0.01
Acid-leached	0.18	0.01
NaCl-added, batch 1	1.22	0.87
NaCl-added, batch 2	1.55	1.20

respectively. The greater stoichiometric equivalent of Na versus Cl indicates that some Na is captured by ion exchange possibly through replacement of other organically bound elements.

For Runs 3 to 7, the deposition of the coating on the bed particles, given as percent increase in mass of the initial bed inventory, versus operating time is given in Figures 5.5. The results are described as follows:

Leaching of the water-soluble sodium (including sodium chloride) from the coal reduced the rate of deposition of the coating on the bed particles, Run 4. The results, however, suggests that both the organically bound sodium and sodium chloride participate in the deposition mechanism.

Leaching part of the acid-soluble inorganics (i.e. Na, Ca, Mg and Al) resulted in further reduction in the rate of deposition of the coating on the bed particles (Run 5).

Addition of NaCl to the coal increased the rate of deposition of the coating on the bed particles (Runs 6 and 7). The increase in the deposition rate became more pronounced when the coal sample with higher concentration of NaCl (Run 7) was used. Additionally, NaCl added to the coal samples enhanced the sticky characteristics of the bed particles to the extent that Run 7 was aborted after 0.5 hour of operation due to defluidisation of the bed. Only one sample could be collected during this run. The characteristics of the coating formed during Runs 3 to 7 will be examined in Section 5.5.

Figure 5.6 gives the rate of deposition of the coating on the bed particles against total sodium in coal. The results indicate this rate increases with increasing Na content of the coal. A linear "fit" can be used for the untreated, water leached and acid leached coal samples. However, a relatively higher deviation from the linear relationship is evident for the samples with added-NaCl. Further work is required to quantify more accurately the effect of various forms of sodium on the rate of deposition of the coating on the bed particles.

Effect of Furnace Temperature

In order to investigate the effect of furnace temperature on the rate of deposition of the coating, combustion tests were carried out at 750° and 700°C (Runs 8 and 9) on the low-mineral coal sample. The results, including those of the test carried out at 800°C (Run 3) are compared, Figure 5.7. As said earlier, the test conducted at 850°C (Run 2) on the low-mineral sample was aborted due to defluidisation of the bed.

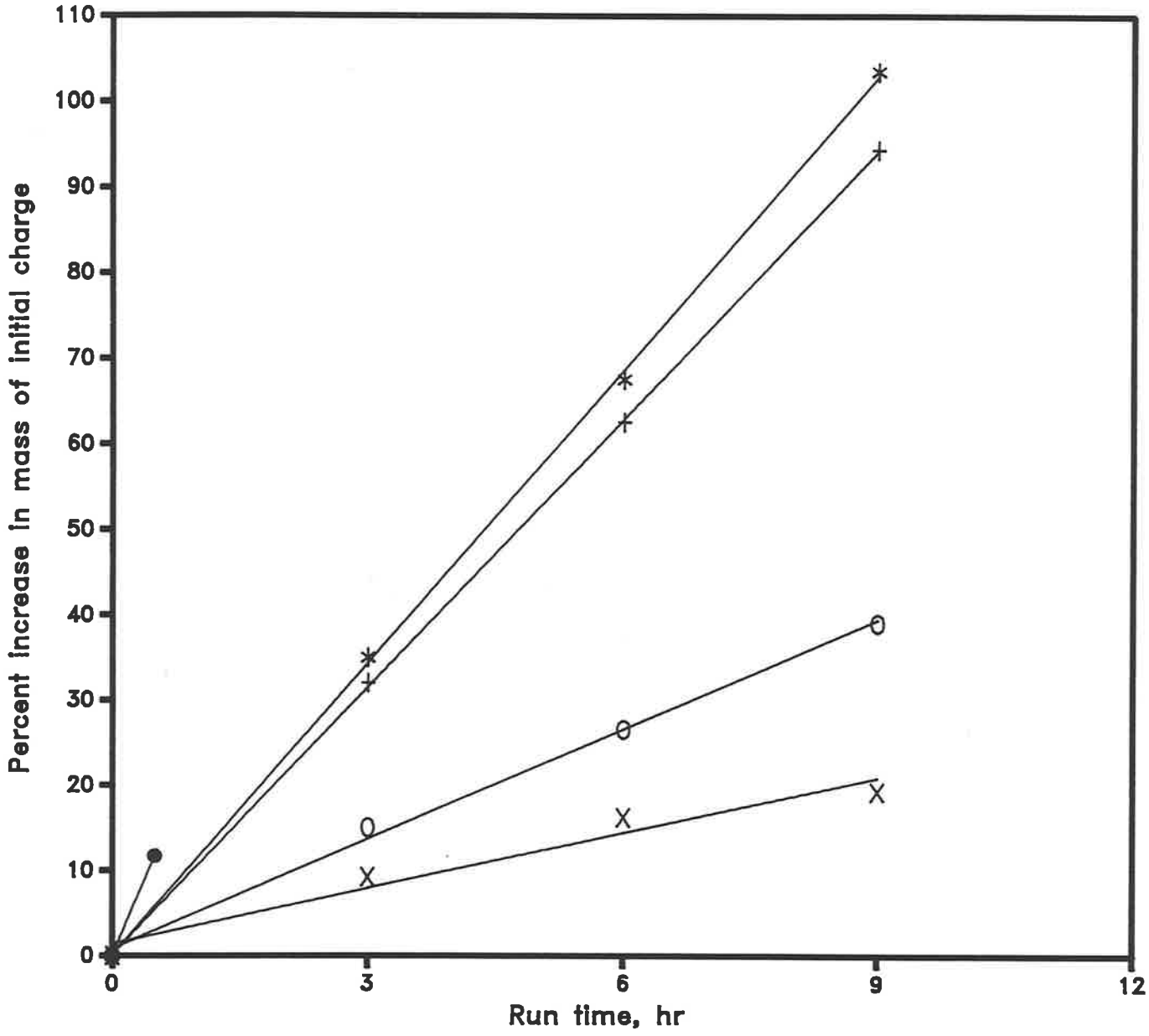

Figure 5.5:
Deposition of coating on the bed particles effect of coal quality

Coal samples:

+ Run 3, low-mineral

0 Run 4, water-leached

X Run 5, acid-leached

* Run 6, NaCl-added (1)

● Run 7, NaCl-added (2)

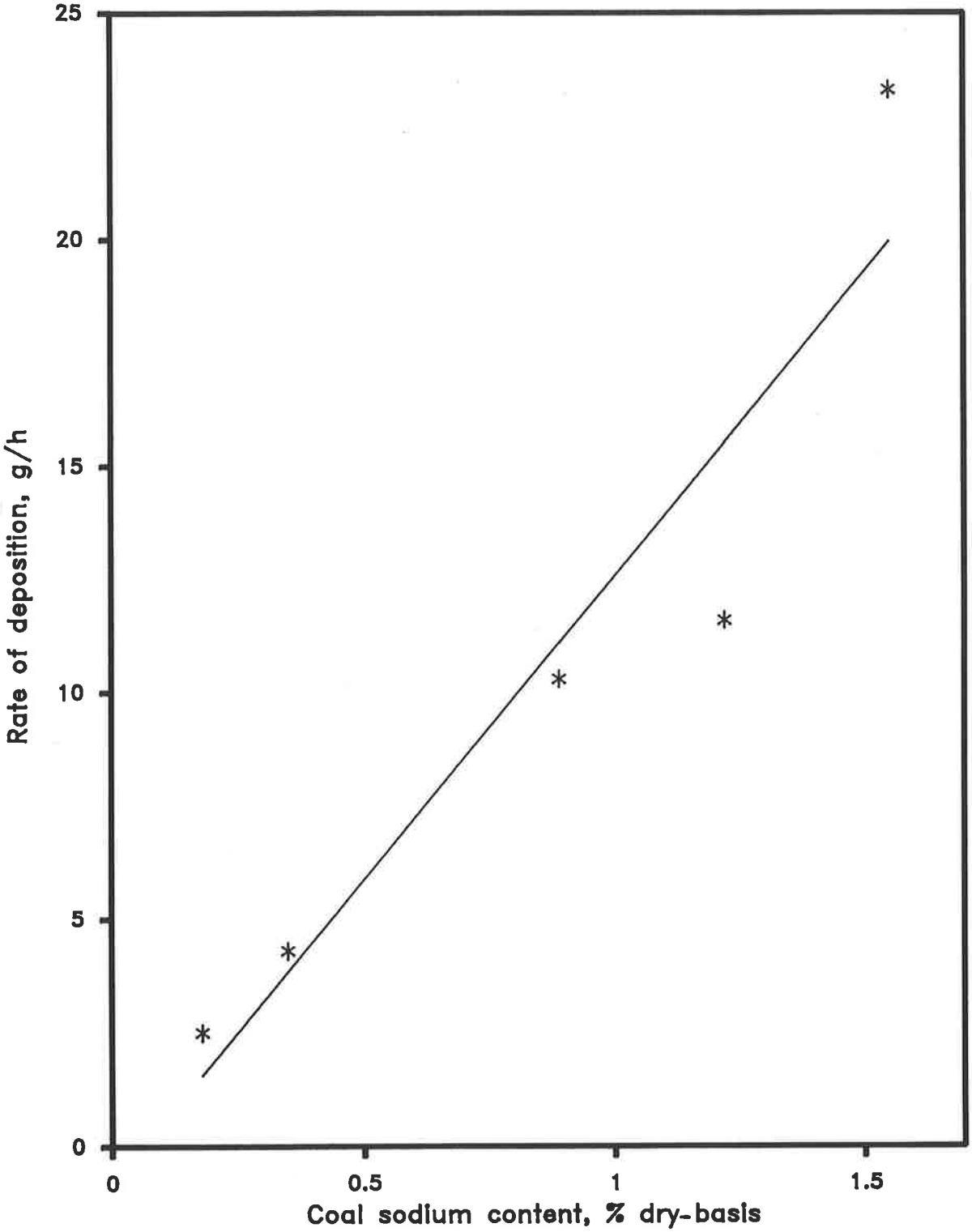

Figure 5.6:
Rate of deposition of coating vs sodium in coal

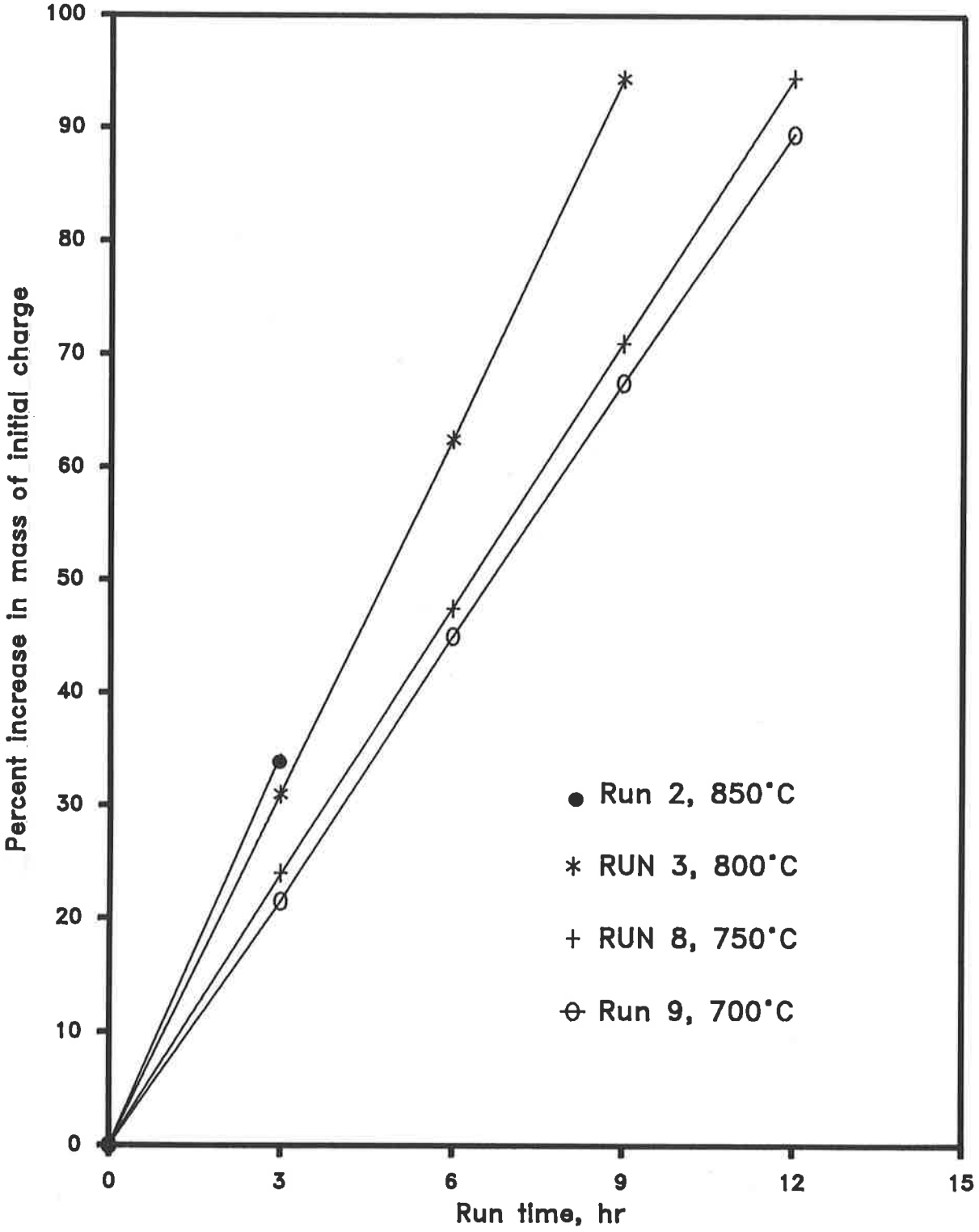

Figure 5.7:
Deposition of coating on the bed particles, effect of furnace temperature

The results indicate that the rate of deposition of the coating on the bed particles increases with furnace temperature, Figure 5.8. The effect of temperature on the chemical composition of the coating will be reported in Subsections 5.3 and 5.5.

Effect of Initial Bed Particle Size

An initial charge of the same amount of sand but of smaller size distribution (0.71 to 0.85 mm) was used to investigate the effect of initial bed particle size on the rate of deposition of the coating (Run 10), Figure 5.9. The combustion tests were carried out at a furnace temperature of 800°C using the low-mineral coal.

The results of Run 3, carried out under the same conditions but with an initial bed inventory of larger size distribution (0.85 to 1.0 mm), is given for comparison. The rate of deposition of coating on the bed particles for the initial charge of smaller size distribution was found to be slightly higher. However, the coating thickness would be smaller due to the greater surface area.

Effect of Bed Material

Dolomite was used as the initial charge to investigate the effect of bed material on the rate of deposition of coating on the bed particles using the low-mineral coal, Run 11. Dolomite, when calcined at temperatures prevailing in FBC, partially breaks down into particles too small to remain in the combustion zone of the FBCS. Therefore, dolomite was first thermally treated and the part remaining in the furnace was used for the combustion experiments.

The results, given in Figure 5.10, show that for the first few hours, the rate of increase in the mass of the initial charge is slow. This could be due to a combination of:

- the breakage of dolomite particles;
- slower rate of interaction between the molten ash on the char's surface and the dolomite particles at the early stages of deposition.

However, it appears that once the bed particles are fully coated, the rate of deposition of the coating on the bed particles becomes the same as that found with silica bed for similar conditions.

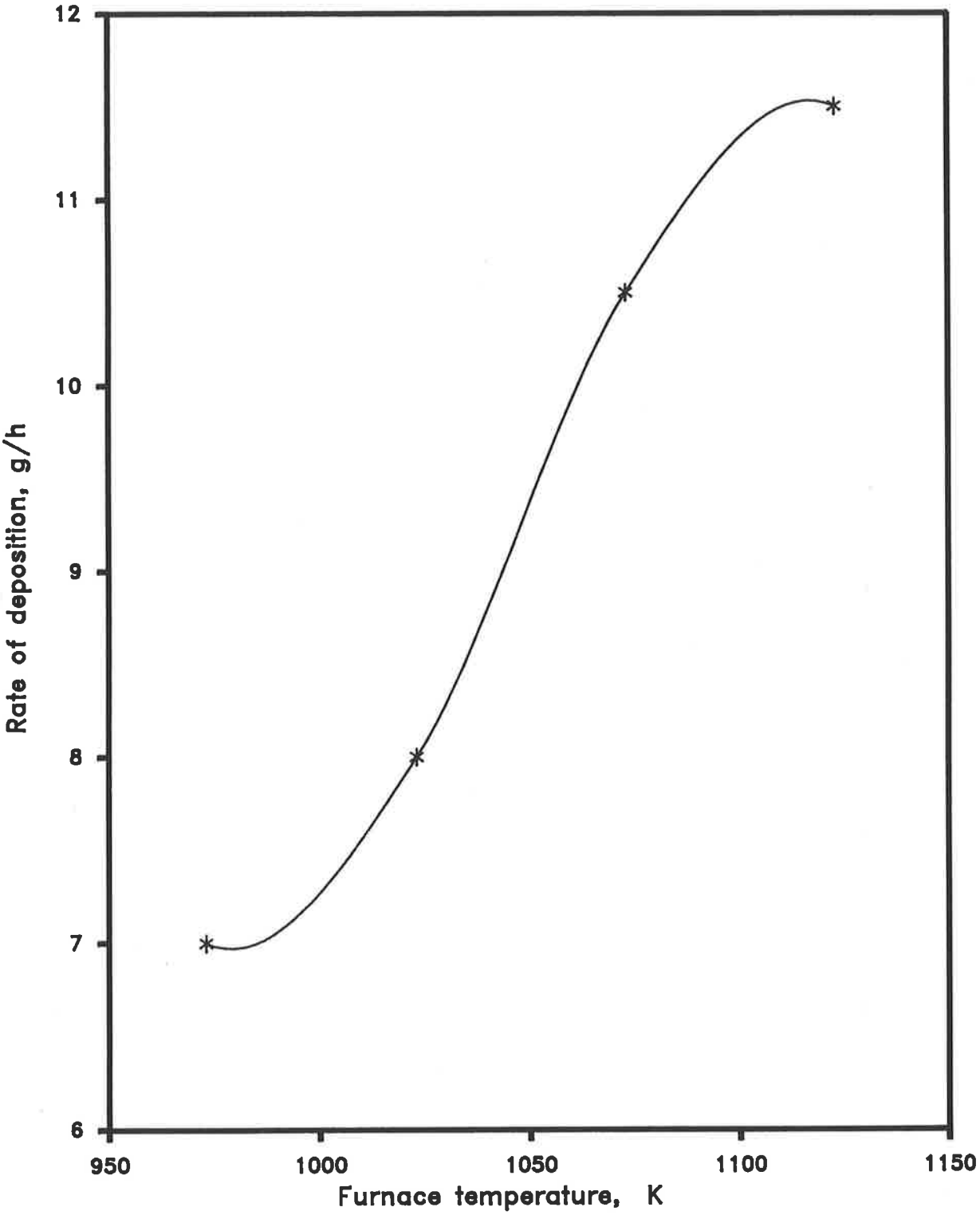

Figure 5.8:
Rate of deposition of coating, effect of furnace temperature

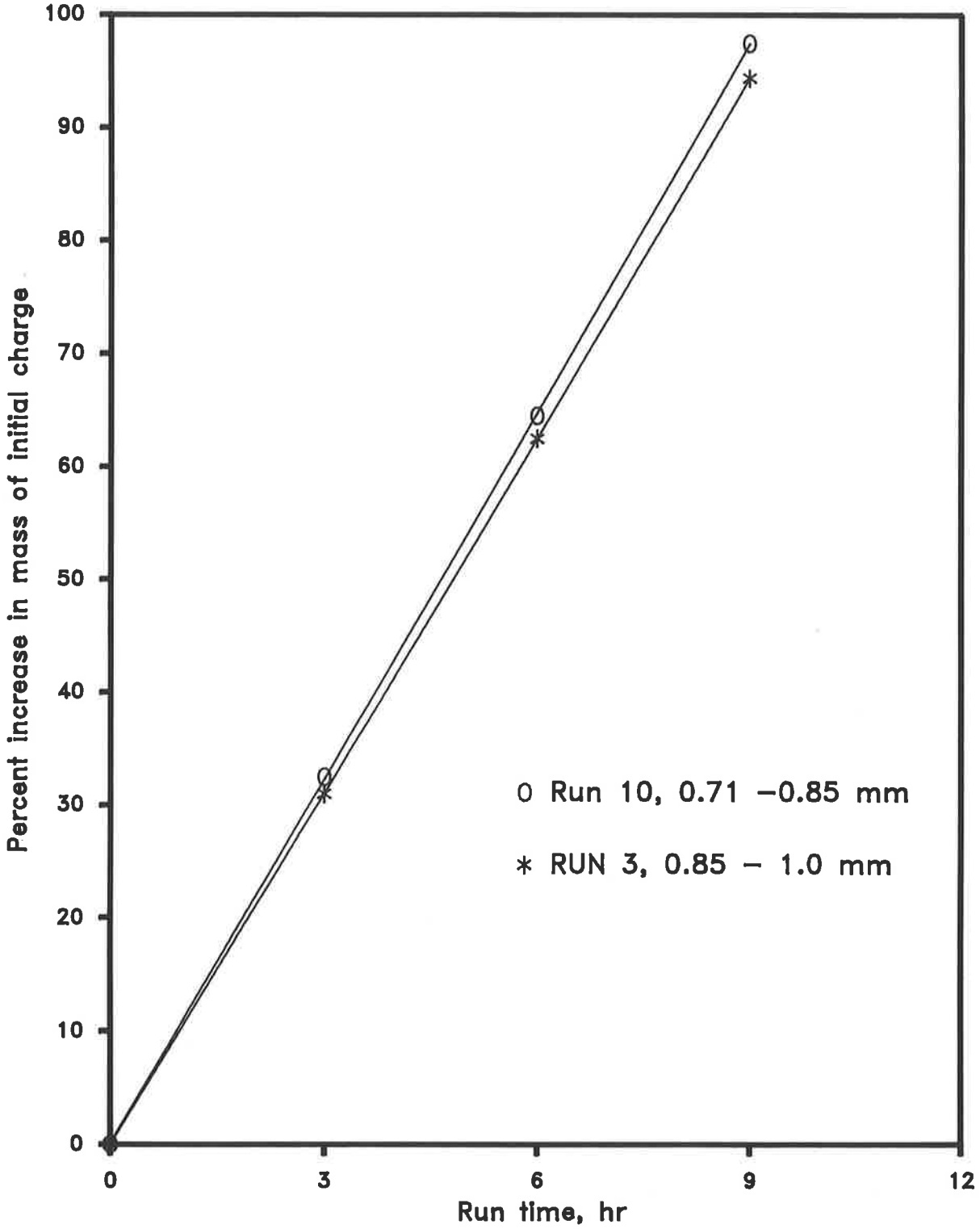

Figure 5.9:
Deposition of coating on the bed particles, effect of size distribution of bed material

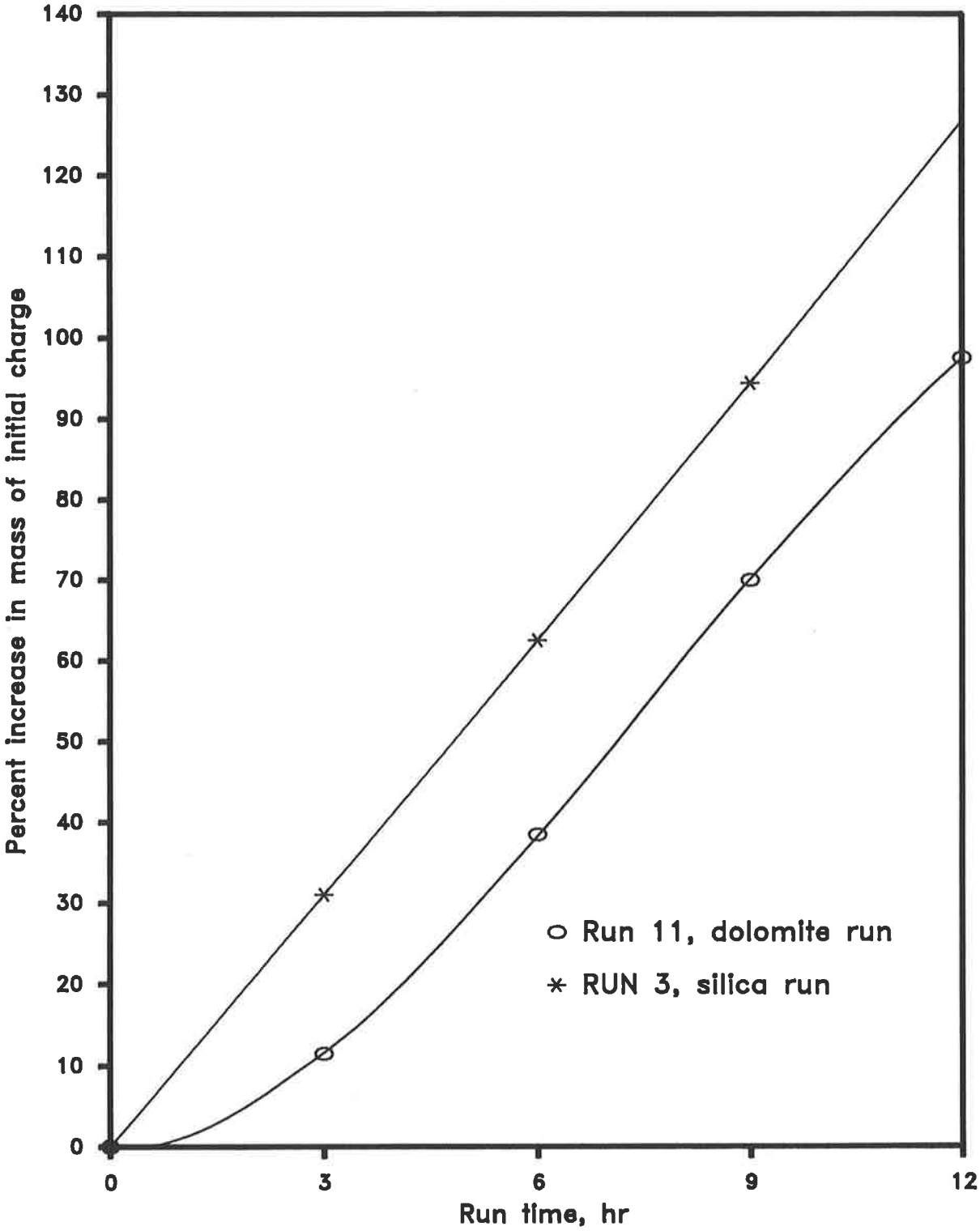

Figure 5.10:
Deposition of coating on the bed particles, effect of bed material

Effect of Excess Oxygen

Due to unstable operation and short duration of the tests (Runs 12 and 13), an assessment of bed particle growth and of deposition of the coating could not be made. The samples collected, however, have been analysed using various analytical methods (Section 5.5).

5.3 CHEMICAL COMPOSITION OF THE COATING

Bed material periodically removed from the furnace was sampled and analysed for the inorganic constituents using the Australian Standard Method AS 1038.14.1 - 1981. The results of the chemical analyses and their recalculations to different bases are given in the Appendix C.

The changes in composition of the inorganic constituents of the bed were plotted against operating time. A typical example is shown in Figure 5.11 for a silica bed run (Run 1). The most significant changes that occurred in the silica bed runs were: a sharp decrease in SiO_2 and a proportional increase in the ash forming inorganic constituents, calculated as SO_3, Na_2O, CaO, MgO and Al_2O_3. The results suggest that the highly sulphated ash, formed from the combustion of high-sodium, high-sulphur coal samples, deposits on the bed particles resulting in a gradual change in the composition of the bed material with operating time. The concentration of chlorine in the samples taken from the bed material was found to be negligible indicating the ash coating does not contain an appreciable amount of Cl compounds.

For the silica bed runs, the composition of the bed calculated on silica-free basis gives the composition of the ash coating on the same basis. Typical results, shown in Figure 5.12 for Run 1, indicate that the composition of the ash adhering to the quartz bed particles does not change significantly with operating time. Therefore, the average values of the compositions are used to compare the chemical characteristics of the coating formed under various conditions (Figures 5.13 to 5.16).

Effect of Coal Quality

Figure 5.13 gives the composition of the ash coating (on a silica-free basis) for Runs 1 and 2. The ash coating in Run 2, conducted with the low-mineral coal sample, has lower concentration of Al_2O_3 and Na_2O, and higher concentration of CaO and SO_3. The concentration of silica in the coatings, which was determined by electron microscopy (Subsection 5.3.2), was much higher for Run 1 compared to that for Run 2. The higher

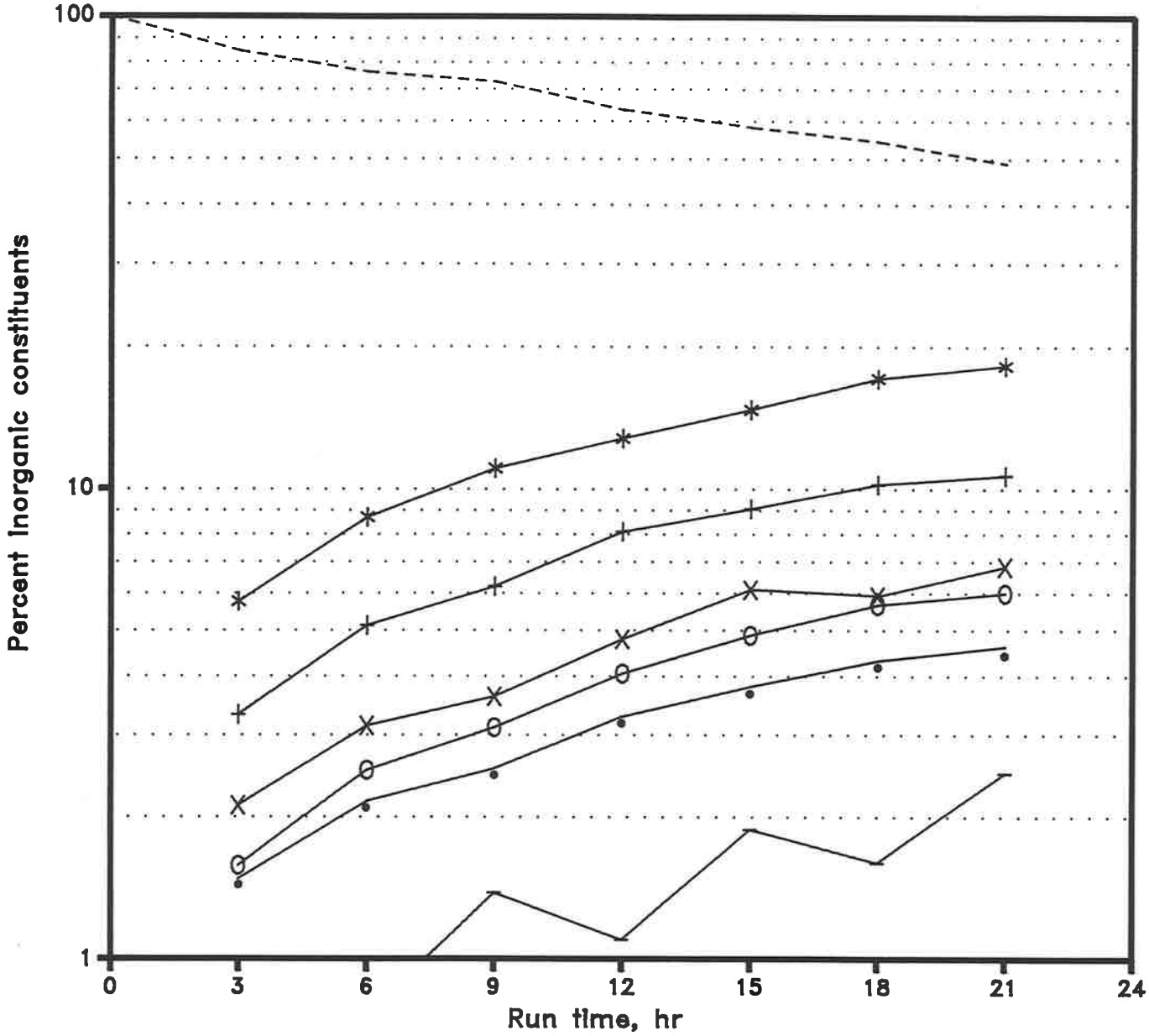

Figure 5.11:
Composition of bed material vs Run time silica run, Run 1

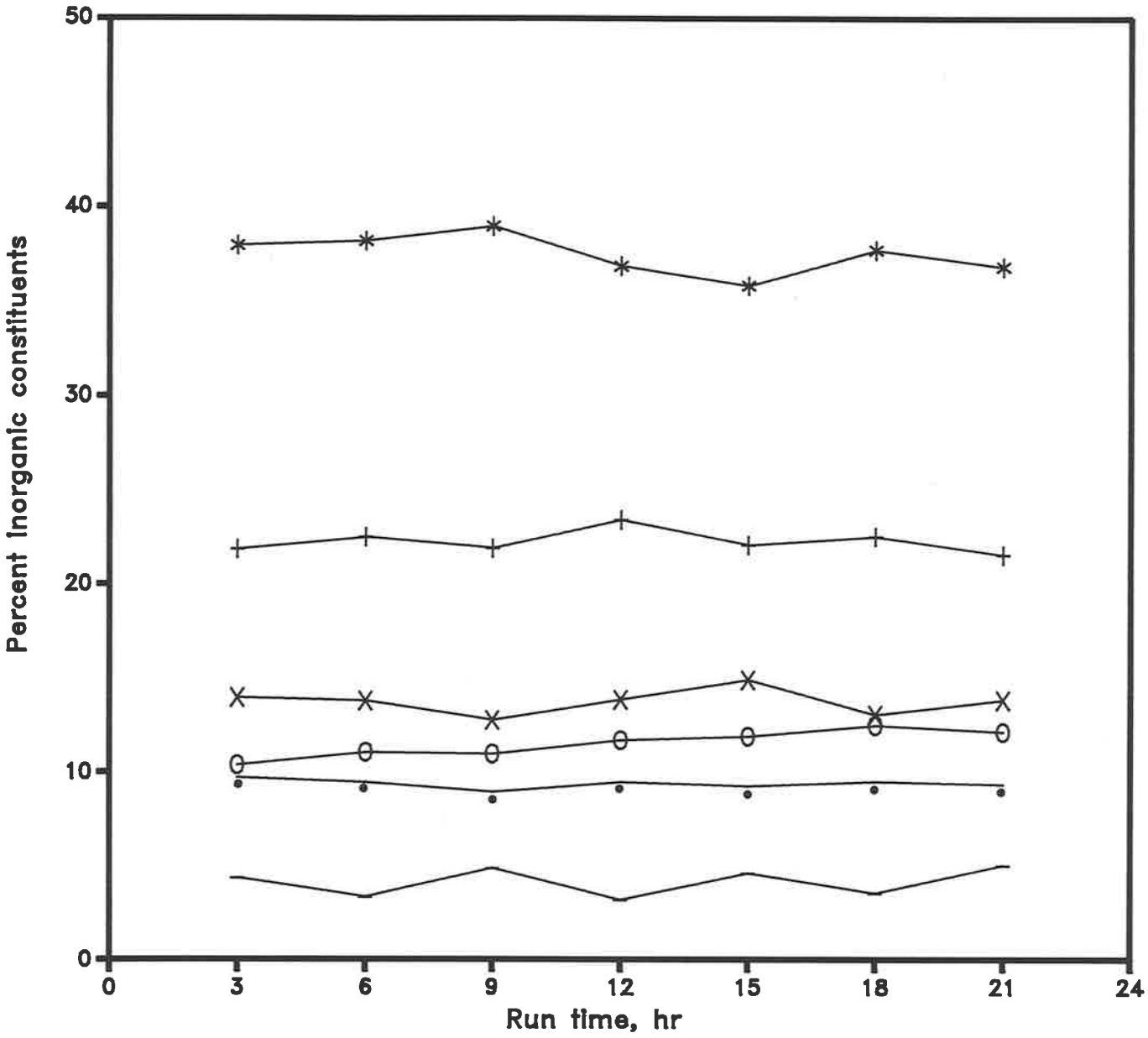

Figure 5.12:
Composition of coating on silica-free basis vs Run time, Run 1

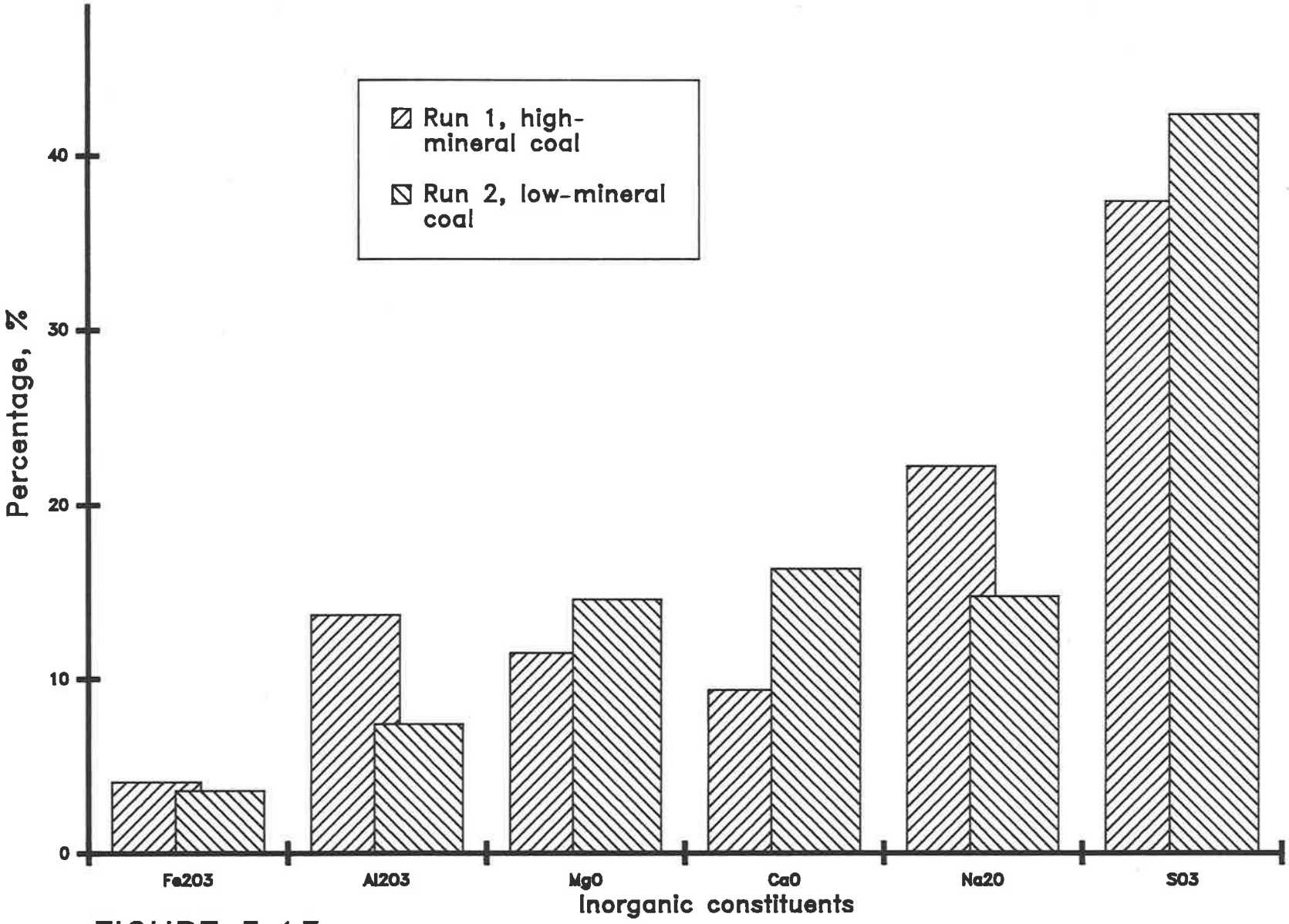

FIGURE 5.13 :

Effect of the mineral matter on coating composition (on silica-free basis)

concentration of Al_2O_3 in the coating of Run 1 is due to the presence of higher concentration of Al containing minerals (such as clays) in the high-mineral coal used in this run. The coal used in Run 2, with an ash composition rich in Ca, Mg and sulphated compounds and low in minerals, appears to have a greater tendency to cause deposition on the bed particles even though the concentration of sodium in the coating in Run 2 is lower than that of Run 1. Further discussions are given in Section 5.6.

Figure 5.14 gives the composition of the ash coating for the low-mineral coal sample (Run 3) and for the coal samples treated with water, acid and two solutions of sodium chloride (Runs 4 to 7 respectively). The removal of water-soluble sodium (Run 4) and part of the organically bound sodium (Run 5) reduces the concentration of sodium in the ash coating. As described in Section 5.2, the removal of sodium also reduces the rate of deposition of the ash coating on the bed particles.

The chemical analyses of the coatings formed during both Run 6 and 7 indicate the presence of a significant amount of chlorine (Appendix C). The proportion of Cl in the coating increases with the amount of NaCl added to the coal. The presence of chloride compounds in these coatings was also detected by electron microscopy and XRD analyses (Subsection 5.5.2 and 5.5.3). The results of these analyses indicate that part of the chlorine in the coating is present as sodium chloride. The Cl compounds seem to have the potential to form lower melting eutectics with other compounds present in the coating, hence resulting in a higher rate of deposition of the coating (in Runs 6 and 7) and in causing the defluidisation of the bed (in Run 7).

The chemical analyses of the coating, given in Figure 5.14, show a slight increase in the content of Na in Run 6. Such an increase is not evident in the case of Run 7. The reduction in the SO_3 concentration of the coating in Run 7 can not be explained.

Effect of Furnace Temperature

Figure 5.15 gives the composition of the ash coating formed during the combustion of the low-mineral sample at various operating temperatures (Runs 3, 8 and 9). The results indicate that the composition of the coating does not change significantly with furnace temperature. This suggests that, within the range tested, the transformations undergone by the inorganic matter during the fluid bed combustion of coal are not markedly affected by the furnace temperature. Similar conclusions were drawn from the results of single particle experiments (Chapter 4).

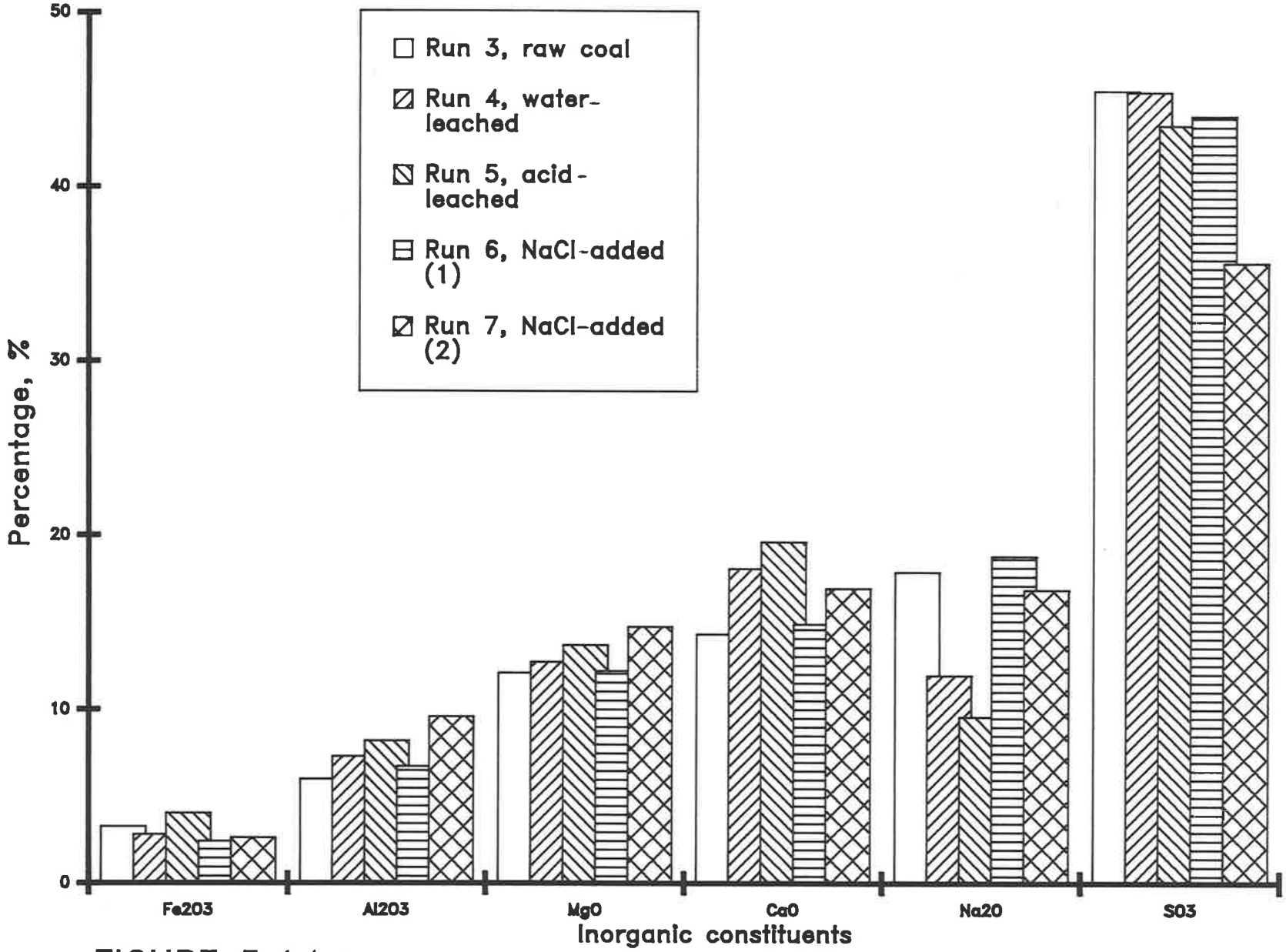

FIGURE 5.14 :

Effect of coal quality on coating composition (on silica-free basis)

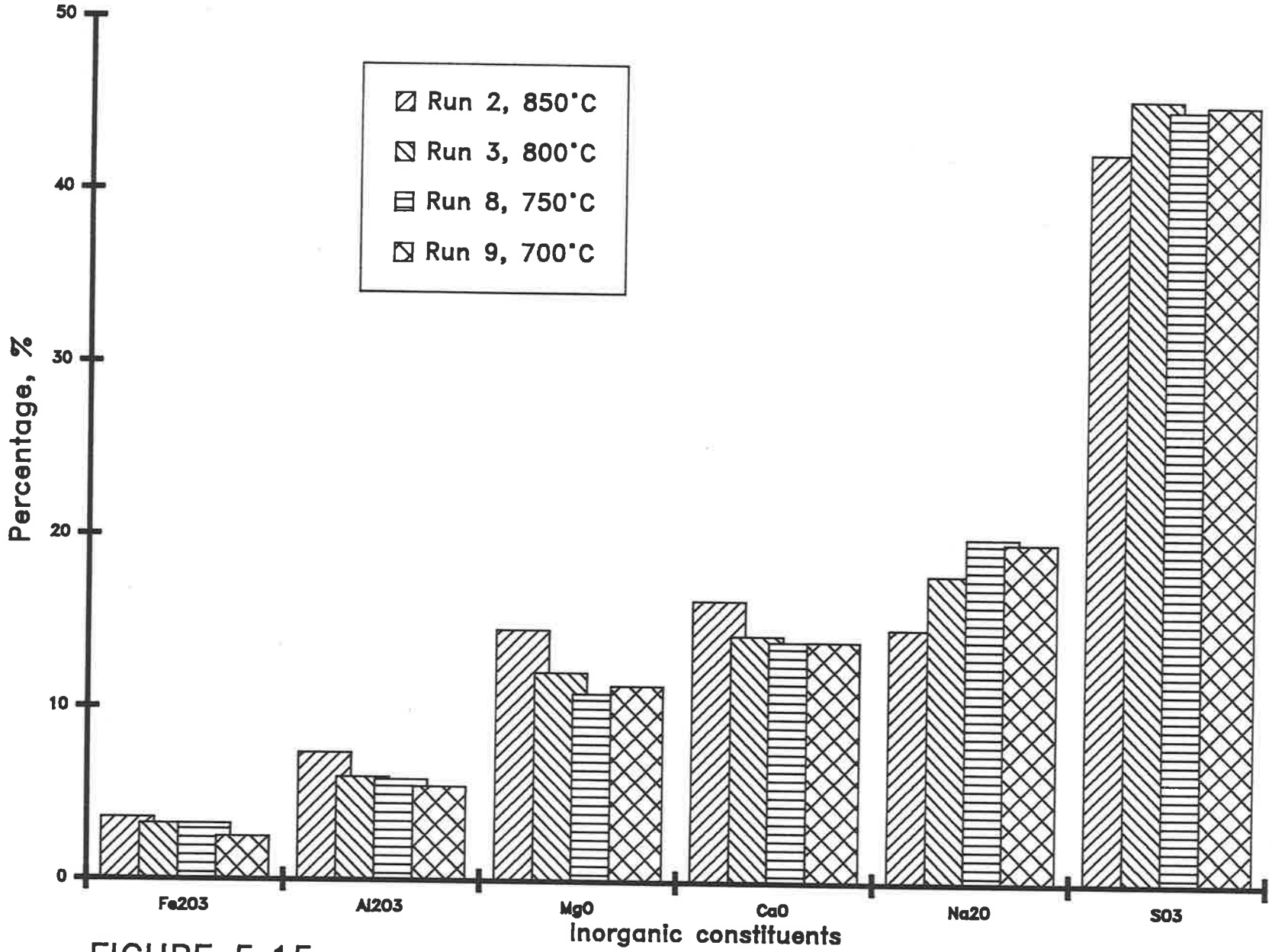

FIGURE 5.15 :

Effect of temperature on coating composition (on silica-free basis)

Effect of Initial Bed Particle Size

The comparison of the coating compositions for Runs 3 and 10 carried out with initial charges of different size distribution is given in Figure 5.16. The results indicate that, as expected, the initial size distribution of the bed material does not have an appreciable effect on the composition of the coating deposited on the bed particles.

Effect of Bed Material

Run 11 was conducted with an initial bed of dolomite. The chemical compositions of the bed material removed periodically from the furnace are shown in Figure 5.17. The composition at zero hour represents that of the initial charge. The dolomite used in the combustion experiment contained 52.5% SiO_2, 16.3% MgO, 15.7% CaO, 6.7% Al_2O_3, 2% Fe_2O_3 and minor quantities of other inorganic constituents. The most significant changes that occurred during the dolomite run were: a sharp decrease in SiO_2 and a proportional increase in the Na and S species, calculated as Na_2O and SO_3. The changes in composition of CaO, MgO, Al_2O_3 and Fe_2O_3 were found to be insignificant.

As dolomite contains most of the inorganic constituents forming the coating, the composition of the coating can not be estimated from the chemical analyses of the bed material. The characteristics of the coating and its interaction with the dolomite bed are investigated by electron microscopy. The results of these investigations are reported in Section 5.5.

Effect of Excess Oxygen

As discussed in Section 3.3, most of the experiments in the FBCS had to be carried out with an excess O_2 in flue gas of about 16%. In order to investigate the effect of excess oxygen on the composition of the coating, Runs 12 and 13 were carried out at excess O_2 levels of 5% and 12% respectively. The compositions of the coatings deposited on the bed particles during these runs, calculated from the chemical analyses of the bed material, are given in Figure 5.18. The results indicate that the concentrations of Na, S and Fe species in the coating slightly reduce with decreasing excess oxygen. The concentrations of Ca, Mg and Al in the coating increase proportionally. It should be noted that, due to difficulties in conducting Runs 12 and 13 over an extended time, the concentrations of the coatings were estimated from a limited number of chemical analyses. Hence, the differences in compositions of the coatings, which are not significant, might be due to analytical and experimental errors. The electron microscopic examination of the coatings formed during Runs 12 and 13, reported in Subsection 5.5.2, does not suggest that these coatings are appreciably different in composition from those of other runs.

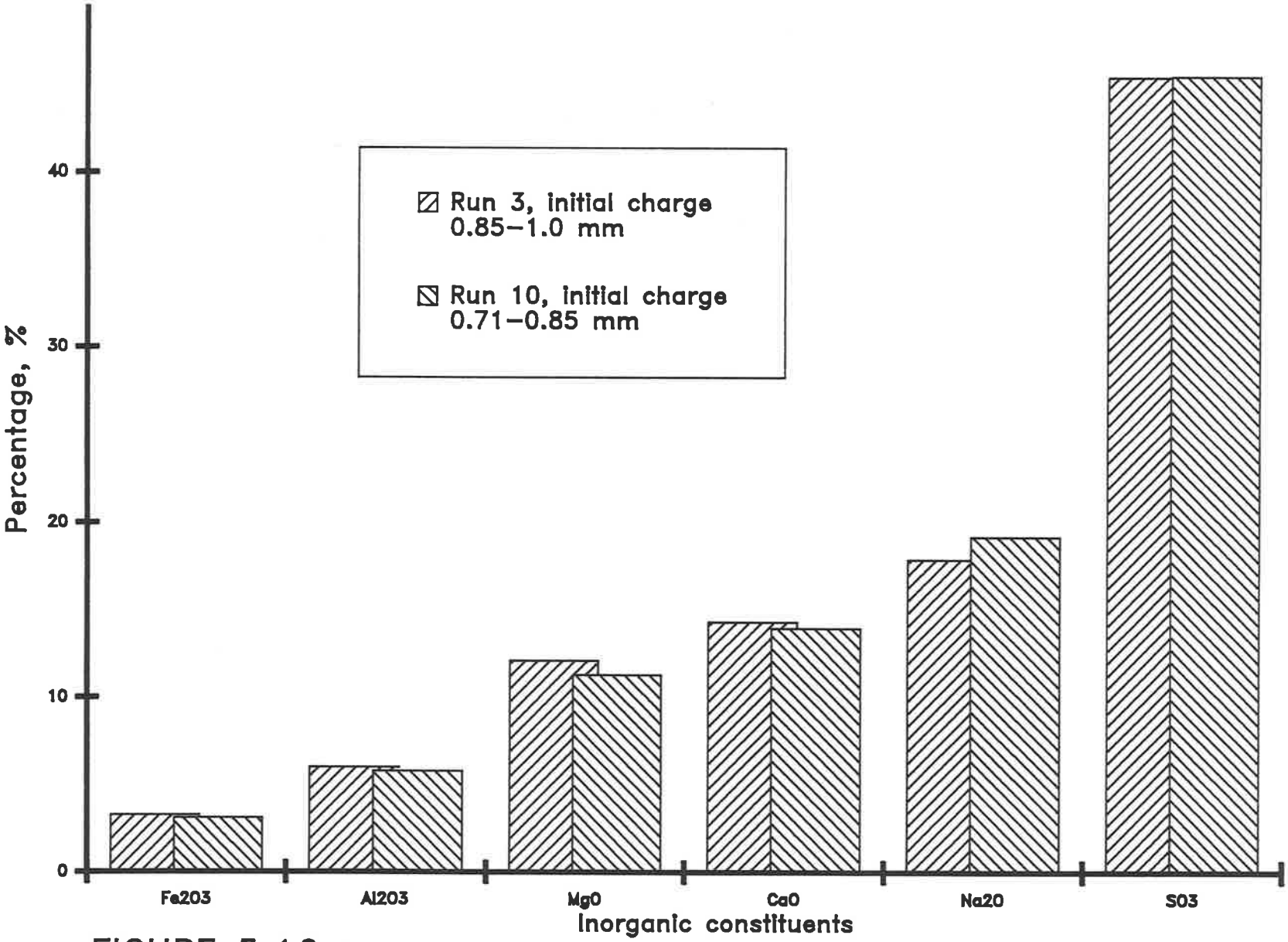

FIGURE 5.16 :

Effect of size distribution of bed material on coating composition (on silica–free basis)

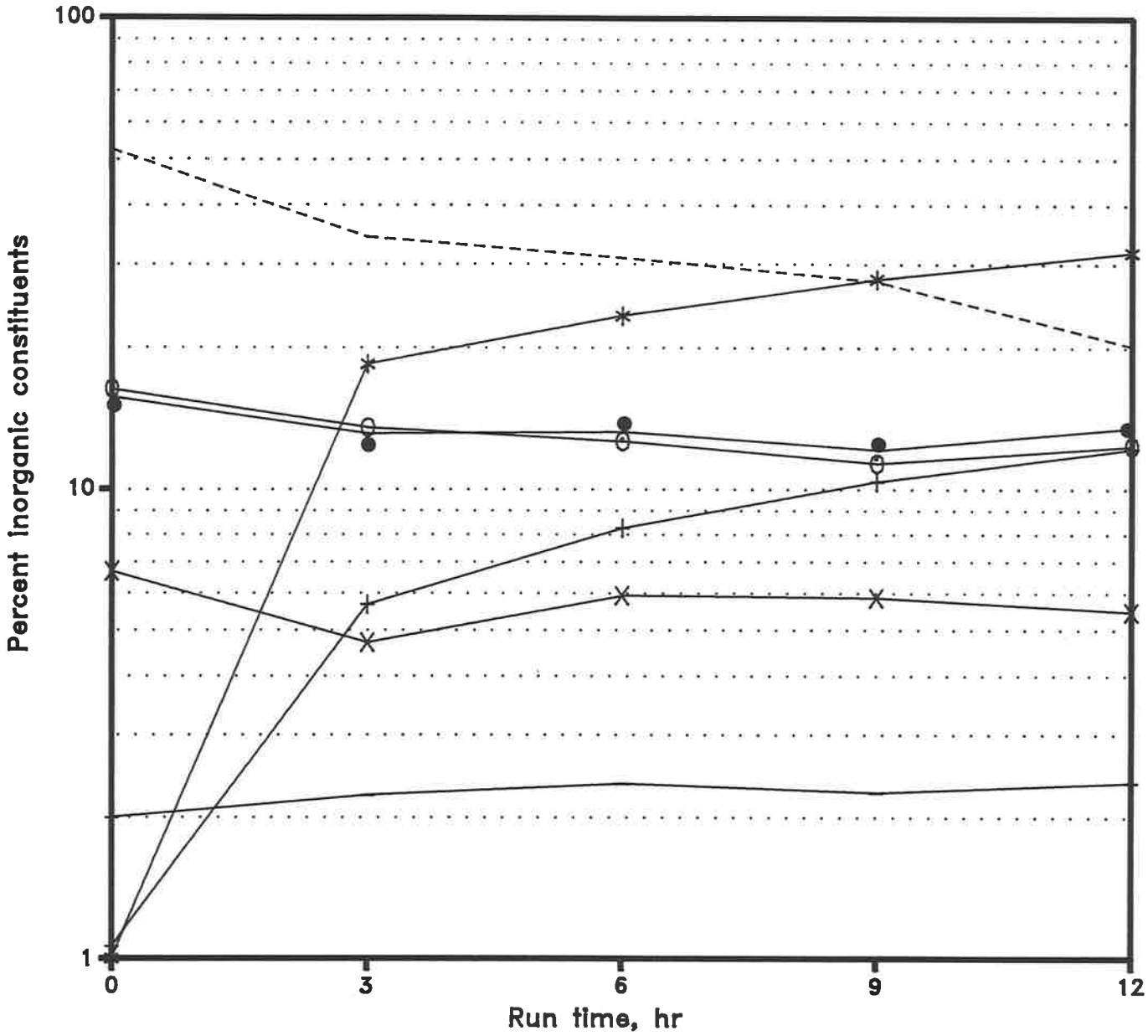

Figure 5.17
Composition of bed material vs Run time dolomite bed, Run 11

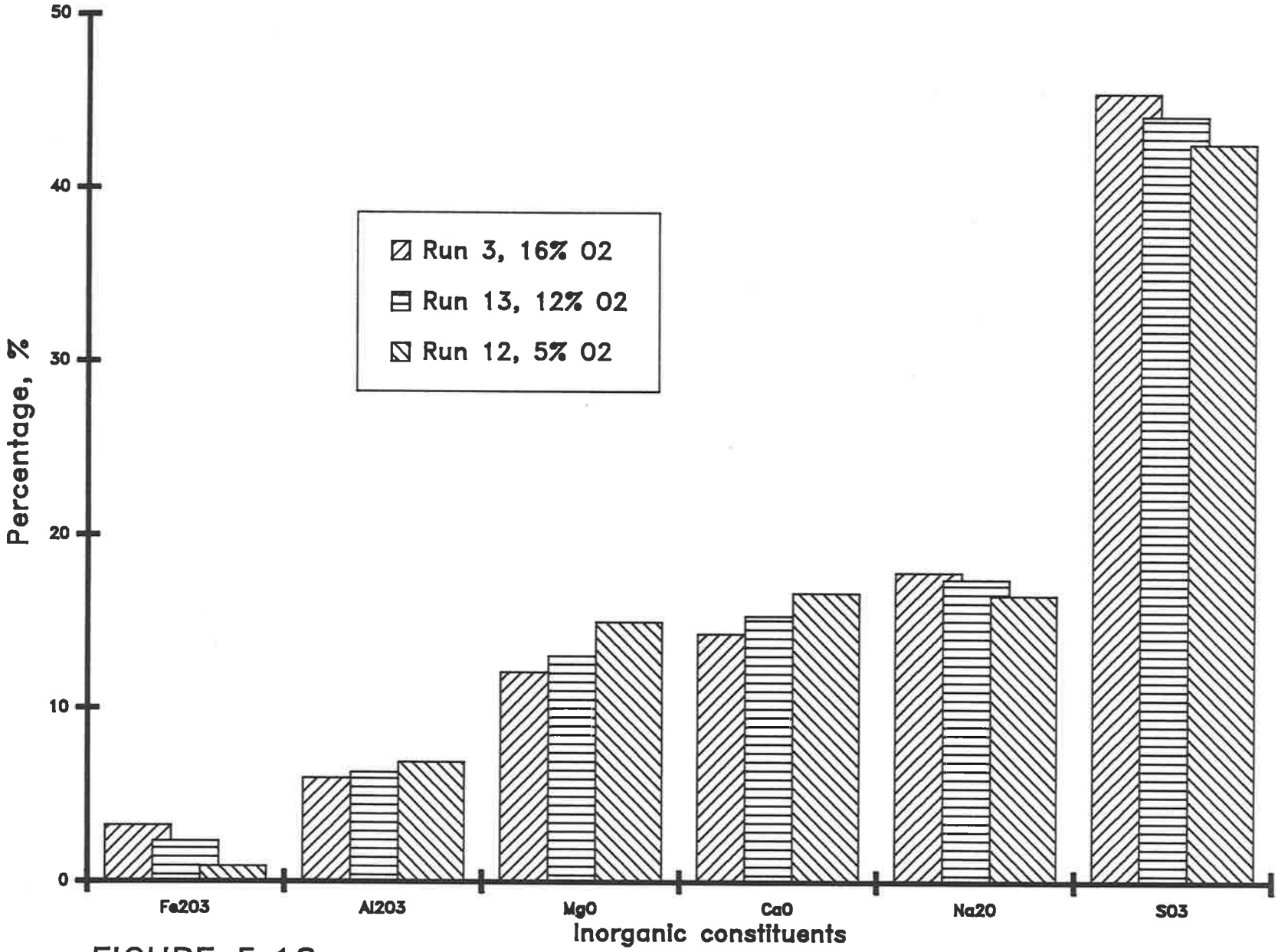

FIGURE 5.18 :

Effect oxygen partial pressure on coating composition (on silica-free basis)

5.4 DISPROPORTIONING OF ASH COMPOSITION

Ash collected in the cyclone was also periodically sampled and analysed by the chemical methods described in Subsection 3.5.1. Figure 5.19 gives the composition of cyclone ash as a function of operating time for Run 1. The results indicate its composition remains relatively constant during the run. However, the concentration of SiO_2 appears to be higher in the first sample taken from the cyclone ash after 3 hours of operation, with a proportional reduction in the concentration of the other inorganic constituents in that sample. Similar results were found in all the silica runs. The higher SiO_2 concentration in the first sample taken from the cyclone ash is due to the breakage of small amount of weaker sand particles at the early stages of the runs.

The composition of the cyclone ash calculated on a silica-free basis (Appendix C) was found to be constant for each run. A typical example is graphically shown in Figure 5.20.

As reported in Section 5.3, the composition of the coating deposited on the bed particles, calculated on a silica-free basis, was also found to be constant for the duration of each run. Hence, the average composition of the ash leaving the combustor (cyclone ash) and that of the ash deposited on the bed particles (coating) were compared with the composition of the coal ash (that is ASTM ash). Typical results (for Runs 1 and 3) are given in Figures 5.21 and 5.22 respectively. The results indicate that, regardless of the coal fired:

- the coating is enriched in S and Na compounds; and
- the cyclone ash is enriched in Ca, Mg and Al compounds.

It appears that the coating is enriched in those species which formed a molten phase on the char's surface during the single particle experiments, Chapter 4. Solid phases consisting mostly of Ca, Mg and Al are preferentially found in the cyclone ash.

A mass balance on the individual inorganic constituents can not be carried out as the amount and composition of the gaseous species, sub-micron particle and furnace wall deposits are not known. Furthermore, the composition of the coating could be determined only on a silica-free basis.

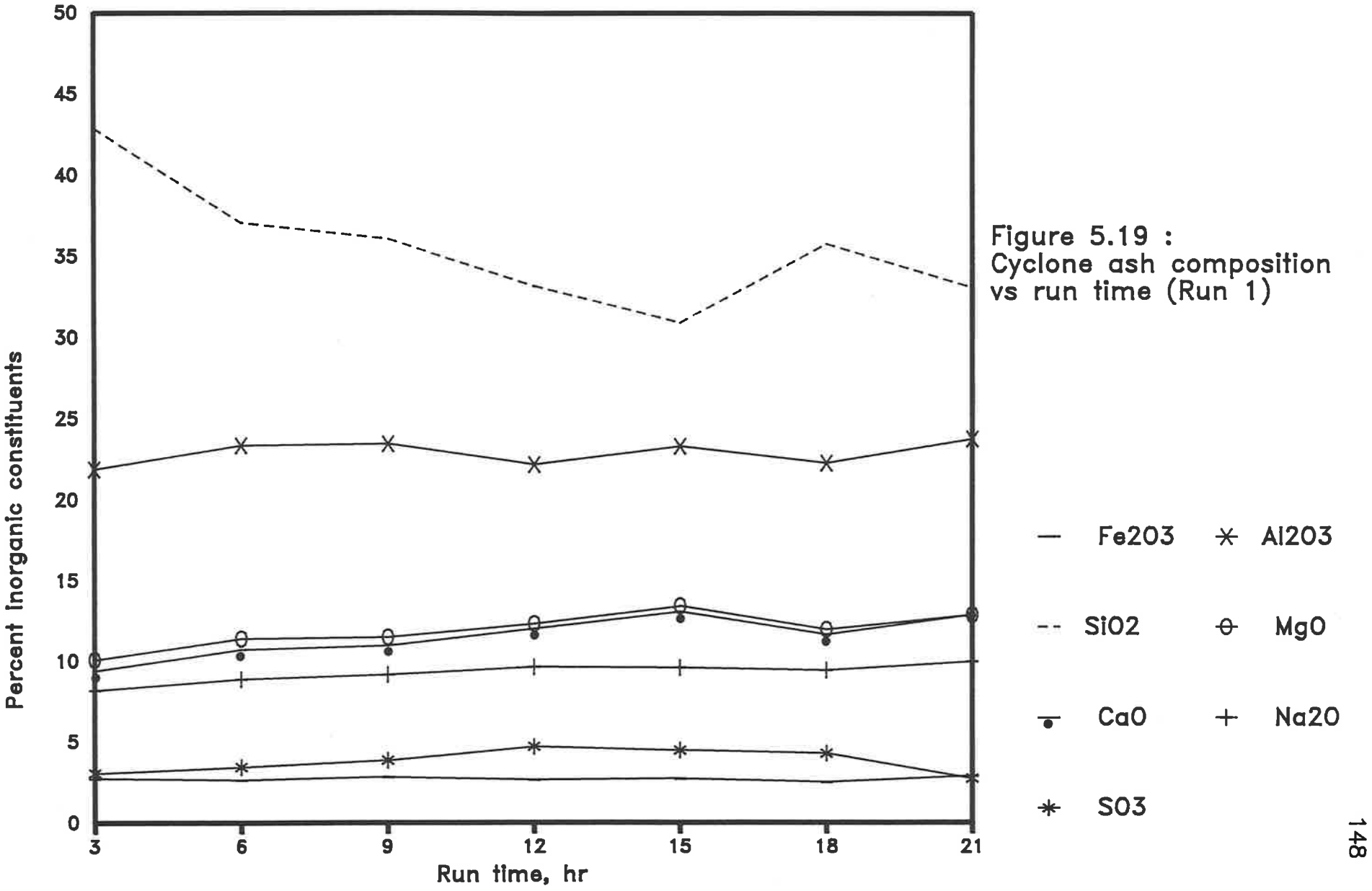

Figure 5.19 :
Cyclone ash composition
vs run time (Run 1)

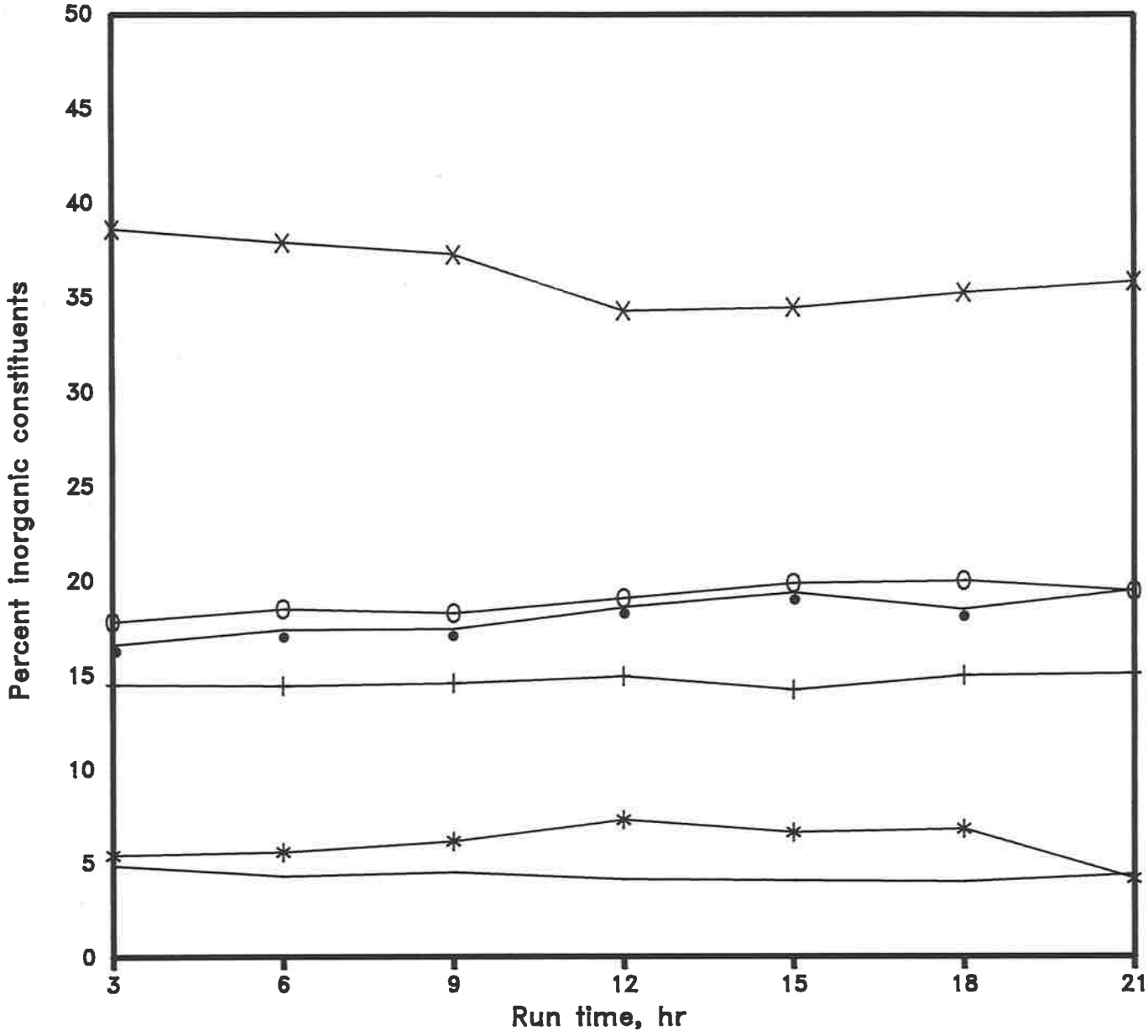

Figure 5.20
Cyclone ash composition (on silica-free basis) vs run time, Run1

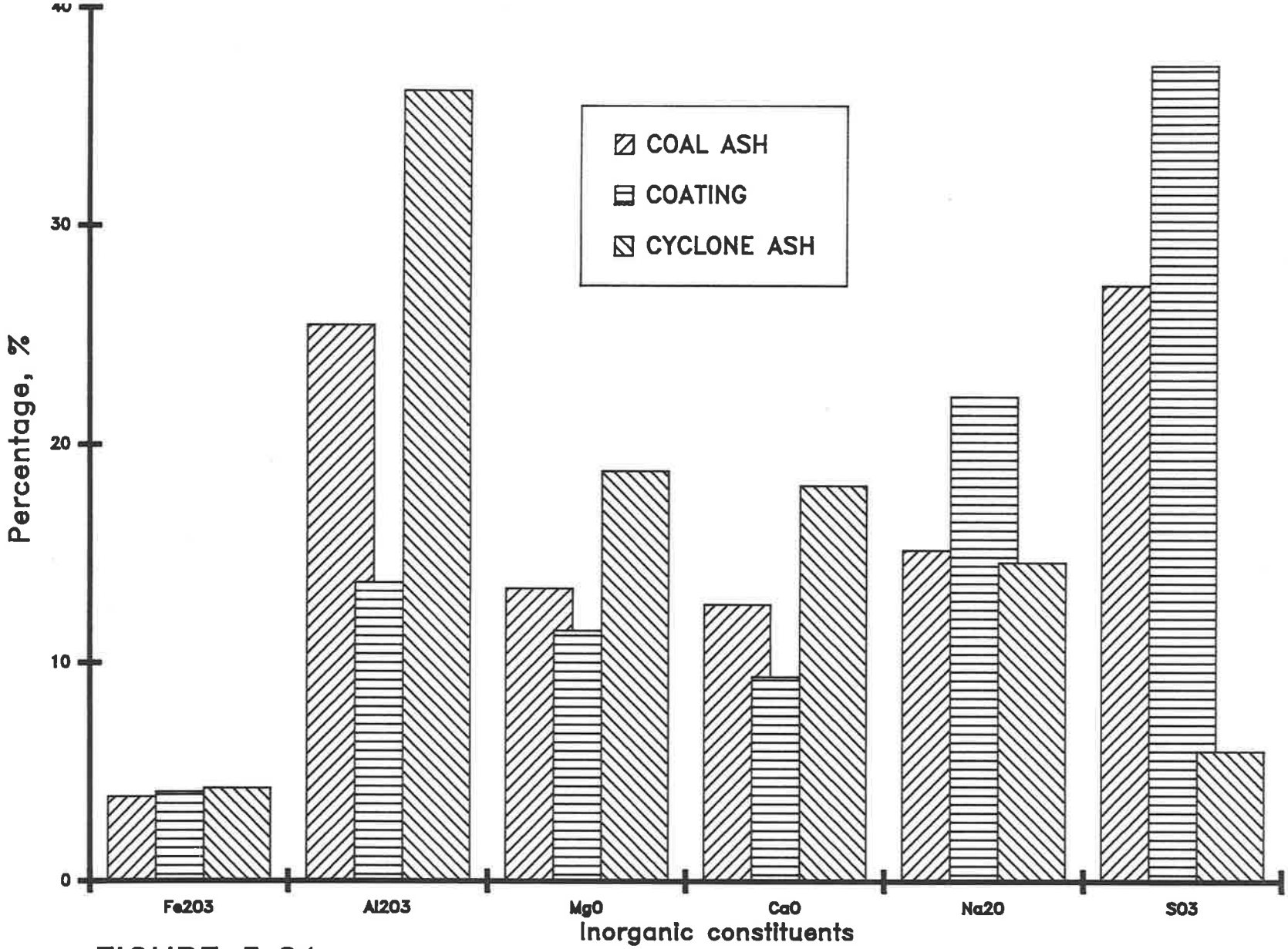

FIGURE 5.21 :

Disproportioning of ash composition, Run 1

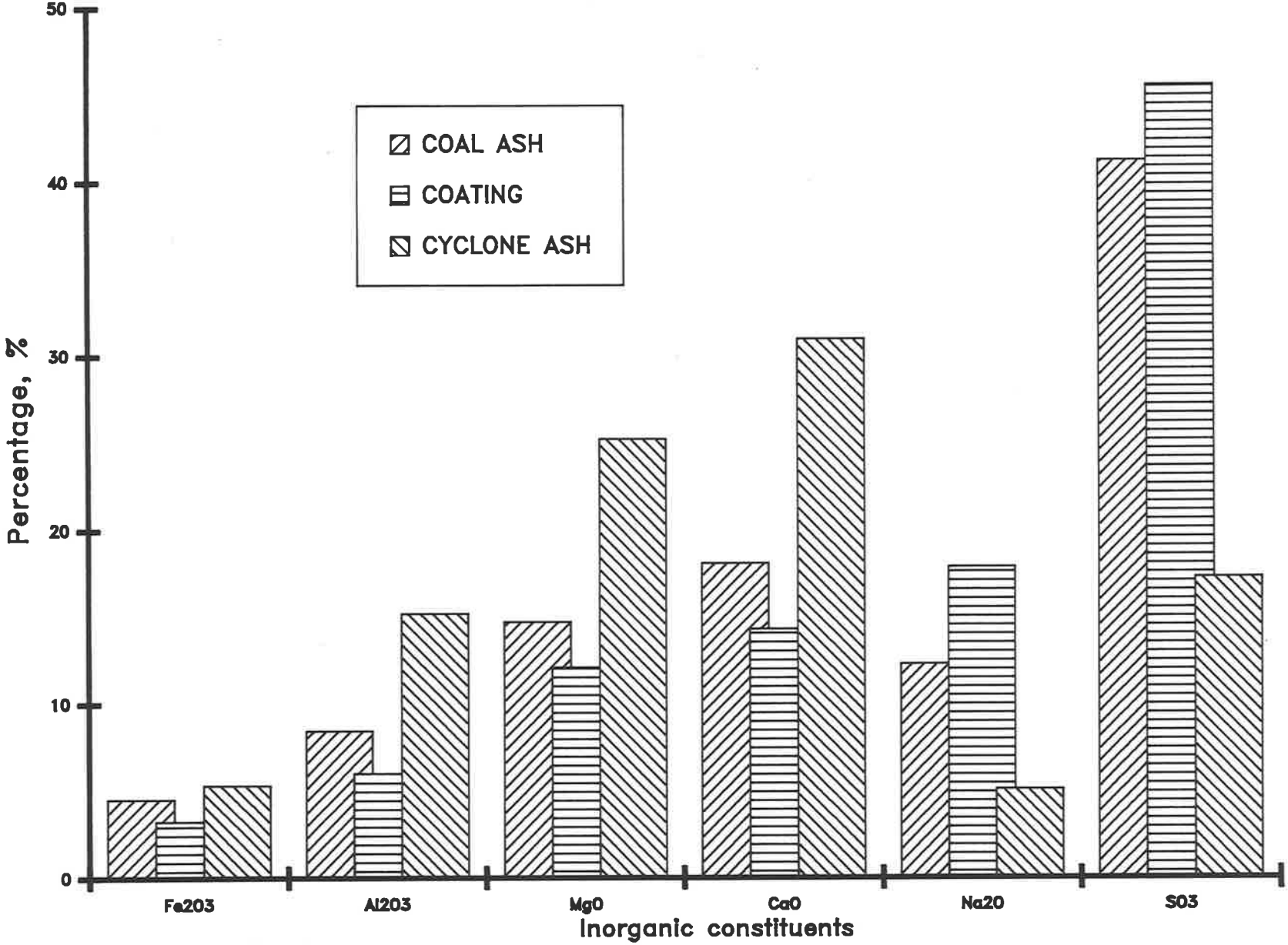

FIGURE 5.22 :

Disproportioning of ash, Run 3

5.5 CHARACTERISATION OF COATING

5.5.1 EXTRACTION METHOD

Samples of bed material and the coal fired in each run were analysed for the water-soluble, acid-soluble, and acid-insoluble inorganic constituents using the extraction methods described in Chapter 3. The results of the analyses of the inorganic matter in coal are presented on a dry-basis (Appendix C). The analyses of the bed material are given as a percentage of total inorganic matter.

Sulphur in Lochiel coal is predominantly organically bound and hence acid insoluble. However, the products of its transformations, which deposit on the bed particles, are water and acid soluble. The proportion of acid and water-soluble sulphur in the coating varies depending on the quality of the coal fired.

About two third of sodium in the raw coal is water soluble and the rest is acid soluble. The analyses of the bed material indicate that sodium is present in the coating as water and acid soluble. The results for the runs carried out with the treated coal samples (Runs 4, 5, 6 and 7) are not conclusive due to the alteration of the ion-exchange positions in the coal as a result of treatment.

Calcium in the coal is mostly organically bound and hence acid soluble. The analyses of the bed material indicate that a significant proportion of calcium in the coating is water soluble.

Similar to calcium, the magnesium in the coal is predominantly organically bound and hence acid soluble. In the coating, however, magnesium is present as acid soluble and acid insoluble; only a small proportion of magnesium is present as water soluble.

A large proportion of aluminium, which is also organically bound, transforms into acid-insoluble compound(s). The remaining aluminium species in the coating are acid soluble. The proportion of water-soluble aluminium in the coating is insignificant.

Iron is present in the coal mostly as acid insoluble. The analyses of the bed material indicate that a proportion of acid-insoluble iron transforms into acid soluble.

The analyses also confirmed that chlorine is not present in the coating in an appreciable proportion. The contents of other inorganic elements (including silicon) in the coating are insignificant.

The extraction method, by its own, can not determine the mineralogical composition of the species present in the coating. However, the results indicate:

- the water-soluble sodium is likely to be sodium sulphate;
- the acid-soluble sodium is likely to be a combination of:
  - + complex compounds of sodium with other inorganic elements;
  - + sodium aluminium silicates; and
  - + sodium sulphate which, due to its intimate distribution with insoluble compounds, does not dissolve in water during the extraction process.
- calcium is likely to be present as calcium sulphate or in combination with other inorganic compounds (such as sodium and magnesium sulphates). The water-soluble calcium could also be attributed to calcium sulphate (solubility 0.2 parts in 100 parts of water, Dean, 1985). Considering that a relatively large amount of water is used for the extraction process (Chapter 3), a significant proportion of calcium sulphate is likely to be dissolved;
- Magnesium and aluminium can form a combination of MgO, Al_2O_3 and Al_2MgO_4 (spinel). A small proportion of water-soluble magnesium in the coating could be attributed to magnesium sulphate. The presence of acid-insoluble Mg and Al species in the coating could be due to the formation of complex compounds (such as silicates). These compounds did not dissolve even in a stronger acid.

The indications given in this section about the possible inorganic species in the coating agree with the thermodynamic calculations reported in Chapter 4 (Subsection 4.4).

5.5.2 ELECTRON MICROSCOPY

The bed material periodically removed from the furnace was also subjected to microscopic examination. Polished cross-sections of the bed particles were examined using an electron microprobe (EMP) equipped with an energy dispersive X-ray analysis system (EDAX). The EMP was operated in the back-scattered electron imaging mode to examine the growth of the bed particles and the composition of the coating deposited on the bed particles.

Duplicate samples were used to study the morphology and the qualitative analysis of the surface of the coating deposited on the bed particles using scanning electron microscopy (SEM). The SEM was operated in the secondary electron image. The description of the electron microscopes used and of the sample preparation are given in Subsection 3.5.2.

FBC of High-Mineral Coal Sample (Run 1)

The growth of the bed particles, due to the formation of coating on their surface, as a function of operating time is shown in Figure 5.23, Micrographs (a) to (e). The intensity of the back-scattered electron image is proportional to the atomic number of the material being subjected to the electron beam. Hence the darker area in the core of the bed particles represents the parent silica bed particles which have lower atomic numbers compared to the material in the coating. The thickness of the coating can be estimated from the bar shown on the bottom left side of the micrographs.

Micrograph (a) shows that a light and scattered coating has formed on the silica bed particles after 0.5 hour in the furnace. The coating seems to be the result of scattered deposition of ash on the bed particles rather than gas-solid interaction or vapour condensation.

After 3 hours in the furnace, Micrograph (b), the coating has become more consolidated and covers the entire surface of the silica sand.

Micrograph (c) shows the growth of the coating after 6 hours in the furnace. The coating appears to have a porous structure.

Micrographs (d) and (e) show the growth of the coating after 12 and 18 hours respectively

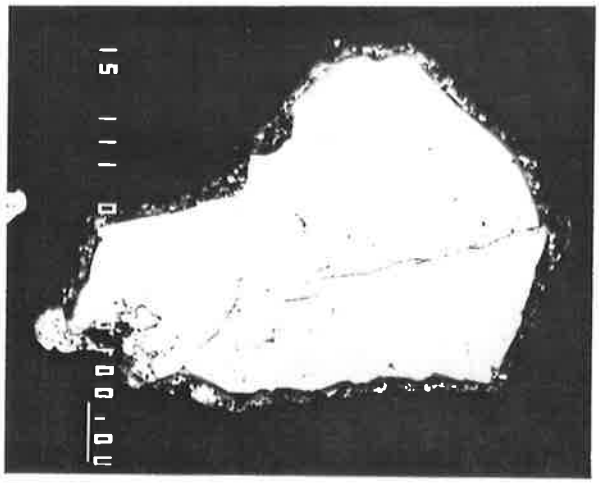

Figure 5.23 (a)= 1/2 hour

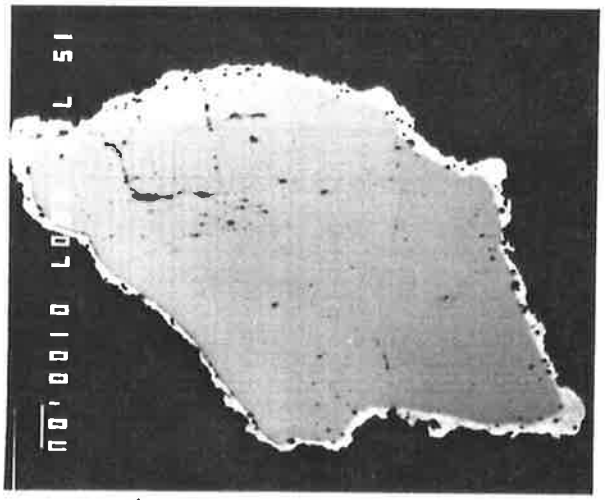

Figure 5.23 (b)= 3 hours

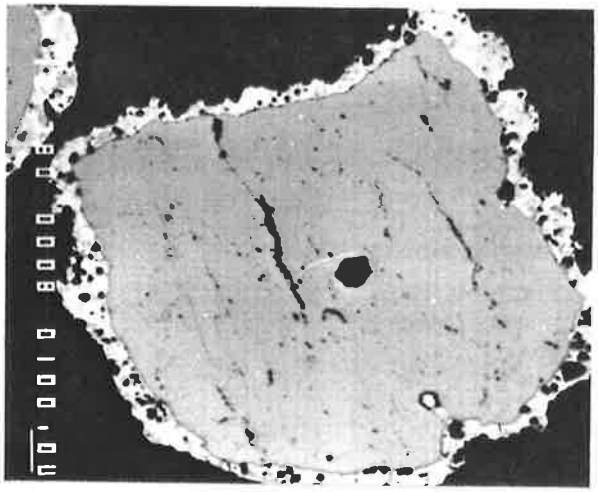

Figure 5.23 (c)= 6 hours

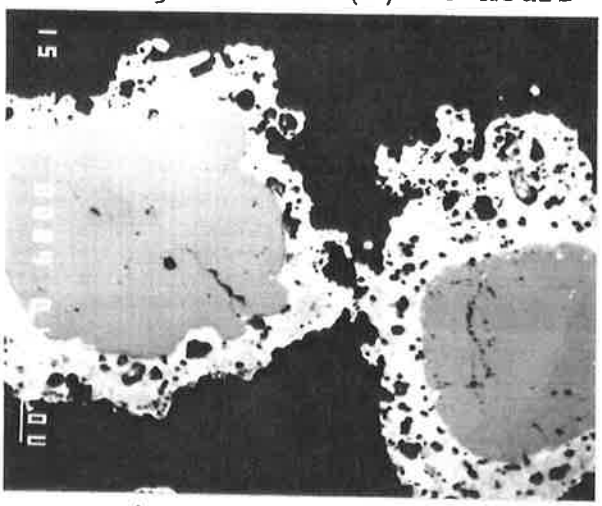

Figure 5.23 (d)= 12 hours

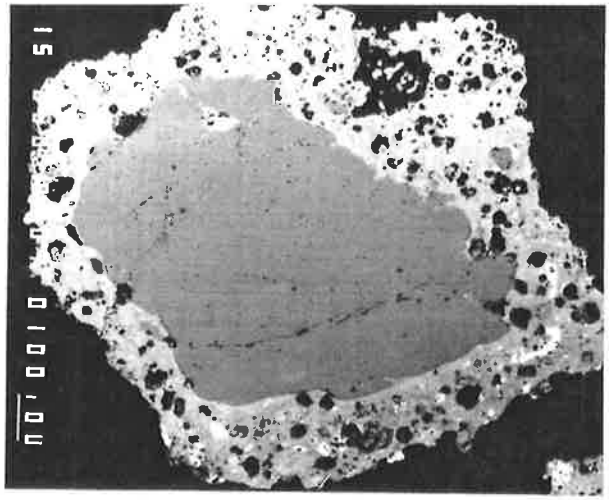

Figure 5.23 (e)= 18 hours

Figure 5.23: **Back-scattered Electron Images of Polished Cross-Sections of Bed Particle After Various Operating Time (Run 1)**- Bright bands around the bed particles show the coating. 100μm bar is shown on the left.

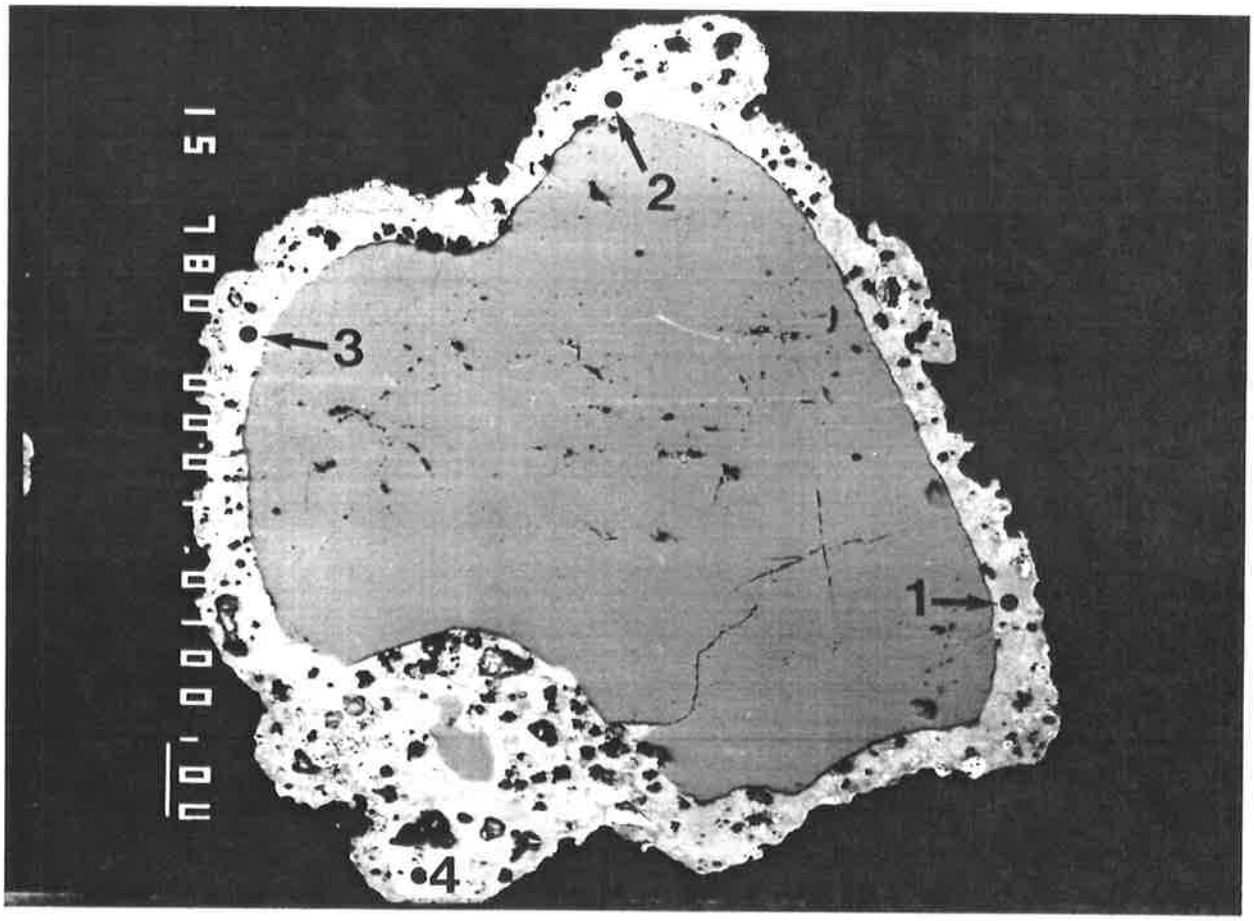

Positions Analysed:	Na_2O	CaO	MgO	SO_3	Al_2O_3	SiO_2	K_2O	P_2O_5	Cl	FeO
1	10.5	15.8	4.6	62.3	5.3	0.6	0.5	-	-	0.3
2	5.7	9.1	17.3	47.1	17.8	1.7	0.4	-	-	0.4
3	6.3	10.7	14.1	54.8	10.9	1.7	0.4	-	-	0.7
4	2.2	32.9	10.3	1.8	17.5	32.0	-	-	-	1.7

Figure 5.24: **Back-scattered Electron Image of a Polished Cross-Section of a Bed Particle (Run 1)** - EDAX analyses of selected positions are presented. Bright bands around the bed particle show the coating. 100μm bar is shown on the left.

Figure 5.24 shows a bed particle removed from the furnace after 9 hours. The porous structure suggests that, while it has adhered to the surface of the silica bed particles, the coating has not undergone extensive fusion. The analyses of the coating show that it is highly sulphated and contains significant amount of sodium, calcium, magnesium and aluminium. Small amount of Fe and K species and almost no chlorine were detected in the coating. The presence of minerals trapped in the coating (Position 4) is evident. The analyses indicate that the composition of the coating is not uniform and, on average, it agrees with those calculated from the chemical composition of the bed material, Section 5.3.

In order to demonstrate the distribution of various elements in the coating, X-ray mapping was carried out on the same sample using the EMP, Figure 5.25. The X-ray images show that the coating consists of a matrix of S, Ca, Na, Mg and Al in which Si and Al containing minerals are embedded. A small amount of Si is intimately distributed through the coating matrix.

Figure 5.26 shows a micrograph of the polished cross-section of a bed particle at high magnification (540x) and gives the analyses of the coating at various distances from the surface of the silica bed particle. The results do not suggest a trend for the variation in concentration of the inorganic species as a function of the distance from the coating-silica interface. The backscattered electron image of the bed particle indicates that, although the coating has formed over 3 periods of 3 hour duration, there is no boundary between the layers of coating formed in each of these periods. In fact, a trial run carried out over 9 hour continuous operation resulted in the formation of a similar coating. This indicates that the periodic removal of the bed from the furnace for weighing, size distribution analysis and sampling did not affect the characteristics of the coating.

The micrograph in Figure 5.26 also shows that there is a clear boundary between the parent silica particle and the coating deposited on it suggesting the lack of chemical reaction between silica and the coating material. The X-ray image of Na, given in Figure 5.26, does not suggest a reaction of this element with silica prior to the deposition of the coating as such reaction would have resulted in a higher concentration of Na on the surface of the parent silica particles. Hence, it appears that the formation of the coating is a physical process caused by the deposition of molten ash on the surface of the bed particles. Once the silica particles are coated, the deposition of molten ash on the existing coating continues exactly at the same rate, Section 5.2.

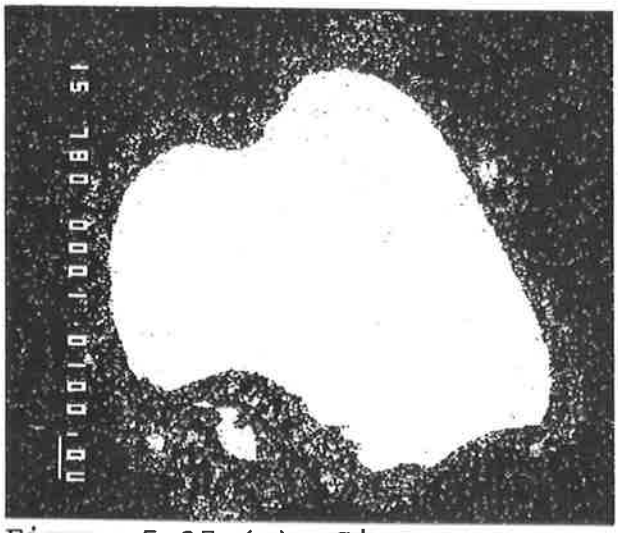

Figure 5.25 (a)= Si

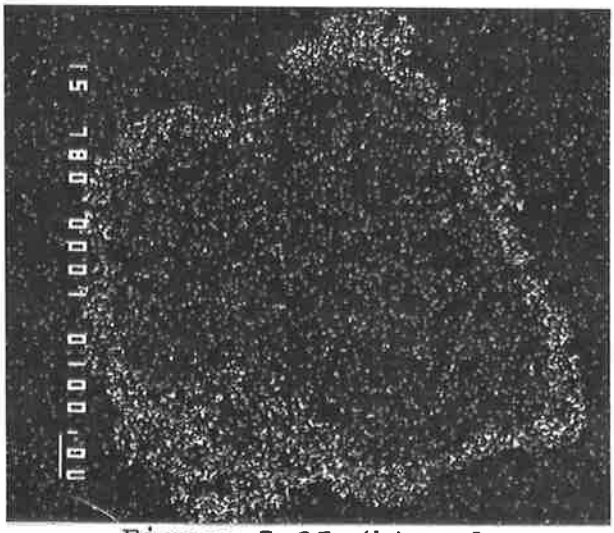

Figure 5.25 (b)= Al

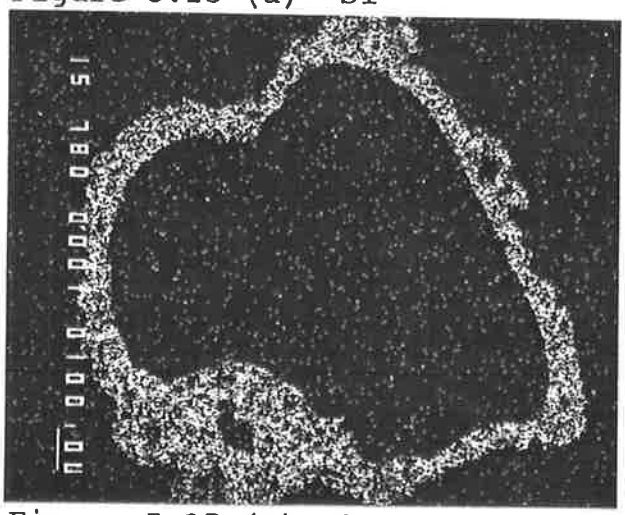

Figure 5.25 (c)= S

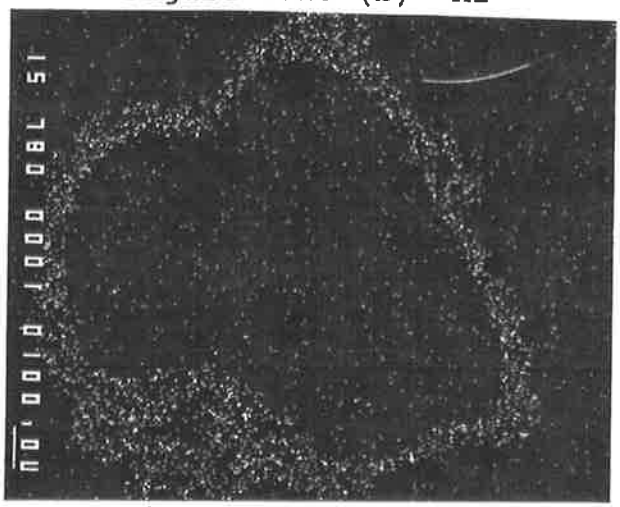

Figure 5.25 (d)= Na

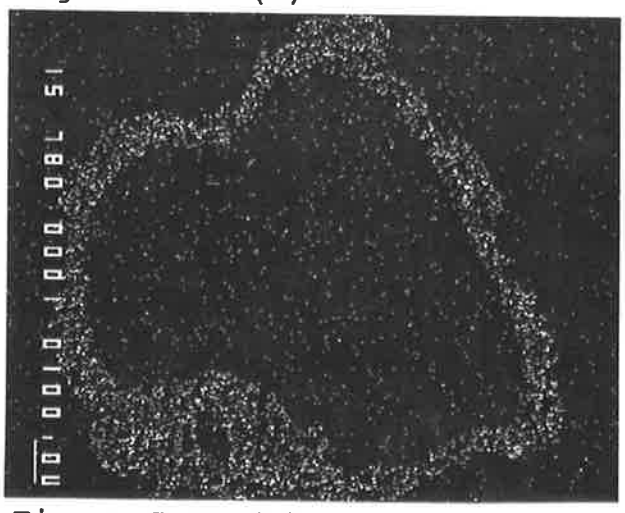

Figure 5.25 (e)= Ca

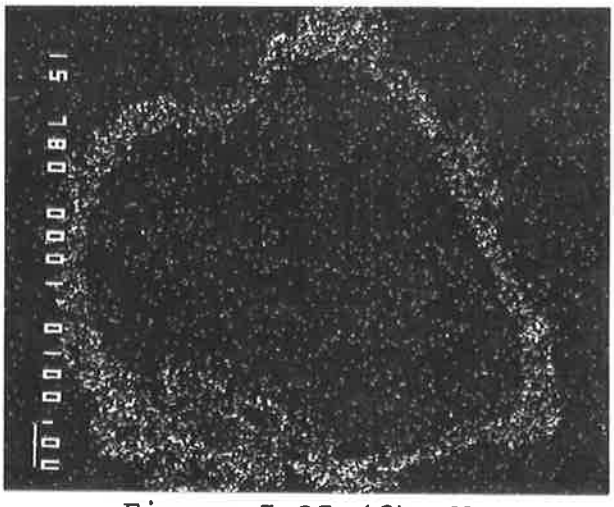

Figure 5.25 (f)= Mg

Figure 5.25: X-ray Images of a Polished Cross Section of a Silica Bed Particle Coated with Ash (Run 1)- Bright spots around the bed particle in Micrograph (a) shows the mineral inclusions. 100 μm bar is shown on the left.

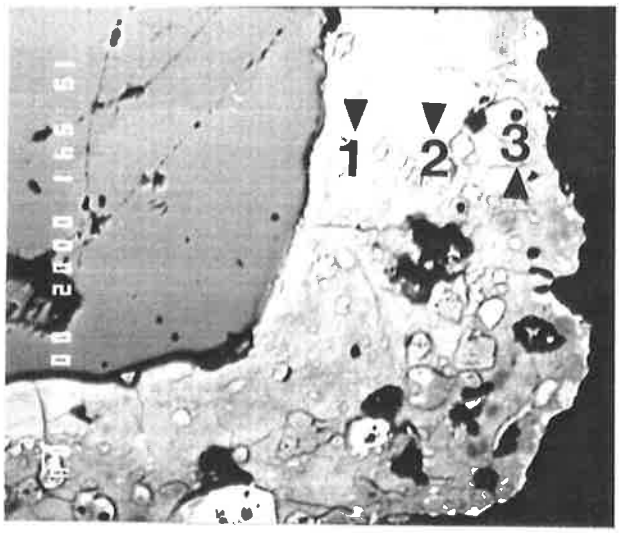

Figure 5.26 (a)= Back-scattered electron image

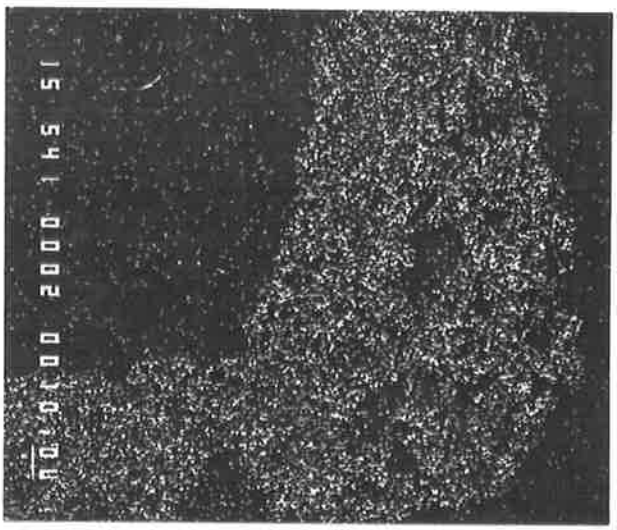

Figure 5.26 (b)= Na X-ray image

Positions Analysed:	Na_2O	CaO	MgO	SO_3	Al_2O_3	SiO_2	K_2O	P_2O_5	Cl	FeO
1	9.0	9.1	11.3	54.9	12.6	1.8	0.4	-	-	0.8
2	6.8	8.2	17.3	52.3	13.7	0.4	0.3	-	-	0.8
3	13.6	8.7	7.5	52.9	15.3	0.3	0.5	-	-	1.2

Figure 5.26: Back-scattered Electron Image and Na X-ray Map of a Polished Cross-Section of a Silica Bed Particle Coated With Ash (Run 1)- EDAX analyses of selected positions are presented. Clear boundary between the coating and silica is evident. 10 μm bar is shown on the left.

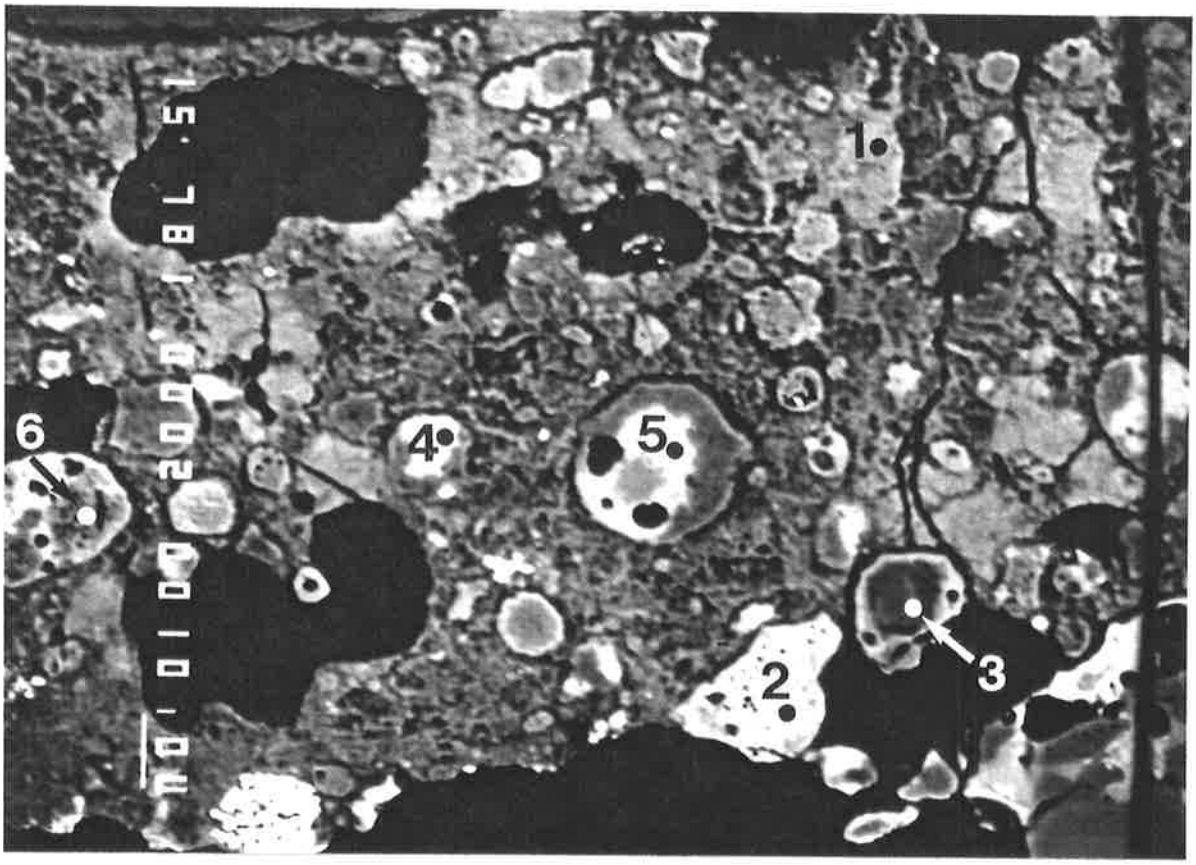

Positions Analysed:	Na_2O	CaO	MgO	SO_3	Al_2O_3	SiO_2	K_2O	P_2O_5	Cl	FeO
1(matrix)	14.4	18.6	2.6	58.3	3.4	2.0	0.3	-	-	0.3
2(mineral)	4.2	29.8	13.1	2.4	16.8	31.7	0.3	0.1	-	1.0
3 "	17.3	1.2	1.5	0.5	38.2	41.0	0.3	-	-	-
4 "	1.6	2.4	49.2	7.2	25.6	13.0	0.1	-	-	0.7
5 "	7.6	21.3	4.5	0.6	30.3	35.2	0.4	-	-	-
6 "	1.8	2.9	48.4	9.9	13.3	22.3	0.2	-	-	0.8

Figure 5.27: Back-scattered Electron Image of a Polished Cross-Section of Coating on a Silica Bed Particle (Run 1) at Higher Magnification - EDAX analyses of selected positions are presented. Minerals embedded in the coating matrix are shown. 10 μm bar is shown on the left.

The heterogeneous nature of the coating is shown at higher magnification (780x) in the back-scattered electron image of a polished cross-section of the coating, Figure 5.27. The spot analyses given indicate the presence of minerals of various size and quality embedded in the coating. The minerals detected include silicates, clays and spinel. Aluminium silicate detected at position 3 contains significant amount of sodium suggesting the reaction of this mineral with gaseous sodium species.

Examination of the secondary electron image of polished cross-sections of the bed particles using SEM, Figure 5.28, gave a better image of the minerals embedded in the coating. The results of EDAX qualitative analyses carried out to identify these minerals are also given. The analyses of the molten matrix in which the minerals are embedded (Positions 1 and 6) indicate the presence of highly sulphated Na and Ca compounds.

The morphology of the surface of bed particles coated with ash, shown in Figure 5.29, confirms that the coating consists of a molten matrix in which solid particles are embedded.

Micrographs showing the back-scattered electron image and the x-ray maps of a polished surface of bed particles at high magnification (1800x) are given Figure 5.30. It is evident that numerous micron size particles of silica and clay minerals are embedded in a matrix of sulphated compounds. The minerals in the coating, which originate from those in the coal, are likely to have been trapped in the ash matrix during the ash formation process prior to the deposition of ash on the bed particles. The presence of minerals trapped in the ash matrix on the char surface was observed during the experiments carried out in the single particle furnace, Section 4.3.

FBC of Low-Mineral Coal Samples (Runs 2 - 13)

The micrographs, given in Figure 5.31, show the back-scattered electron image of the polished cross-sections of bed particles coated during the FBC of the low-mineral coal sample. The image of the coating shown is different from that formed with the high-mineral coal sample. As expected, there is no indication of the presence of a significant number of minerals in the matrix of the coating. EDAX analyses indicate that the coating consists mostly of S, Na, Ca, Mg and Al. The distribution of these compounds is not uniform throughout the coating matrix. The concentration of Cl in the coating is insignificant. The average composition of the coating is similar to that of the ash formed on the char's surface during the single particle combustion experiments using similar coal, Section 4.3.

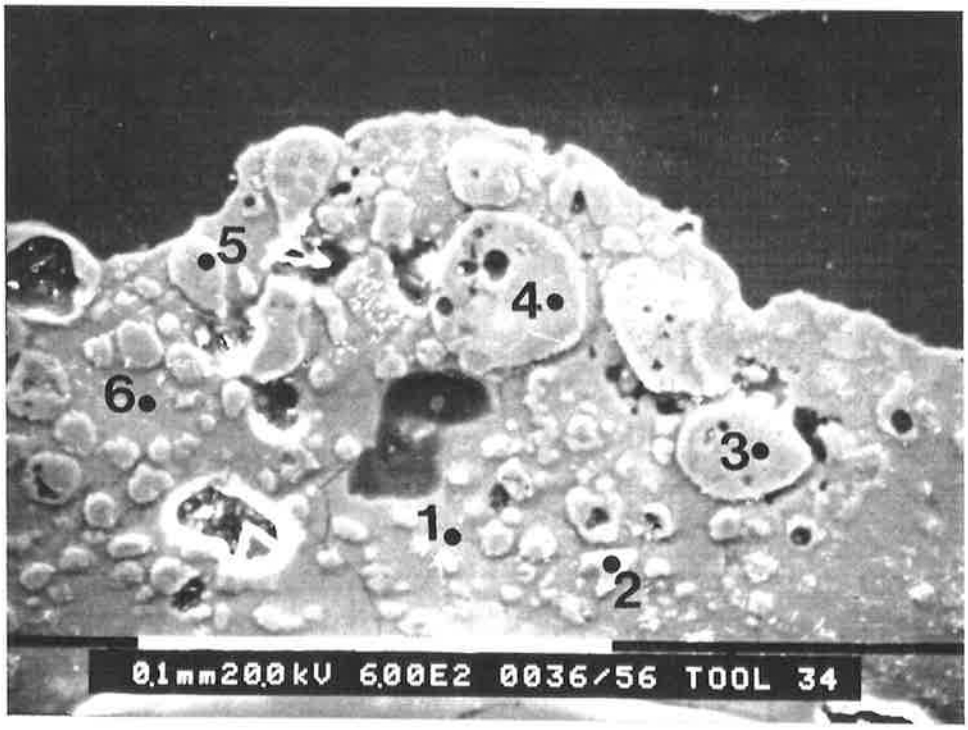

1: S, Ca, (Al, Na, Mg)
2: Si
3: Si, Al, Ca, (Na, S)
4: Si, Ca, Al, Mg
5: Si, Ca, Al, (Mg, Na, S)
6: S, Ca, (Al, Na, Mg)

Figure 5.28: Secondary Electron Image of a Polished Cross-Section of Coating on a Silica Bed Particle (Run 1)- Major and minor (in bracket) elements detected at selected positions by EDAX system are presented. 0.1 mm bar is shown at the bottom.

Figure 5.29 (a) :
Magnification x 150

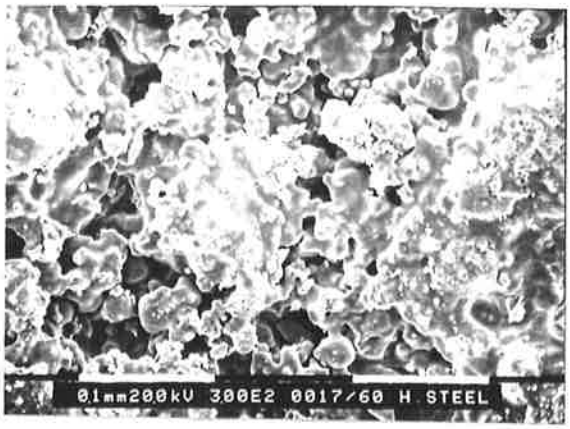

Figure 5.29 (b) :
Magnification x 300

Figure 5.29 (c) :
Magnification x 600

Figure 5.29: **Secondary Electron Images of the surface of a Bed Particle Coated with Ash (Run 1)** - Molten matrix in which solid phases are embedded is shown.

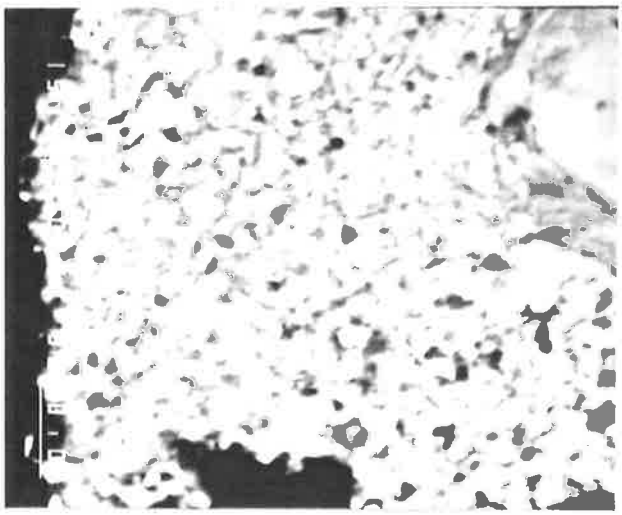

Figure 5.30 (a)= Micrograph

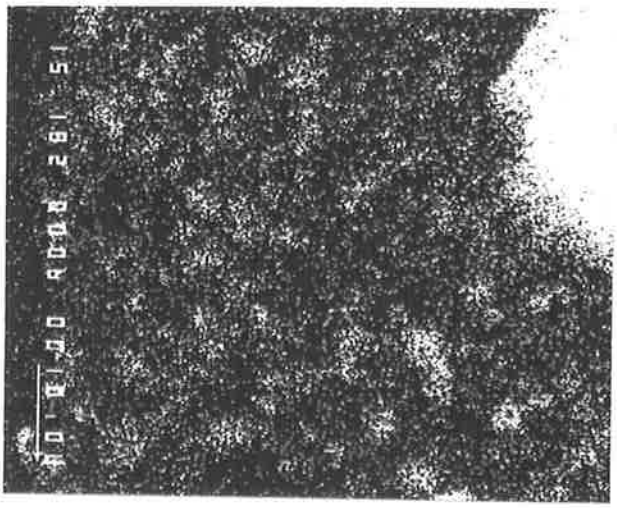

Figure 5.30 (b)= Si

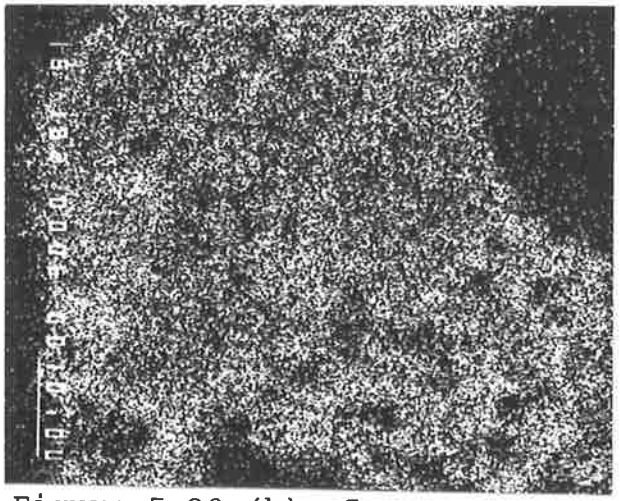

Figure 5.30 (b)= S

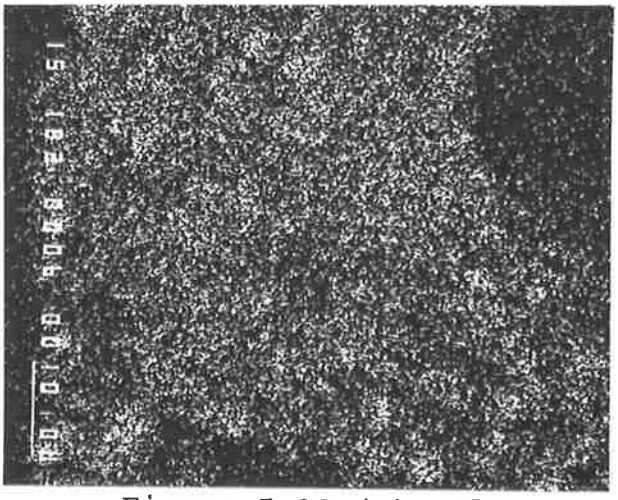

Figure 5.30 (c)= Al

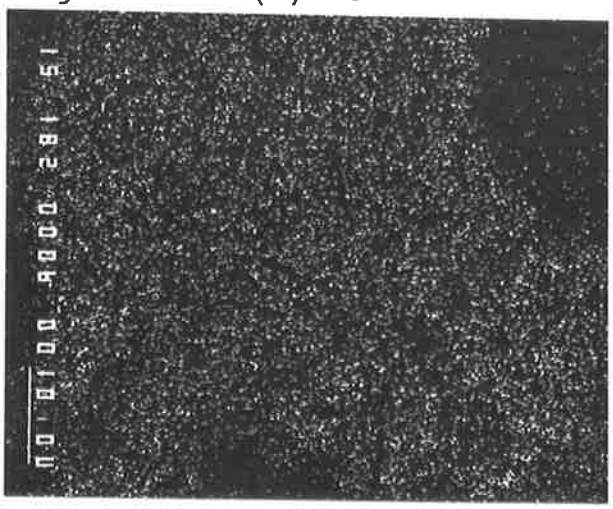

Figure 5.30 (e)= Na

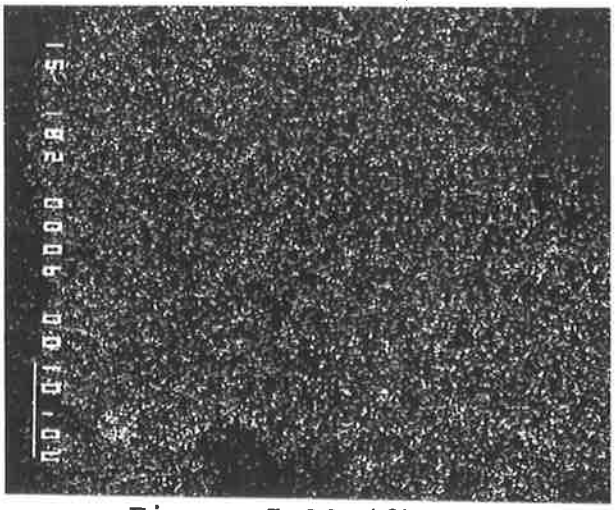

Figure 5.30 (f)= Ca

Figure 5.30 : Back-scattered Electron Image and X-ray Maps of a Polished Cross-Section of Coating on a Silica Bed Particle (Run 1) - Bright spots in the x-ray maps of Si and Al show the minerals. 10μm bar is shown on the left.

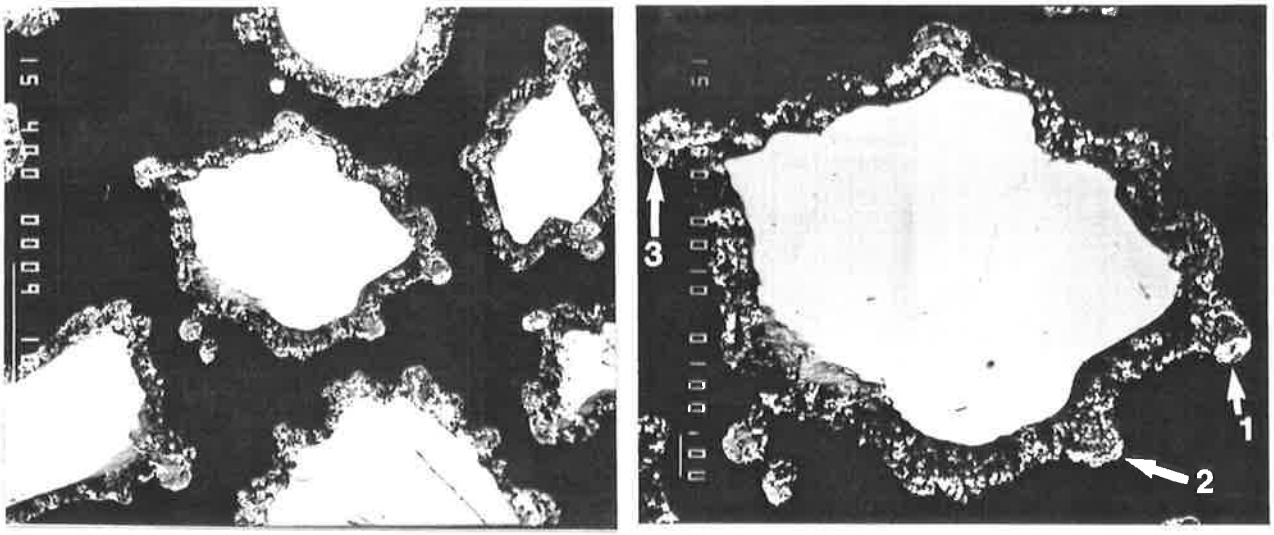

Positions Analysed:	Na_2O	CaO	MgO	SO_3	Al_2O_3	SiO_2	K_2O	P_2O_5	Cl	FeO
1	8.4	16.7	17.4	45.5	7.2	3.0	0.4	-	0.5	0.5
2	9.7	17.0	15.1	46.2	6.6	4.2	0.3	-	0.2	0.3
3	8.4	17.6	16.7	47.5	8.6	1.5	0.3	-	0.2	0.5

Figure 5.31: Back-scattered Electron Images of Polished Cross-Sections of Bed Particles Coated During the Combustion of the Low-Mineral Coal Sample (Run 3)- EDAX analyses of selected scans are presented. 100μm bar is shown on the left.

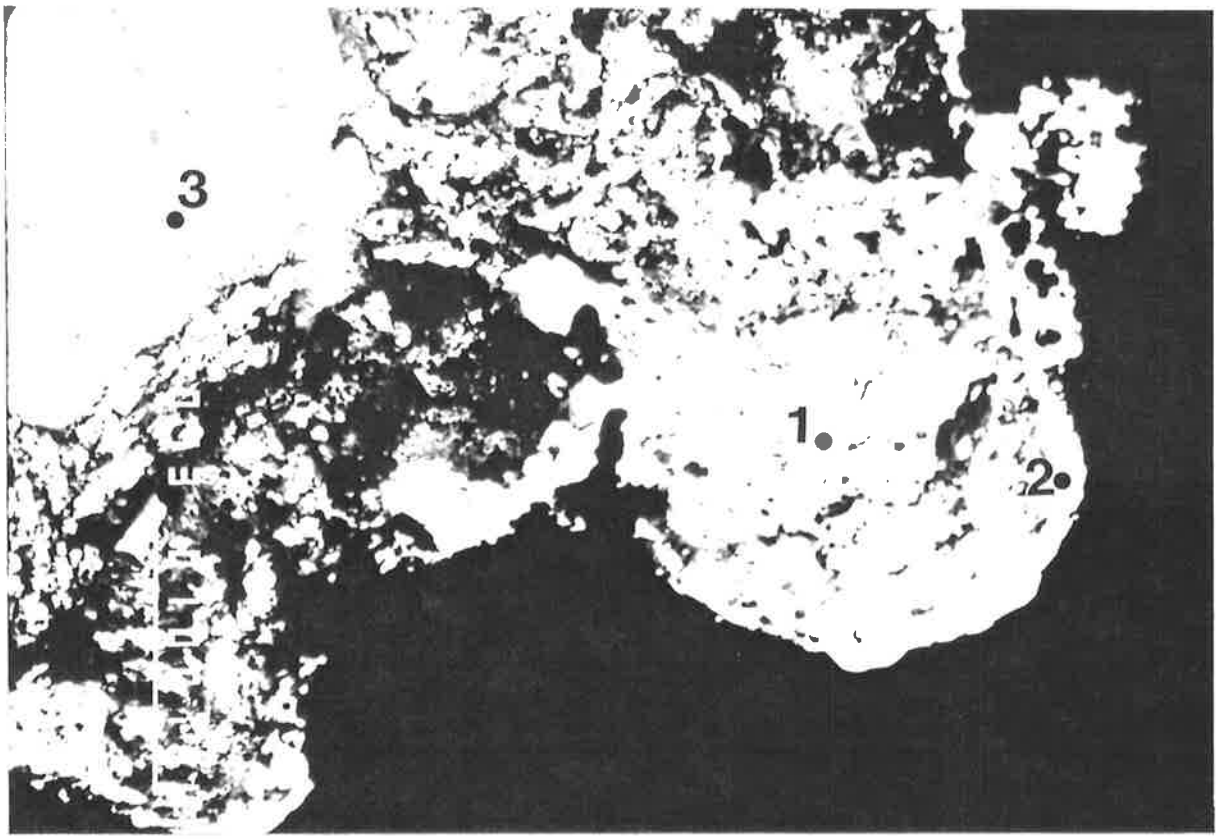

Positions Analysed:	Na_2O	CaO	MgO	SO_3	Al_2O_3	SiO_2	K_2O	P_2O_5	Cl	FeO
1	0.4	33.3	0.4	65.3	0.2	0.4	-	-	-	0.2
2	0.3	30.3	7.5	58.0	3.8	-	-	-	-	-
3	-	-	-	-	-	99.9	-	-	-	-

Figure 5.32: Back-scattered Electron Image of a Polished Cross-Section of the Coating Formed on a Silica Bed Particle During the Combustion of the Low-Mineral Coal Sample (Run 3) - EDAX analyses of Selected Points are presented. 100 μm bar is shown on the left.

EDAX analyses of the coating, shown at higher magnification in Figure 5.32, indicate that the brighter areas evident in the micrographs are enriched in Ca and S, possibly in the form of $CaSO_4$. These areas appear to be more consolidated.

Figure 5.33 shows the distribution of inorganic elements in the coating deposited on a silica bed particle. The X-ray images of selected elements are also shown. The distribution of sodium in the coating is shown in the next figure. The Si image indicates the presence of only a few Si containing mineral inclusions. The bright area at the bottom of the Si image is part of the parent silica bed particle. It is also evident that a small amount of Si is intimately distributed through the coating matrix. The sub-micron Si containing particles in the coating are likely to originate from the inherent minerals in coal, Chapter 4.

The x-ray images, shown in Figure 5.33, indicate the enrichment of certain compound at various locations. The bright areas appear to be rich in $CaSO_4$ and the darker areas are rich in Mg and Al which are likely to be present as alumina phases and/or oxides. Despite these partial enrichments, the elements of S, Ca, Mg and Al seem to be intimately distributed through the coating matrix. The enrichment of compounds in certain locations could have occurred due to diffusion of these compounds after the deposition of the coating.

The distribution of Na in the coating, given in the micrographs of Figure 5.34, show the enrichment of Na in certain locations with a corresponding depletion of Ca. Both Na and Ca seem to be associated with S. Enrichment of Mg and Al corresponds with the depletion of sulphated compounds. Despite the localised enrichment, Na is intimately distributed through the coating matrix. The bright spot shown in the X-ray image of Al indicates the presence of a clay mineral inclusion.

The morphology of the surface of the bed particles coated with the ash was examined using SEM operating on a secondary electron mode. The micrographs, shown in Fig 5.35, indicate that the surface of the bed particles has a nodular shape. This is also evident in the micrograph showing the polished cross-section of the bed particles, Figure 5.31. The reason for the nodular shape of the coating deposited on the bed particles during the combustion of low-mineral coal sample is not known.

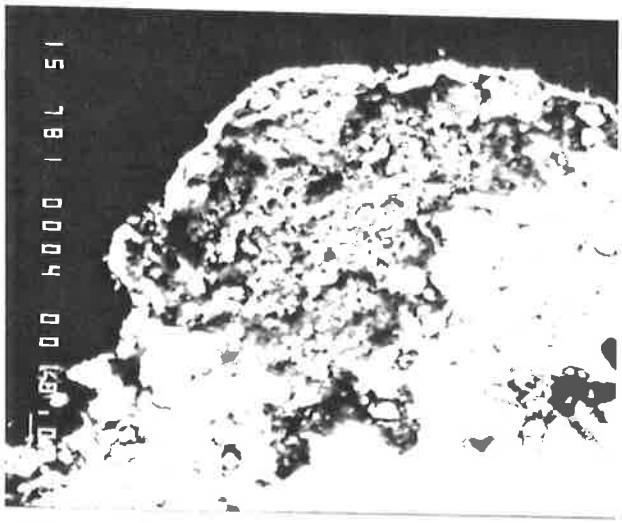

Figure 5.33 (a)= Micrograph

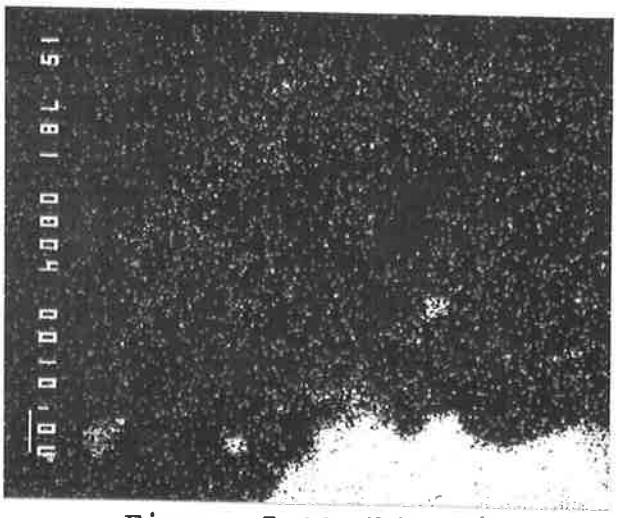

Figure 5.33 (b)= Si

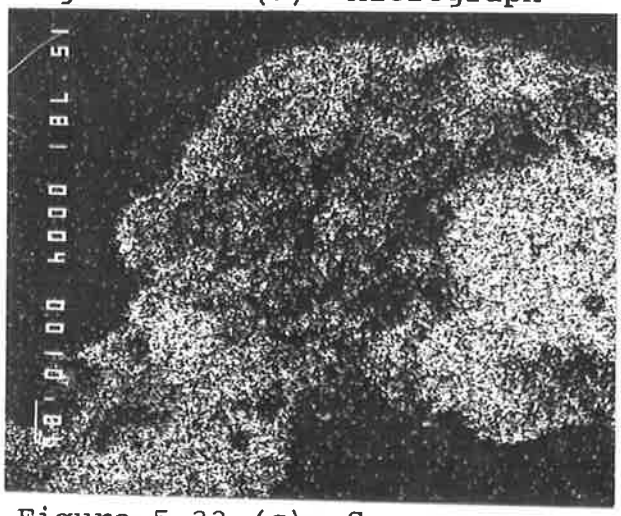

Figure 5.33 (c)= S

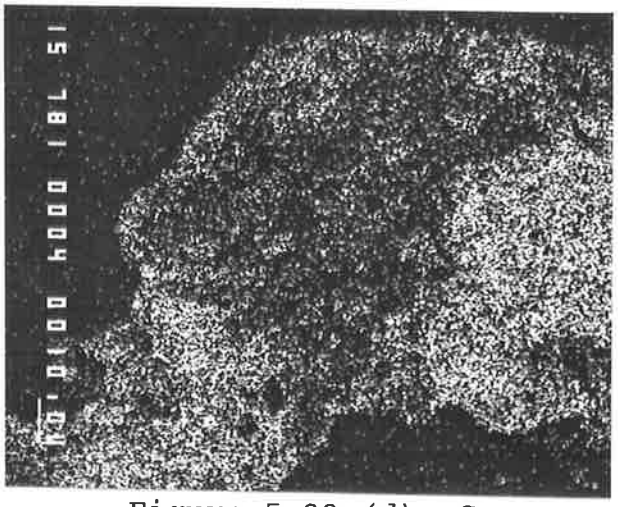

Figure 5.33 (d)= Ca

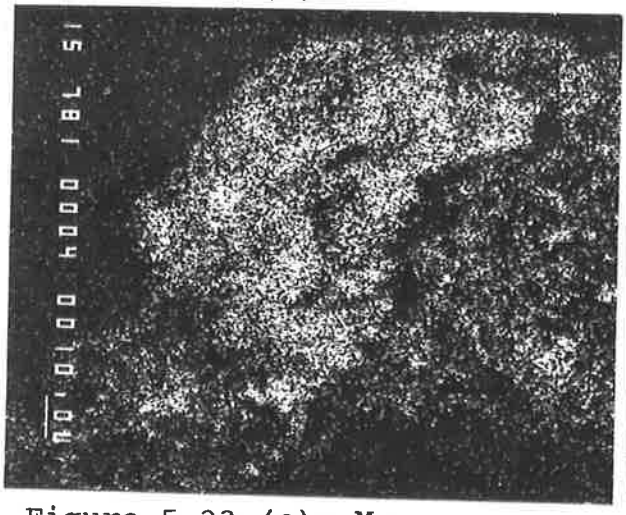

Figure 5.33 (e)= Mg

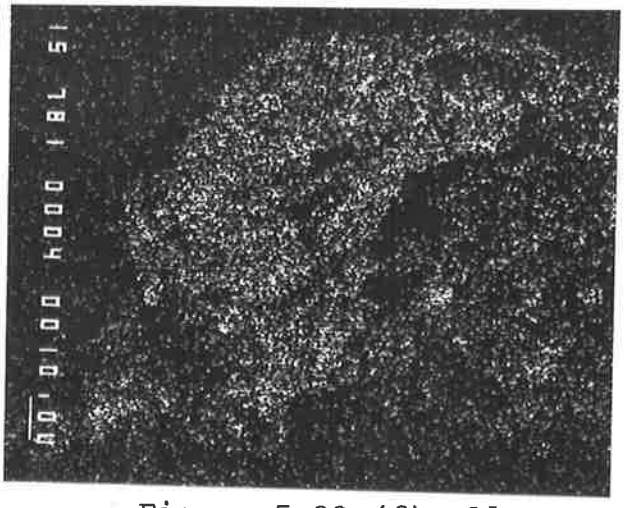

Figure 5.33 (f)= Al

Figure 5.33: Back-scattered Electron Image and X-ray Maps of a Polished Cross-Section of the Coating on a Silica Bed Particle (Run 3) - Localised enrichment of certain elements are shown. 10μm bar is shown on the left.

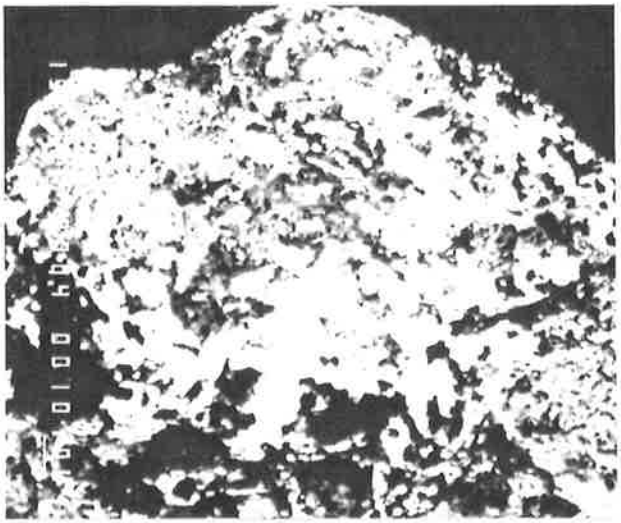

Figure 5.34 (a)= Micrograph

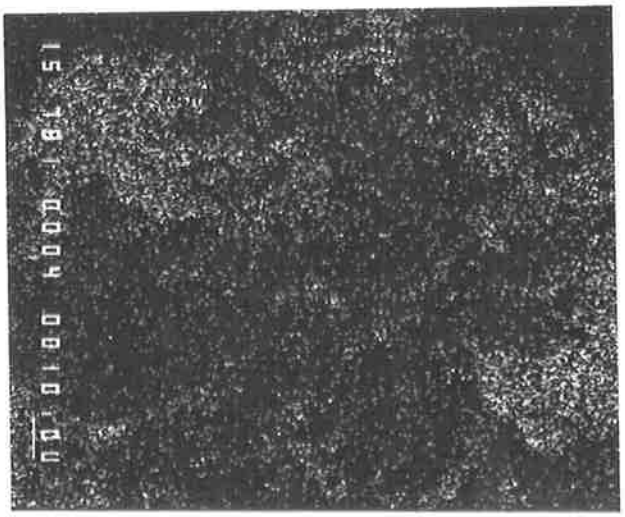

Figure 5.34 (b)= Na

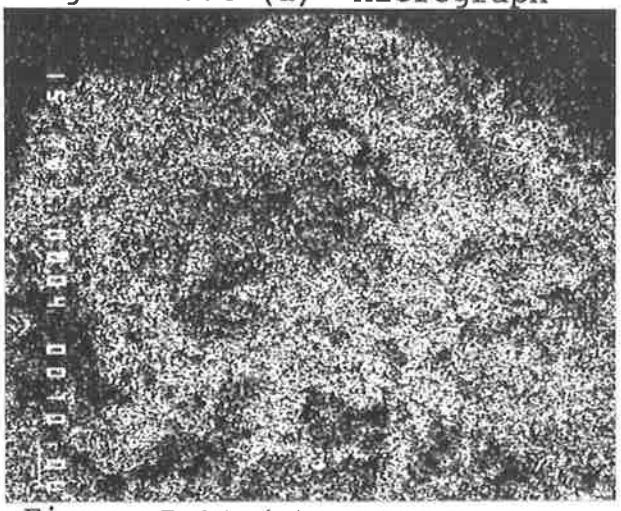

Figure 5.34 (c)= S

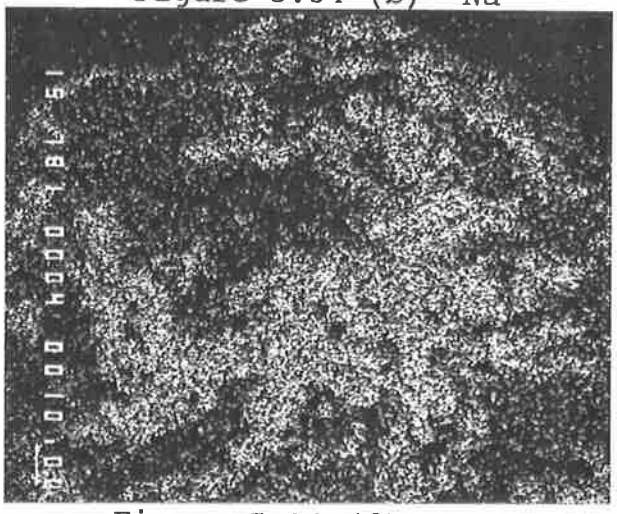

Figure 5.34 (d)= Ca

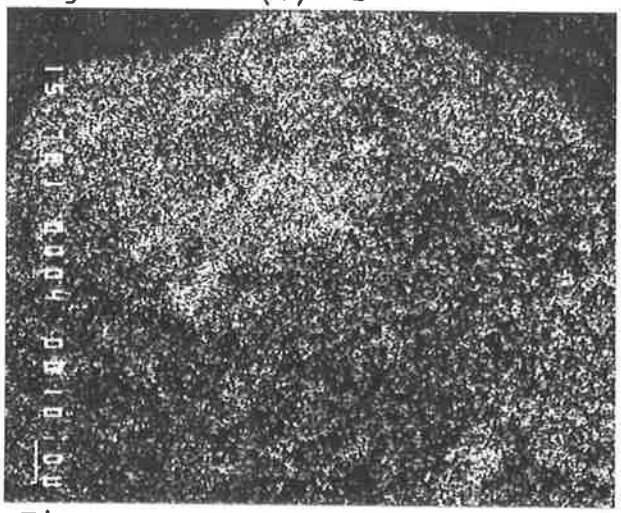

Figure 5.34 (e)= Mg

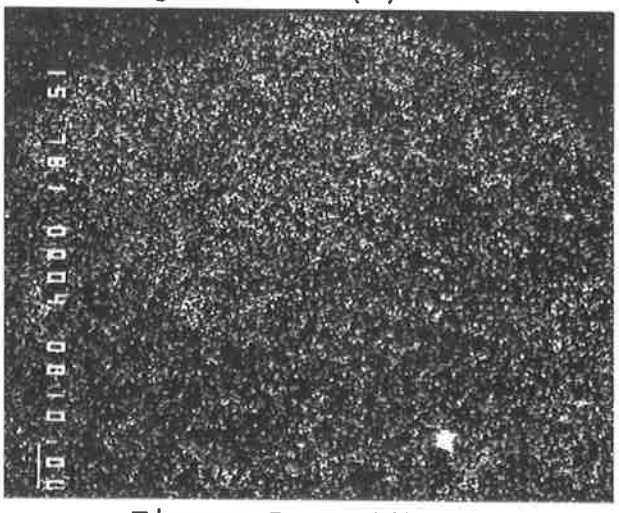

Figure 5.34 (f)= Al

Figure 5.34: Back-scattered Electron Image and X-ray Maps of a Polished Cross-Section of the Coating on a Silica Bed Particle (Run 3) Showing the Localised Enrichment of Na - 10μm bar is shown on the left.

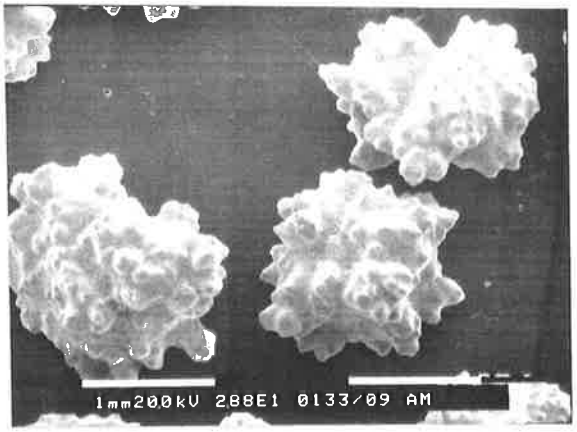

Figure 5.35 (a) :
Magnification x 28

Figure 5.35 (b) :
Magnification x 78

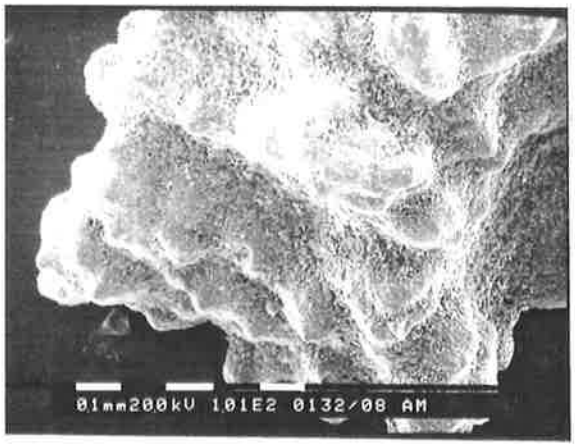

Figure 5.35 (c) :
Magnification x 100

Figure 5.35: **Secondary Electron Images of the surface of a Bed Particle Coated with Ash (Run 3)** - The nodular surface of the coating is shown.

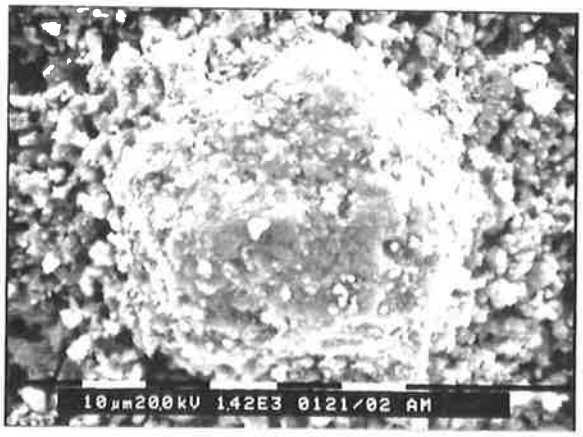

Figure 5.36 (a) :
Magnification x 1420

Figure 5.36 (b) :
Magnification x 2400

1: S, Ca, (Na)
2: Ca, Mg, Al, (Na, S)

Figure 5.36: Secondary Electron Images of the surface of a Bed Particle Coated with Ash at High Magnifications (Run 3) - Major and minor (in bracket) elements in the molten matrix and the solid phases detected by EDAX are shown.

A secondary electron micrograph (SEM) and the EDAX qualitative analyses of the surface of the bed particles coated with ash are given in Figure 5.36. The smooth molten matrix, positions designated as (1), consists mainly of sulphated compounds of Ca and Na. The rough areas, designated as (2), indicate the presence of Mg and Al as well as S, Ca and Na. It is evident that the low temperature melting compounds formed from S, Ca and Na have a molten morphology, whereas, the high temperature melting compounds of Ca, Mg and Al appear to have a solid morphology.

The Effects of Other Variables

Microscopic examination of the bed particles removed from the furnace during Runs 2,3,4,5,8,9,10,12 and 13 indicated that the characteristics of the coating do not change significantly with:

- operating temperature (Runs 2,3,8,9);
- particle size distribution of the initial charge (Run 10); and
- excess O_2 in the flue gas (Runs 12 and 13).

These observations are in agreement with the results of chemical analyses, Section 5.3.

Water and acid leaching of coal, Runs 4 and 5 respectively, reduced the concentration of Na in the coating by a small margin. There was no significant change in the morphology of the coating. It was, however, found that only a small amount of coating deposited on the bed particles during these runs.

The addition of NaCl to the coal sample, Runs 6 and 7, increased the average concentration of Cl in the coating. Figure 5.37 shows the back-scattered image of a polished cross-section of the coating on a bed particle. Figure 5.38 shows the X-ray images of the major elements found in the coating. The X-ray image of Cl indicates that this element is intimately distributed in the coating matrix except in a few locations where it is present as inclusions in association with other inorganic elements. One of the Cl inclusions is identified as sodium chloride. Other Cl inclusions can not be identified.

With the exclusion of Cl, the content and the distribution of other inorganic elements in the coating seem to be similar to that formed with the untreated low-mineral coal sample (Run 3). The presence of Cl compounds is considered to be responsible for the high rate of deposition of the coating and for the enhanced stickiness of the bed particles which resulted in the defluidisation of the bed, Section 5.2.

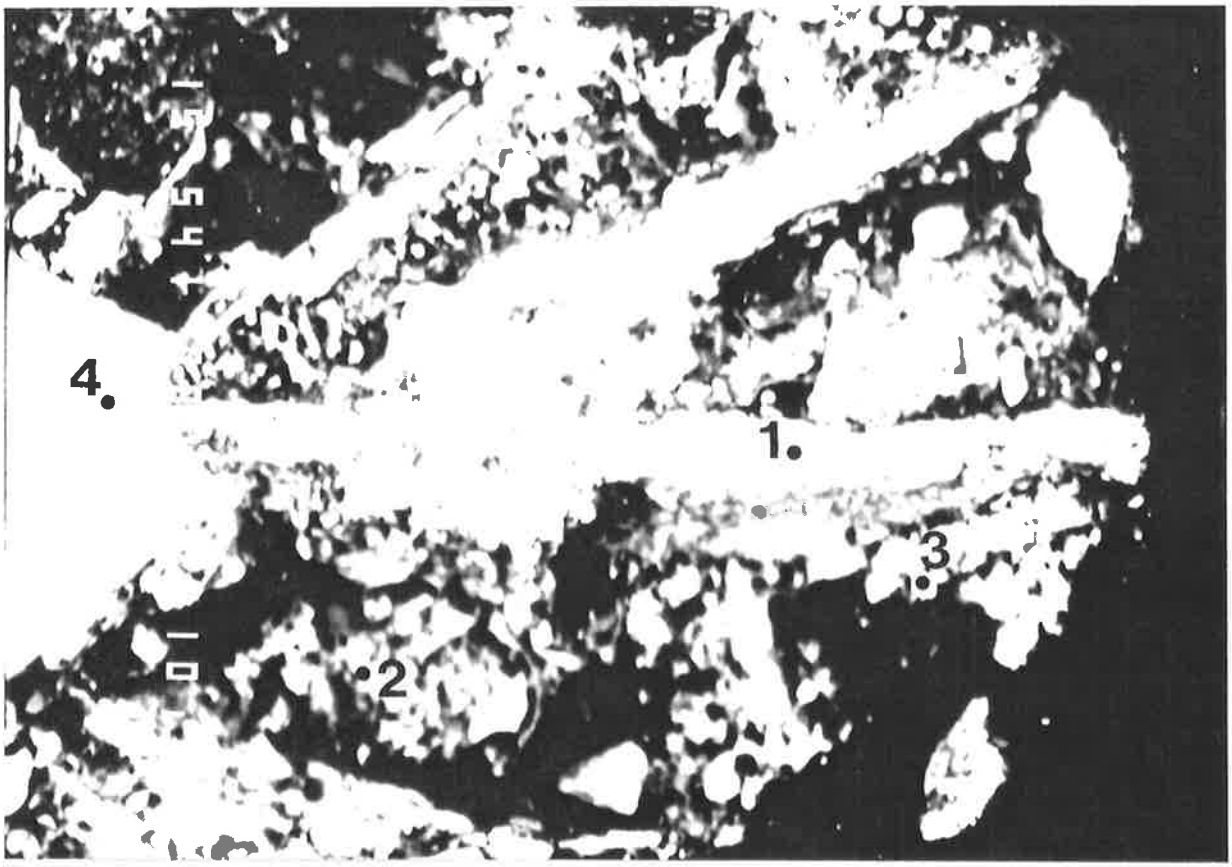

Positions Analysed:	Na_2O	CaO	MgO	SO_3	Al_2O_3	SiO_2	K_2O	P_2O_5	Cl	FeO
1	5.2	7.1	38.7	29.9	15.4	1.5	0.5	-	0.9	0.2
2	9.2	7.1	26.3	45.8	9.8	0.2	-	-	1.0	-
3	29.9	13.8	1.6	15.1	1.1	2.3	0.9	-	35.2	-
4	-	-	-	-	-	99.0	-		-	-

Figure 5.37: Back-scattered Electron Image of a Polished Cross-Section of the Coating Formed on a Silica Bed Particle During the Combustion of the Low-Mineral Coal Sample Added with NaCl (Run 6) - EDAX analyses of selected positions are presented.

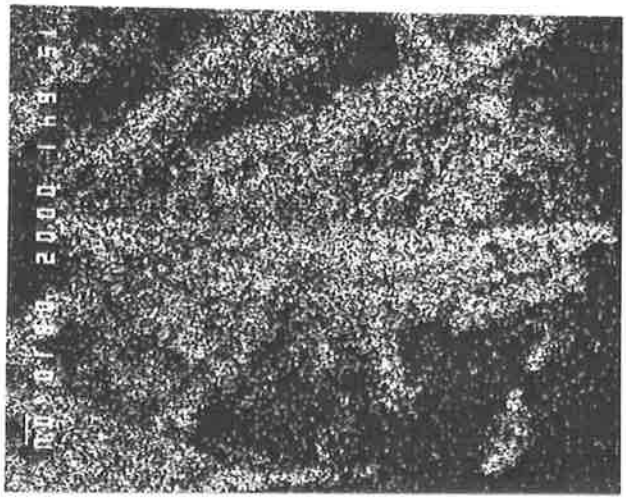

Figure 5.38 (a)= S

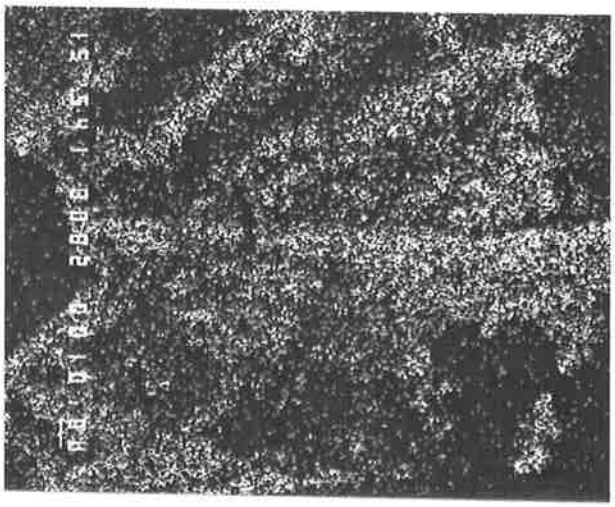

Figure 5.38 (b)= Ca

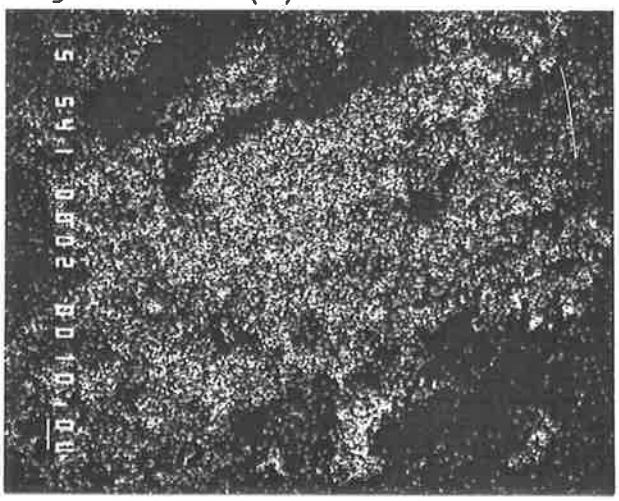

Figure 5.38 (c)= Mg

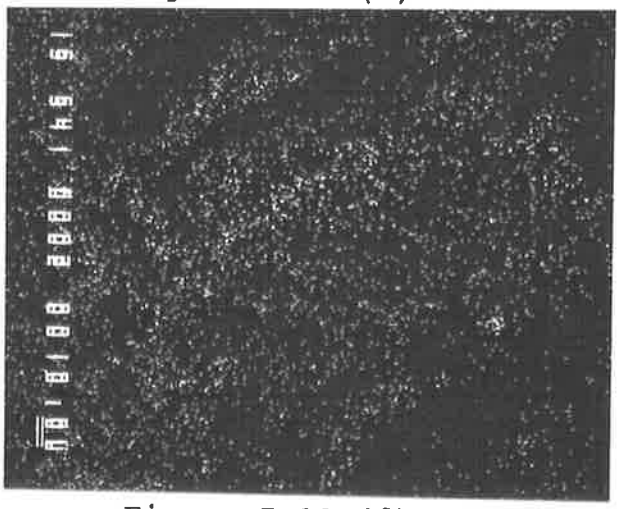

Figure 5.38 (d)= Na

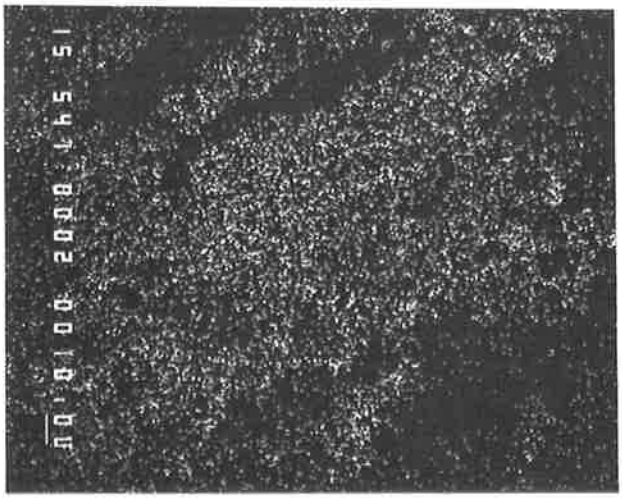

Figure 5.38 (e)= Al

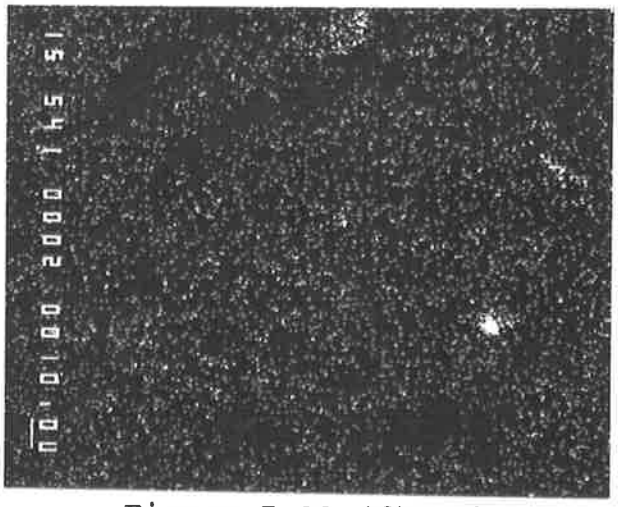

Figure 5.38 (f)= Cl

Figure 5.38: Back-scattered Electron Image and X-ray Maps of a Polished Cross-Section of the Coating on a Silica Bed Particle Showing the Distribution of Cl (Run 6)- 10μm bar is shown on the left.

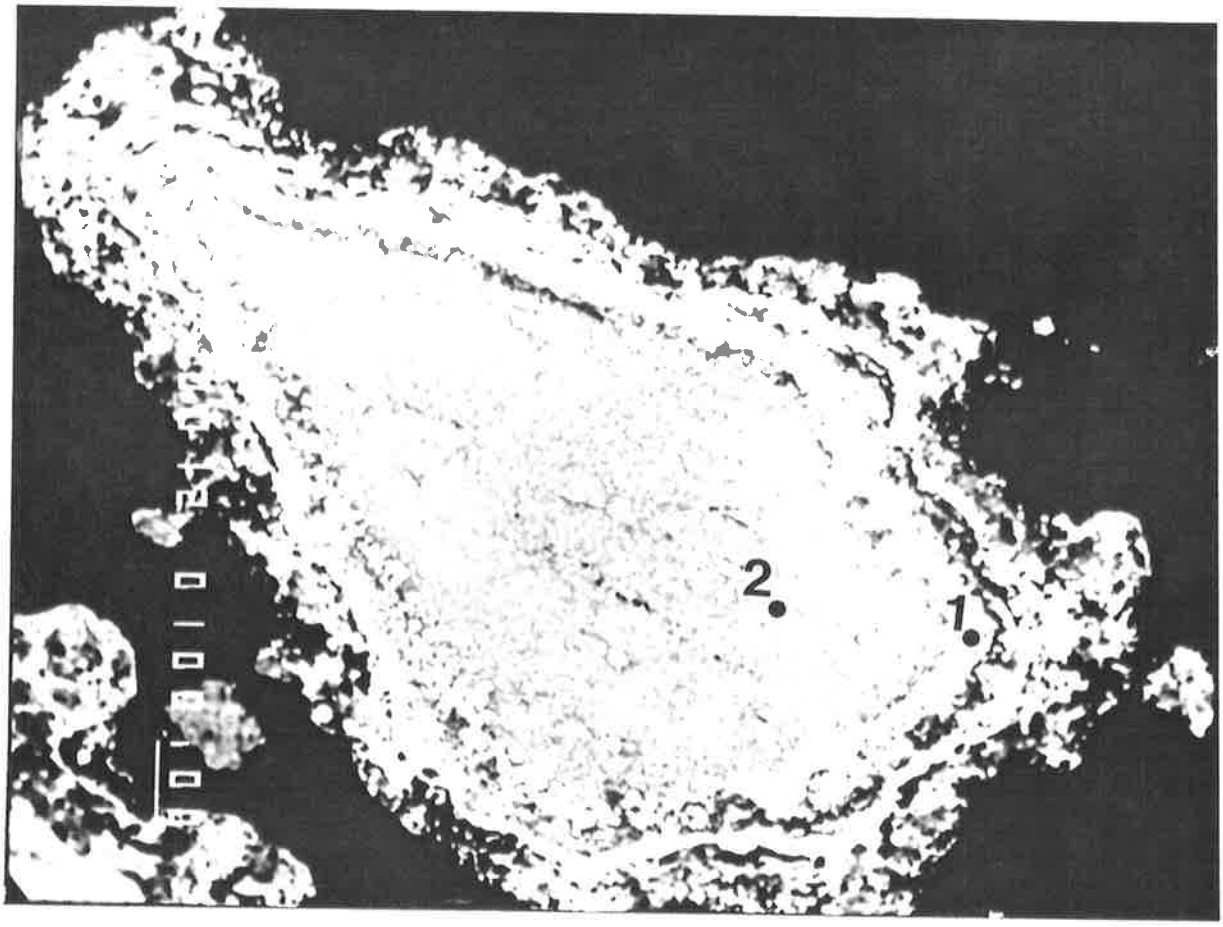

Positions Analysed:	Na_2O	CaO	MgO	SO_3	Al_2O_3	SiO_2	K_2O	P_2O_5	Cl	FeO
1	0.4	28.0	14.1	55.8	0.2	0.3	-	-	-	0.9
2	0.8	54.5	39.8	1.7	0.3	0.2	-	-	0.2	2.1

Figure 5.39: **Back-scattered Electron Image of a Polished Cross-Section of the Coating Formed on a Dolomite Bed Particle (Run 11)** - EDAX analyses of selected positions are presented. 100 μm bar is shown on the left.

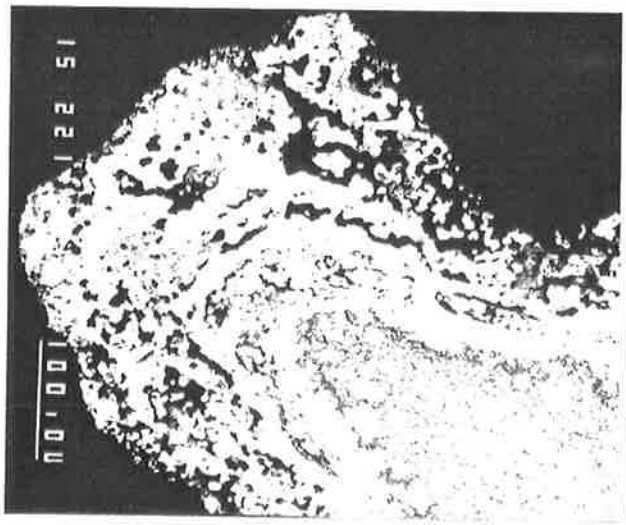

Figure 5.40 (a)= Micrograph

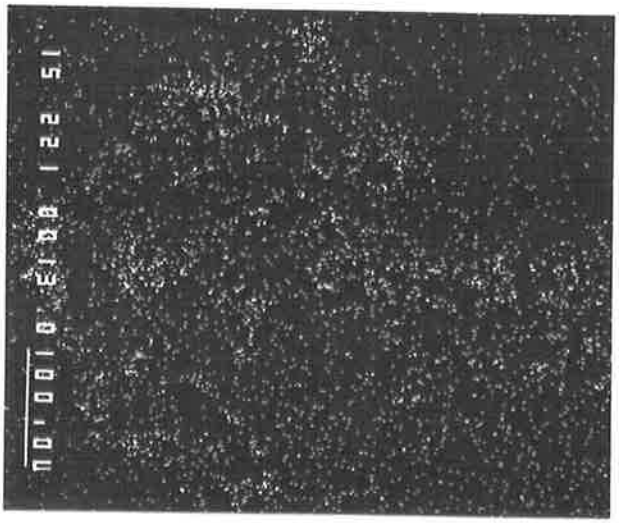

Figure 5.40 (b)= Na

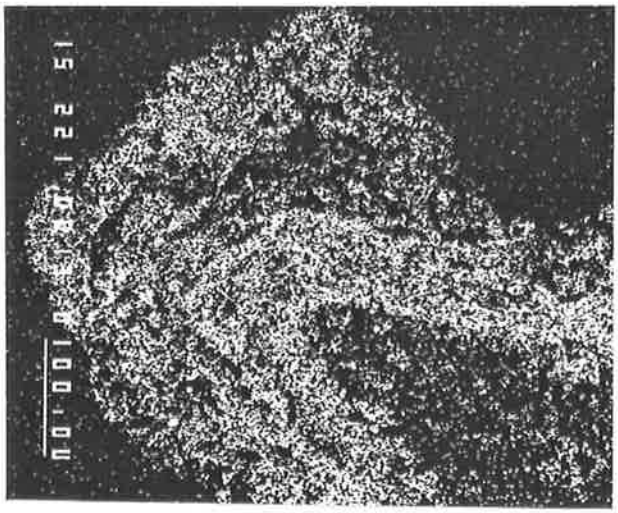

Figure 5.40 (c)= S

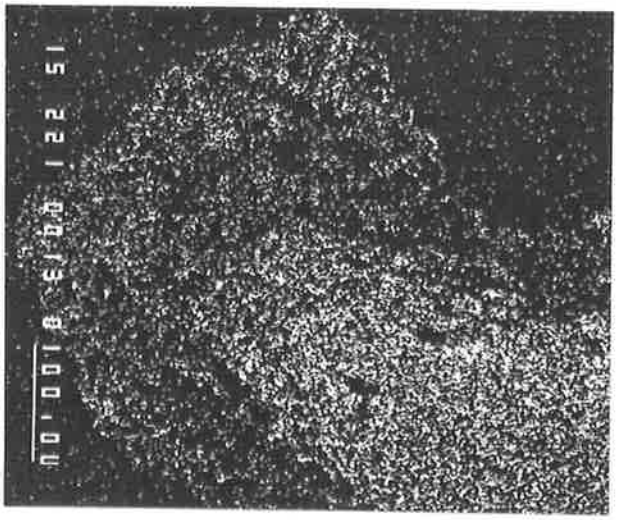

Figure 5.40 (d)= Mg

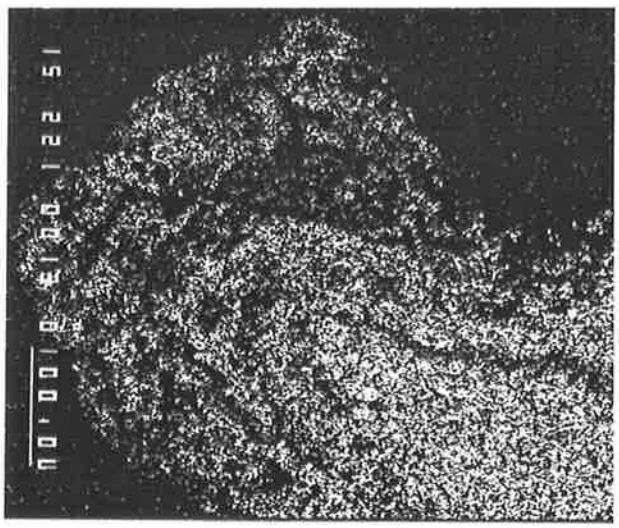

Figure 5.40 (e)= Ca

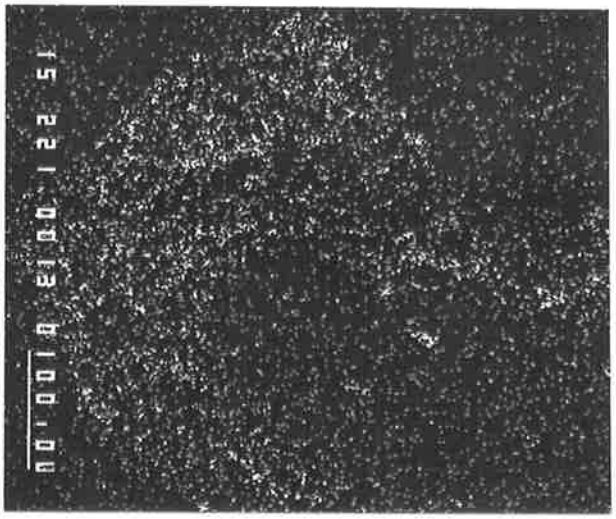

Figure 5.40 (f)= Al

Figure 5.40: **Back-scattered Electron Image and X-ray Maps of a Polished Cross-Section of Coating on a Dolomite Bed Particle (Run 11)** - 100 μm bar is shown on the left.

The formation of the coating on a dolomite bed particle, Run 11, is shown in Figure 5.39. The composition of the coating on the dolomite particles was found to be the same as those deposited on silica bed particles under similar conditions. The layered configuration of the dolomite bed particle, shown in the micrograph, indicates the penetration of S into the weak structure of the dolomite and its reaction with Ca.

The X-ray images of the top corner of the same dolomite particle, are given in Figure 5.40. The penetration of sulphur into the parent bed particle is evident. With the exclusion of the reaction between S and dolomite forming $CaSO_4$, there is no indication of chemical reaction between the inorganic matter and dolomite.

5.5.3 X-RAY DIFFRACTION ANALYSES

Samples of bed material and cyclone ash were used for mineralogical analysis using XRD. The procedure for sample preparation and the description of the equipments used are given in Subsection 3.5.3.

The minerals and compounds identified in these samples, listed in Table 5.6, are categorised as MAJOR, MINOR and TRACE. The assessment of relative abundance is based on the peak heights.

Some of the diffraction lines obtained could not be assigned, at the present state of the knowledge, to minerals and compounds. Many of these unknowns were MINOR or TRACE components. In other samples, the diffraction pattern could be matched with the shifted lines of known minerals and compounds indicating cation substitution in the crystal structure and/or distortion of crystals.

The presence of unknown compounds and shifted diffraction patterns highlight the complexity of the transformations experienced by the inorganic matter during the FBC of low-rank coals.

Quartz detected in the samples of bed material is related to the parent silica bed material. Although most of the samples taken from the bed material contained significant amount of coating, only anhydrite was identified as a major phase in the sample of bed material obtained from runs burning the low-mineral coal. The presence in the coating of anhydrite is also evident in the micrographs given in Subsection 5.5.2.

SAMPLE	RUN	MAJOR	MINOR	TRACE	COMMENTS
bed material	1	quartz	thenardite anhydrite periclase spinel	magnesioferrite Na-Ca-sulphate	unidentified lines assigned to Na-Ca-sulphate type phases
bed material	2	quartz	anhydrite periclase thenardite	magnesioferrite spinel Na-Ca-sulphate	
bed material	3	quartz anhydrite	thenardite periclase	magnesioferrite Na-Ca-sulphate spinel	
cyclone ash	3	periclase	thenardite tricalcium-aluminate lime quartz	mayenite spinel thenardite? unidentified	tricalcium-aluminate phase $Ca_3Al_2O_6$ unidentified phase at 2.13A
bed material	4	quartz anhydrite	periclase thenardite	Na-Ca-sulphate magnesioferrite	
cyclone ash	4	periclase anhydrite	tricalcium-quartz lime	magnesioferrite thenardite? mayenite	
bed material	5	quartz andydrite	periclase	magnesioferrite thenardite Na-Ca-sulphate	
cyclone ash	5	periclase anhydrite	tricalcium-aluminate quartz	magnesioferrite thenardite? mayenite	
bed material	6	quartz anhydrite	periclase thenardite spinel Na-Ca-sulphate	magnesioferrite	
cyclone ash	6	periclase	anhydrite tricalcium-aluminate quartz halite lime	magnesioferrite mayenite	

Table 5.6: ***X-Ray Diffraction Analyses of Bed Material and Cyclone Ash.***

SAMPLE	RUN	MAJOR	MINOR	TRACE	COMMENTS
bed material	7	quartz anhydrite	halite periclase	Na-Ca-sulphate	unidentified phase at 3.733A
cyclone ash	7	organic C	halite periclase tricalcium-aluminate anhydrite quartz	lime mayenite?	
bed material	8	quartz anhydrite	thenardite periclase	magnesioferrite spinel Na-Ca-sulphate	
cyclone ash	8	periclase	tricalcium-aluminate anhydrite lime quartz	mayenite halite? thenardite?	
bed material	9	quartz anhydrite	periclase thenardite	magnesioferrite spinel Na-Ca-sulphate	
cyclone ash	9	periclase	tricalcium-aluminate anhydrite lime halite	quartz mayenite	
bed material	13	quartz	anhydrite periclase Na-Ca-sulphate		
cyclone ash	13	organic C	anhydrite quartz periclase	halite magnesioferrite tricalcium-aluminate	

Table 5.6 Continued: ***X-Ray Diffraction Analyses of Bed Material and Cyclone Ash.***

Minor phases identified in the bed material samples included thenardite, periclase, anhydrite and in some samples spinel and magnesioferrite. Shifted diffraction pattern of Na-Ca-sulphate was considered to be due to the substitution of foreign elements such as Mg for Ca in this compound. Halite was found in the bed material obtained from Run 7 carried out with the sample of coal with added NaCl (batch 2). Cl compounds were detected in this sample by electron microscopy, Subsection 5.5.2. Chemical analyses of the samples of bed material from Runs 6 and 7, firing coals impregnated with sodium chloride, confirmed the presence of Cl compounds in these samples, Section 5.3. However, due to the low concentration of Cl compounds in the sample of bed material from Run 6, these compounds were not detected in this sample by XRD.

Trace compounds and minerals detected in the samples of bed material included: Na-Ca-sulphate, thenardite, magnesioferrite and spinel. In one of the samples, Run 8, mayenite ($Ca_{12}\ Al_{14}\ O_{33}$) was also identified.

In addition to the phases identified in the samples of bed material tricalcium aluminate ($Ca_3\ Al_2\ O_6$) and lime were found in some of the cyclone ash samples. The presence of mayenite in these samples is more evident. Periclase was identified as a major phase in almost all the cyclone ash samples analysed by XRD. In two samples, Runs 4 and 5, anhydrite was also detected as a major phase. In two of the samples, Runs 7 and 13, containing significant amount of unburnt carbon, inorganic compounds could not be detected as major phases.

The results indicate that Na is present in the samples as thenardite and Na-Ca-sulphate in which some of the cations are substituted. Calcium is present as anhydrite and aluminate, that is mayenite and tricalcium aluminate. Magnesium is found as periclase (MgO) and spinel (magnesium aluminate).

Thenardite, Na-Ca-sulphate and anhydrite are more abundant in the coating deposited on the bed particles. These compounds have low melting points or can form low melting eutectics. Compounds having higher melting points, that is oxides and alumina phases are more abundant in the cyclone ash. None of the compounds identified suggests a chemical reaction between the inorganic matter and the silica bed. The compounds detected in the coating are similar to those found in the ash prepared in a crucible at 600°C, Section 4.4.

It should be noted that, due to the limitation of the XRD method, compounds having small concentration in the samples can not be detected. Additionally, as demonstrated by the X-ray mapping of various elements using the electron microprobe, the compounds formed from the transformations of the inorganic matter are intimately distributed in the ash which deposits on the surface of the bed particles. Upon cooling the ash, first from the char particle temperature to the furnace temperature and then to the ambient temperature, some of its compounds may not form a complete crystalline structure to be identified by XRD. Furthermore, as indicated in the case of Na-Ca-sulphate, foreign elements may substite for some of the atoms in a crystal resulting in the shifting of the diffraction pattern of the pure compound.

In the case of Na-Ca-sulphate, Mg is likely to substitute for Ca. Chemical analyses of the bed material using the extraction method, Appendix C, indicate that a small proportion of Mg in the coating is water soluble presumably as sulphate. Evidence of mixed sulphates of sodium and magnesium have been found during the X-ray diffraction studies of some deposits formed during pc combustion and in magnesium-rich ash, Drummond, et al. (1977). Hence, it appears that the particle coating generally contains various sulphates of the 3-component system $CaSO_4$ - $MgSO_4$ - Na_2SO_4, of which the compounds of series Na-Ca-sulphate are the most pronounced.

5.5.4 THERMOMECHANICAL ANALYSES

The process by which the particles are bonded together is called sintering. Several investigators have reported that sintering can occur at a few hundred degrees below the initial deformation temperature defined by the ASTM ash fusion test (Stallmann and Neavel, 1980; Huffman et al., 1981; Hsieh and Roberts, 1985). The ASTM ash fusion test determines the shape-temperature dependence of molded ash cones and defines the following characteristic temperatures: the initial deformation temperature (IDT); the hemispherical temperature (HT); and the fluid temperature (FT).

The onset of sintering is the temperature at which particles begin to stick together or sinter. Hence, it determines the minimum temperature at which the particles have the potential to form agglomerates. The initial sintering temperature is measured using a dilatometer. The sample is placed in a cylindrical sample holder and a vertical shaft is pushed against the

sample in the cylinder. A constant force is applied to the shaft and the sample in the cylinder is heated at a pre-defined rate. The expansion or contraction of the sample is transferred to a gauge and the change of length of the sample is plotted against temperature.

At first, the sample increases in length due to thermal expansion. Then, with increasing temperature a point is reached where the rate of expansion begins to decrease. This indicates the onset of a phenomenon that is competing with thermal expansion, that is, sintering or densification. The initial sintering temperature (T_S) is defined as the temperature at which the thermal expansion and the shrinkage of the sample become equal.

Sintering tests were carried out on samples of bed material from each run using a thermomechanical analysis (TMA) instrument. The type of the instrument used is given in Subsection 3.5.4. In each test, a few bed particles coated with ash were placed in the sample holder and the length change of the samples were recorded as a function of temperature. The curves showing the rate of length change of the samples were also recorded.

All samples exhibited a sharp expansion (approx. 0.2%) at about 700°C which was followed by a contraction (Figures 5.41 to 5.44). The results of the thermogravimetric analysis, reported in Subsection 5.5.5, show that at about the same temperature the samples experience a weight gain under oxidising atmosphere.

It is suggested that the expansion of the samples is probably due to the oxidation of iron compounds formed from the transformation of pyrites which are present in the coal. Chemical analysis, XRD analysis and microscopic examination of the bed particles confirm the presence of Fe compounds in the coating. Pyrite decomposes to pyrrhotite at about 500° to 600°C (Srinivasachar and Boni, 1980). In the presence of oxygen, pyrrhotite then oxidises to magnetite and finally to haematite. During the ash formation process, the oxidation of pyrrhotite and other Fe compounds may occur partially as these compounds are likely to become embedded in the molten ash and hence become isolated from oxygen. During TMA tests, in the presence of air, oxygen penetrates through the pores of the coating resulting in further oxidation of these compounds.

The thermomechanical behaviour of the samples of Run 1 to 5 were found to be identical, a typical example is given in Figure 5.41. The results indicate that, although the agglomerating propensities of the bed particles in these runs were found to be different, Chapter 6, the onset of sintering (initial sintering temperature) of the bed particles is not affected by:

- the presence of minerals in the coating, Run 1; and
- the leaching of the coal samples by water and acid, Runs 4 and 5.

It appears that compounds other than the minerals are responsible for the initiation of the sintering mechanism and that these compounds are present in the coating of bed particles in Runs 1 to 5. The difference in the sintering (agglomerating) propensity of the bed material from these runs is considered to be, amongst other variables, due to the amount of these compounds present in the coating of the bed particles, Chapter 6.

The results, shown in Figure 5.41, also indicate that, after having reached the onset of sintering at about 700°C, the contraction slightly exceeds the thermal expansion.

Thermomechanical behaviour of the bed material from Run 6, carried out with the coal sample impregnated with NaCl (batch 1), is shown in Figure 5.42. The results indicate that the onset of sintering of this sample is the same as that of other samples described earlier. The marked difference in the behaviour of this sample is a more extensive contraction after the onset of sintering at about 700°C. The coating of the bed particles in this sample contain small amount of Cl compounds (about 0.5%), Section 5.3. In runs carried out with the untreated coal sample, the amount of Cl determined by the chemical method was about 0.04%.

Rapid contraction (melt down) occurred with the bed material from Run 7, carried out with the coal sample impregnated with larger amount of NaCl (batch 2), Figure 5.43. In addition to the onset of sintering at about 700°C, two extensive contractions occurred at about 720° and 800°C which are illustrated by the graph showing the rate of length change. The chemical and EDAX analyses of the bed material obtained from this run suggest that significant amount of Cl compounds (about 5.0% Cl) is present in the coating of the bed particles.

The thermomechanical behaviour of the bed material from Runs 2, 3 and 8, carried out at 850°, 800° and 750°C respectively, were found to be identical, Figure 5.41. The results confirm the results of chemical and EDAX analyses of the samples which indicated that, within the range tested, the furnace temperature does not have a marked effect on the characteristics of the coating deposited on the bed particles, Section 5.3 and Subsection 5.5.2.

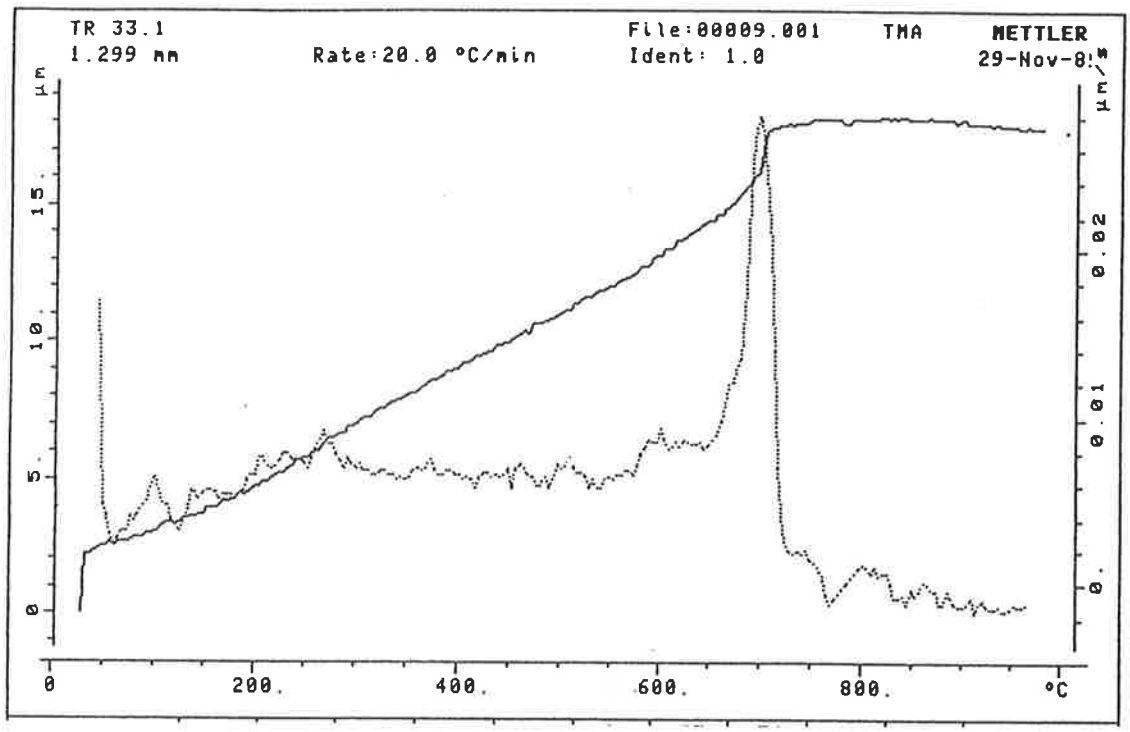

Figure 5.41: Thermomechanical Behaviour of the Ash Coating (Runs 1 to 5)

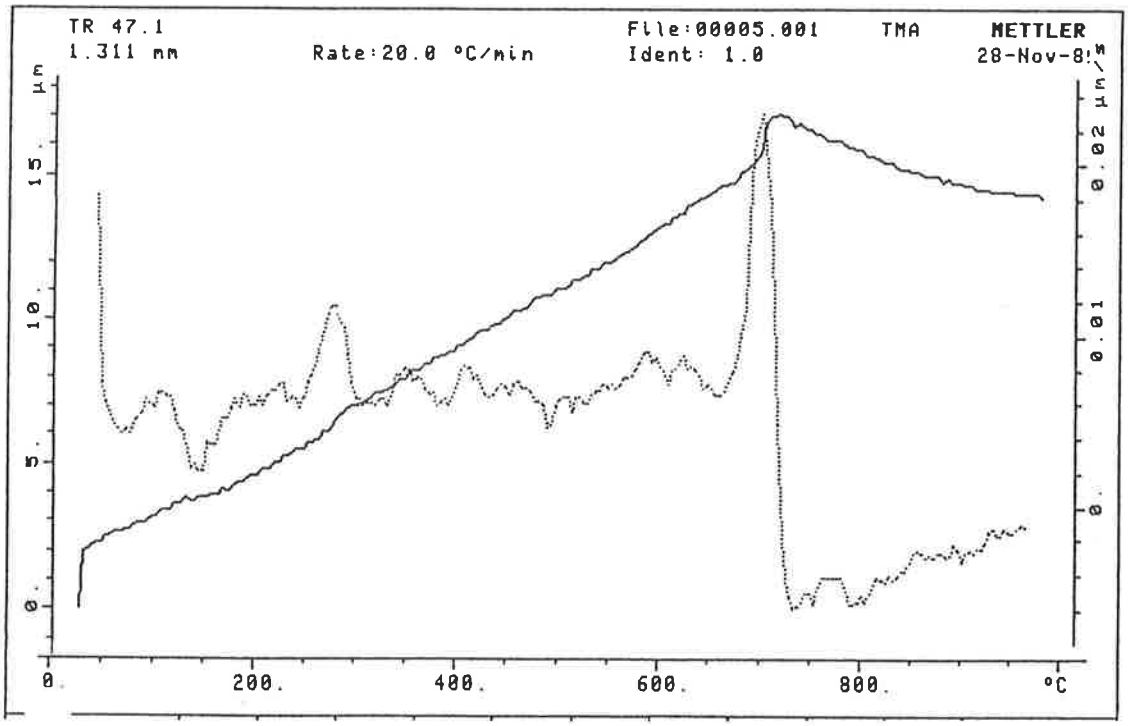

Figure 5.42: Thermomechanical Behaviour of the Ash Coating (Run 6)

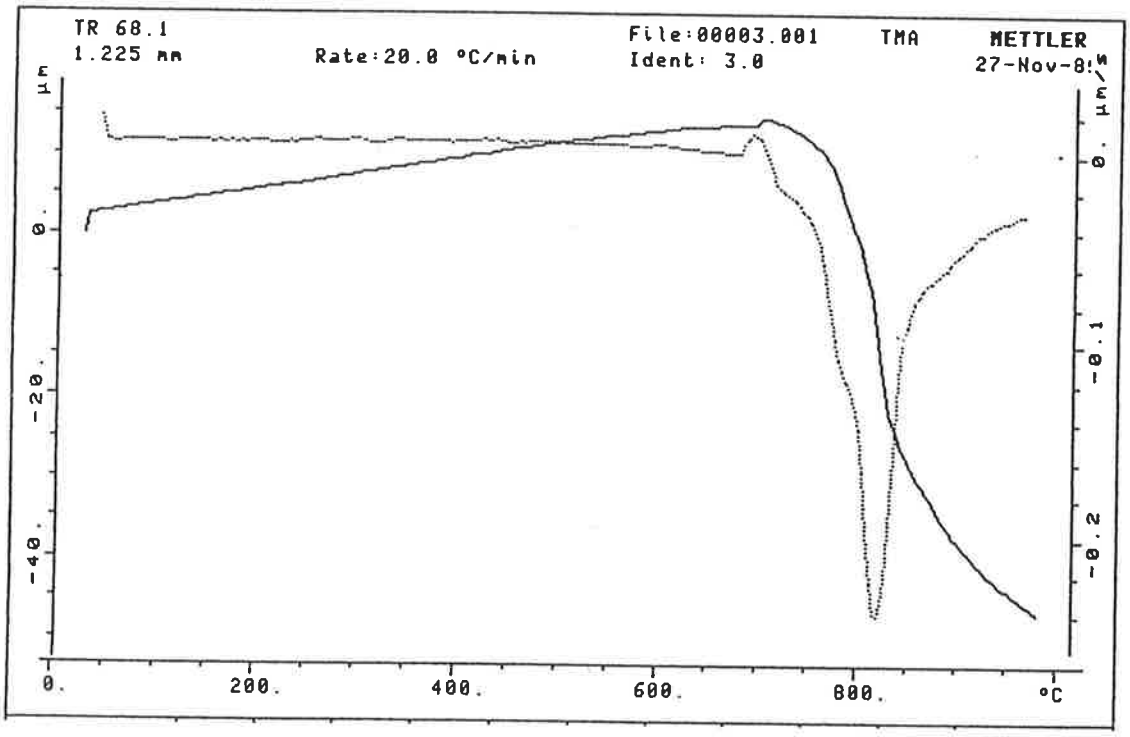

Figure 5.43: Thermomechanical Behaviour of the Ash Coating (Run 7)

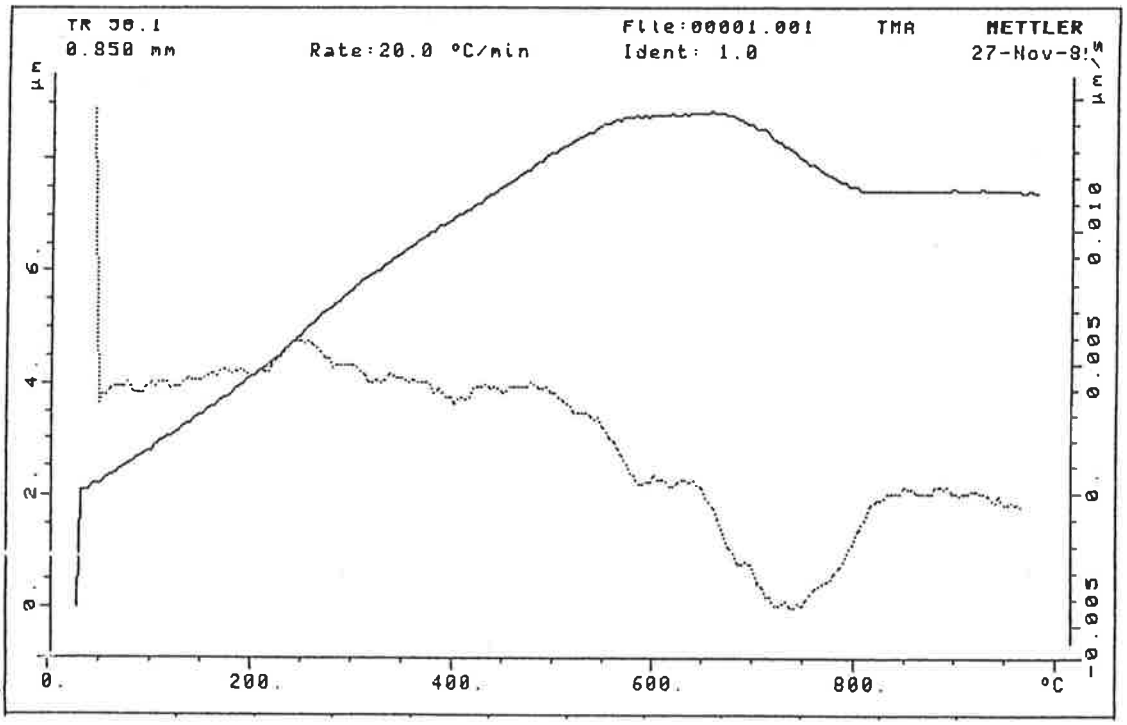

Figure 5.44: Thermomechanical Behaviour of the Ash Coating (Run 11)

The thermomechanical behaviour of a sample of bed material obtained at a furnace temperature of 700°C, Run 9, exhibited an earlier contraction at about 450°C. DTA/TGA analyses, Subsection 5.5.5, indicated that this contraction coincides with an exothermic reaction which is the characteristics of carbon combustion. The presence of carbon in the coating of the bed particles from this run, which is the result of operating the furnace at a low temperature, was detected by XRD analysis, Subsection 5.5.3. The loss of ignition carried out on a sample of the bed material from this run confirmed the presence of a significant amount of carbon in this sample.

In addition to the contraction at about 700°C, dolomite bed particles coated with ash, Run 11, exhibited an earlier contraction due to transformation of dolomite (Subsection 5.5.4), Figure 5.44. These contractions are illustrated by the graph showing the rate of length change (Figure 5.44). Similar contraction at 700°C indicates that the coating on the bed particles contains the same compounds which are responsible for the sintering of the bed particles in other runs. Microscopic examination and EDAX analyses of the coating on the dolomite bed particles confirm that the coating of the bed particles in the dolomite run has the same characteristic as that in the silica runs.

The thermomechanical behaviour of the bed material from Runs 12, and 13, carried out at lower O_2 levels, was similar to that of Run 3 shown in Figure 5.41. Again, the results agree with the results of EDAX and chemical analyses which indicated that the composition of the coating on the bed particles does not change with excess oxygen, Section 5.3.

5.5.5 SIMULTANEOUS DTA/TGA ANALYSES

Simultaneous TGA/DTA analyses were carried out on selected samples of bed material. The description of the instruments is given in Subsection 3.5.5. All samples were analysed under oxidising conditions. A few samples were also tested under nitrogen environment. For the analyses, the bed particles were ground and the coating of the bed particles was removed in the form of powder. Analyses were also carried out on a few granular samples of bed material. The results are given in Figure 5.45.

The samples first exhibited a broad exotherm, due to the combustion of the residual unburnt carbon, during which a few endotherms occured (due to the loss of adsorbed and crystalline

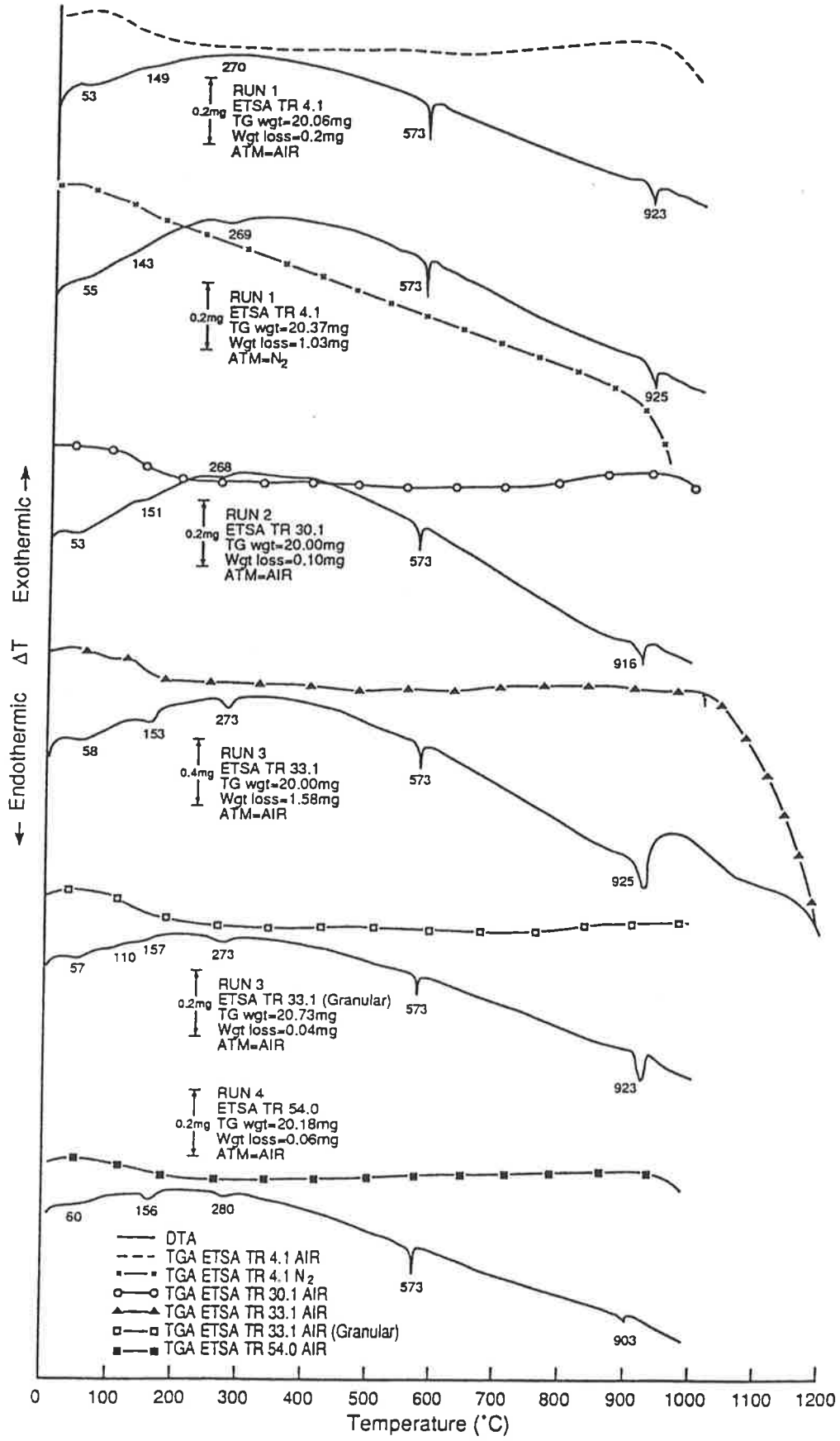

Figure 5.45: DTA/TGA Behaviour of the Bed Particles

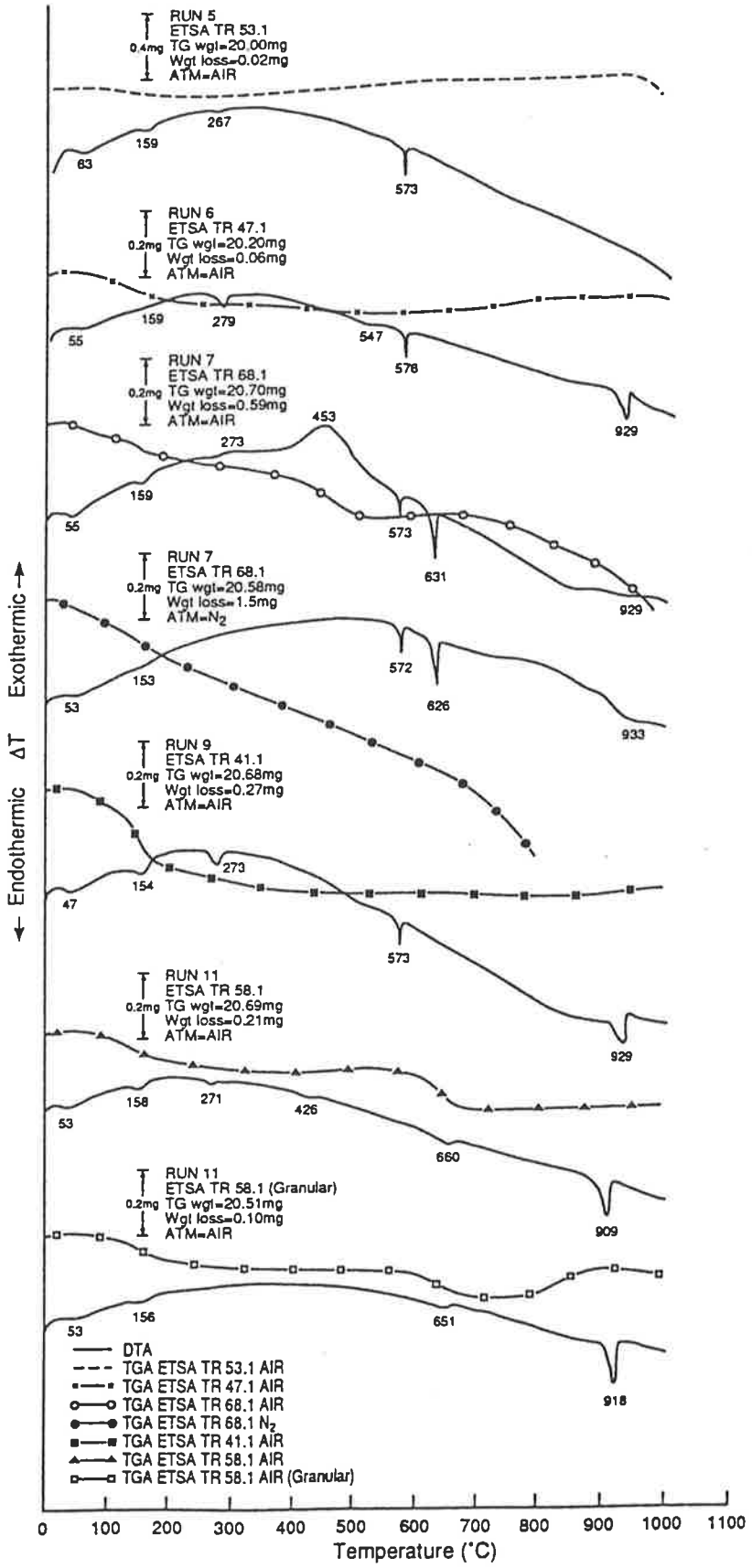

Figure 5.45: DTA/TGA Behaviour of the Bed Particles (Cont'd.)

water). In the silica runs, the endothermic transformation of silica occurs at about 573°C. In the dolomite run, the endotherms at about 426°C and 660°C are attributed to dolomite transformations.

The DTA/TGA behaviour of the samples of Run 1 to 5 was found to be similar. Figure 5.45 shows that a broad endothermic process occurs after the transformation of silica which suggests some of the compounds in the samples undergo a slow process of melting. The results also suggest that the sintering of the bed particles detected by the TMA at about 700°C, Subsection 5.5.4, is likely to have been caused by the formation of melt(s). Except in the bed material obtained from Run 5, an endothermic peak was also detected at above 900°C which indicates melting of a new compound of a significant proportion.

Of the compounds identified by the XRD analyses, Subsection 5.5.3, the 3-component system Na_2SO_4 - $CaSO_4$ - $MgSO_4$ is likely to form low melting point eutectics. A eutectic of Na_2SO_4 and $MgSO_4$ melts at about 670°C and a eutectic of Na_2SO_4 and $CaSO_4$ melts at about 900°C, phase diagrams are given in Figure 2.2. Pure Na_2SO_4 also melts at about 900°C.

It is suggested that the broad endotherm detected in all samples at about 700°C is due to the Na_2SO_4 and $MgSO_4$ eutectic. The endothermic peak detected at above 900°C is likely to be due to the formation of the Na_2SO_4 and $CaSO_4$ eutectic as well as melting of pure Na_2SO_4. Due to the presence of a significant amount of Na and Ca sulphates in the coating of bed particles in Runs 1 to 3, a sharp peak was detected as a result of endothermic transformation (melting) of these sulphates. The coatings formed during Runs 4 and 5, with the water and acid leached coal samples respectively, contain lesser proportions of Na_2SO_4 and, hence, exhibited either a weak endothermic peak (Run 4) or no peak at all (Run 5) at above 900°C.

The analyses of the coating from Run 3 was continued up to 1200°C. After the formation of a melt at 925°C, the sample underwent melt down with a parallel weight loss due to the vaporisation of melt(s).

The results of DTA/TGA analyses for Run 6 is similar to those of Runs 1 to 3. Run 6 was carried out with a coal sample impregnated with NaCl (batch 1). A weak endothermic peak was detected at about 547°C which can not be explained.

The coating formed during Run 7, with a coal sample impregnated with a larger proportion of NaCl, exhibited an additional endothermic peak at about 631°C which suggests the formation of a new melt at this temperature. However, this melt did not cause an appreciable contraction of the sample during TMA test, Subsection 5.5.4. It should be noted that the slope of the DTA graph is sharper than that of the other runs indicating a more extensive endothermic process after the formation of the peak at 631°C. The relatively large weight loss of this sample, detected by the TGA, suggests that a significant amount of melt(s) is formed which partly evaporates from the sample. The results agree with the results of TMA tests which indicated a melt down of this sample after 700°C.

The enhanced exothermic process observed at lower temperatures (with a peak shown at 453°C) is due to the combustion of unburnt carbon present in this sample.

The coating of the bed particles in Run 7 contains a significant amount of sodium chloride which can form three additional melts as follows:

- a eutectic of NaCl and Na_2SO_4 at 621°C;
- a eutectic of NaCl and $CaSO_4$ at 721°C;
- pure NaCl melting at 801°C.

The endothermic peak detected at about 631°C could be attributed to the eutectic of NaCl and Na_2SO_4. The other two melts are likely to be responsible for enhancing the contraction process shown in Figure 5.43.

A sample of coating from Run 9, carried out at 700°C, was also analysed by the DTA/TGA. This sample exhibited similar DTA/TGA behaviour to those of samples from runs carried out at higher temperatures, that is Runs 2 and 3. The larger weight loss and the greater exotherm detected at lower temperatures (200° - 400°C) is due to the larger proportion of unburnt carbon in this sample. The results confirm the results of other analyses that, within the range tested, the combustion temperature does not have a significant impact on the characteristics of the coating.

The results of DTA/TGA analyses of a sample of coating from Run 11, with a dolomite bed, confirmed that the coating formed on dolomite bed particles have the same characteristics as those formed on silica particles. The additional endothermic peaks detected are related to the transformations of dolomite which was present in this sample.

The results of DTA/TGA analyses carried out on a selected sample under N_2 atmosphere are also given in Figure 5.45. The results show a gradual and significant weight loss which can not be explained.

The results of analyses carried out on powdered and granular samples were found to be similar. With powdered samples, the endothermic peaks detected at low temperatures were more enhanced.

5.6 LARGE PILOT PLANT STUDIES

The FBCS was designed to simulate the stirred environment of the circulating fluid bed combustion (CFBC) systems. The bench scale systems, however, can not simulate all of the design parameters of a full scale plant. In order to validate the physico-chemical processes experienced during combustion of coal in the FBCS, samples of bed material and fly ash collected in the bag filter during the pilot plant testing of Lochiel coal in a 300 kg/h CFBC pilot plant, owned and operated by Lurgi Gmbh of Frankfurt, Federal Republic of Germany, were characterised by electron microscopy and X-ray diffraction techniques. The results of these characterisation are given in this section. The description of the Lurgi pilot plant is given elsewhere (Beisswenger et al., 1985).

The coal used during the pilot plant tests was similar in composition to that of the high-mineral coal sample used in Run 1. The pilot plant tests were carried out at various combustor temperatures using various quantities of ballast (coal overburden) and reactive material. Hence, the bed material collected in these tests contained particles of various compounds. Nonetheless, the chemical analyses of bed material indicated a gradual increase in the concentration of elements found in the ash. The composition of the ash in the bed could not be determined due to the presence in the bed of additives containing the same elements as those found in the ash.

Microscopic Examination

Due to the continuous addition of large amount of overburden and dolomite to the combustor, the bed material in the pilot plant was continuously replaced with fresh material. This resulted in a small amount of ash being accumulated in the combustor.

A micrograph of the backscattered electron image of a polished cross-section of the bed material obtained from the pilot plant, given in Figure 5.46, shows the variety of compounds present. Some of the silica particles appear to have a thin layer of coating. Due to the continuous introduction of fresh bed material, some of the silica particles do not have any coating at all.

Figure 5.47 shows a micrograph of a polished cross-section of bed particles at higher magnification. EDAX analyses of the coating indicate that the coating consists mostly of compounds of S, Ca, Na, Mg and Al. While the same elements are found in the coating of bed material obtained from the FBCS, the concentration of Na in the coating of pilot plant bed material seems to be lower, whereas, the concentration of Si is higher.

The distribution of the inorganic elements in the coating of the same bed particles is shown in Figure 5.48 in the form of X-ray maps. The silica particles on the right and the spinel particle on the left are coated by the ash. The concentration of S in the coating appears to be non-uniform. Si is intimately distributed in the matrix of the coating.

Microscopic examination of other material present as bed particles indicates that the coating is indiscriminately formed on all material. Figure 5.49 shows a back-scattered electron image of a polished cross-section of a clay particle coated with ash. The X-ray image of S, shown in this figure, indicates that the clay particle has been coated with sulphated compounds. Due to the structure of clays, the ash has penetrated the particle.

Figure 5.50 shows a back-scattered electron micrograph and X-ray images of a polished cross-section of dolomite particles. The X-ray image of Al shows the formation of coating on the dolomite bed particles. The bright spots in this image is either due to non-uniform distribution of Al in the coating or due to the presence of clay particles trapped in the coating.

SEM examination of the surface of the coated bed particles obtained from the pilot plant tests, Figure 5.51, shows similar morphology and composition to those found in the FBCS.

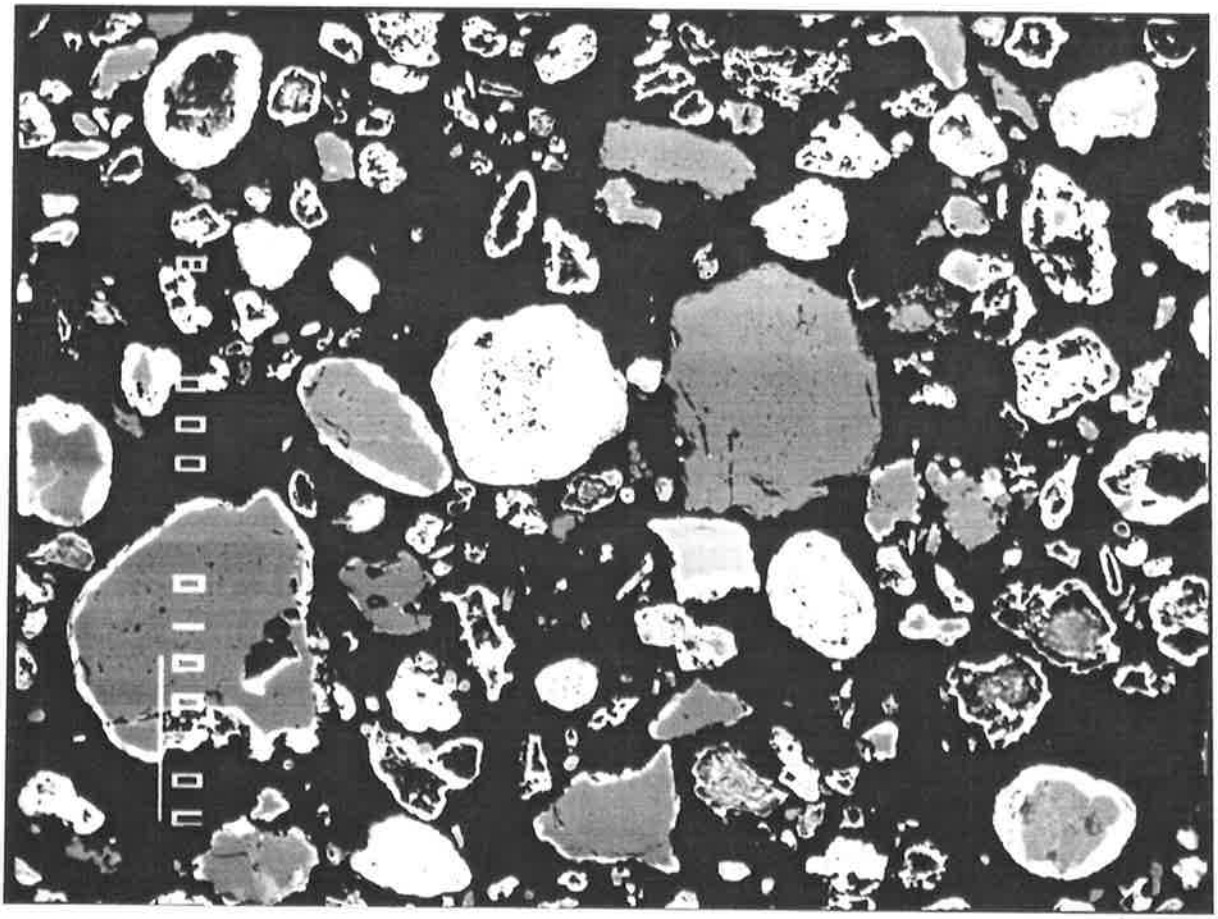

Figure 5.46: **Back-scattered Electron Image of a Polished Cross-Section of Bed Material from Pilot Plant Tests** - Bright band around some of the bed particles shows the formation of coating. 100 μm bar is shown on the left.

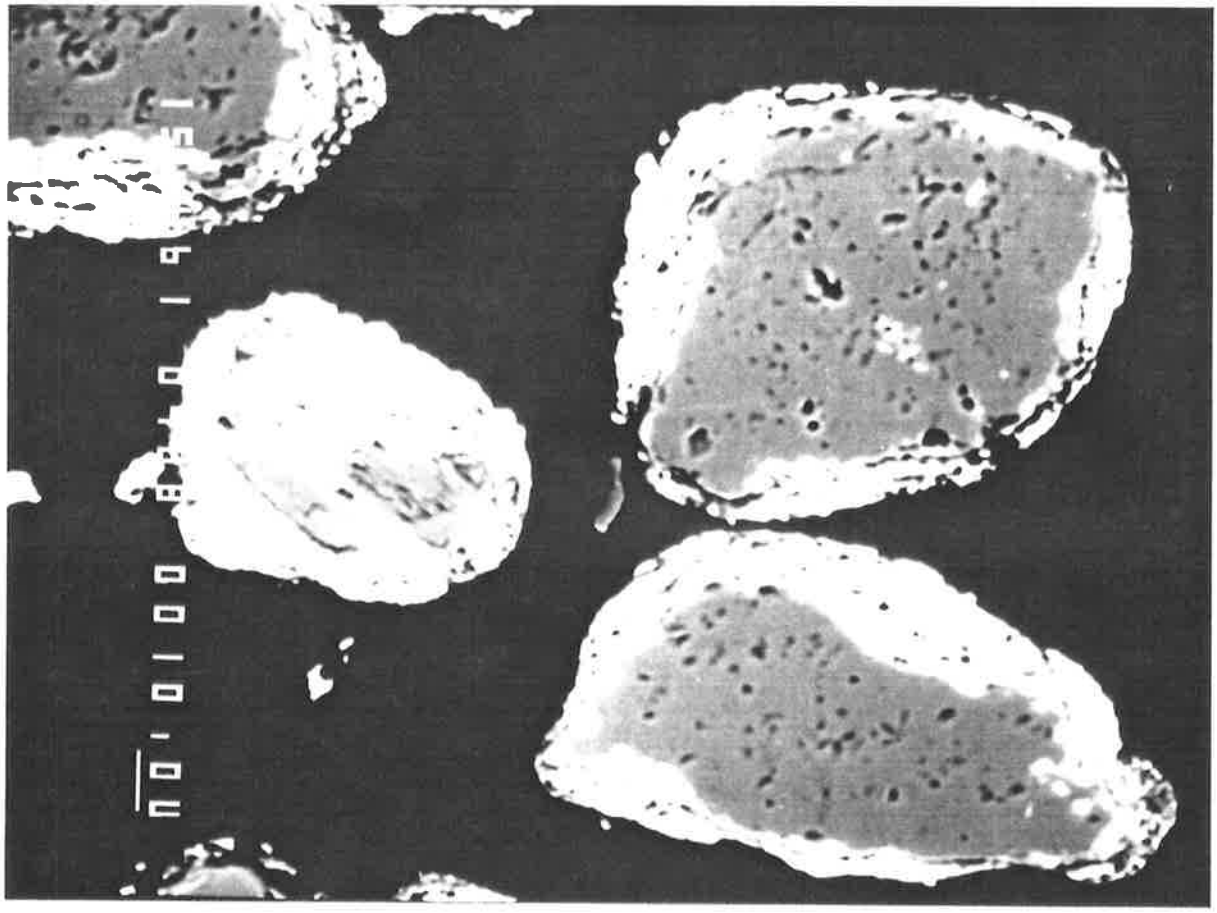

Positions Analysed:	Na_2O	CaO	MgO	SO_3	Al_2O_3	SiO_2	K_2O	P_2O_5	Cl	FeO
1	1.3	30.9	9.5	46.7	3.5	6.8	-	-	-	0.9
2	1.5	28.8	5.5	57.7	2.6	2.1	-	-	-	2.1

Figure 5.47: **Back-scattered Electron Image of a Polished Cross-Section of the Bed Particles Coated During the Pilot Plant Tests** - EDAX analyses of selected positions in the coating are presented. 10 m bar is shown on the left.

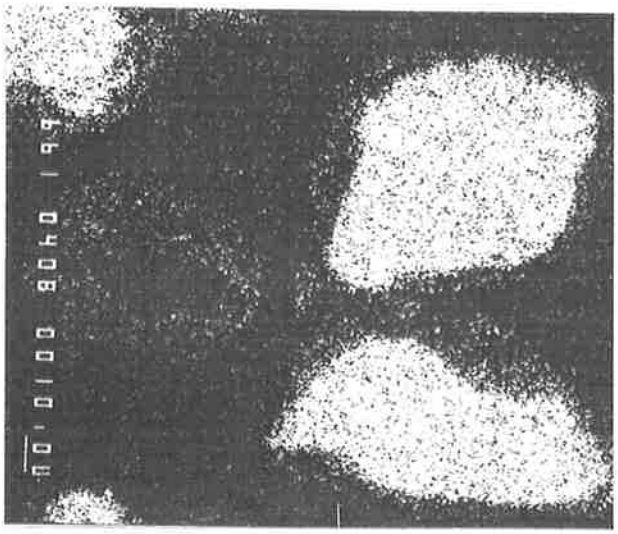

Figure 5.48 (a)= Si

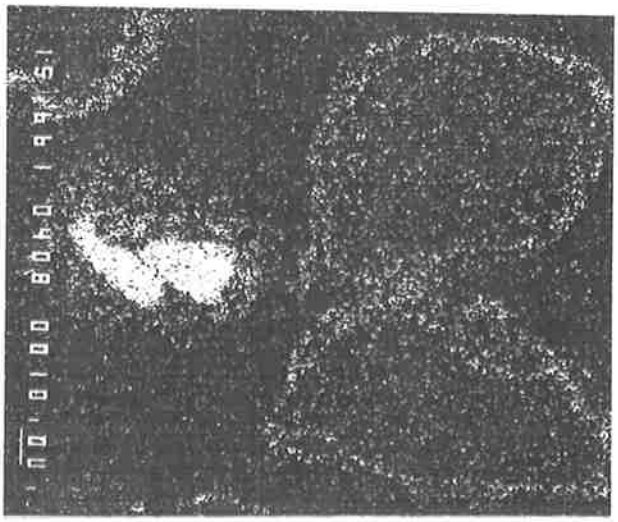

Figure 5.48 (b)= Al

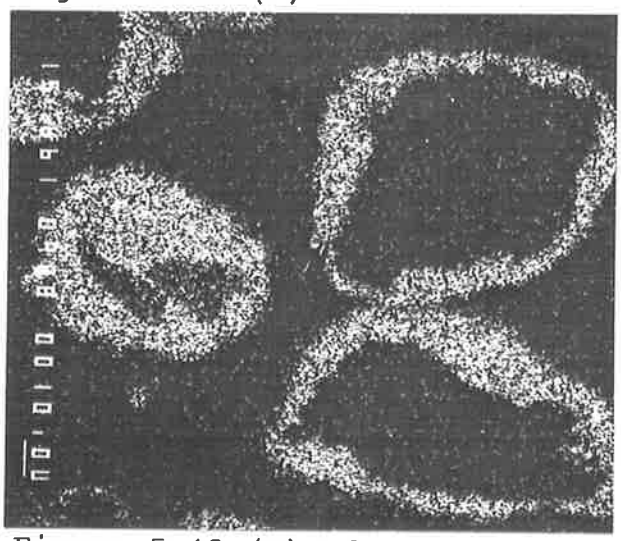

Figure 5.48 (c)= Ca

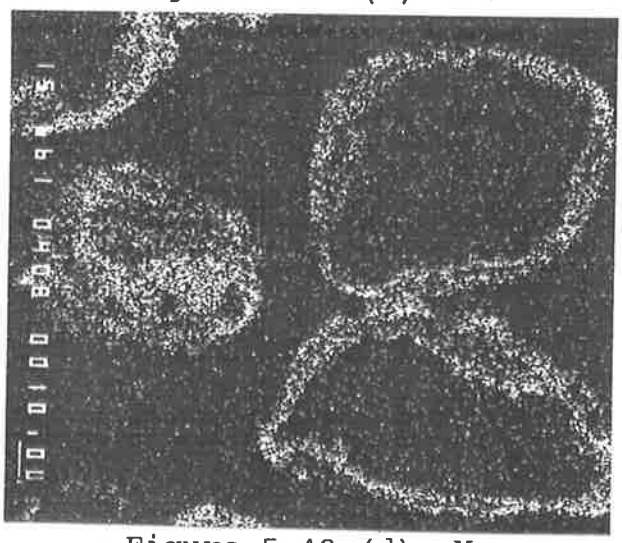

Figure 5.48 (d)= Mg

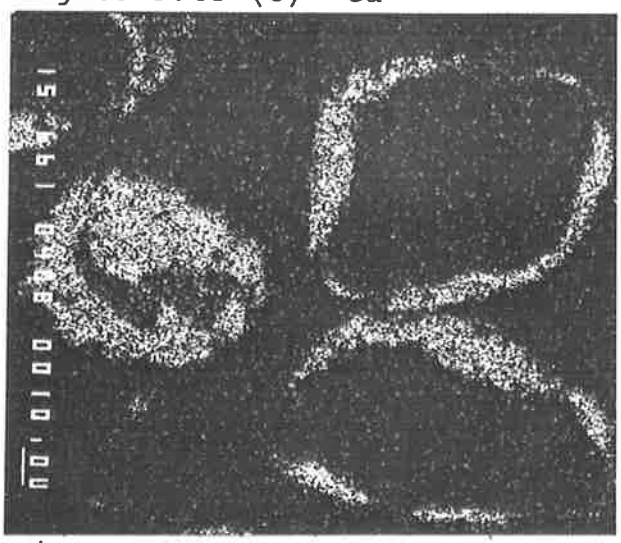

Figure 5.48 (e)= S

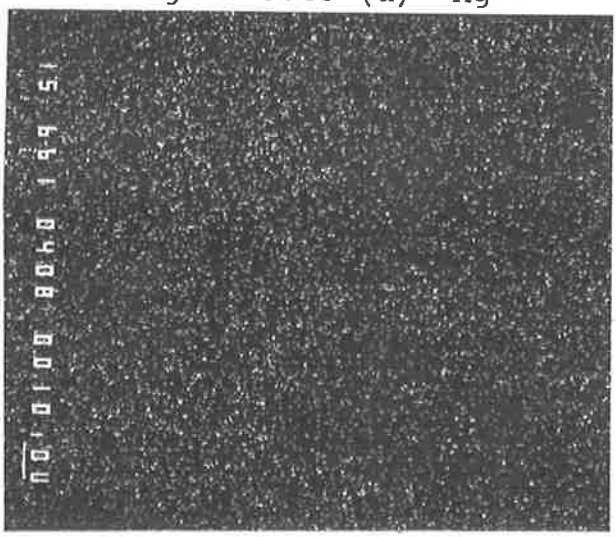

Figure 5.48 (F)= Cl

Figure 5.48: X-ray Maps of a Polished Cross-Section of the Bed Particles Coated during the Pilot Plant Tests - 10 μm bar is shown on the left.

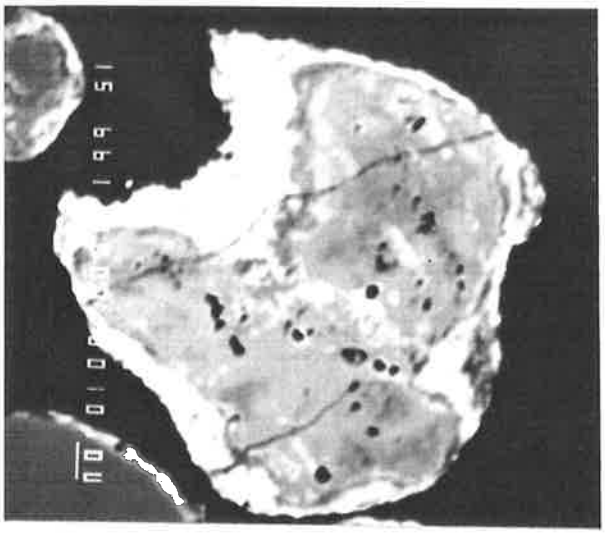

Figure 5.49 (a)= Back-scattered electron image

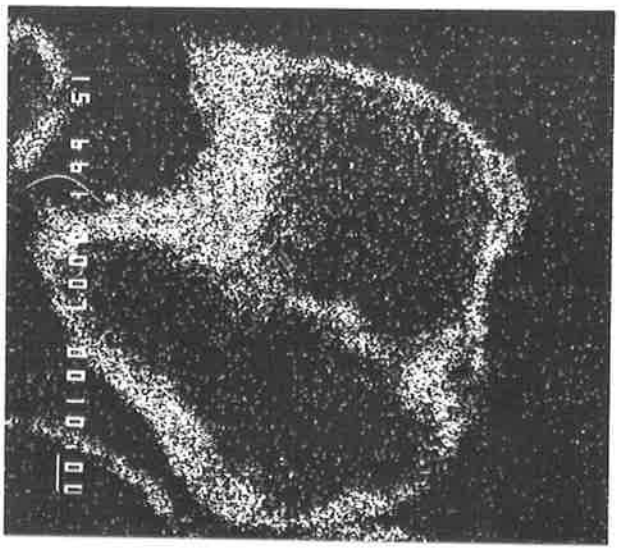

Figure 5.49 (b)= Sulphur X-ray image

Figure 5.49: Back-scattered Electron Image and Sulphur X-ray Map of a Polished Cross-Section of a Clay Bed Particle Coated With Ash - 10μm bar is shown on the left.

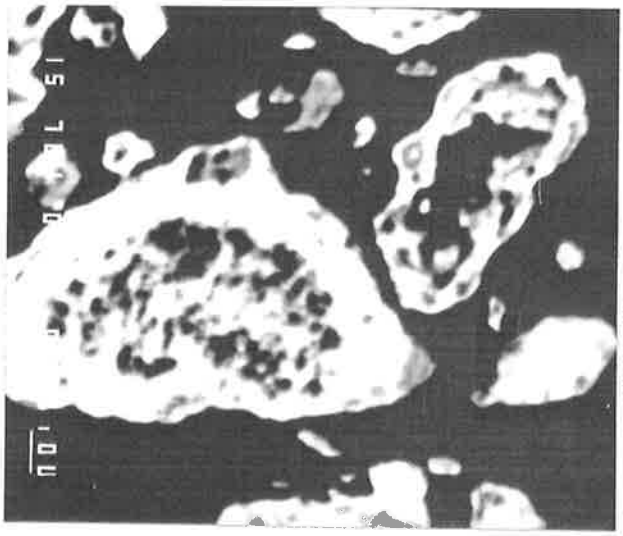

Figure 5.50 (a)= Micrograph

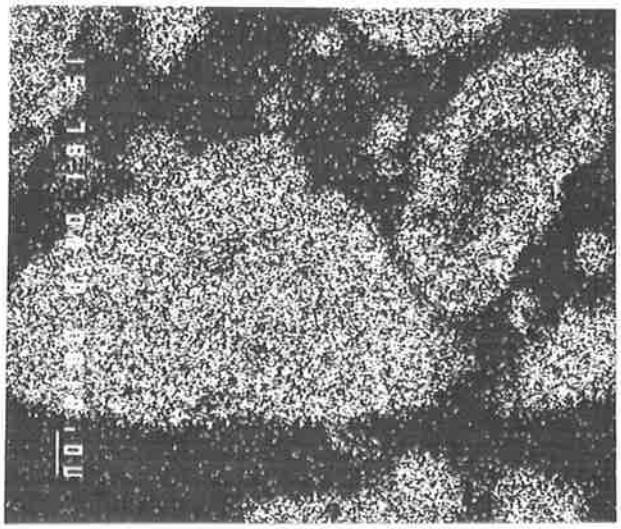

Figure 5.50 (b)= S

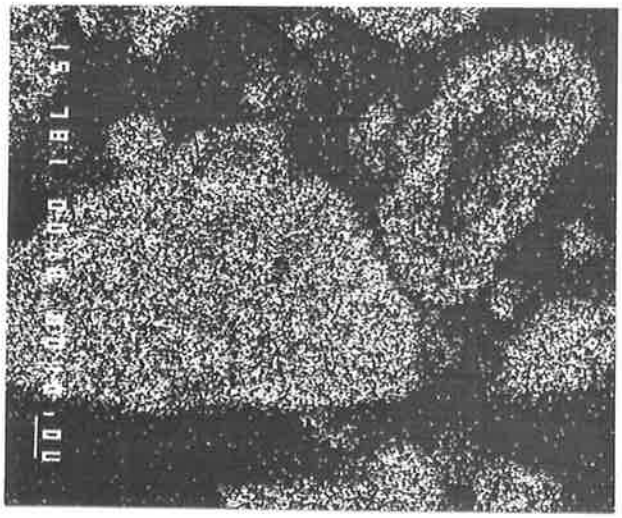

Figure 5.50 (c)= Ca

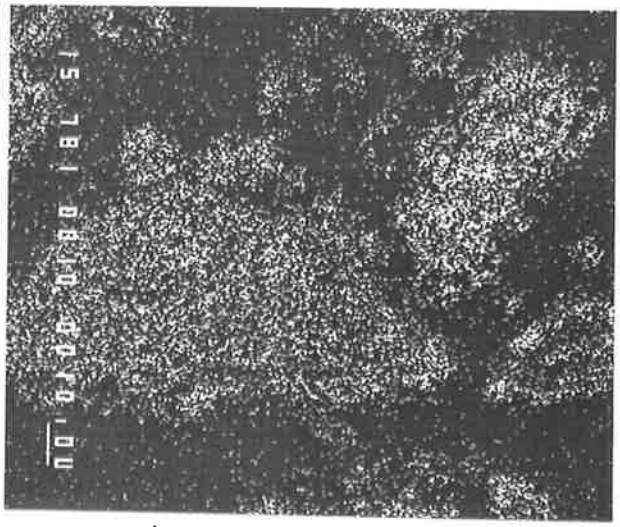

Figure 5.50 (d)= Mg

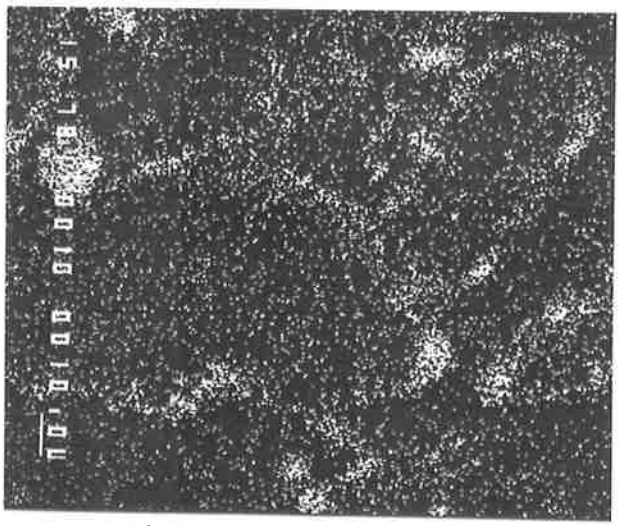

Figure 5.50 (e)= Al

Figure 5.50: **X-ray Images of a Polished Cross-Section of a Dolomite Bed Particle Coated with Ash** - Al image shows the coating formed on the bed particles.

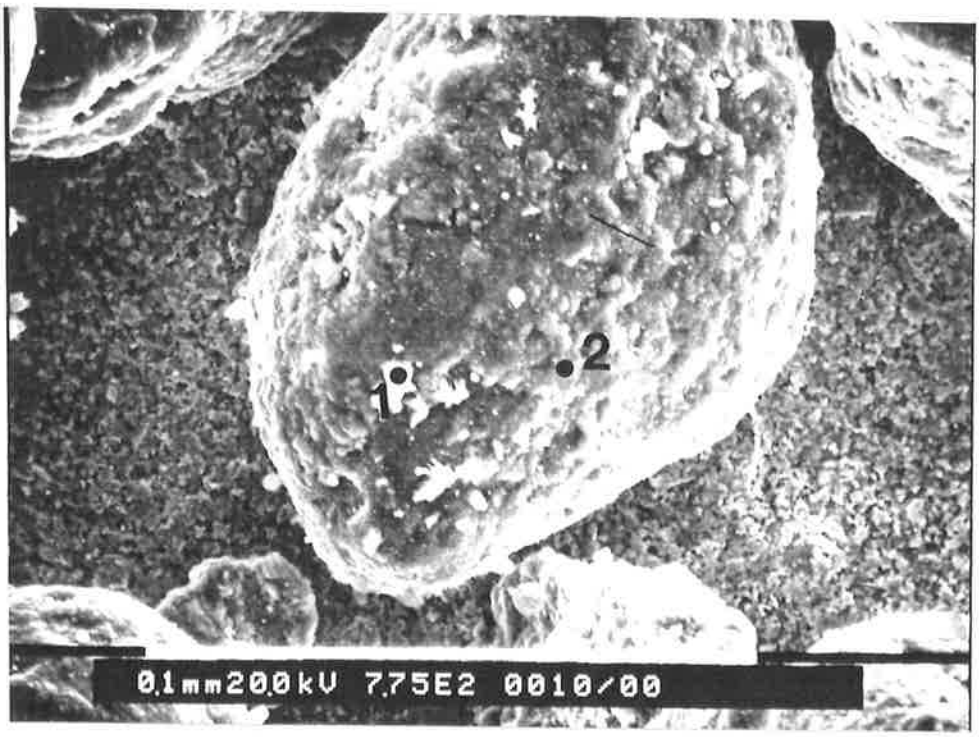

Magnification x 775

1: S, Ca, (Na,Mg,Al,Si)
2: Ca, S, Mg, (Al,Si)

Figure 5.51: Secondary Electron Image of the surface of a Bed Particle Coated with Ash during the Pilot Plant Tests - Major and minor (in bracket) elements at selected positions detected by EDAX are presented.

X-ray Diffraction Analysis

Numerous compounds were detected by XRD analysis of the samples taken during the pilot plant tests. Most of these compounds were introduced to the combustor as the additives. Hence, it is difficult to determine which of these compounds have been formed from the inorganic matter in coal. However, as the additives employed did not contain an appreciable amount of sodium and chlorine, the presence of compounds containing these elements can be attributed to the coal's inorganic matter.

The major crystalline Na compound identified in the bed material was $Na_4\ Ca(SO_4)$. The characteristic of the peaks assigned to $Na_4\ Ca(SO_4)$ suggests that this compound may contain foreign elements such as Mg. It appears that the ash formed during these tests, which is then deposited on the bed particles, contained various sulphates of the 3-component system $CaSO_4$ - $MgSO_4$ - Na_2SO_4, of which the compounds of series Na, Ca and SO_4 are the most pronounced.

Thenardite (Na_2SO_4) was only found in those bag filter samples in which Na to Ca ratio was high (i.e. tests with lesser amount of dolomite addition). Thenardite could be the hydration product of $Na_4\ Ca(SO_4)$.

The chemical analysis as well as XRD analysis of bed material indicate that NaCl is absent from the bed material. NaCl was only found in the bag filter samples containing fine particles. The presence of NaCl in the filter samples is considered to be the result of partial vaporisation of NaCl in coal and its subsequent condensation on finer particles. HCl was detected in the flue gas indicating the reactions of NaCl with other compounds in the combustor.

Examination of the samples obtained from the pilot plant tests confirms that the ash forms a coating on the bed particles. Although the conditions under which the coal was fired in the pilot plant, that is with various additives, was different from those in the FBCS, the characteristics of the coating deposited on the bed particles in both systems appear to be similar. Sodium is present in the coating as complex sulphates of Na, Ca and possibly Mg in a 3-component system. The lack of Cl in the bed material and its presence in the bag filter ash and in the flue gas as HCl is in agreement with the findings of single particle experiments and the fluid bed combustion experiments carried out in the FBCS.

The formation of the coating on silica as well as other compounds present in the bed agrees with the hypothesis that the deposition of the coating is a physical process by which the ash transfers from the char surface to the surface of the bed particles with which it has lesser interfacial tension.

5.7 DISCUSSION

5.7.1 MECHANISM OF COATING DEPOSITION

The mechanism of the deposition of the coating on the bed particles during the CFBC of high-sodium, high-sulphur low-rank coals and the role of the inorganic matter in this mechanism can be determined using the results of the experiments carried out in the SPF and in the FBCS.

The SPF experiments indicated that the combustion of low-rank coals with high content of sodium and sulphur results in the formation of a highly sulphated ash matrix on the char's surface, Section 4.3. The ash matrix includes a molten phase in which solid particles are embedded. The molten phase consists mostly of S, Na and part of Ca in the form of sodium sulphate (thenardite), calcium sulphate (anhydrite) and complex sodium-calcium sulphates in which Na is likely to be substituted by other cations such as Mg. The solid phases present in the ash matrix include:

a) large mineral inclusions which are trapped in the ash matrix during the ash formation process;

b) sub-micron silica particles, intimately distributed in the coal matrix, which are also trapped in the ash matrix; and

c) solid compounds formed from the organically bound Ca, Mg and Al, that is, aluminates and oxides in a multi-component system.

The solid compounds in groups b and c become intimately distributed in the ash matrix.

The combustion experiments carried out in the FBCS and the chemical and microscopic examination of the solid products indicated that:

- the bed particles become coated in the stirred environment of the FBCS;

- the rate of deposition of the coating does not change with operating time;
- the average composition and the characteristics of the coating do not change with operating time;
- there is no indication of chemical reaction between gaseous species, such as those of Na, and silica forming molten phases;
- there is a clear boundary between the coating and silica particles;
- the coating has similar characteristics to those of the ash formed on the char surface, that is a molten matrix (rich in Na, Ca and S) in which solid phases (minerals and the species formed from the organically bound Ca, Mg and Al) are embedded;
- the chemical composition of the coating and the compounds identified in the coating by XRD are similar to those of the ash formed on the char surface.

The results indicate that in CFBC systems, where the bed particles and the char particles collide vigorously, the molten ash matrix formed on the char's surface transfers to the surface of the bed particles with which it has lesser interfacial tension. This results in the formation of a coating on the bed particles which has similar characteristics to those of the ash formed on the char's surface. A proportion of the molten ash matrix not transferred to the surface of the bed particles is collected in the cyclone as fly ash.

Comparison of the chemical composition of the coating, cyclone ash and the coal ash (ASTM ash) indicates that the coating is enriched in Na and S species which constitute the molten matrix of the coating. The disproportioning of the inorganic matter in the combustor can occur either on the char surface during the ash formation process and/or during the deposition of ash on the bed particles. The former appears more likely since a portion of the solid phases exposed on the char surface can escape into the gas phase prior to being trapped in the molten ash matrix. This results in the depletion of the ash matrix in elements forming the minerals and in the organically bound elements forming the solid phases during combustion, that is Ca, Mg and Al. The ash transferred to the surface of the bed particles in the combustor would then become enriched in those elements forming the molten phases, that is Na and S.

It is also possible that the molten phases in the ash matrix are preferentially deposited on the bed particles resulting in the disproportioning of the inorganic matter in the combustor in favour of those species which are likely to have lower melting points.

The results confirm the hypothesis described earlier (Section 5.1) that the mechanism of deposition of coating on the bed particles is:

- collision of bed particles with burning char particles covered in molten ash in the stirred environment of CFBC;
- transfer of molten ash from the surface of burning char particles to the bed particles.

The theoretical evaluation of the deposition of the coating on the bed particles is given in Chapter 7.

5.7.2 EFFECT OF VARIABLES

The chemical analyses of the coating calculated on silica-free basis, Section 5.3, indicate that the composition of the coating changes slightly with the variables investigated. Leaching of coal with water and acid results in a marginal reduction in the concentration of sodium in the coating. The addition of sodium chloride to the coal results in a residual concentration of Cl compounds in the coating. Combustion of the high-mineral coal sample results in the formation of a coating with numerous mineral inclusions.

While the chemical composition of the coating deposited on the bed particles is affected only marginally by certain variables, the rate of deposition of coating changes markedly with coal quality and furnace temperature. The effect of excess oxygen on the rate of deposition of the coating could not be determined due to the limitation of the FBCS. A summary of findings is given in Table 5.7 which compares the composition and the rate of deposition of the coating for various runs with those of Run 3, carried out at 800°C using the low-mineral coal sample.

For the same firing rate, the rate of deposition of the coating is expected to be governed by the:

- content of the inorganic matter in the coal being fired;
- chemical composition of the ash formed on the char's surface;
- operating temperature;
- fluidisation velocity;

Table 5.7: ***Effect of Operating Variables on Composition and Rate of Deposition of Coating.***

Run No	Variable	Composition					Depos. Rate	Comments
		Na	Cl	S	Ca	Mineral		
1	increasing minerals	0	0	(-)	(-)	(+)	(-)	less sticky
4	decreasing WS inorganic	(-)	(-)	0	0	0	(-)	
5	decreasing AS inorganic	(-)	(-)	0	(-)	0	(-)	
6 7	increasing NaCl	0	(+)	0	0	0	(+)	more sticky
2 3 8 9	decreasing Furnace Temp.	0	0	0	0	0	(-)	less sticky
11	decreasing bed size	0	0	0	0	0	0	
12 13	decreasing excess O_2	0	0	0	0	0	?	

WS = Water-soluble
AS = Acid-soluble

(0) = no significant change
(+) = significant increase
(-) = significant decrease

- initial charge and size distribution of the bed inventory;
- system geometry.

The content of the inorganic matter in coal determines the rate of formation of ash on the char's surface and, in turn, the rate of deposition of ash on the bed particles. The chemical composition of the ash formed on the char's surface and the operating temperature determine the stickiness of the ash. The other factors listed above determine the number of collision between the char and the bed particles. Thus, the variation in the rate of deposition of coating experienced in various runs can be explained as follows:

- The higher proportion of mineral inclusions in the molten ash matrix formed on the char surface of the high-mineral coal, Run 1, is likely to reduce the stickiness of the ash and hence its tendency to deposit on the bed particles.
- Given the same rate of combustion, the lower content of the inorganic elements in the coal samples fired in Runs 4 and 5, resulting from leaching the samples with water or acid, is expected to reduce the rate of formation of ash. The chemical and EDAX analyses of the ash, Sections 5.3 and 5.5, indicate that the concentration of sodium in the ash and, most likely, its stickiness decreases with decreasing amount of sodium in the coal. Therefore, the lower rate of deposition of the coating experienced in Runs 4 and 5 is considered to be due to a combination of the above two reasons.
- The addition of NaCl to the coal fired in Runs 6 and 7 is expected to increase the rate of formation of ash on the char's surface. The presence of Cl compounds in the ash enhances the stickiness of the molten ash, Subsection 5.5.4. The latter appears to be the main reason for the increase in the rate of deposition of the coating.
- Furnace temperature was found to have a minor effect on the composition of coating but a significant effect on the rate of deposition of coating on the bed particles. The stickiness of the molten ash, governed by its surface tension and viscosity (Chapter 7), is expected to increase with increasing temperature resulting in an increase in the rate of deposition of the coating.
- The rate of deposition of the coating for the charge having smaller size distribution was found to be slightly higher. This charge, containing larger number of bed particles per unit mass, is expected to have more collisions with the burning char particles in the furnace resulting in more ash deposition on the bed particles.

Chapter 6

AGGLOMERATION AND DEFLUIDISATION

6.1 INTRODUCTION

The combustion experiments carried out in the single particle furnace (SPF) showed that, for operating conditions relevant in fluid bed combustors, the inorganic matter in low-rank coals containing Na and S forms a molten ash matrix on the char's surface. The combustion experiments carried out in the FBCS, described in Chapter 5, demonstrated that the molten ash transfers from the surface of burning char particles to that of the bed particles with which it has less interfacial tension. By doing so, the molten ash is cooled to the furnace temperature. At this temperature, some of the species in the coating may remain molten and in this condition the bed particles are capable of sintering together and forming agglomerates.

The main purpose of the investigation reported in this chapter was to study the mechanisms by which the bed particles agglomerate and/or defluidise. While conducting the combustion experiments in the FBCS, the effect of certain variables on the rate of agglomeration and the onset of defluidisation was also investigated. The results, however, are considered to be only indicative as substantial experimental work, beyond the scope of this project, is

required for exact quantification.

The variables investigated are: operating time; coal quality; bed temperature; bed particle size distribution; and bed material. The effect of excess O_2 in the flue gas on the rate of agglomeration could not be determined due to the unstable and short duration of the tests carried out at lower excess O_2 levels.

The details of the experimental procedure and the experimental program are given in Subsection 3.4.3.

6.2 CHARACTERISTICS OF AGGLOMERATES

In order to determine the mechanism of agglomeration, samples of bed material removed from the FBCS were examined by electron microscopy. The bed material contained agglomerates of two or more bed particles, coated with the molten ash, forming a linear shape and, more often, a cluster of bed particles, Figure 6.1.

The micrographs given in Figure 6.2 show the back-scattered electron images of the cross-section of the bed agglomerates. The slightly shaded areas in the centre of the bed particles represent pure quartz, and the bands surrounding the quartz represent the sulphated coating. The micrographs show that agglomerates are formed as a result of sintering of the coating present on the bed particles. It should be noted that, despite sintering together, the coating on the bed particles has maintained its irregular shape. The presence of sharp angles and irregularity on the surface of the coatings suggests that neither melting nor substantial softening has occurred. It appears, however, that at the interface between bed particles a limited coalescence has taken place resulting in the formation of a bond between the coatings on the bed particles.

A secondary electron image of the cross-section of an agglomerate, given in Figure 6.3, shows the morphology of the bond formed between two silica bed particles. The presence of pores in the junction between bed particles confirms that the coating has not experienced substantial softening.

In general, the bond formed between the bed particles was found to be weak. Rolling an agglomerate of bed particles between the fingers resulted in the breakage of the bond holding the bed particles together. The formation of a weak bond between the particles is also an indication of the limited coalescence at the interface between the bed particles.

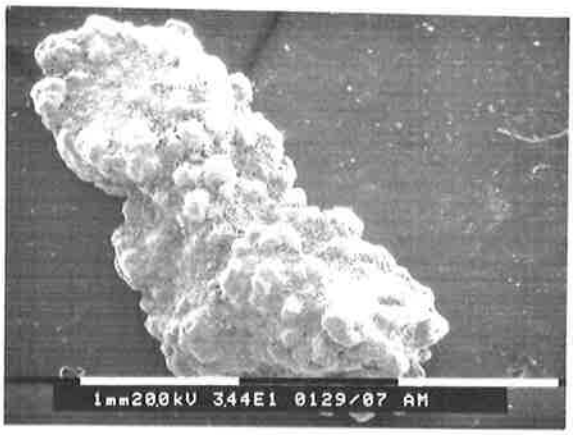

Figure 6.1 (a) : An agglomerate consisting of two bed particles

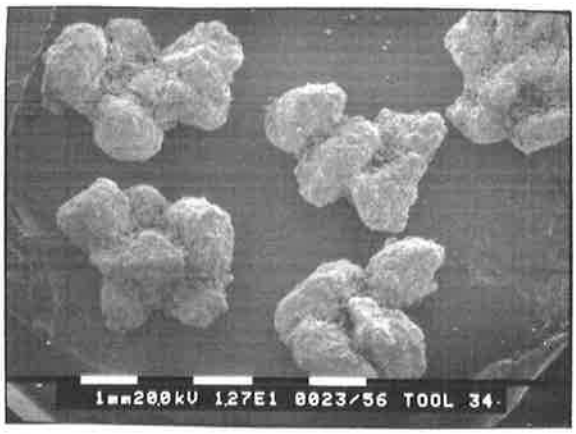

Figure 5.36 (b) : Agglomerates consisting of more than two bed particles

Figure 6.1: Secondary Electron Images of the Surface of Agglomerates.

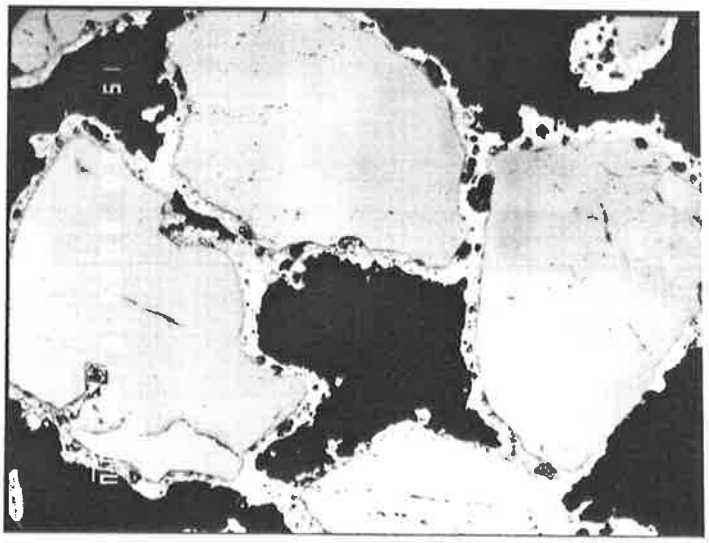

Figure 6.2 (a) Magnification x 60

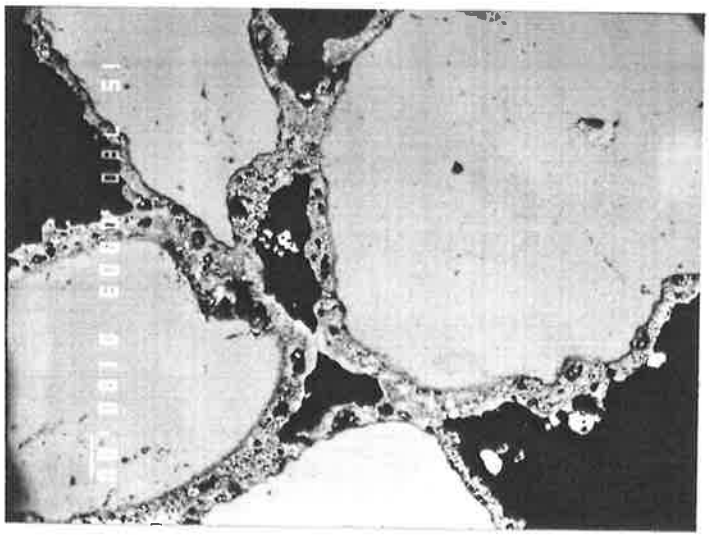

Figure 6.2 (b) Magnification x 78

Figure 6.2: Back-scattered Electron Image of Polished Cross-sections of Agglomerates formed during Run 1.

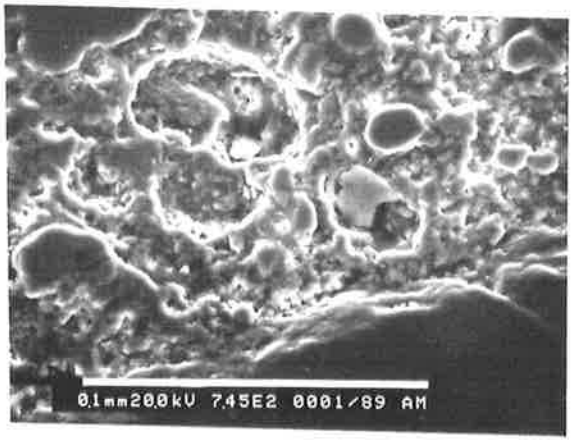

Figure 6.3 (a) :
Magnification x 745

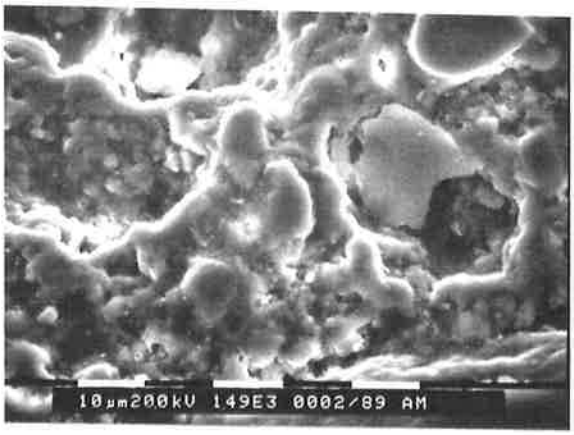

Figure 6.3 (b) :
Magnification x 1490

Figure 6.3 : Secondary Electron Images of Polished Cross-Section of Agglomerates Showing the Interface (Bond) Between the Bed Particles (Run 3).

Figure 6.4 shows the secondary electron image of the surface of an agglomerate at various magnifications. Micrograph (a) shows an agglomerate of a few bed particles sintered together. Micrograph (b) shows one of the bed particles and the porous junctions formed with the neighbouring particles at higher magnification (71.5x). Micrograph (c) shows the junction between two bed particles at yet higher magnifications (170x). The junction consists of numerous bonds formed between the coatings of the bed particles. The porosity of the junction and the numerous bonds formed between the bed particles is shown at higher magnification (570x) in Micrographs (d) and (e). The characteristics of the junction, shown in these micrographs, confirm that only a limited coalescence has taken place at the interface between the coatings of the bed particles.

EDAX analyses of the agglomerates were carried out to determine whether specific conditions at a particular location in the coating of a bed particle resulted in its sintering with other particles. Figures 6.5 and 6.6 show, respectively, the backscattered electron image and the X-ray maps of a polished cross-section of an agglomerate formed during Run 1 with the high-mineral coal sample. The X-ray images, Figure 6.6, indicate that Na, Ca, S, Mg and Al are the major inorganic elements distributed in the coating around the bed particles including the interface between the bed particles.

The distribution of the inorganic elements in the interface between two bed particles is shown at higher magnification in Figure 6.7. The presence of mineral inclusions in the coating, originating from the minerals in the high-mineral coal sample, is evident. Microscopic examination of the agglomerates indicates that the coating at the interface between the bed particles has the same characteristics as in other positions around the bed particles. It can, therefore, be concluded that agglomeration occurs as a result of random collision between the bed particles coated with ash.

6.3 EFFECT OF VARIABLES

Bed material, removed periodically from the FBCS, was sieved and the proportion of the agglomerates in the bed material was determined according to the criteria described in Subsection 3.4.3. The results were then plotted as a function of operating time for various runs (Figures 6.8 to 6.11).

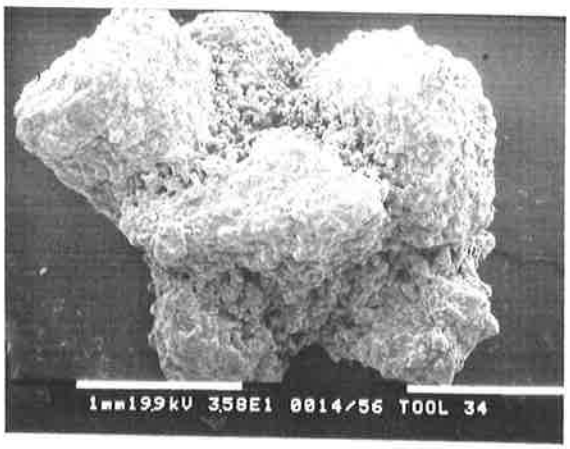

(a):Magnification x 35.8

(b): Magnification x 71.5

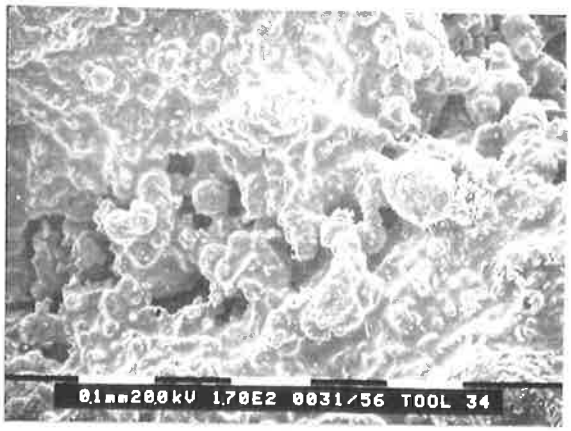

(c): Magnification x 170

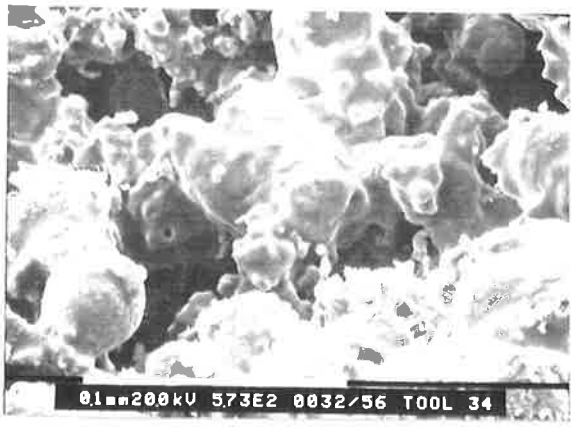

(d): Magnification x 573

(e): Magnification x 573

Figure 6.4: Secondary Electron Image of the Surface of Agglomerates and Their Interface (Bond) Formed During Run 3.

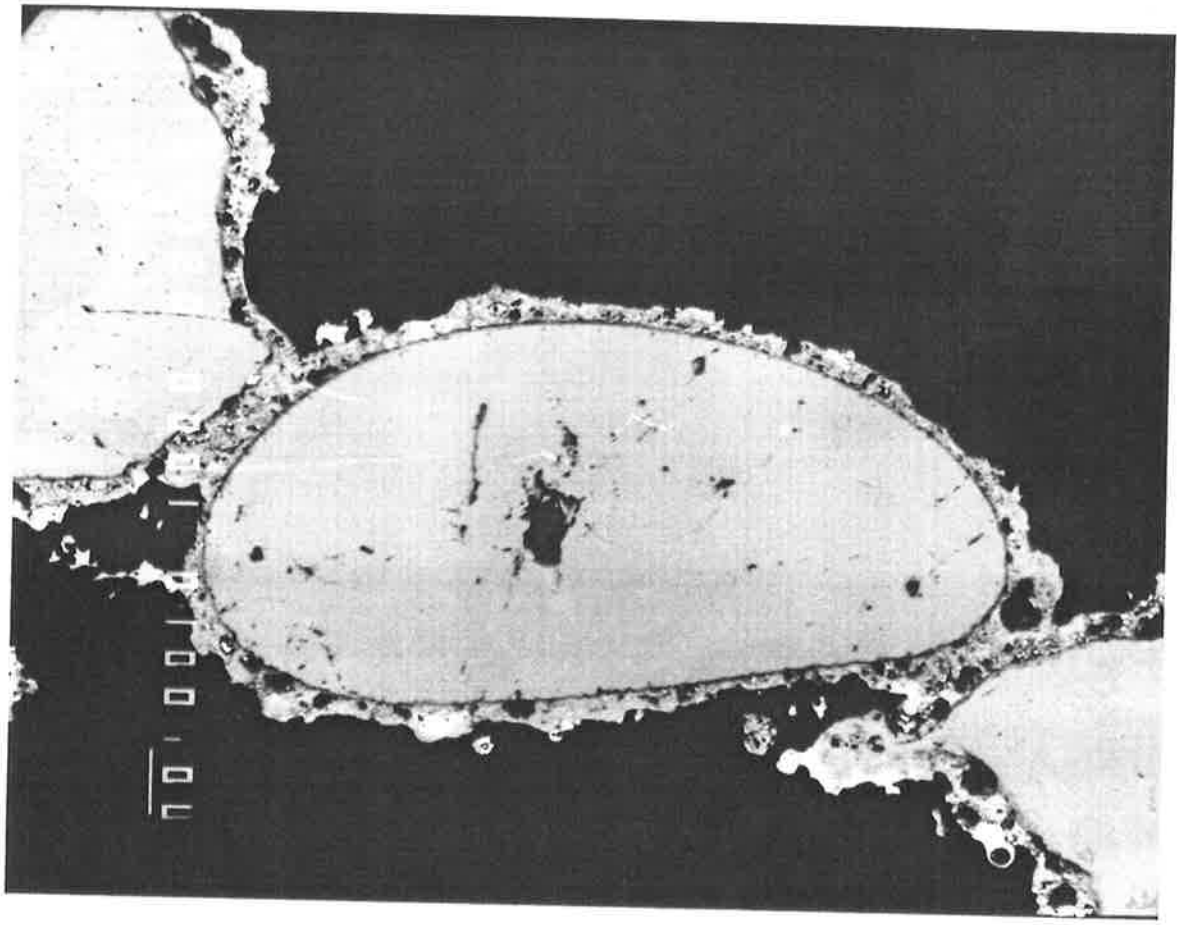

Figure 6.5: Back-scattered Electron Image of the Polished Cross-section of an Agglomerate Formed During Run 1.

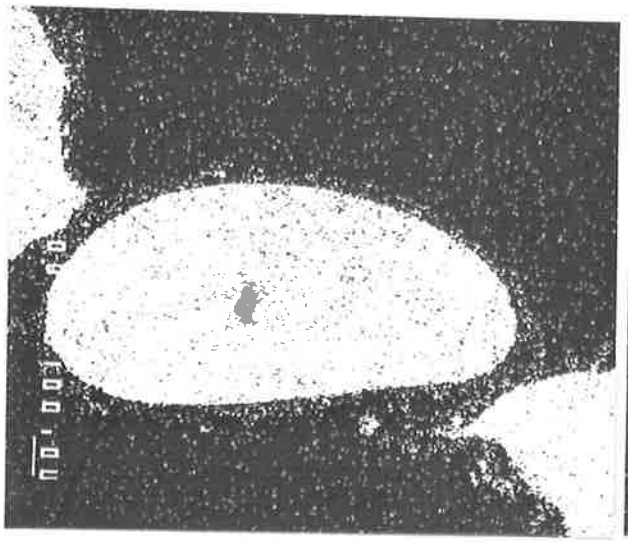

Figure 6.6 (a)= Si

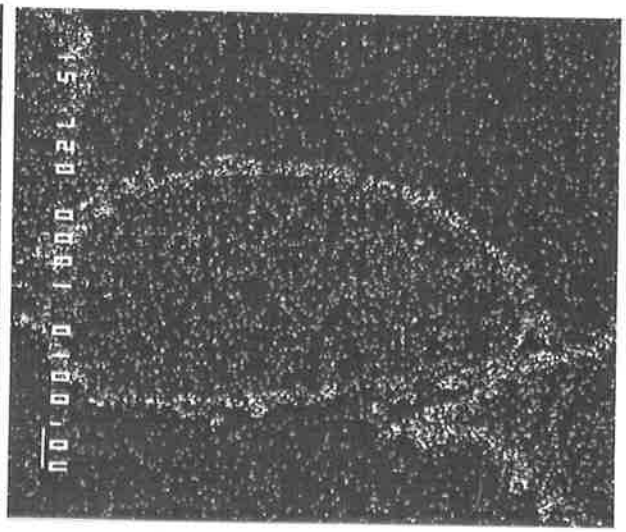

Figure 6.6 (b)= Al

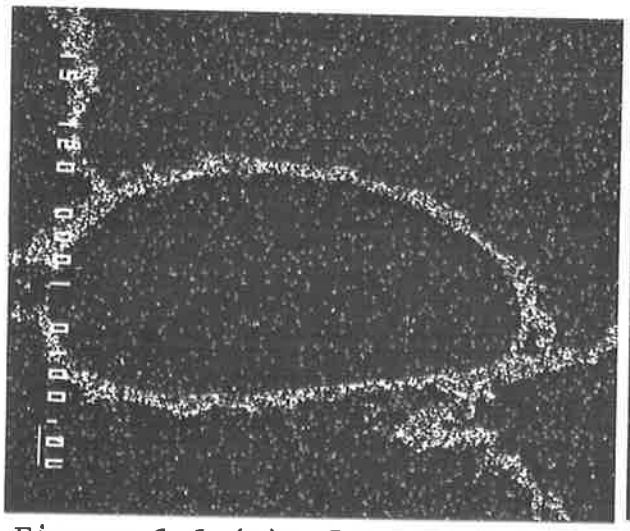

Figure 6.6 (c)= S

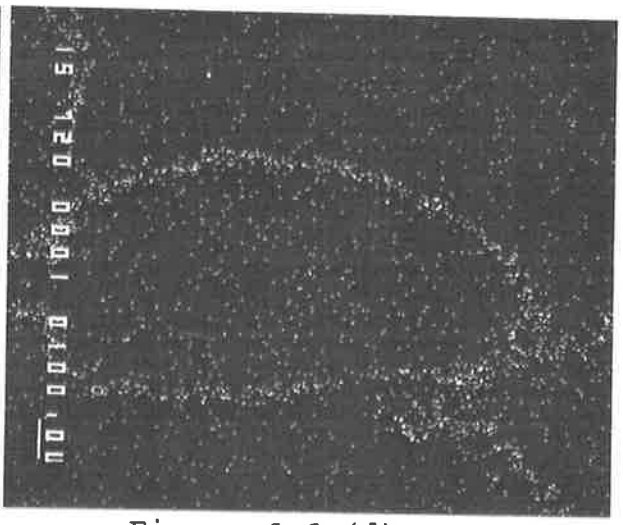

Figure 6.6 (d)= Na

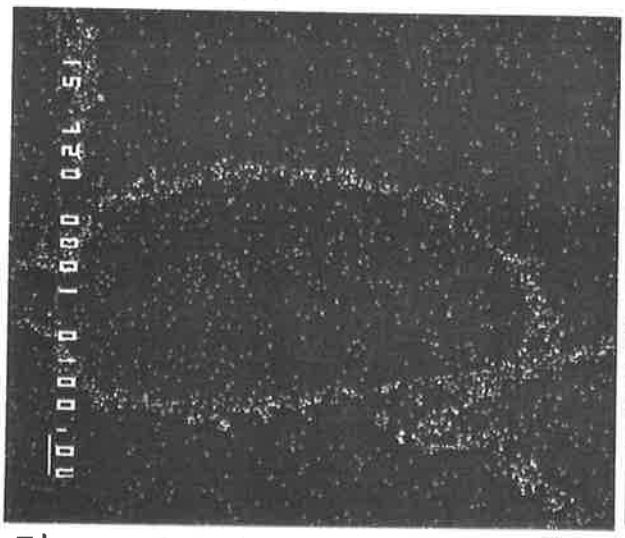

Figure 6.6 (e)= Ca

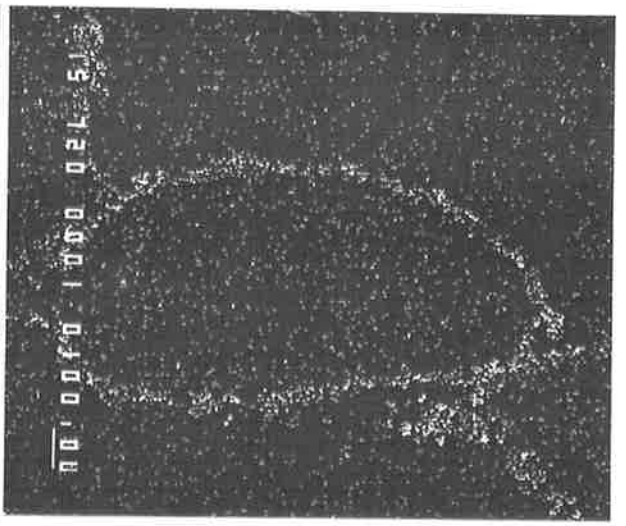

Figure 6.6 (F)= Mg

Figure 6.6: X-ray Maps of the Polished Cross-section of an Agglomerate Formed During Run 1.

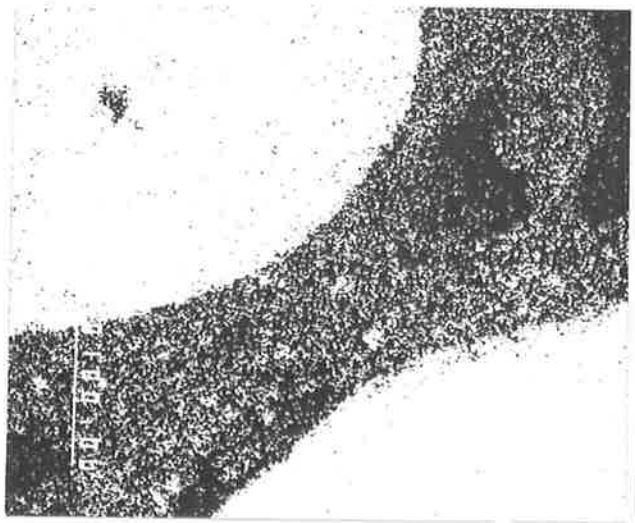

Figure 6.7 (a)= Si

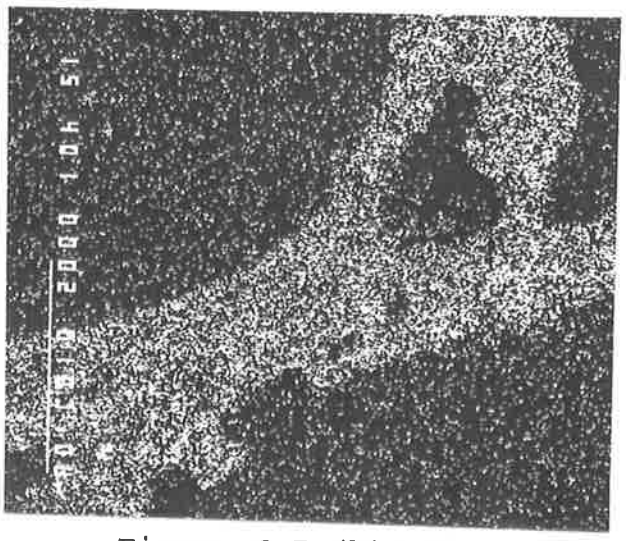

Figure 6.7 (b)= Al

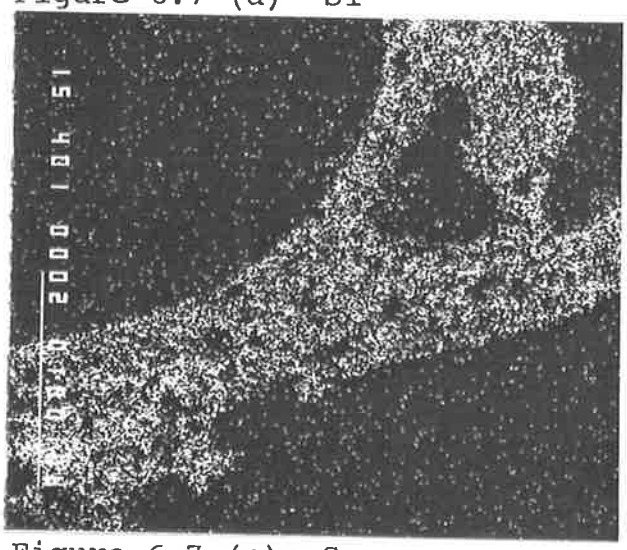

Figure 6.7 (c)= S

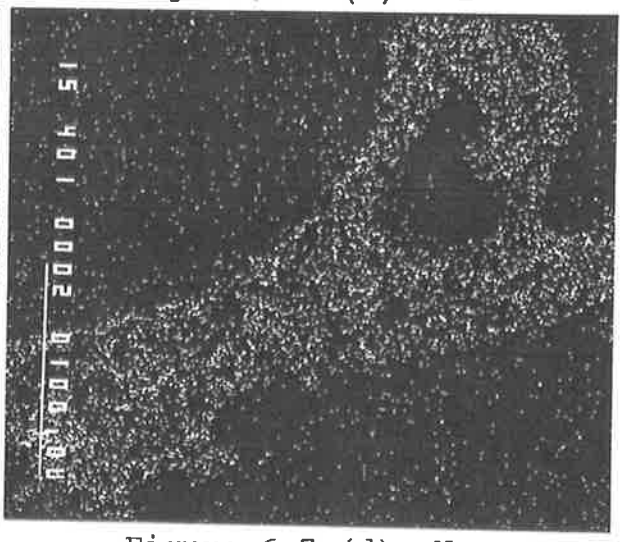

Figure 6.7 (d)= Na

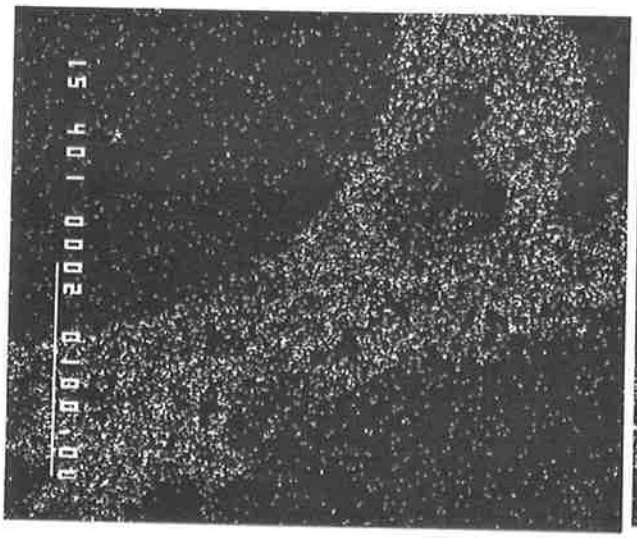

Figure 6.7 (e)= Ca

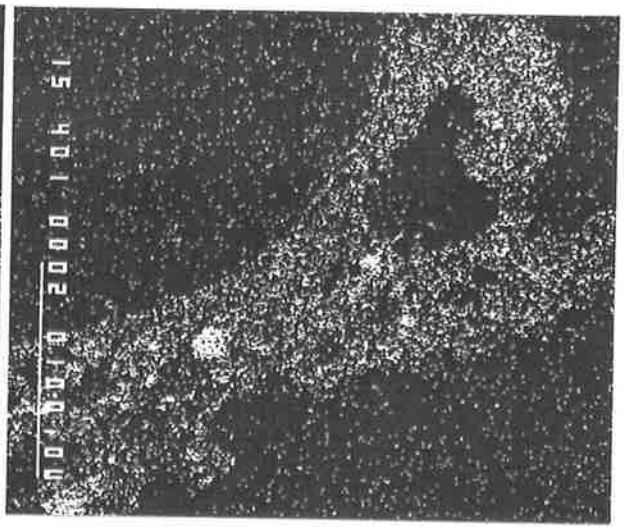

Figure 6.7 (F)= Mg

Figure 6.7: X-ray Maps of the Polished Cross-section of an Agglomerate at Higher Magnification.

Effect of Operating time/Coating Thickness

The results presented in Figures 6.8 to 6.11 indicate that the rate of agglomeration of the bed particles is a function of operating time. As the thickness of the coating on the bed particles changes with operating time, it is considered that, amongst other variables, the rate of agglomeration is governed by the coating thickness.

Due to the differences in the rate of deposition of the coating and/or in the size distribution of the initial charge in various runs, the thickness of the coating on the bed particles for the same operating time may not be the same. Consequently, in order to evaluate the effect of variables, the rate of agglomeration has to be plotted as a function of coating thickness.

The thickness of the coating on the bed particles at various operating times can be determined by the following methods:

- examination of the cross-section of the bed particles removed periodically from the furnace using electron microscope;
- calculation, given the rate of deposition of the coating, operating time, particle size, mass and density of the initial charge (Appendix D).

The results of calculation of the coating thickness at various operating times are presented in Table 6.1. The coating thickness estimated by examining the cross-section of the bed particles by electron microscopy is also given in Table 6.1.

Using the method described in Appendix D, the rate of agglomeration was calculated as a function of coating thickness, Figures 6.12 to 6.14. The results indicate that for agglomeration to commence, or for the onset of defluidisation, a minimum thickness of coating referred to as "critical thickness" has to be deposited on the bed particles. The values of the "critical thickness" for various runs were estimated from Figures 6.12 to 6.14, the results are presented in Table 6.2.

Effect of Coal Quality

The effect of coal quality on the extent of agglomeration is shown in Figure 6.12. Run 1, with the high-mineral coal sample, was carried out at 850°C. Other runs, shown in Figure 6.12, were carried out at 800°C.

Although Run 1, with the high-mineral coal, was conducted at higher bed temperature, the rate of agglomeration in this run for the same coating thickness is less than that of Run 3, with the low-mineral coal sample. The coating on the bed particles in both runs have the

Table 6.1: ***Coating Thickness.***

Run hr	3	6	9	12	15	18
Run 1	21(25)*	39(35)	57(60)	74(70)	90(95)	105(110)
2	47(55)					
3	43(45)	79(75)	114(120)			
4	18(25)	36(35)	53(50)			
5	11(15)	22(25)	33(40)			
6	48(50)	89(80)	126(115)			
7	16(10)+					
8	33(25)	64(60)	94(105)	117(120)		
9	31(25)	59(65)	85(75)	109(110)		
10	38(45)	70(60)	99(110)			

* values in brackets are coating thicknesses estimated by examining the cross-section of the bed particles using electron microprobe.

\+ coating thickness after 0.5 hour of operation.

Note: Runs 2 and 7 defluidised after 3.5 hours and 0.5 hour respectively.

Table 6.2: ***Critical Thickness, micron.***

Run No	1	2	3	4	5	6	7	8
	38	*	27	+	+	15	*	55

* defluidised

\+ did not reach the "critical thickness"

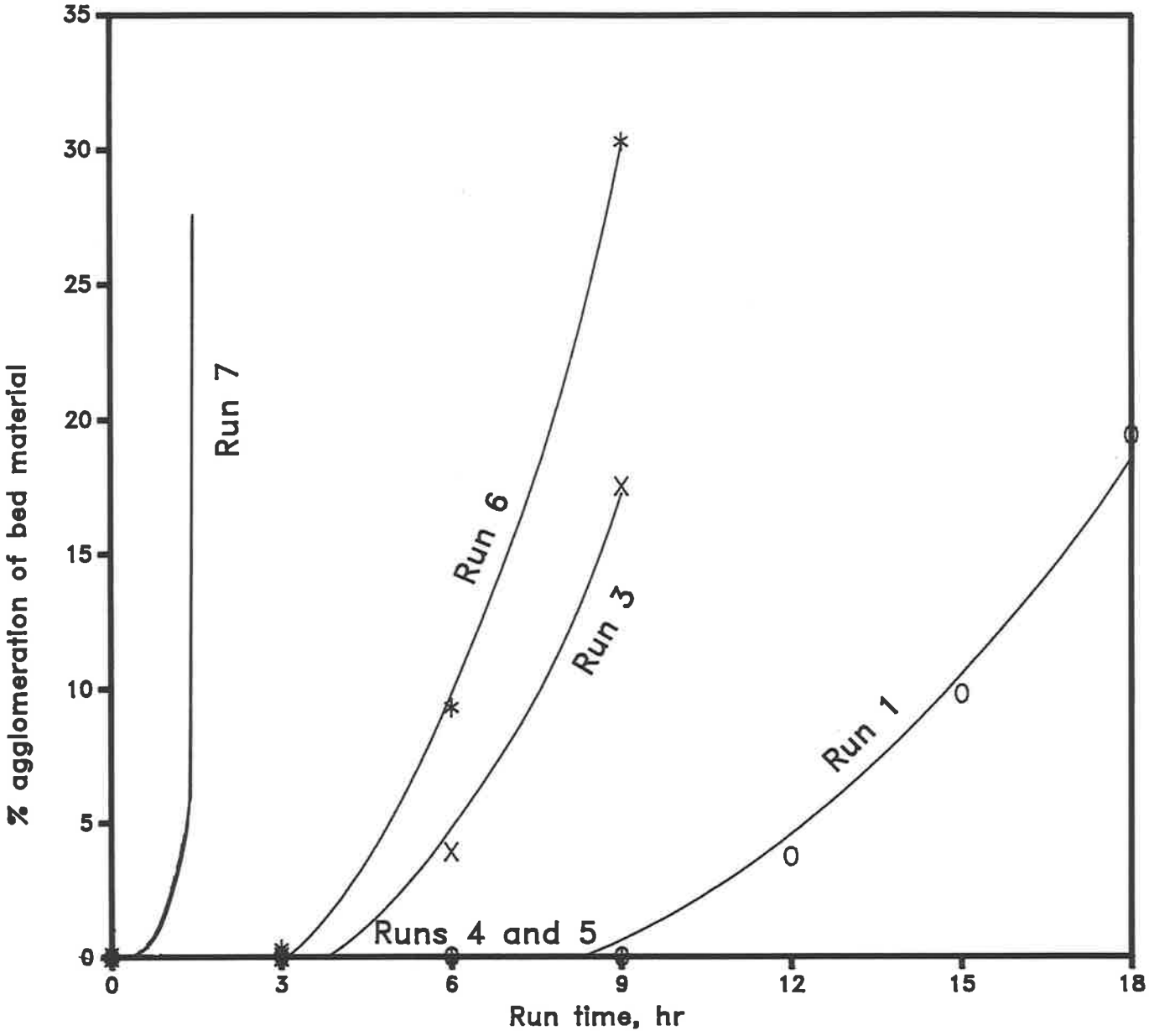

Figure 6.8
Agglomeration of Bed Material vs Run Time
Effect of Coal Quality

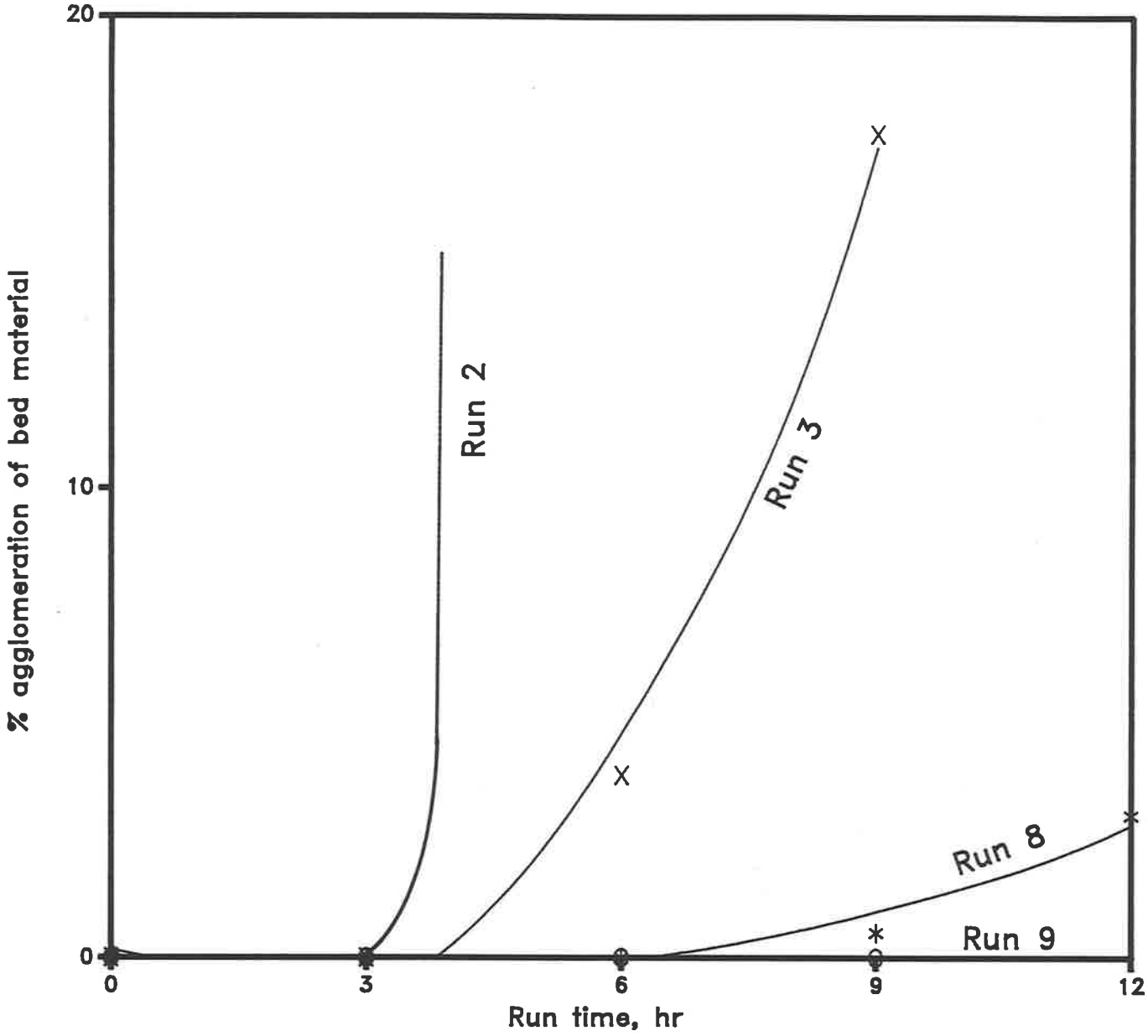

Figure 6.9
Agglomeration of Bed Material vs Run Time Effect of Temperature

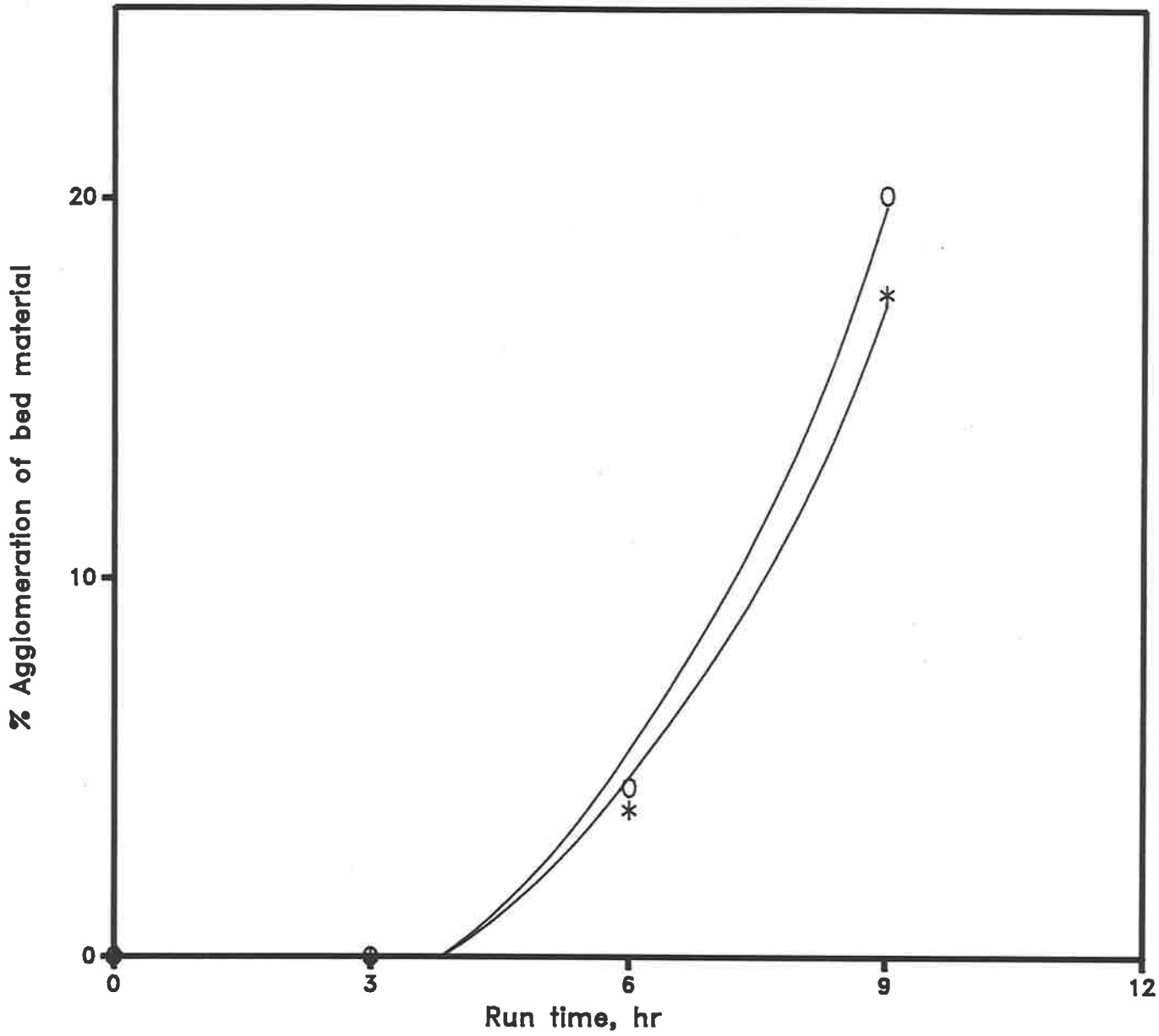

Figure 6.10
Agglomeration of Bed Material vs Run time
Effect of Bed Particle Size

Initial charge:

* 0.85–1.0 mm, Run 3

o 0.71–0.85 mm, Run 10

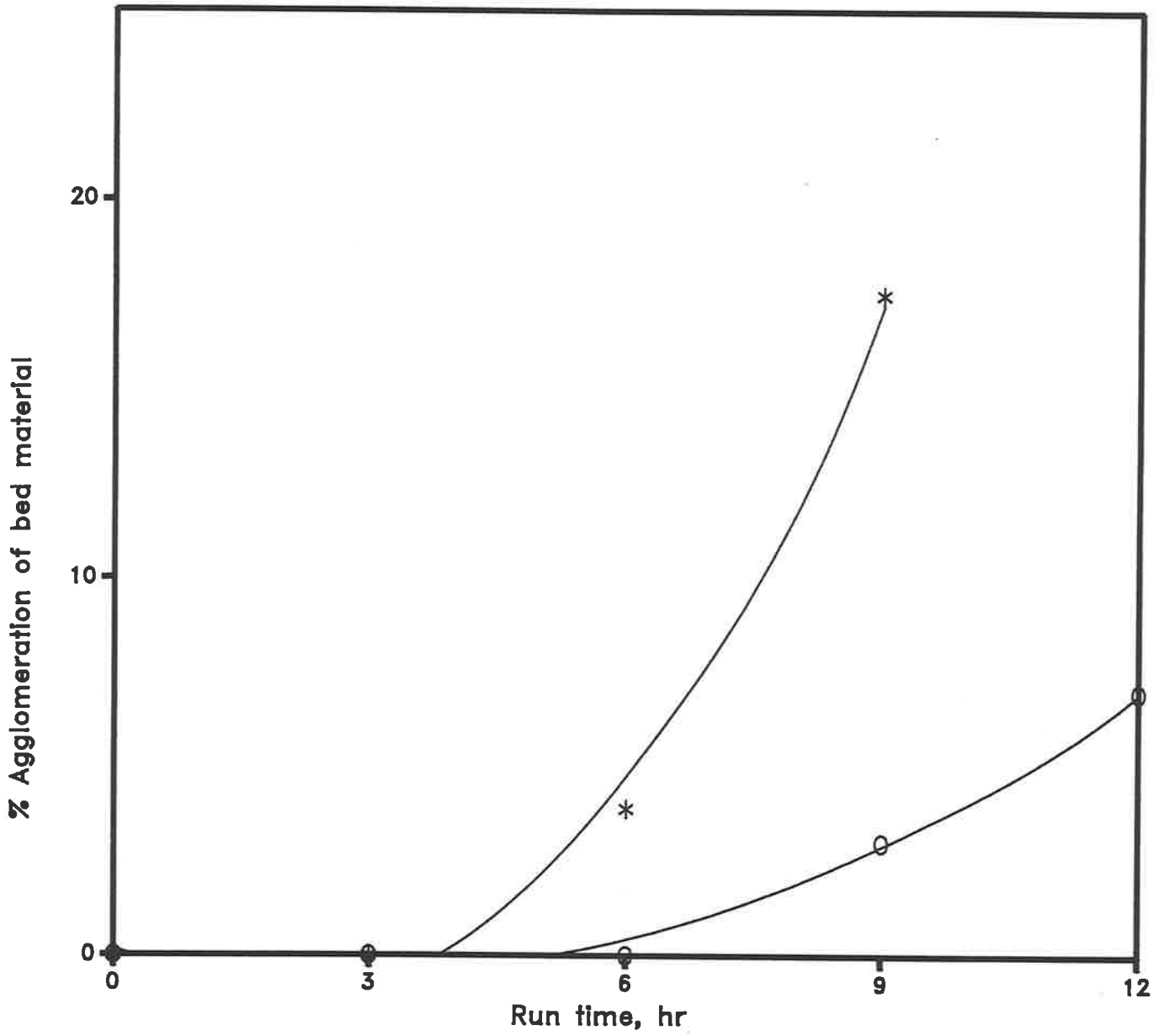

Figure 6.11
Agglomeration of Bed Material vs Run Time
Effect of Bed Material:

* Silica bed, Run 3

0 Dolomite bed, Run 11

same melt and thus have the same initial sintering temperature (Chapter 5). However, a larger proportion of mineral inclusions in the coating of the bed particles in Run 1 appears to reduce the agglomeration propensities of the bed particles.

Runs 4 and 5 carried out with the water and acid-leached samples of coal resulted in the formation of a relatively thin coating on the bed particles at the conclusion of the tests. Given the lower content of sodium compounds in the coating of the bed particles in these runs (Chapter 5), it appears that a larger "critical thickness" is required for agglomeration to commence in these runs. As the main objective of the project was to determine the role of the inorganic matter in the mechanisms of agglomeration and defluidisation, these runs were not extended beyond 9 hours.

The addition of sodium chloride to the coal in Runs 6 resulted in an increase in the agglomeration propensities of the bed particles. The coating deposited on the bed particles during this run was found to contain an appreciable amount of Cl compounds (about 1.1%, on silica-free basis). The increase in the agglomeration propensities of the bed particles in this runs is due to the presence of additional melt (NaCl eutectics) in their coating. Figure 6.12 shows that the "critical thickness" decreases with the addition of NaCl to the coal.

Run 7, with a coal sample containing a larger proportion of NaCl, defluidised after 0.5 hour of operation. The coating of the bed particles in this run contained about 5.0% Cl. Contrary to agglomeration, defluidisation was found to be an instantaneous process. After defluidisation, the bed settled in the conical distributor of the FBCS with fluidising gas blowing a hole through the mass of particles.

Effect of Bed Temperature

The effect of bed temperature on the extent of agglomeration is shown in Figure 6.13. Run 9 carried out at 700°C, which is equal to the initial sintering temperature of the bed particles, did not result in the formation of agglomerates even after the deposition of a significant amount of coating. The "critical thickness" in Run 8, carried out at 750°C, is larger than that of Run 3, carried out at 800°C. It appears that the "critical thickness" decreases with temperature. At 850°C, the fluid bed defluidised after 3.5 hours of operation, Run 2.

In Chapter 5 it was reported that the composition of the coating is not appreciably affected by the furnace temperature (Section 5.3). The results were confirmed by TMA and DTA/TGA

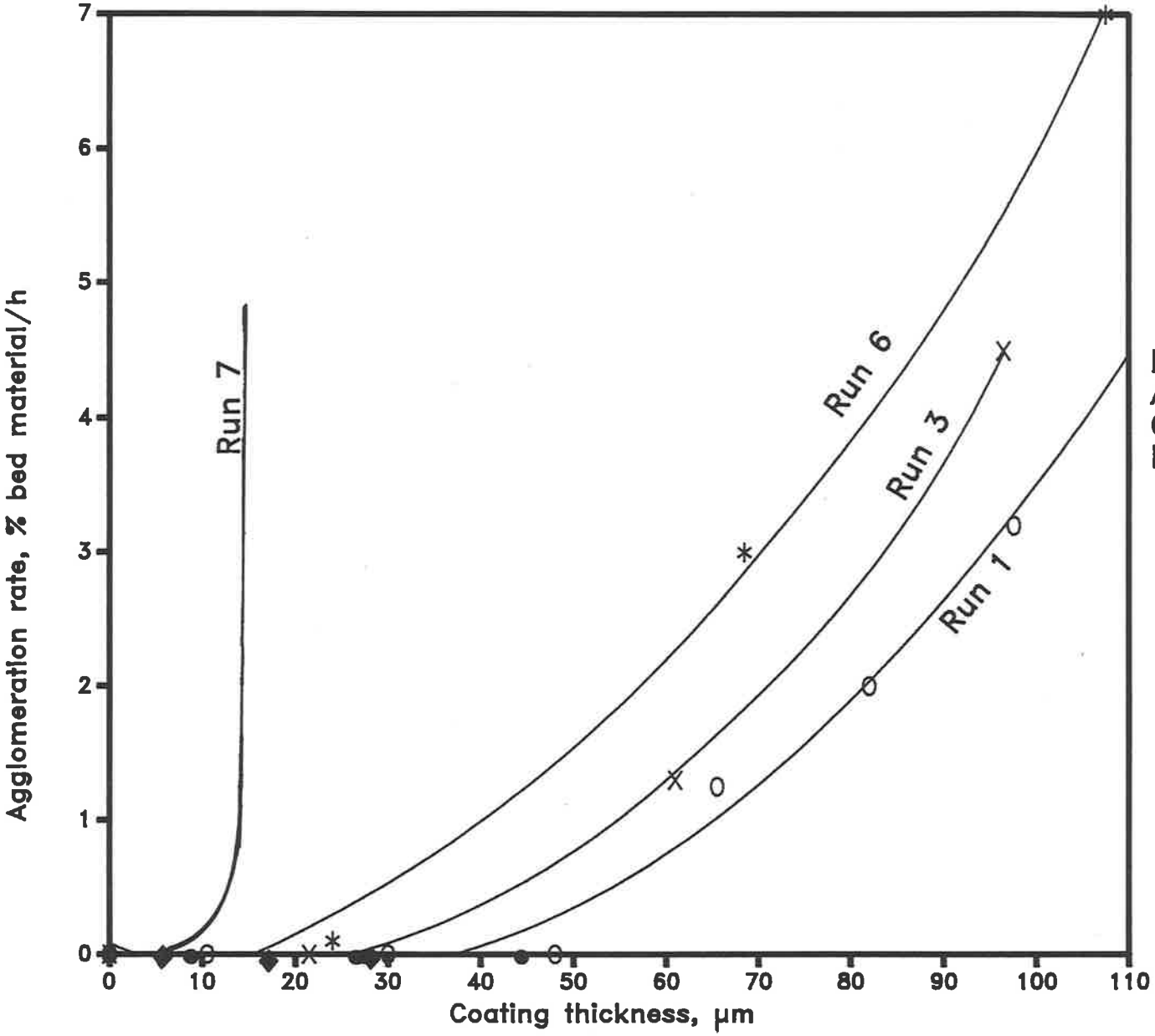

Fig 6.12
Agglomeration Rate vs
Coating Thickness
Effect of Coal Quality

o Run 1
x Run 3
● Run 4
◆ Run 5
* Run 6

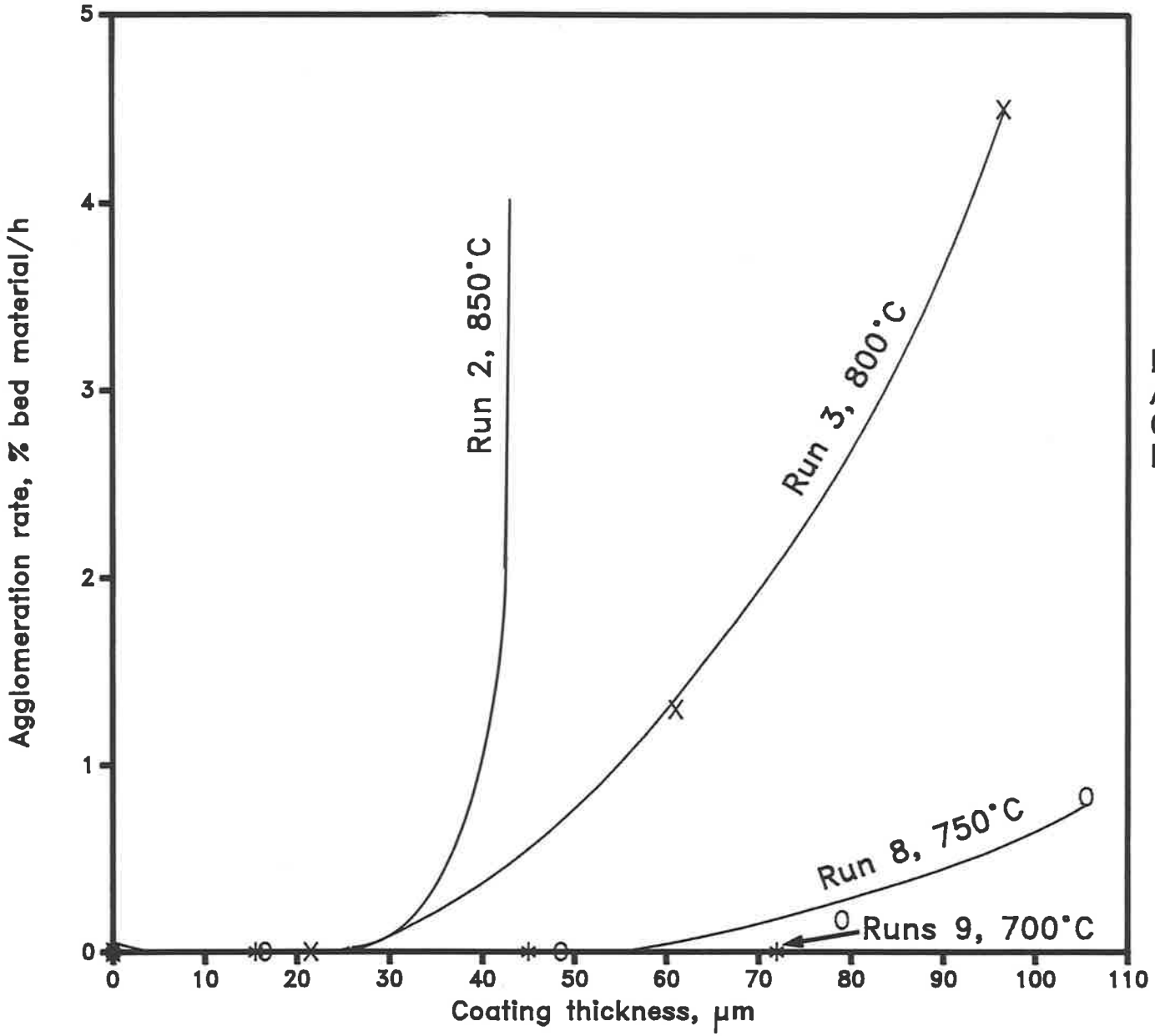

Figure 6.13
Agglomeration Rate vs
Coating Thickness
Effect of Temperature

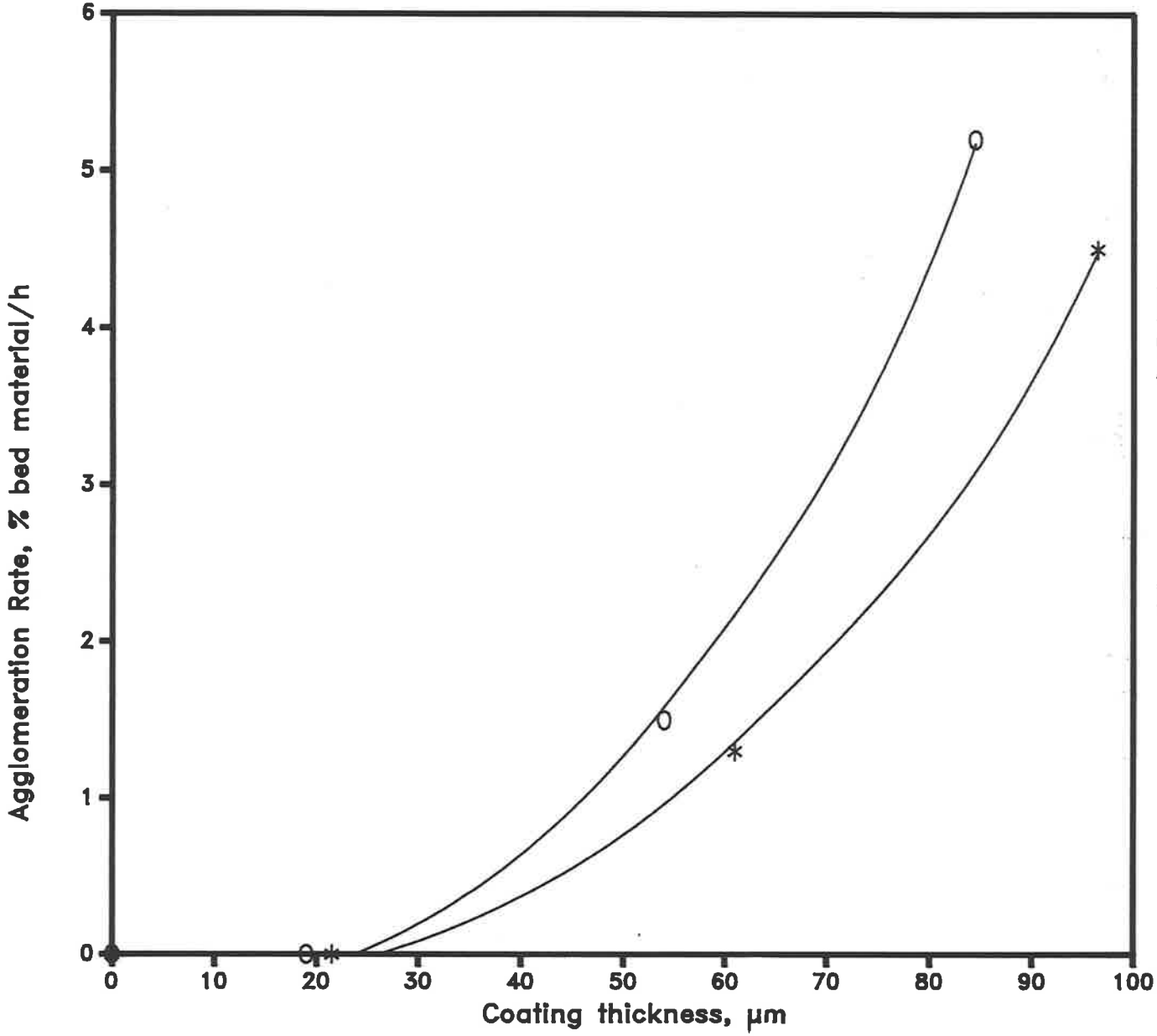

Fig 6.14
Rate of Agglomeration vs Coating Thickness – Effect of Bed Particle Size

Initial charge:

* 0.85–1.0 mm, Run 3

o 0.71–0.85 mm, Run 10

analyses which indicated that the coating formed at various temperatures has the same initial sintering temperature. It it, therefore, considered that temperature influences the extent of agglomeration by altering the physical properties of the coating (Chapter 7).

It is interesting to note that, while the bed particles do not agglomerate at furnace temperature equal to the initial sintering temperature (Run 9), the deposition of ash on the bed particles occurs at this temperature (Figure 5.7). The reason is that the ash on the char surface is at much higher temperature than the furnace temperature. Therefore, when the furnace is operating at the initial sintering temperature or less, the ash on the char surface would still be molten and thus can deposit on the bed particles.

Effect of Bed Size Distribution

The effect of size distribution of the initial charge on the rate of agglomeration is shown in Figure 6.14. The results indicate that, for the same coating thickness, the rate of agglomeration of the bed particle of smaller size distribution is higher. This is because the smaller particles have smaller momentum (Chapter 7).

Effect of Bed Material

Due to the breakage and the loss of dolomite particles in Run 11, described in Chapter 5, the extent of agglomeration for this run could not be determined accurately.

6.4 DISCUSSION

6.4.1 Agglomeration Mechanism

Microscopic examination of the bed material indicates that agglomerates are formed by bonding of the coating deposited on the bed particles (Section 6.2). Whilst it forms a bond, the coating on the bed particles maintains its structure, which indicates that neither substantial melting nor softening of the coating occurs.

Sintering is caused by the system's attempt to reduce its surface free energy. Two particles in mutual contact form a system which is thermodynamically unstable because its total surface free energy is not at minimum. In time, the two particles will bond together in order to decrease the total surface area and hence the total surface free energy of the system. The formation of bond involves a limited coalescence at the position of contact between the particles.

Hence, for sintering to take place, the particles must be heated to temperatures which render them capable of coalescing. This temperature which is referred to as the "onset of sintering" is measured by dilatometric techniques (Subsection 5.5.4).

Sintering may take place in a solid state or in the presence of a liquid phase. Formation of an interface between two particles can be achieved by one or a combination of the following mechanisms:

- solid state sintering, where the interface is formed by means of surface diffusion, grain boundary diffusion, volume diffusion;
- sintering by viscous flow, where the interface is formed by means of a viscous material (silicates);
- sintering due to evaporation-condensation, where the interface is formed by vapour condensation.
- sintering due to the presence of liquid, where the interface is formed by viscous flow.

Substantial sintering with small amounts of melt is possible if solids are dissolved at the point of contact thus forcing the particles closer together by the effect of surface forces acting in the melt surface. This type of sintering, known as "sintering with a reactive liquid", requires a certain solubility of the solid phase in the melt.

The theoretical studies on solid state sintering are based on results from sintering pure oxides. Most multi-component systems, such as coal ash, may contain a melt at the combustion temperature. When present in sufficient amount, the melt may cause sintering of the particles. Phenomenologically, the process is analogous to the coalescence of water drops on a glass plate through the effect of surface tension. The interface, once formed, gradually widens until the two drops completely coalesce. This process proceeds rapidly because of the low viscosity of water which allows the rapid deformation of the drops. In the case of a solid matrix containing a liquid phase, the coalescence of particles is slow and incomplete.

The results of TMA and DTA/TGA analyses, described in Chapter 5, indicate that sintering of the bed particles in the FBC systems is indeed caused by the presence of a liquid phase in the coating. The liquid phase is intimately distributed within the matrix of the coating. The amount of melt in the coating of the bed particles has been sufficient to render them capable of sintering together and forming agglomerates.

It should be noted that only a small proportion of the inorganic matter in the coating may remain molten at furnace temperature. The molten morphology of the coating, evident from the micrographs of the bed particles and their coating, is due to the higher temperatures experienced by the inorganic matter while on the char's surface. Once transferred to the surface of the bed particles, the ash is cooled to the furnace temperature. At this temperature, most of the molten species in ash may solidify. The species in the coating which remain molten at the furnace temperature are responsible for the sintering (agglomeration) of the bed particles.

The melt detected by TMA and DTA/TGA analyses at about 700°C, was attributed to the Na_2SO_4 - $MgSO_4$ eutectic, Chapter 5. The amount of $MgSO_4$ present in the coating of the bed material is small. Three additional melts were detected in the samples of bed material obtained from Runs 6 and 7, conducted with the coal samples impregnated with sodium chloride. The additional melts, at about 620°, 720° and 800°C, detected in these samples were correspondingly attributed to (Subsection 5.5.4):

. NaCl and Na_2SO_4 eutectic at 612°C ;

. NaCl and $CaSO_4$ eutectic at 721°C; and

. NaCl pure, melting point 801°C.

The uniform distribution of the melt(s) in the matrix of the coating confirms that agglomerates are formed as a result of random collision between the bed particles. The results presented elucidate the mechanism of formation of agglomerates and the role of the inorganic matter, particularly Na and S, in this mechanism.

6.4.2 Defluidisation Mechanism

The results of experiments indicate that, as in agglomeration, the main driving force for the defluidisation is the sintering propensity of the bed particles due to the presence of a molten phase in their coating. The following variables, which enhance the agglomeration propensity (Section 6.3), were also found to encourage defluidisation:

- higher furnace temperatures;
- higher proportion of melt in the coating;

- lack of mineral inclusions in the coating; and
- higher coating thickness.

Defluidisation occurred as early as half an hour after the start up with a fresh bed inventory (Run 7) and it was found to be a sharp phenomenon: a well fluidised bed defluidised suddenly. In Run 2, examination of the bed material removed from the furnace after 3 hours did not show the presence of an appreciable amount of agglomerates. However, the bed defluidised suddenly after another 0.5 hour of operation.

These observations suggest that defluidisation is caused by particle interactions which result in an increase in the minimum fluidisation velocity required to maintain the bed particles in suspension. The interaction force between the bed particles increases with the coating thickness and temperature. Further discussions on the mechanism of defluidisation is given in Chapter 7.

6.5 SUMMARY AND CONCLUSIONS

The results reported in this chapter indicate that agglomeration occurs by random collision of the bed particles coated with ash and the formation of an interface (bond) between their coating. The deposition of the coating on the bed particles is the result of transformations of the inorganic matter present in the coal, in particular, S, Na, Ca, Mg and NaCl. The details of these transformations are reported in the earlier chapters.

The results also suggest that defluidisation is caused by the interactions of the bed particles coated with ash. These interactions result in an increase in the minimum fluidisation velocity required to maintain the bed particles in suspension.

The sintering force between the bed particles responsible for agglomeration and defluidisation is the result of a molten phase present in the coating of the bed particles. Hence, for these processes to occur:

- the furnace temperature has to exceed the initial sintering temperature of the coating; and
- a minimum thickness of coating referred to as the "critical thickness" has to be deposited on the bed particles.

Once these conditions are satisfied, the rate of agglomeration and the defluidisation propensities increase with:

- the furnace temperatures;
- the amount of melt in the coating;
- decreasing proportion of mineral inclusions in the coating; and
- increasing coating thickness.

Chapter 7

THEORETICAL EVALUATION

7.1 INTRODUCTION

In accordance with the objective of this thesis, the role of the inorganic matter in agglomeration and defluidisation mechanisms were investigated by experimentation and extensive analytical work (Chapters 4, 5 and 6). While conducting these experiments, the effect of certain variables on the rate of agglomeration and the onset of defluidisation was also studied (Chapter 6).

Of the variables investigated, the chemical composition and mode of occurrence of the inorganic matter, furnace temperature and coating thickness were found to have a marked impact on the rate of agglomeration and the onset of defluidisation. This chapter evaluates theoretically the agglomeration and defluidisation processes in an attempt to establish the effect of these variables.

As reported in the previous chapters, agglomeration and defluidisation are caused by the interaction of bed particles coated with sticky material. The interaction occurs due to the presence of a molten phase in their coating. A sintering model describing this type of

interaction is employed to derive expressions for the agglomeration rate and the onset of defluidisation in terms of intrinsic physical properties of the ash coating and operating variables.

It should be noted that models which can describe the agglomeration and defluidisation processes quantitatively are not yet available (Chapter 2). The mechanisms of agglomeration and defluidisation reported earlier (Chapters 5 and 6) and the correlations presented in this chapter are the first steps towards developing such models. Further investigations, beyond the scope of this project, are required for establishing quantitative models of agglomeration and defluidisation. Recommendations for further work are given in Chapter 8.

7.2 DEPOSITION OF COATING

The experimental work reported in Chapter 5 indicates that the molten ash on the char surface transfers to the surface of the bed material as a result of collisions between the char and the bed particles. The reason for the occurrence of this process can be explained by considering the molten ash/char interface phenomena.

The work of adhesion, W_a, of a liquid to a solid surface is given by:

$$W_a = \pi + \sigma(1 + \cos\theta) \qquad (7.1)$$

where σ is the surface tension of the molten ash and θ is the contact angle at the solid-liquid interface (Raask ,1985).

The work of cohesion, W_c, of a liquid is given by

$$W_c = 2\sigma \qquad (7.2)$$

When θ is equal to zero, the work of adhesion can be expressed as follows:

$$W_a = \pi + 2\sigma \qquad (7.3)$$

Thus, for perfect wetting, that is when the angle of contact is zero, the work of adhesion is higher than the work of cohesion.

Using a heating microscope, Raask (1966a) investigated the wetting characteristics of coal ash slags on carbon, silica, alumina and other materials. The angle of contact between the melt and the solid surfaces were determined. It was found that the coal-ash slags had a large angle of contact with the carbon surface and a small angle of contact with the surface of refractory oxides. It can, therefore, be concluded that the molten ash would transfer from the surface of char particles to the surface of bed particles with which it has a lesser interfacial tension.

The rate of deposition of coating is a function of the following variables:

- firing rate;
- content of the inorganic matter in the coal being fired;
- chemical composition of the ash formed on the char's surface;
- fluidisation velocity;
- bed temperature;
- initial charge and size distribution of the bed inventory;
- system geometry.

The results of the experiments carried out indicate that, with the exclusion of the dolomite run, the rate of deposition of the coating on the bed particles is independent of the operating time, Chapter 5.

Of the variables given above, the effect of temperature and composition of the inorganic matter on the rate of deposition of coating were investigated, Chapter 5. A plot of logarithm of the rate of deposition, R_{ab} versus the reciprocal of temperature, given in Figure 7.1, shows the linear relationship which is the characteristics of the Arrhenius equation.

$$R_d = K_c e^{-\frac{E}{RT}} \qquad (7.4)$$

where E is defined as the activation energy of the process, T is the absolute temperature in K, R is the Universal Gas Constant, and K_c is the pre-exponential factor.

The values of E and K_c, calculated from Figure 7.1 and Equation 7.4, are respectively 30.5 kJ/mole and 251.3 g/h.

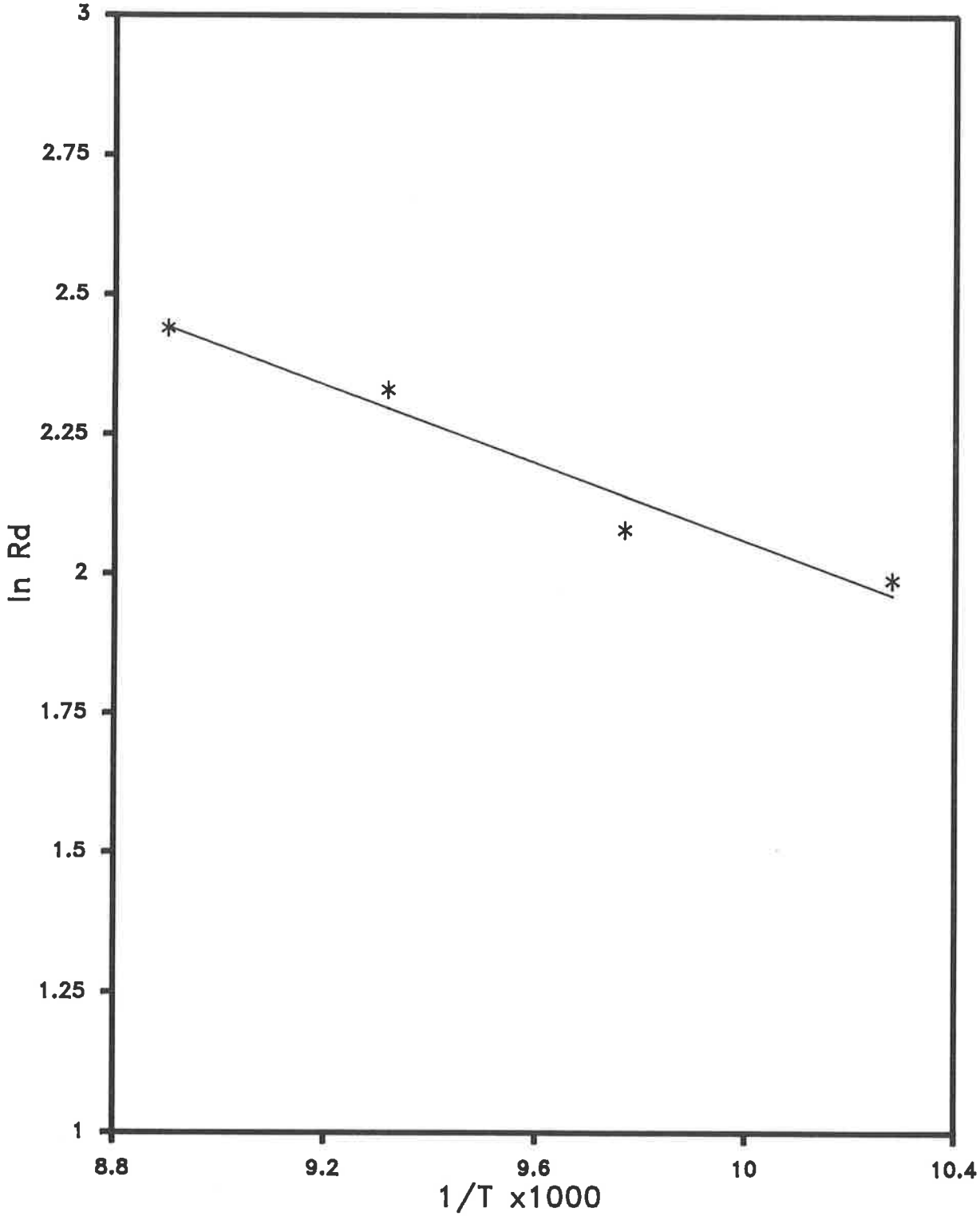

Figure 7.1:
Logarithm of the Rate of Deposition of Coating (g/h) vs Inverse of Furnace Temperature (K)

The results of the experiments reported in Chapter 5 indicate that the coating deposition occurs at bed temperatures even less than the initial sintering temperature. It should be noted that the ash prior to deposition is at a char particle temperature which could be up to a few hundred degrees higher than that of the bed. Hence, while the bed temperature is at or below the initial sintering temperature, the ash on the char surface is molten and is capable of depositing on the bed particles.

The relationship between the rate of deposition of the coating and the content of sodium in coal is graphically given in Figure 5.6. The results indicate that the rate of deposition of the coating increases with the Na content of the coal; a linear "fit" can be used. The results for the runs carried out with NaCl-added coal samples show relatively larger deviation from the linear "fit".

It was reported in Chapter 5 that impregnation of coal with sodium chloride results in a residual amount of sodium chloride in the coating deposited on the bed particles with the resultant formation of additional molten phases which would markedly affect the rate of deposition of the coating. These results and those of the experiment carried out with a high-mineral sample, Run 1, indicate that the mode of occurrence of the inorganic matter in coal has a marked effect on the characteristics of the ash and its rate of deposition on the bed particles. The findings illustrate the difficulties involved in formulating the rate of deposition of the coating in terms of measurable parameters such as the content of the inorganic matter in coal.

7.3 SINTERING THEORY, FRENKEL MODEL

The results of TMA and DTA/TGA analyses, described in Chapter 5, indicated that sintering of the bed particles is caused by the presence of a liquid phase in the coating. The liquid phase is intimately distributed within the solid matrix of the coating in proportions sufficient for the coating to acquire the characteristics of a viscous material. Hence, the sintering model developed by Frenkel (1945) can be employed for a system of particles coated with such material.

This model, schematically shown in Figure 7.2, describes the rate of coalescence of particles under the influence of surface tension which causes a viscous flow. Frenkel was able to derive an equation relating the growth of an interface between two spherical particles at constant temperature:

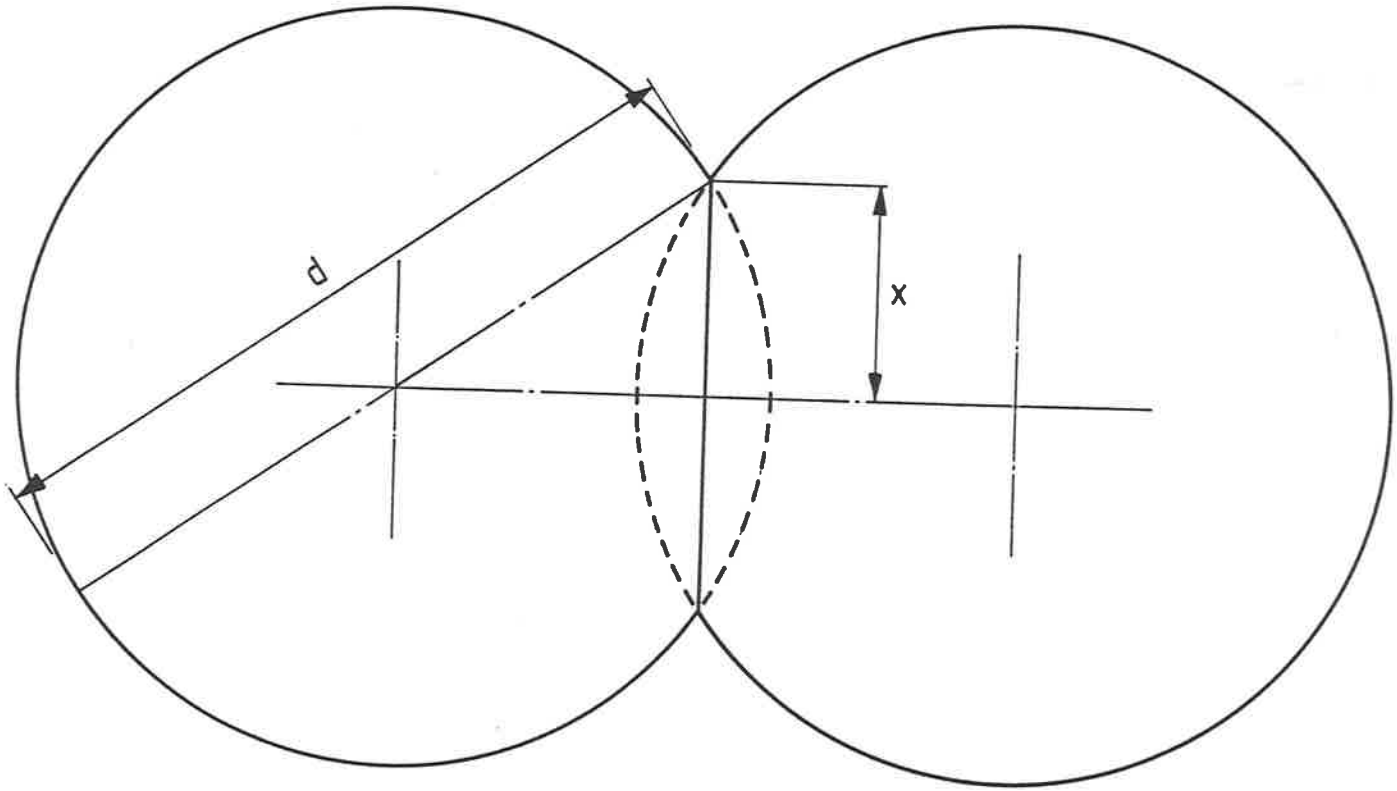

Figure 7.2: Schematic Illustration of Frenkel Model

$$x^2 = \frac{3d\sigma}{4\mu} t_c \qquad (7.5)$$

where x = radius of interface assumed to be circular

d = diameter of spherical particles

σ = surface tension

μ = viscosity

t_c = contact time

Thus, the cross-sectional area of the interface (S_r) formed between two particles as a function of time can be derived from the above equation:

$$S_r = \frac{3\pi d\sigma}{4\mu} t_c \qquad (7.6)$$

From this equation, the rate of formation of an interface (R_i) between two spherical particles of the same radius can be derived as follows:

$$R_i = \frac{3\pi d\sigma}{4\mu} \qquad (7.7)$$

The magnitude of R_i gives an indication of sintering propensity of the particles. From this equation, it is evident that the sintering propensity of the particles increases with its size and the surface tension, and decreases with increasing viscosity of the material forming the particles. The rapid coalescence of water droplets, described earlier as an analogy to sintering of the bed particles in the presence of a molten phase, is primarily due to the low viscosity of water.

The proportion of melt in the coating and furnace temperature are expected to affect the sintering propensities of the bed particles by altering the physical properties of the coating, that is surface tension and viscosity.

7.4 AGGLOMERATION

The binding force between two colliding particles (F_b) is directly proportional to:

- the rate of formation of an interface (R_i); and
- the binding strength (B), resulting from cohesion (Van der Waal's forces) between the molecules of the material in the interface.

$$F_b \propto R_i \times B \tag{7.8}$$

Thus, using the rate of formation of interface derived from the Frenkel model, the binding force between two particles of diameter d can be obtained as follows:

$$F_b \propto \frac{d\sigma B}{\mu} \tag{7.9}$$

Surface tension changes very little with temperature, whereas viscosity is strongly temperature-dependent. Thus, the binding force between two particles is expected to change strongly with temperature. As the viscosity of a liquid decreases with increasing temperature, the following equation is used to correlate the viscosity with temperature:

$$\mu = \frac{\mu_0}{(T - T_s)^n} \quad \textbf{for} \quad T > T_s \tag{7.10}$$

where n is a constant

μ_0 is the viscosity of the coating material at a reference temperature, say T_s;

T is the bed temperature; and

T_s is the initial sintering temperature determined by dilatometric methods.

Ignoring the effect of temperature on the cohesion (Van der Waal) force between the molecules, the relationship between the binding force and temperature can be shown by combining Equations 7.9 and 7.10:

$$F_b \propto \frac{d\sigma B}{\mu_0}(T - T_s)^n \quad \textbf{for} \quad T > T_s \tag{7.11}$$

At bed temperatures less than or equal the initial sintering temperature, T_s, the particles would not be sticky and hence the binding force would be equal to zero.

When two particles collide, they tend to rebound due to the kinetic energy of the particles before the collision process. The probability of effective collisions in forming agglomerates is considered to be directly proportional to binding force and inversely proportional to the momentum of the bed particles (P). Thus, the rate of agglomeration (R_a) in a multi-particle fluid bed system can be expressed as follows:

$$R_a = k_f \frac{F_b}{P} \tag{7.12}$$

where k_f is proportional to the collision frequency of the particles which, in turn, depends on the number of bed particles per unit volume and system geometry. Equation 7.12 is in accordance with work reported in the literature concerning agglomeration tendency (Chapter 2) of sticky bed particles.

The momentum of the bed particles can be expressed in terms of their velocity (U_p), diameter (d) and density (ρ_p):

$$P = \frac{\pi}{6} \rho_p d^3 U_p \tag{7.13}$$

Due to the complexity of the hydrodynamics of fluid bed systems, it is difficult to derive an accurate expression for the particle velocity. It can, however, be considered that U_p is a function of excess gas velocity. That is:

$$U_p = k_u (U - U_m)^m \quad \textbf{for} \quad U > U_m \tag{7.14}$$

where k_u and m are constant; and

U_m is the minimum fluidisation velocity.

Then, the momentum of the bed particles can be expressed as follows:

$$P = \frac{\pi k_u}{6} \rho_p d^3 (U - U_m)^m \tag{7.15}$$

By incorporating Equations 7.11 and 7.15 into Equation 7.12, the rate of agglomeration can be expressed in terms of operating variables (that is fluidisation velocity and temperature) and intrinsic properties of the bed material (that is σ, B and μ_0):

$$R_a = K_a \frac{1}{\rho_p d^2} \frac{\sigma B}{\mu_0} \frac{(T - T_s)^n}{(U - U_m)^m} \qquad (7.16)$$

where $K_a = 6 \frac{k_f}{(\pi k_u)}$

The first term in this equation (K_a) is determined by the system geometry and the number of particles and the second term shows the effect of particle size and density.

Should the bed particles acquire stickiness due to the presence of a coating on their surface, the binding force between the bed particles is expected to be a function of the coating thickness. In this case, Equation 7.11 can be written as follows:

$$F_b \propto \frac{(d_0 + 2\delta)\sigma B}{\mu_0} (T - T_s)^n f(\delta) \qquad (7.17)$$

where δ is the coating thickness.

d_0 is the initial particle diameter

When δ is equal to zero, that is at the start of combustion with a fresh bed inventory, $f(\delta)$ and hence F_b becomes equal to zero. As δ increases, the binding force changes according to Equation 7.17.

Using the binding force given by Equation 7.17, the rate of agglomeration for a fluid bed system containing bed particles with sticky coating can be determined as follows:

$$R_a = K_a \frac{1}{\rho_p (d_0 + 2\delta)^2} \frac{\sigma B}{\mu_0} \frac{(T - T_s)^n}{(U - U_m)^m} f(\delta) \qquad (7.18)$$

It should be noted that the minimum fluidisation velocity (U_m) in this equation is also a function of furnace temperature and physical properties of the coating (Chapter 2). The expressions for the minimum fluidisation velocity are given in the following section.

7.5 DEFLUIDISATION

Gluckman and his collaborators (Gluckman et. al. ,1975) noted that fluid beds, made of copper particles, poly-propylene beads or glass particles, are suddenly defluidised at a velocity defined by the bed temperature; both velocity and temperature correlated linearly. The true minimum fluidisation velocity calculated from this correlation intercepted the theoretical minimum fluidisation velocity, calculated from the standard formula, at the initial sintering temperature. Although they could not elaborate on the principles governing the defluidisation, they concluded that defluidisation is a well-ordered phenomenon obeying precise rules.

A reasonable conclusion from this work is that the binding force between the sticky bed particles has to be included in the balance between gravity, drag force and buoyancy.

As in agglomeration, the binding force between the bed particles is the result of the system's attempt to reduce its surface energies when two particles collide. Thus, the Frenkel model can be employed where the binding between the particles is due to the presence of a molten phase. Hence Equation 7.11 can be used to express the binding force between two particles. The total binding force (F_t) per unit volume of bed in a multi-particle system, which has to be overcome by the kinetic energy of the system, can be expressed as follows:

$$F_t = N \frac{d\sigma B}{\mu_0}(T - T_s)^n \qquad (7.19)$$

where N is proportional to the number of particles per unit volume of the fluid bed.

The pressure drop per unit length of fluid bed can be written in a general form as follows (Ergun, 1952):

$$\frac{\Delta P}{L} = 72\alpha \frac{(1-\epsilon)^2}{\epsilon^3}\frac{\mu_f U}{(\phi d)^2} + \frac{3\beta}{4}\frac{(1-\epsilon)}{\epsilon^3}\frac{\rho_f U^2}{\phi d} \qquad (7.20)$$

where ΔP = pressure drop across the bed

ϵ = voidage

ϕ = sphericity

ρ_f = fluid density
μ_f = fluid viscosity; and
ρ_p = particle density

α and β are dimensionless correlation factors. By conducting a large number of experiments, Ergun (1952) found that the values of α and β are 2.08 and 2.33 respectively.

The fluidisation of a bed of sticky particles requires that the pressure drop per unit length of the bed to be at least equal to the sum of the weight of the bed and the total binding force per unit volume of the bed:

$$(1-\epsilon_{mf})(\rho_p-\rho_f)g + F_t = 72\alpha\frac{(1-\epsilon_{mf})^2}{\epsilon_{mf}^3}\frac{\mu_f U_m}{(\phi d)^2} + \frac{3\beta}{4}\frac{(1-\epsilon_{mf})}{\epsilon_{mf}^3}\frac{\rho_f U_m^2}{\phi d} \qquad (7.21)$$

where ϵ_{mf} = voidage at the minimum fluidisation velocity
ρ_p = particle density
g = normal gravitational acceleration

Solving the above quadratic equation, the true minimum fluidisation velocity can be expresses as follows:

$$U_m = \frac{48\alpha}{\beta}\frac{\mu_f(1-\epsilon_{mf})}{(\phi d)\rho_f}\left\{-1+\sqrt{\frac{\beta}{1728}\frac{\epsilon_{mf}^3(\phi d)^3\rho_f}{(1-\epsilon_{mf})^2\mu_f}\left[(\rho_p-\rho_f)g+\frac{F_t}{1-\epsilon_{mf}}\right]+1}\right\} \qquad (7.22)$$

where F_t is given by Equations 7.19

As a simplification, the kinetic energy loss term in Equation (7.22) can be neglected as the Reynolds number is small at minimum fluidisation velocity for small particle size (Reynolds number for Run 2 was calculated to be 2.3). The expression for U_m can be written as follows:

$$U_m = \frac{1}{72\alpha}\frac{\epsilon_{mf}^3}{(1-\epsilon_{mf})}\frac{(\phi d)^2}{\mu_f}\left[(\rho_p-\rho_g)g+\frac{F_t}{1-\epsilon_{mf}}\right] \qquad (7.23)$$

Assuming the particles are spherical (that is ϕ equal to 1.0), the voidage at the minimum fluidisation velocity can be estimated to be 0.415 (Wen and Yu; 1966). Inserting the values of ϕ, ϵ_{mf} and α in Equation 7.23:

$$U_m = \frac{1}{1228}\frac{d^2}{\mu_f}(\rho_p - \rho_g)g + \frac{F_t}{0.585} \qquad (7.24)$$

Equation 7.25 can be written in terms of the theoretical minimum fluidisation velocity (U_0) for non-sticky particles:

$$U_m = U_0 + \frac{1}{718}\frac{d^2}{\mu_f}F_t \qquad (7.25)$$

Replacing F_t from Equation 7.19:

$$U_m = U_0 + \frac{N}{718\mu_f}\frac{d^3\sigma B}{\mu_0}(T - T_s)^n \qquad (7.26)$$

Should the bed particles acquire stickiness due to the deposition on their surface of sticky coating, the total binding force would be a function of coating thickness. That is

$$F_t = N\frac{(d_0 + 2\delta)\sigma B}{\mu_0}(T - T_s)^n f(\delta) \qquad (7.27)$$

By using this equation and employing the same procedure, the minimum fluidisation velocity for fluid bed systems containing bed particles covered with sticky material can be determined:

$$U_m = U_0 + \frac{N}{718\mu_f}\frac{(d_0 + 2\delta)^3\sigma B}{\mu_0}(T - T_s)^n f(\delta) \qquad (7.28)$$

Equations 7.26 and 7.28 illustrate that, at temperatures higher than the initial sintering temperature of the bed particles, the true minimum fluidisation velocity (U_m) is higher than the theoretical minimum fluidisation velocity (U_0) for non-sticky bed particles. U_m is a function of: number of particles per unit volume, particle size, intrinsic physical properties of the sticky material, bed temperature and coating thickness.

The existence of a relationship between the minimum fluidisation velocity and temperature in fluid bed systems operating at temperatures higher than the initial sintering temperature of the bed particles has been confirmed experimentally (Gluckman et al., 1975; Basu, 1982). Gluckman and his collaborators have also confirmed that this relationship becomes stronger with the sintering propensity of the bed particles. They, however, could not explain their observations theoretically.

Based on the experimental results, Gluckman and his collaborators (1975) suggested a linear relationship between the true minimum fluidisation velocity and temperature, that is n equal to 1. Furthermore, without applying the sintering theory, Basu (1982) employed a similar theoretical approach to that given in this section and assumed the binding force between the bed particles to be proportional to bed temperature.

It should be noted that due to the difficulty in accurately determining the onset of defluidisation and because of the limited data available, further experimental work would be needed to confirm the exact relationship.

7.6 DISCUSSION

In the previous section, a number of equations were developed for the agglomeration rate and for the onset of defluidisation. In these equations, the effect of coal quality is expressed in terms of intrinsic properties of the ash coating. These equations also describe the effect of operating variables such as fluidisation velocity and temperature.

Equations 7.16, 7.18, 7.26 and 7.28 can be simplified by assuming that the values of m and n in these equations are equal to 1. The linear relationship between U_m and temperature, determined experimentally (Gluckman et al., 1975; and Basu, 1982), suggests that n can be assumed to be equal to 1. It is also reasonable to assume that the particle velocity is directly proportional to the excess gas velocity (that is $m = 1.0$). Given these assumptions, one can rewrite Equations 7.18 and 7.28 as follows:

$$R_a = K_a \frac{1}{\rho_p (d_0 + 2\delta)^2} \frac{\sigma B}{\mu_0} \frac{(T - T_s)}{(U - U_m)} f(\delta) \qquad (7.29)$$

$$U_m = U_0 + \frac{N}{718\mu_f} \frac{(d_0 + 2\delta)^3 \sigma B}{\mu_0} (T - T_s) f(\delta) \qquad (7.30)$$

Equation 7.29 can be rewritten in the following form:

$$U = U_m + \frac{K_a}{R_a \rho_p (d_0 + 2\delta)^2} \frac{\sigma B}{\mu_0} (T - T_s) f(\delta) \qquad (7.31)$$

where U_m is given by Equation 7.30.

The operating regimes of fluid bed systems, in which all variables in Equations 7.30 and 7.31 except fluidisation velocity and temperature are kept constant, can be illustrated by plotting these equations on a $U - T$ diagram, Figure 7.3.

On the basis of the assumptions made (that is m and n equal to 1.0) the true minimum fluidisation velocity (U_m) becomes a linear function of furnace temperature (Equation 7.30). U_m intercepts the theoretical minimum fluidisation velocity for non-sticky particles (U_0) at the initial sintering temperature (T_s). The slope of U_m versus furnace temperature is a function of sintering propensity of the bed particles (amongst other variables) which is determined by the intrinsic physical properties of the coating deposited on the bed particles.

Equation 7.31 gives a family of curves relating the fluidisation velocity (U) to furnace temperature for constant rates of agglomeration. Given the same assumptions, that is m and n equal to 1.0, these curves also become linear. They all intercept at $U = U_m$ and $T = T_s$. The slopes of these curves are also a function of intrinsic physical properties of the coating, amongst other variables.

At temperatures lower than the initial sintering temperature, the agglomeration rate is zero for all values of fluidisation velocity (Zone A). At higher temperatures and for U greater than U_m the fluid bed operates under agglomerating regime (Zone B). In this zone, the rate of agglomeration is determined by the fluidisation velocity and temperature. It increases with temperature and decreases with increasing fluidisation velocity. Figure 7.3 shows the fluidisation velocity-temperature relationship for two arbitrary rates of agglomeration (a and b) where a is greater than b. Any pair of fluidisation velocity - temperature below U_m results in defluidisation (Zone C). This figure explains the phenomenon discovered by Godel (1966) which was described in Chapter 2.

The instantaneous defluidisation of bed material experienced during Runs 2 and 7 suggests that defluidisation is governed by the principles which determine the minimum fluidisation velocity rather than those which govern the rate of agglomeration. It should be noted that,

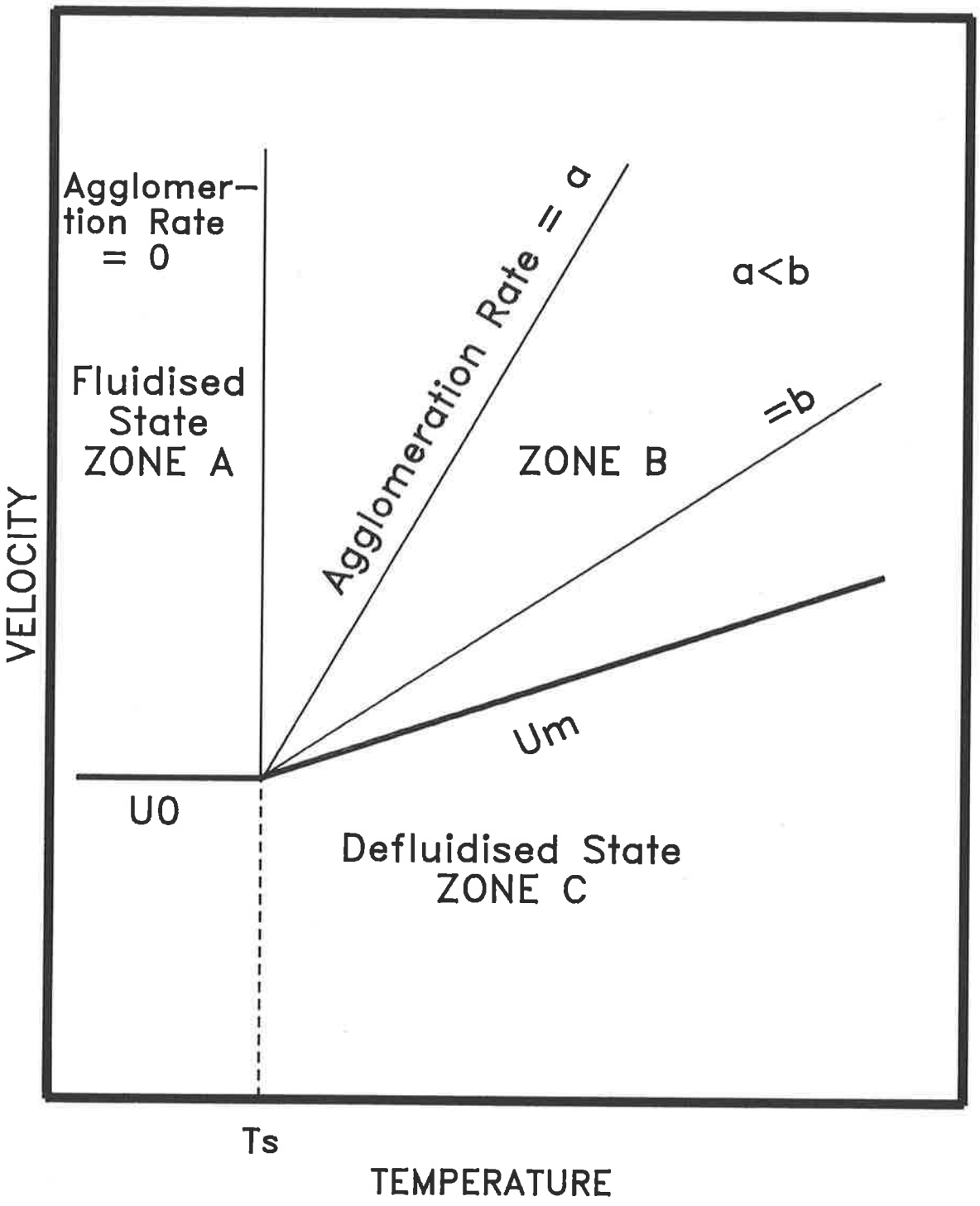

FIGURE 7.3: HIGH TEMPERATURE REGIMES OF FLUIDIZED BED OPERATION SHOWING THE AGGLOMERATING ZONE (ZONE B)

in these runs, the minimum fluidisation velocity was reached as the thickness of the coating on the bed particles increased with operating time, as illustrated in Figure 7.4. Based on this hypothesis, it can be suggested that clinker formation in fluid bed systems occur after the bed has defluidised.

Burning the same coal as in Run 2 but operating at lower temperatures (Runs 3, 8 and 9) did not result in defluidisation for the duration of the runs. With the exclusion of Run 9, the FBCS operated under an agglomerating regime (Zone B) during these runs. Agglomeration did not occur during Run 9 which operated near the initial sintering temperature.

The operating regimes of the FBCS can be illustrated using data collected from various experiments, Figure 7.5. It should be noted that only those runs during which all variables except temperature and fluidisation velocity were maintained could be shown on the same $U-T$ diagram. In Runs 2, 3, 8 and 9, the composition of coating and hence the intrinsic physical properties of the bed particles were the same (Chapter 5). However, the bed particles in these runs acquired different coating thickness for the same operating time. Therefore, the values of agglomeration rate for Runs 3, 8 and 9, shown in Figure 7.5, are calculated from the experimental results (Figure 6.13) for the same coating thickness of 80 micron (an arbitrarily selected value). The true minimum fluidisation curve (U_0) is drawn to pass above the coordinates of Run 2 which defluidised prior to reaching the coating thickness of 80 micron. The theoretical minimum fluidisation velocity for non-sticky particles (U_0) was calculated using the Ergun equation (Appendix A). The initial sintering temperature of the bed particles in these runs (700°C) is also shown.

The rate of agglomeration designated to the curves shown in Figure 7.5 and the slope of the minimum fluidisation curve (U_m) are only indicative as further experimentation at various fluidisation velocity is required to determine the exact relationships. Nonetheless, Figure 7.5 shows that a qualitative agreement exists between the experimental results and theory.

This project can be considered the starting basis to generate quantitative models for the agglomeration and defluidisation processes. Details of further work required is given in Chapter 8. The scope of the current project, specifically the investigation of the role of the inorganic matter, did not include this additional work.

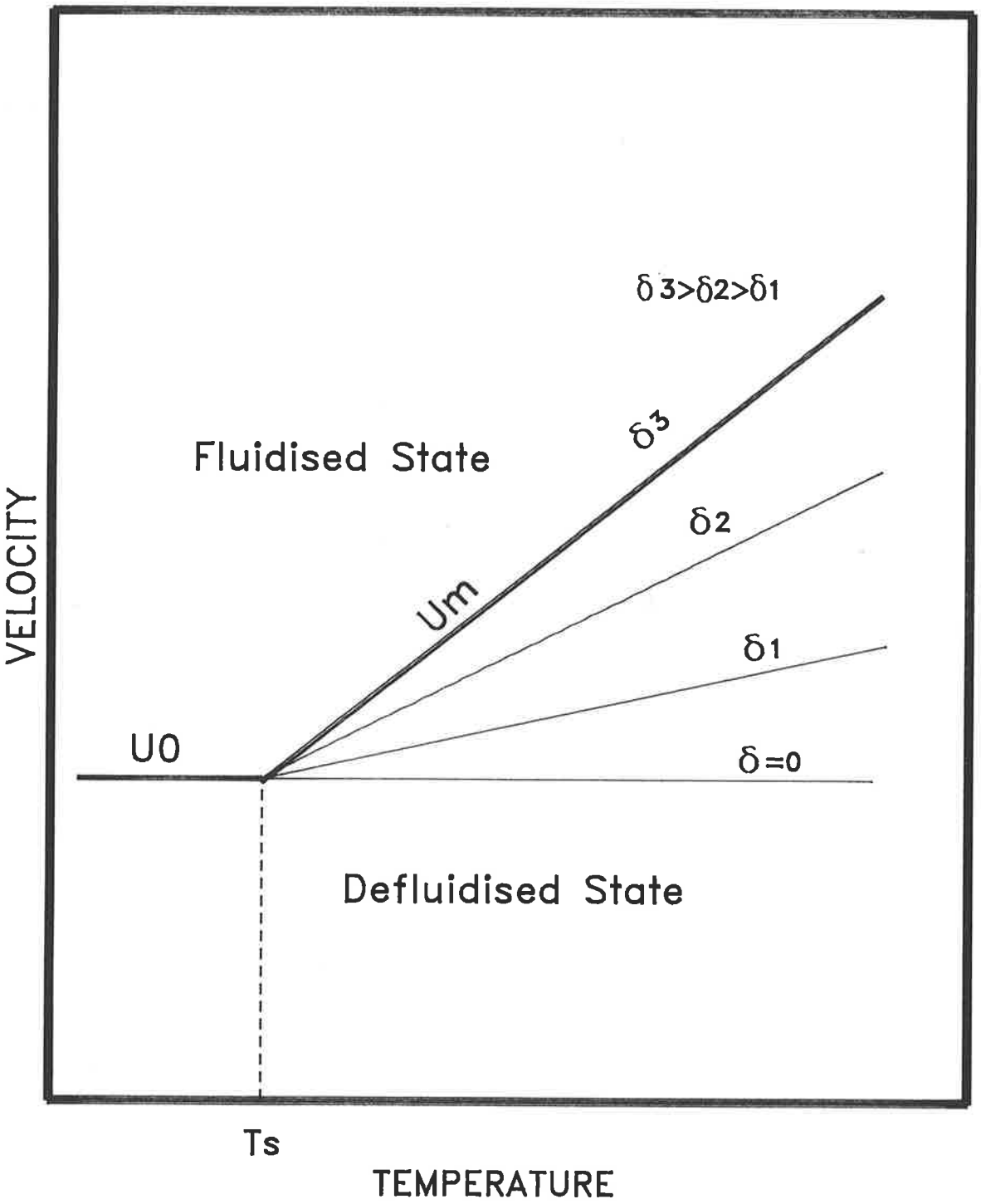

FIGURE 7.4: HIGH TEMPERATURE REGIMES OF FLUIDISED BED OPERATION EFFECT OF COATING THICKNESS

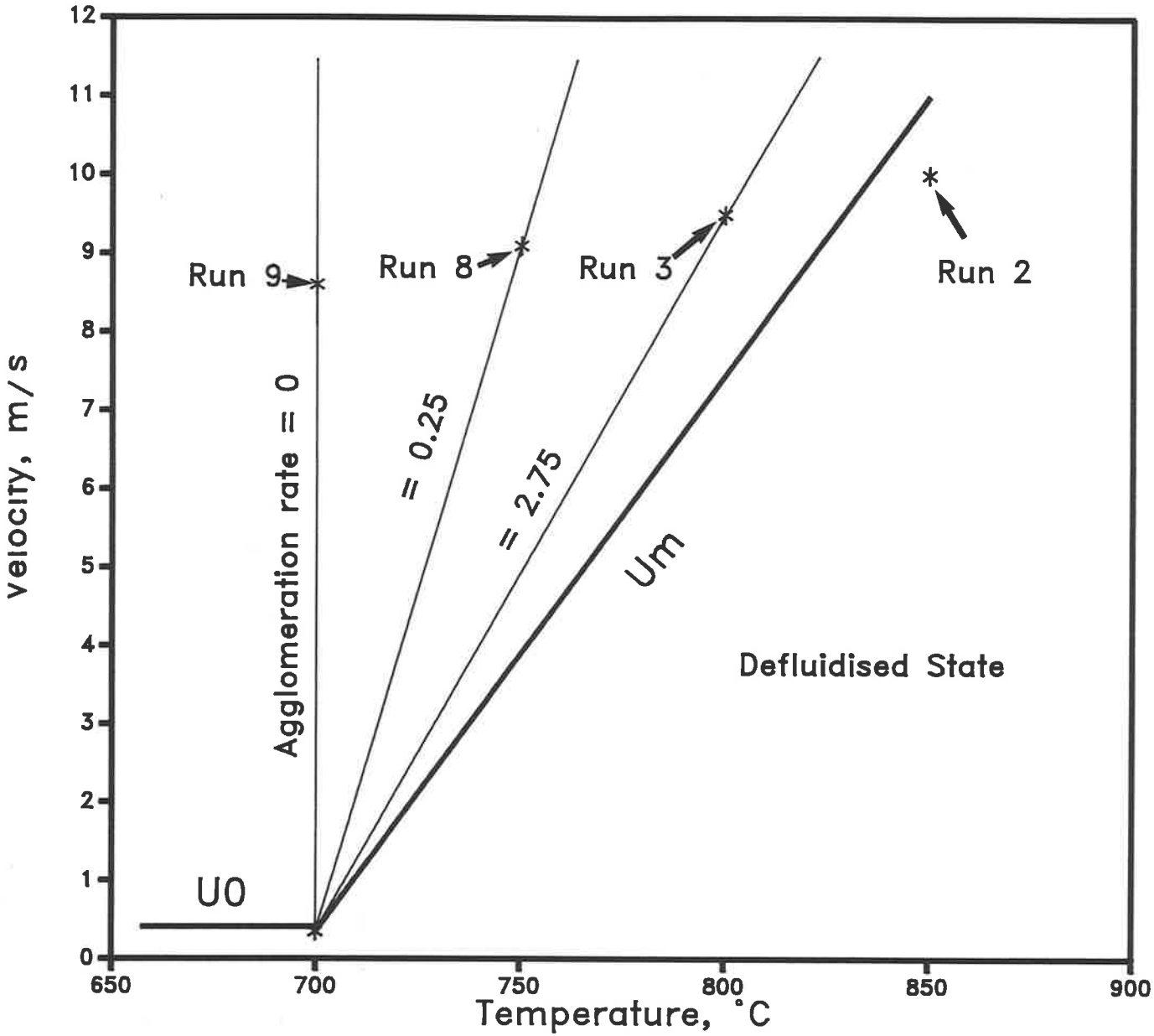

Fig 7.5: High Temperature Regimes of the FBCS Operation At a Constant Coating Thickness (80 μ)

Chapter 8

CONCLUSIONS, IMPLICATIONS AND RECOMMENDATIONS

8.1 CONCLUSIONS

The major conclusions derived from the results of the experimental program and theoretical evaluations are presented as follows:

- Under the conditions of FBC systems burning high-sodium high-sulphur low-rank coals, the extent of vaporisation of sodium species including sodium chloride is small. Sodium chloride reacts with other compounds inside the char and/or on the char's surface resulting in a disproportionate release of chlorine possibly as hydrochloric acid. Sodium species remaining in the char, including those from sodium chloride reactions, participate in the ash formation process.
- The presence of the organically bound sulphur in the coal results in the formation of sulphates of sodium and calcium. Formation of a small amount of magnesium sulphate is also possible. These sulphates form low melting eutectics which cause the deposition of ash on the surface of the inert bed particles. The deposition occurs as a result of collision of the bed particles with the burning char particles.

- The nature and the proportion of the inorganic matter in coal, particularly sodium and sulphur, have a profound effect on the rate of deposition of ash on the bed particles (coating of the bed particles). The furnace temperature was also found to have a marked effect on the rate of deposition of the coating. The deposition of ash on the bed particles occurs irrespective of the nature of the bed material.

- The inorganic matter disproportionates in the fluid bed combustors. The ash deposited on the bed particles will be enriched in those species having the potential to form low melting compounds. The ash collected in the cyclone will be enriched in solid species including the mineral inclusions in coal. The composition of ash coating does not change significantly with bed temperature, bed size distribution and with the composition of the bed material. However, the proportion of sodium chloride and the organically bound elements in coal have a profound effect on the composition of the ash coating.

- Some of the species in the ash coating deposited on the bed particles may remain molten at bed temperature. The molten phase present in the coating of the bed particles render them capable of sintering together and forming agglomerates or causing defluidisation.

- For agglomeration or defluidisation to occur:

  a) the furnace temperature has to exceed the initial sintering temperature of the coating; and

  b) a minimum thickness of coating referred to as the "critical thickness" has to be deposited on the bed particles.

- Once these conditions are satisfied, the rate of agglomeration and the defluidisation propensities are governed principally by the proportion of the molten phase, the characteristics of the coating matrix, the coating thickness and furnace temperature.

- The stages involved in the agglomeration process are as follows:

  + the formation of a sticky coating on the surface of the bed particles;

  + collision of the bed particles; and

  + formation of an interface between the coatings due to viscous flow caused by the system's attempt to reduce its surface energies.

- The stages involved in the defluidisation process are similar to those of agglomeration. However, for defluidisation to occur, the bed particles do not necessarily have to remain sintered together (that is, to form agglomerates). The interaction force between the bed particles may be sufficient to alter the balance between the forces of gravity, buoyancy and drag with the resultant defluidisation of the bed above the theoretical minimum fluidisation velocity for non-sticky bed particles. Contrary to agglomeration, defluidisation is an instantaneous process.

- Using the Frenkel sintering model, one can derive expressions for the rate of agglomeration and the onset of defluidisation in terms of: operating variables (such as fluidisation velocity and temperature), intrinsic physical properties of the coating (surface tension, viscosity and binding strength) and the coating thickness (or operating time). The equations derived can be used as a basis for the development of agglomeration and defluidisation models.

8.2 PRACTICAL IMPLICATIONS

The results obtained have a number of practical implications which are described as follows:

- Compared with pc fired systems, evaporation of a smaller proportion of sodium compounds, including sodium chloride, during FBC is expected to reduce fouling of the heat transfer surfaces caused by vapour condensation. However, the presence of low melting compounds formed from Na, Ca, S and possibly magnesium could result in fouling of these surfaces through the adhesion of sticky particles of ash and bed material. Furthermore, the release of chlorine as hydrochloric acid could aggravate the risk of high temperature corrosion.

- The growth of bed particles due to the deposition of ash, which occurs at bed temperatures even below the initial sintering temperature of the ash, is expected to alter the hydrodynamics of the fluid bed combustors and thus the heat transfer regimes. The bed material has to be bled from the combustor continuously and fresh material has to be added to the system in order to maintain the size of the bed particles at the required limit. The thickness of the coating on the bed particles at the steady condition is determined by the rate of deposition of the coating and the rate of renewing the bed inventory.

- Burning coals in fluid bed combustors at temperatures higher than the initial sintering temperature of the bed particles would result in the formation of agglomerates and/or defluidisation of the bed. Any pair of values of fluidisation velocity and bed temperature above the true minimum fluidisation velocity, typically shown in Figure 7.3, is likely to cause agglomeration. Below this curve, the bed would defluidise instantaneously.

- If, due to combustion reasons, a fluid bed has to operate at temperatures higher than the initial sintering temperature of the bed particles, one can control agglomeration and defluidisation by either increasing the fluidisation velocity and/or maintaining the thickness of the coating below the "critical thickness". The latter is achieved by controlling the rate of bleeding of the bed inventory and adding an equivalent amount of fresh material to the bed.

- It is also possible to avoid defluidisation and reduce the rate agglomeration by reducing the sintering propensity of the bed particles through the use of additives which could alter the physical characteristics of the coating deposited on the bed particles.

- Knowing the high temperature regimes of fluid bed operation (typically shown in Figure 7.3), would assist in selecting the optimum operating conditions for any particular fluid bed system either for avoiding agglomeration and defluidisation or for constant rate of agglomeration under stable conditions (for example in agglomerating gasifiers).

8.3 RECOMMENDATIONS FOR FURTHER WORK

The results of this study have increased the knowledge on the behaviour of the inorganic matter during FBC of high-sodium, high-sulphur low-rank coals and on the mechanism of agglomeration and defluidisation. However, ongoing work is desirable to extend the knowledge, particularly in the following areas:

Transformation of the Inorganic Matter

The results of carbonisation tests carried out on single particles of coal indicated the formation of acid insoluble compounds from the organically bound Ca, Mg and Al. These compounds could not be identified by the analytical techniques employed. Identification of these compounds would assist in better understanding of the inorganic transformations under the reducing environment prevailing inside the char particles during combustion.

Reaction of Gaseous Inorganic Species with Bed Material

Although no evidence was found to suggest the reaction of gaseous species with the bed material, specially designed experiments to confirm the findings would be beneficial in ensuring that the only mechanism by which the bed particles acquire stickiness is by the deposition of molten ash on the bed particles.

Fouling and Corrosion of the Heat Transfer Surfaces

The mechanisms of fouling of the heat transfer surfaces by vapour condensation and by the adhesion of sticky material need to be investigated. The effect of fouling and gaseous HCl on corrosion of metals and refractories should be evaluated.

Effect of the Ballast Material (Additives)

The effect of various additives (amount, composition and size distribution) on the characteristics of the coating deposited on the bed particles has to be investigated in order to optimise the operating conditions for fluid bed systems operating with sticky bed particles.

Quantitative Description of Agglomeration and Defluidisation

To develop quantitative models for agglomeration and defluidisation, further work should be directed towards the following:

Stage 1- Validation of the equations presented in Chapter 7 using bed material of known physical properties (such as polyethylene beads) in a fluid bed system operating at various temperatures and velocities.

Stage 2- Empirical determination of the agglomeration rate and the onset of defluidisation using spent bed material of known coating thickness and composition in a fluid bed system operating at various temperatures and velocities.

Stage 3- Establishment of a data base of intrinsic physical properties of the coating (such as viscosity, surface tension and binding strength) and finding the parameters in the equations presented in Chapter 7 using the results of Stage 2.

Nomenclature

Ar	Archimedes dimensionless number
B	binding strength
c_p	heat capacity
d	particle diameter
d_0	initial particle diameter
d_f	furnace diameter (cylindrical section)
E	activation energy
F_b	binding force between two colliding particles
F_t	total binding force per unit volume of fluid bed
g	normal gravitational acceleration
K_a	$6\frac{k_f}{(\pi k_u)}$
K_c	pre-exponential factor
k_f	collision frequency
k_u	constant
L	lengh of fluid bed
M	mass of bed inventory
m	constant
m_a	mass flow rate of combustion air

m_c	mass of coating on bed particles
n	constant
N	number of particles per unit volume of fluid bed
N_b	number of bed particles in bed inventory
P	momentum of bed particles
Q_d	air heater duty
Q_v	volumetric flow rate
Q_m	mass flow rate
R	Universal Gas Constant
Re_{mf}	Reynolds number at the minimum fluidisation velocity
R_a	rate of agglomeration
R_d	rate of deposition of coating
R_i	rate of formation of an interface
r	radius of bed particles
S_r	cross-sectional area of interface
T	furnace temperature
t	operating time of the furnace
t_c	contact time between two sticky particles
T_0	outlet air heater temperature
T_i	ambient temperature
T_s	initial sintering temperature
U	fluidisation velocity (superficial)
U_0	theoretical minimum fluidisation velocity for non-sticky particles
U_m	minimum fluidisation velocity
U_p	particle velocity

W_a	work of adhesion of a liquid
W_c	work of cohesion of a liquid
x	radius of interface between two particles

Greek Symbols

α	dimensionless correlation factor
β	dimensionless correlation factor
δ	coating thickness
ϵ	voidage
ϵ_{mf}	voidage at the minimum fluidisation velocity
μ	ash viscosity
μ_0	ash viscosity at a reference temperature
μ_f	fluidising gas viscosity
ρ_f	fluidising gas density
ρ_p	particle density
ΔP	pressure drop across the bed
ϕ	sphericity
θ	contact angle at the solid-liquid interface
σ	surface tension

Appendix A

FLUID BED COMBUSTION SYSTEM CALCULATIONS AND PRE-COMMISSIONING

A.1 Calculations

A cylindrical furnace of 77 mm ID was selected. In order to keep the bed material in the conical section at the bottom of the furnace (combustion zone), a fluidisation velocity of 1 to 2 m/s in the cylindrical part of the furnace was considered to be adequate. Based on these velocities, the coal throughput and combustion air flow rate were calculated for various levels of excess air. The diameter of the narrow end of the conical section of the furnace was then selected to provide an average fluidisation velocity of 5 to 10 m/s in the combustion zone.

Combustion air requirement:

The volumetric and mass flow rates (Q_v and Q_m respectively) of the fluidising gas is given by:

$$Q_v = \frac{\pi}{4} d_f^2 U \qquad (A.1)$$

$$Q_m = \rho_f Q_v \qquad (A.2)$$

where d_f is diameter of the cylindrical section of the furnace,

U is fluidisation velocity at the combustion temperature,

ρ_f is the gas density at the combustion temperature

Given $d_f = 0.077$ m and gas density (at 800°C) = 0.31 kg/m^3, the volumetric and mass flow rates of flue gas were calculated for two fluidisation velocities:

	U = 1 m/s	U = 2 m/s
Q_V (m^3/s) x 10^3	4.65	9.31
Q_m (kg/s) x 10^3	1.44	2.88

In order to determine the combustion air requirement, combustion calculations were carried out for various excess oxygen using the ultimate and proximate analyses of air-dried Lochiel coal (20% moisture).

Combustion air and flue gas for 1 kg of fuel

Excess air	vol.% O_2 (dry-basis)	kg flue gas	nm^3 flue gas
25	4.2	8.4	6.4
100	10.5	13.0	9.9
200	14.0	19.0	14.6
300	15.7	25.0	19.3

The coal throughput and combustion air (at ambient conditions) were then calculated as follows (sample calculation):

U = 1 m/s

excess air = 25%

flue gas/kg fuel = 6.4 nm^3 (from combustion calc.)

@ 800°C = 6.4 x 1073/273 = 25.15 m^3

coal throughput = $4.65 \times 10^{-3}/25.15$ = 185×10^{-6} kg/s
= 665 g/h

combustion air (mass)/kg fuel = 8.4 - 1 = 7.4 kg (from combustion calculation)

combustion air (vol.)/kg fuel = $7.4 \times 22.414/28.9 = 5.735$ nm^3

combustion air flow rate = 0.665×5.735 = 3.814 nm^3/h
= 63.5 L/minute

The results of calculations are presented in the following table:

	coal throughput, kg/h		air flow rate, L/min	
% excess air	1 m/s	2 m/s	1 m/s	2 m/s
25	0.665	1.330	63.5	127.0
100	0.429	0.858	66.4	132.8
200	0.291	0.582	67.6	135.2
300	0.220	0.440	68.1	136.2

Based on these results, the diameter of the narrow end of the conical distributer was selected (26 mm ID) in order to obtain an average fluidisation velocity of 5 to 10 m/s in the combustion zone.

Air heater duty

The air heater duty (Q_d) is calculated by:

$$Q_d = m_a c_p (T_0 - T_i) \qquad (A.3)$$

where m_a is mass flow rate of combustion air

c_p is heat capacity of air

T_0 outlet air heater temperature

T_i ambient temperature

Given c_p = 1071 J/kg° C, T_0 = 700°C and T_i = 25°C, the air heater duty was calculated for the maximum air flow rate of 150 L/minute:

	U = 1 m/s	U = 2 m/s
Q_d, kW	0.918	1.836

Minimum fluidisation velocity

The minimum fluidisation velocity for particle diameter of 0.925 mm was calculated as follows:

From Howard (1989):

$$Ar = 150\frac{1-\epsilon_{mf}}{\Phi^2\epsilon_{mf}^3}Re_{mf} + \frac{1.75}{\Phi\epsilon_{mf}^3}Re_{mf}^2 \qquad (A.4)$$

where Ar is Archimedes number, and

Re_{mf} is Reynolds number at the minimum fluidisation velocity.

$$Ar = \frac{\rho_f(\rho_p - \rho_f)gd^3}{\mu_f^2} \qquad (A.5)$$

where d = particle diameter (0.925×10^{-3} m)

Φ = sphericity assumed equal to 1.0

ϵ_{mf} = voidage at the minimum fluidisation velocity (= 0.417)

ρ_f = gas density (0.31 kg/m^3 at 800°C)

ρ_p = particle density (2.50×10^3 kg/m^3)

μ_f = gas viscosity (0.047 centipoise)

g = normal gravitational acceleration

Calculating Ar from Equation A.5 and inserting the values of the variables in Equation A.4:

Ar = 2882

Re_{mf} = 2.298

$$Re_{mf} = \frac{d\rho_f U_0}{\mu_f} \qquad (A.6)$$

where U_0 is the minimum fluidisation velocity for non-sticky particles.

From Equation A.6:

$U_0 = 0.35$ m/s

A.2 Pre-commissioning Results

The coal particle size distribution before and after the coal is fed through the screw feeder is given in Figure A.1. The characteristic curve of the screw feeder is given in Figure A.2.

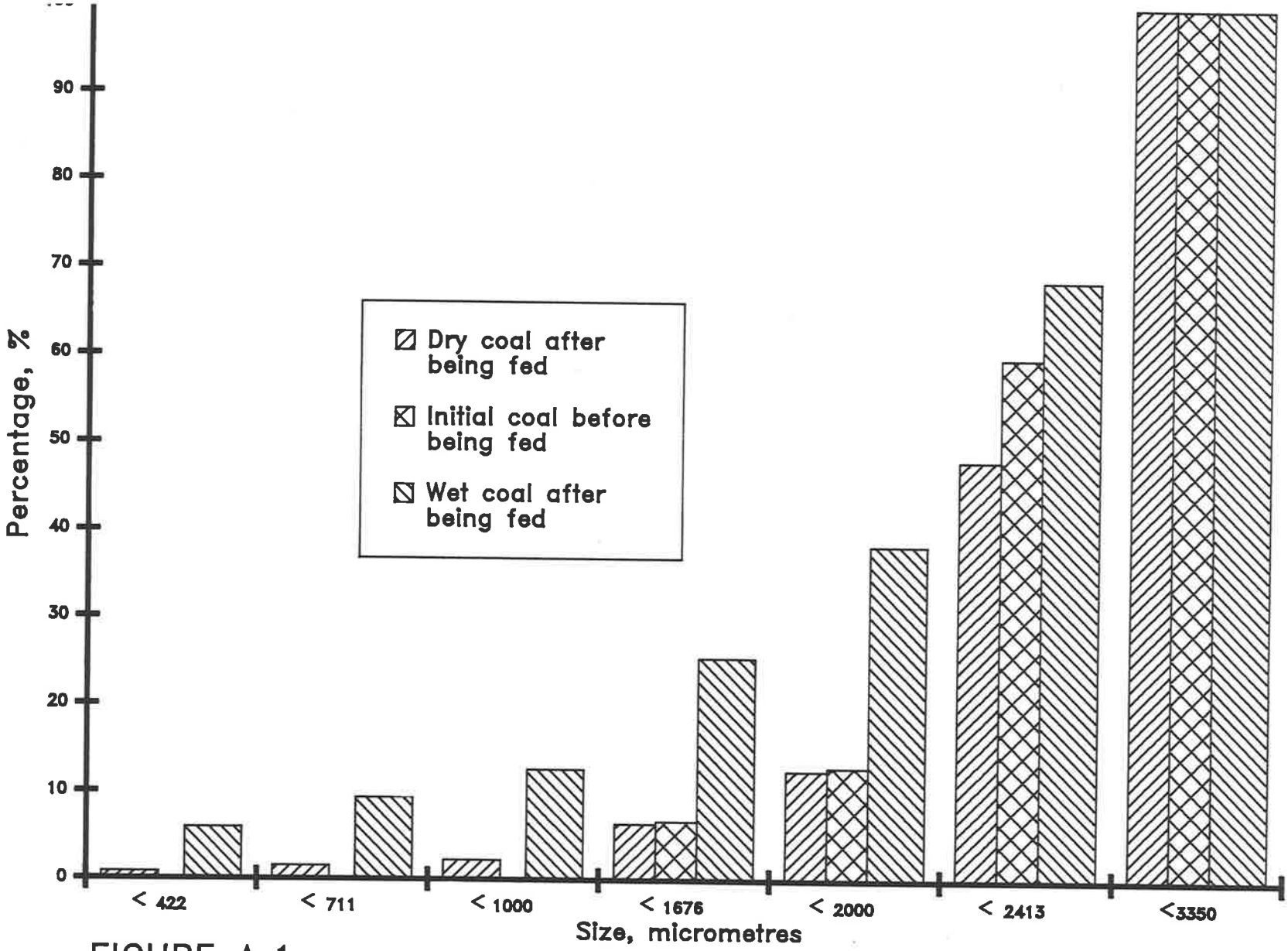

FIGURE A.1:

Graph of size distribution of coal after being fed through the screw feeder.

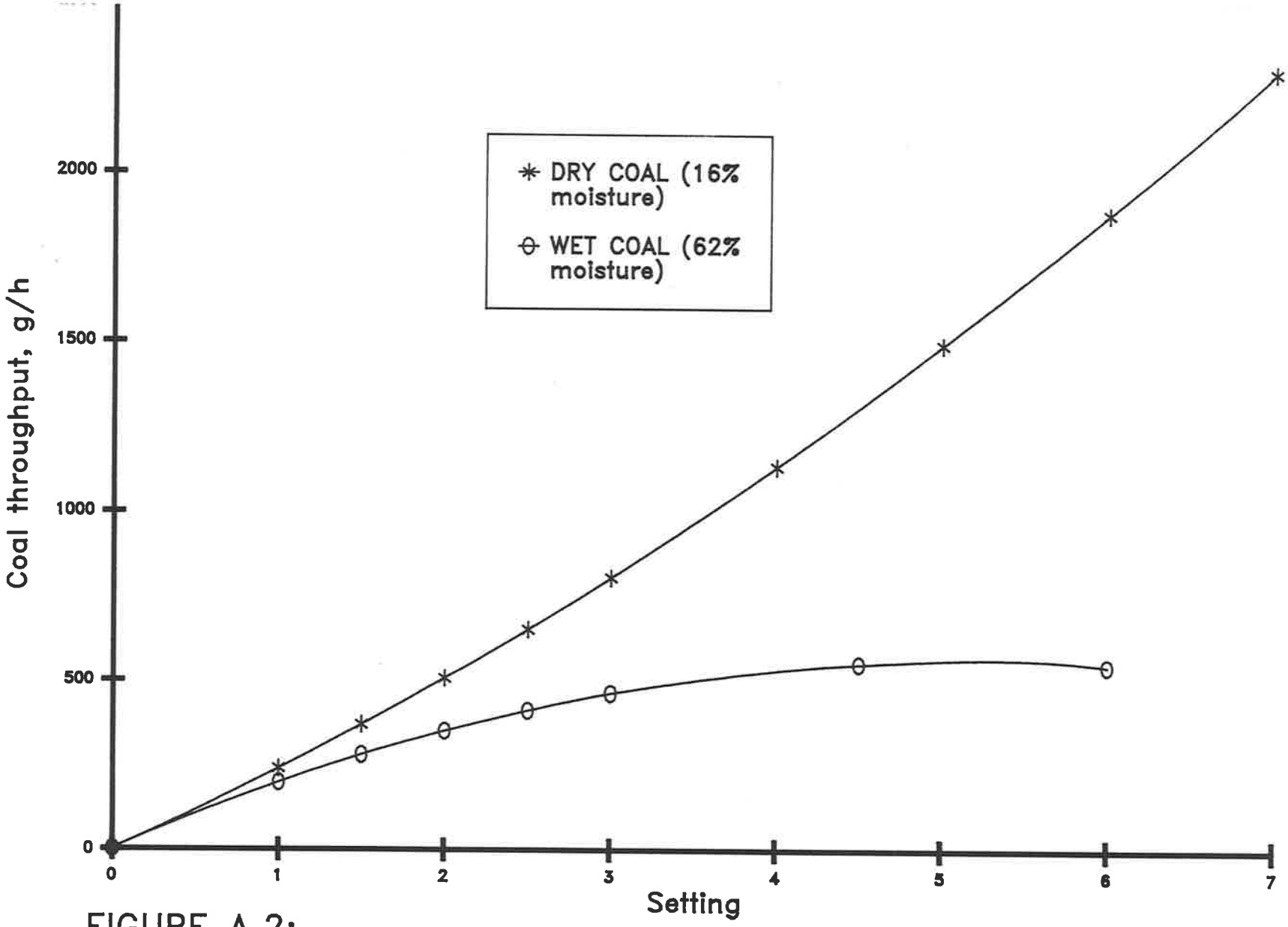

FIGURE A.2:

Characteristic Curve of the Screw Feeder

Appendix B

CHEMICAL ANALYSIS (EXTRACTION METHODS) SINGLE PARTICLE EXPERIMENTS

The product particles withdrawn from the single particle furnace were analysed for the inorganic elements (Na, Cl, Ca, Mg and SO_4) using the extraction methods described in Chapter 3. The results are presented as micrograms of the inorganic elements in the total mass of the product particles.

Given the initial mass of the product particles prior to combustion or carbonisation, the results were then re-calculated per 100 mg of the initial mass of the product particles. By comparing the amount of the inorganic elements in the product particles with those in the same amount of raw coal, the percent loss of various elements were calculated. A sample calculation is given as follows:

Carbonisation test at 700°C and 7.5 mm coal particle size:

initial mass of the single coal particle (wet coal) = 302 mg
mass of the product particle = 235.6 mg
percent mass loss during carbonisation or combustion = 22%

Results of Chemical Analysis of Product Particle

	micrograms in the product particle
Na (total)	1070
Na water soluble (WS)	710
Na acid soluble (AS)	338
Na acid insoluble (AI)	22
Ca (total)	1477
Ca water soluble (WS)	22
Ca acid soluble (AS)	1430
Ca acid insoluble (AI)	25
Mg (total)	1024
Mg water soluble (WS)	14
Mg acid soluble (AS)	995
Mg acid insoluble (AI)	15
Cl all water soluble	771
SO_4 water soluble (WS)	184

The results are multiplied by 100/302 to calculate the amount of the inorganic elements in a product particle of 100 mg initial mass.

Inorganic elements in a Product Particle of 100 mg Initial Mass

	micrograms in the product particle of 100 mg initial mass	micrograms in 100 mg of raw coal
Na (total)	354.3	350.0
Na water soluble (WS)	235.1	233.0
Na acid soluble (AS)	111.9	109.0
Na acid insoluble (AI)	7.3	8.0
Ca (total)	489.1	503.0
Ca water soluble (WS)	7.3	7.0
Ca acid soluble (AS)	473.5	489.0
Ca acid insoluble (AI)	8.3	7.0
Mg (total	339.1	347.0
Mg water soluble (WS)	4.6	3.0
Mg acid soluble (AS)	329.5	339.0
Mg acid insoluble (AI)	5.0	5.0
Cl all water soluble	215.6	219.0
SO_4 water soluble (WS)	60.9	0.0

The results are then compared with the amount of the inorganic elements in 100 mg of raw coal to determine the percent loss of Na, Ca, Mg and Cl.

Percent Loss of the Inorganic Elements

	percent loss
Na	-1.2*
Ca	2.8
Mg	2.3
Cl	1.5

* the negative sign is considered as no change in mass

COMBUSTION TEST, T= 700 C, d= 5.5 mm

		PRODUCT PARTICLE			
Initial mass, mg		118.00	127.00	134.00	122.00
Wt loss, %		49.10	74.80	91.00	98.40
Time ,s		10.0	20.0	30.0	40.00
		MICROGRAMS			
Na(TOTAL)		404.0	316.0	218.0	34.0
Na(WS)		348.0	290.0	194.0	28.00
Na(AS)		48.0	21.0	19.0	4.00
Na(AI)		8.0	5.0	5.0	2.00
Ca(TOTAL)		576.8	519.0	342.0	86.0
Ca(WS)		5.0	32.0	56.0	38.00
Ca(AS)		513.0	427.0	177.0	21.00
Ca(AI)		58.8	60.0	109.0	27.00
Mg(TOTAL)		392.0	370.0	239.0	64.0
Mg(WS)		4.0	24.0	32.0	22.00
Mg(AS)		362.0	292.0	122.0	17.00
Mg(AI)		26.0	54.0	85.0	25.00
Cl		183.6	83.8	33.4	1.40
SO_4 (WS)		88.8	130.0	166.9	152.40
	COAL	CALC. PER 100 mg OF INITIAL MASS			
Na(TOTAL)	342.0	342.4	248.8	162.7	27.9
Na(WS)	233.0	294.9	228.3	144.8	23.0
Na(AS)	109.0	40.7	16.5	14.2	3.3
Na(AI)	.0	6.8	3.9	3.7	1.6
Ca(TOTAL)	496.0	488.8	408.7	255.2	70.5
Ca(WS)	7.0	4.2	25.2	41.8	31.1
Ca(AS)	489.0	434.7	336.2	132.1	17.2
Ca(AI)	.0	49.8	47.2	81.3	22.1
Mg(TOTAL)	342.0	332.2	291.3	178.4	52.5
Mg(WS)	3.0	3.4	18.9	23.9	18.0
Mg(AS)	339.0	306.8	229.9	91.0	13.9
Mg(AI)	.0	22.0	42.5	63.4	20.5
Cl	219.0	155.6	66.0	24.9	1.1
SO_4 (WS)	.0	75.3	102.4	124.6	124.9
		PERCENT LOSS OF INORGANICS			
Na	.0	-.1	27.2	52.4	91.9
Ca	.0	1.4	17.6	48.5	85.8
Mg	.0	2.9	14.8	47.8	84.7
Cl	.0	29.0	69.9	88.6	99.5

COMBUSTION TEST, T= 700 C, d = 7.5 mm

		PRODUCT PARTICLES			
Initial mass, mg	302.00	285.00	296.00	296.00	307.00
Wt loss, %	24.50	53.70	74.00	87.50	95.00
Time ,s	10.0	20.0	30.0	40.00	50.00
		MICROGRAMS			
Na(TOTAL)	1024.0	828.5	647.0	564.0	326.3
Na(WS)	648.0	625.0	603.0	546.00	321.80
Na(AS)	331.0	199.0	38.0	11.00	2.50
Na(AI)	45.0	4.5	6.0	7.00	2.00
Ca(TOTAL)	1477.0	1248.0	1048.8	1009.0	671.5
Ca(WS)	11.0	8.0	12.0	105.00	225.50
Ca(AS)	1424.0	1185.0	921.8	794.00	263.70
Ca(AI)	42.0	55.0	115.0	110.00	182.30
Mg(TOTAL)	1021.0	879.0	741.0	718.0	488.7
Mg(WS)	7.0	10.0	16.0	7.00	21.90
Mg(AS)	981.0	803.0	616.0	599.00	313.10
Mg(AI)	33.0	66.0	109.0	112.00	153.70
Cl	516.5	383.0	189.6	117.70	35.60
SO_4 (WS)	340.0	1100.0	960.0	650.00	430.00
	COAL	CALCULATED PER 100 mg OF INITIAL MASS			
Na(TOTAL)	342.0	339.1	290.7	218.6	190.5	106.3
Na(WS)	233.0	214.6	219.3	203.7	184.5	104.8
Na(AS)	109.0	109.6	69.8	12.8	3.7	.8
Na(AI)	.0	14.9	1.6	2.0	2.4	.7
Ca(TOTAL)	496.0	489.1	437.9	354.3	340.9	218.7
Ca(WS)	7.0	3.6	2.8	4.1	35.5	73.5
Ca(AS)	489.0	471.5	415.8	311.4	268.2	85.9
Ca(AI)	.0	13.9	19.3	38.9	37.2	59.4
Mg(TOTAL)	342.0	338.1	308.4	250.3	242.6	159.2
Mg(WS)	3.0	2.3	3.5	5.4	2.4	7.1
Mg(AS)	339.0	324.8	281.8	208.1	202.4	102.0
Mg(AI)	.0	10.9	23.2	36.8	37.8	50.1
Cl	219.0	171.0	134.4	64.1	39.8	11.6
SO_4 (WS)	.0	112.6	386.0	324.3	219.6	140.1
		PERCENT LOSS OF INORGANICS			
Na	.0	.9	15.0	36.1	44.3	68.9
Ca	.0	1.4	11.7	28.6	31.3	55.9
Mg	.0	1.1	9.8	26.8	29.1	53.5
Cl	.0	21.9	38.6	70.8	81.8	94.7

COMBUSTION TEST, T= 700 C, d = 9.0 mm

		PRODUCT PARTICLES				
Initial mass, mg		570.00	581.00	541.00	564.00	549.00
Wt loss, %		38.40	55.20	72.30	81.70	89.20
Time ,s		20.0	30.0	40.0	50.00	60.00
		MICROGRAMS				
Na(TOTAL)		1828.0	1651.0	1380.0	1238.0	990.0
Na(WS)		1380.0	1408.0	1296.0	1190.00	920.00
Na(AS)		440.0	237.0	80.0	46.00	70.00
Na(AI)		8.0	6.0	4.0	2.00	.00
Ca(TOTAL)		2702.8	2479.0	2101.0	2079.0	1709.0
Ca(WS)		38.0	22.0	38.0	62.00	206.00
Ca(AS)		2450.0	2270.0	1830.0	1730.00	1230.00
Ca(AI)		214.8	187.0	233.0	287.00	273.00
Mg(TOTAL)		1906.5	1802.0	1490.0	1496.0	1240.0
Mg(WS)		30.0	22.0	30.0	44.00	56.00
Mg(AS)		1684.0	1648.0	1284.0	1246.00	942.00
Mg(AI)		192.5	132.0	176.0	206.00	242.00
Cl		1026.0	496.2	364.1	244.30	92.78
SO_4 (WS)		607.6	626.1	634.8	509.10	581.40
	COAL	CALCULATED PER 100 mg OF INITIAL MASS				
Na(TOTAL)	342.0	320.7	284.2	255.1	219.5	180.3
Na(WS)	233.0	242.1	242.3	239.6	211.0	167.6
Na(AS)	109.0	77.2	40.8	14.8	8.2	12.8
Na(AI)	.0	1.4	1.0	.7	.4	.0
Ca(TOTAL)	496.0	474.2	426.7	388.4	368.6	311.3
Ca(WS)	7.0	6.7	3.8	7.0	11.0	37.5
Ca(AS)	489.0	429.8	390.7	338.3	306.7	224.0
Ca(AI)	.0	37.7	32.2	43.1	50.9	49.7
Mg(TOTAL)	342.0	334.5	310.2	275.4	265.2	225.9
Mg(WS)	3.0	5.3	3.8	5.5	7.8	10.2
Mg(AS)	339.0	295.4	283.6	237.3	220.9	171.6
Mg(AI)	.0	33.8	22.7	32.5	36.5	44.1
Cl	219.0	160.0	85.4	67.3	43.3	16.9
SO_4 (WS)	.0	106.6	107.8	117.3	90.3	105.9
		PERCENT LOSS OF INORGANICS				
Na	.0	6.2	16.9	25.4	35.8	47.3
Ca	.0	4.4	14.0	21.7	25.7	37.2
Mg	.0	2.2	9.3	19.5	22.4	34.0
Cl	.0	26.9	61.0	69.3	80.2	92.3

COMBUSTION TEST, T = 770 C, d = 7.5 mm

		PRODUCT PARTICLES				
Initial mass, mg		597.00	621.00	610.00	583.00	604.00
Wt loss, %		37.00	70.00	85.00	89.00	93.00
Time ,s		10.0	20.0	30.0	35.00	40.00
		MICROGRAMS				
Na(TOTAL)		1945.0	1492.0	1183.0	1032.0	846.0
Na(WS)		1340.0	1380.0	1132.0	944.00	692.00
Na(AS)		600.0	107.0	46.0	83.00	128.00
Na(AI)		5.0	5.0	5.0	5.00	26.00
Ca(TOTAL)		2822.0	2327.4	1982.0	1780.0	1649.0
Ca(WS)		22.0	30.0	184.0	272.00	435.00
Ca(AS)		2720.0	2055.4	1600.0	1260.00	907.00
Ca(AI)		80.0	242.0	198.0	248.00	307.00
Mg(TOTAL)		1967.0	1650.0	1424.0	1266.0	1185.0
Mg(WS)		18.0	44.0	96.0	58.00	24.00
Mg(AS)		1882.0	1467.0	1150.0	1010.00	951.00
Mg(AI)		67.0	139.0	178.0	198.00	210.00
Cl		1109.0	565.0	345.0	235.00	115.00
SO_4 (WS)		650.0	1040.0	1420.0	890.00	600.00
	COAL	CALCULATED PER 100 mg OF INITIAL MASS				
Na(TOTAL)	342.0	325.8	240.3	193.9	177.0	140.1
Na(WS)	233.0	224.5	222.2	185.6	161.9	134.6
Na(AS)	109.0	100.5	17.2	7.5	14.2	1.2
Na(AI)	.0	.8	.8	.8	.9	4.3
Ca(TOTAL)	496.0	472.7	374.8	324.9	305.3	273.0
Ca(WS)	7.0	3.7	4.8	30.2	46.7	72.0
Ca(AS)	489.0	455.6	331.0	262.3	216.1	150.2
Ca(AI)	.0	13.4	39.0	32.5	42.5	50.8
Mg(TOTAL)	342.0	329.5	265.7	233.4	217.2	196.2
Mg(WS)	3.0	3.0	7.1	15.7	9.9	4.0
Mg(AS)	339.0	315.2	236.2	188.5	173.2	157.5
Mg(AI)	.0	11.2	22.4	29.2	34.0	34.8
Cl	219.0	185.8	91.0	56.6	40.3	19.0
SO_4 (WS)	.0	108.9	167.5	232.8	152.7	99.3
		PERCENT LOSS OF INORGANICS				
Na	.0	4.7	29.7	43.3	48.2	59.0
Ca	.0	4.7	24.4	34.5	38.4	45.0
Mg	.0	3.7	22.3	31.7	36.5	42.6
Cl	.0	15.2	58.5	74.2	81.6	91.3

COMBUSTION TEST, T = 830 C, d = 7.5 mm

		PRODUCT PARTICLES				
Initial mass, mg		602.00	300.00	602.00	302.00	585.00
Wt loss, %		39.00	75.00	86.00	91.00	94.00
Time ,s		10.0	20.0	30.0	35.00	40.00
Na(TOTAL)		1969.0	678.0	1051.0	424.0	606.0
Na(WS)		1420.0	614.0	980.0	354.00	532.00
Na(AS)		544.0	59.0	66.0	65.00	69.00
Na(AI)		5.0	5.0	5.0	5.00	5.00
Ca(TOTAL)		2876.0	1066.0	1686.0	710.0	1098.0
Ca(WS)		44.0	8.0	90.0	98.00	316.00
Ca(AS)		2722.0	933.0	1360.0	450.00	475.00
Ca(AI)		110.0	125.0	236.0	162.00	307.00
Mg(TOTAL)		2004.0	739.0	1186.0	490.0	763.0
Mg(WS)		30.0	10.0	42.0	34.00	12.00
Mg(AS)		1880.0	630.0	956.0	342.00	527.00
Mg(AI)		94.0	99.0	188.0	114.00	224.00
Cl		1025.0	215.0	285.0	95.00	65.00
SO_4 (WS)		860.0	430.0	890.0	180.00	520.00
	COAL	CALCULATED PER 100 mg OF INITIAL MASS				
Na(TOTAL)	342.0	327.1	226.0	174.6	140.4	103.6
Na(WS)	233.0	235.9	204.7	162.8	117.2	134.6
Na(AS)	109.0	90.4	19.7	11.0	21.5	1.2
Na(AI)	.0	.8	1.7	.8	1.7	.9
Ca(TOTAL)	496.0	477.7	355.3	280.1	235.1	187.7
Ca(WS)	7.0	7.3	2.7	15.0	32.5	54.0
Ca(AS)	489.0	452.2	311.0	225.9	149.0	81.2
Ca(AI)	.0	18.3	41.7	39.2	53.6	52.5
Mg(TOTAL)	342.0	332.9	246.3	197.0	162.3	130.4
Mg(WS)	3.0	5.0	3.3	7.0	11.3	2.1
Mg(AS)	339.0	312.3	210.0	158.8	113.2	90.1
Mg(AI)	.0	15.6	33.0	31.2	37.7	38.3
Cl	219.0	170.3	71.7	47.3	31.5	11.1
SO_4 (WS)	.0	142.9	143.3	147.8	59.6	88.9
		PERCENT LOSS OF INORGANICS				
Na	.0	4.4	33.9	49.0	58.9	69.7
Ca	.0	3.7	28.4	43.5	52.6	62.2
Mg	.0	2.7	28.0	42.4	52.6	61.9
Cl	.0	22.3	67.3	78.4	85.6	94.9

CARBONISATION TEST, T= 700 C, D= 7.5 MM

		PRODUCT PARTICLES					
Initial mass, mg	302.00	291.00	292.00	293.00	299.00	303.00	305.00
Wt loss, %	22.00	36.50	46.90	54.90	63.90	72.30	75.40
Time, s	10.0	20.0	30.0	40.00	60.00	90.00	120.00
		MICROGRAMS					
Na(TOTAL)	1070.0	1056.0	1049.0	1033.0	1049.0	1033.0	1043.0
Na(WS)	710.0	690.0	706.0	708.00	826.00	910.00	900.00
Na(AS)	338.0	346.0	313.0	285.00	195.00	90.00	90.00
Na(AI)	22.0	20.0	30.0	40.00	28.00	33.00	53.00
Ca(TOTAL)	1477.0	1576.0	1455.0	1423.0	1496.0	1445.0	1593.0
Ca(WS)	22.0	36.0	12.0	10.00	8.00	30.00	28.00
Ca(AS)	1430.0	1515.0	1410.0	1375.00	1405.00	1130.00	745.00
Ca(AI)	25.0	25.0	33.0	38.00	83.00	285.00	820.00
Mg(TOTAL)	1024.0	1075.0	1033.0	981.0	1058.0	1067.0	1094.0
Mg(WS)	14.0	10.0	10.0	8.00	8.00	32.00	18.00
Mg(AS)	995.0	1050.0	1000.0	945.00	970.00	725.00	333.00
Mg(AI)	15.0	15.0	23.0	28.00	80.00	310.00	743.00
CL	651.0	620.0	524.0	464.00	394.00	337.00	374.00
SO_4 (WS)	184.0	224.0	224.0	209.00	140.00	82.00	41.00
	COAL	CALCULATED PER 100 MG OF INITIAL MASS					
Na(TOTAL)	350.0	354.3	362.9	359.2	352.6	350.8	340.9	342.0
Na(WS)	233.0	235.1	237.1	241.8	241.6	276.3	300.3	295.1
Na(AS)	109.0	111.9	118.9	107.2	97.3	65.2	29.7	29.5
Na(AI)	8.0	7.3	6.9	10.3	13.7	9.4	10.9	17.4
Ca(TOTAL)	503.0	489.1	541.6	498.3	485.7	500.3	476.9	522.3
Ca(WS)	7.0	7.3	12.4	4.1	3.4	2.7	9.9	9.2
Ca(AS)	489.0	473.5	520.6	482.9	469.3	469.9	372.9	244.3
Ca(AI)	7.0	8.3	8.6	11.3	13.0	27.8	94.1	268.9
Mg(TOTAL)	347.0	339.1	369.4	353.8	334.8	353.8	352.1	358.7
Mg(WS)	3.0	4.6	3.4	3.4	2.7	2.7	10.6	5.9
Mg(AS)	339.0	329.5	360.8	342.5	322.5	324.4	239.3	109.2
Mg(AI)	5.0	5.0	5.2	7.9	9.6	26.8	102.3	243.6
CL	219.0	215.6	213.1	179.5	158.4	131.8	111.2	122.6
SO_4 (WS)	.0	60.9	77.0	76.7	71.3	46.8	27.1	13.4
		PERCENT LOSS OF INORGANICS					
Na	.0	-1.2	-3.7	-2.6	-.7	-.2	2.6	2.3
Ca	.0	2.8	-7.7	.9	3.4	.5	5.2	-3.8
Mg	.0	2.3	-6.5	-2.0	3.5	-2.0	-1.5	-3.4
Cl	.0	1.6	2.7	18.1	27.7	39.8	49.2	44.0

CARBONISATION TEST, T= 770 C, D =7.5 mm

		PRODUCT PARTICLES					
Initial mass	288.00	292.00	288.00	295.00	289.00	298.00	280.00
Wt loss, %	37.80	40.00	54.20	60.30	67.20	74.80	76.10
Time ,s	10.0	20.0	30.0	40.00	60.00	90.00	120.00
		MICROGRAMS					
Na(TOTAL)	1026.0	1033.0	997.0	988.0	966.0	962.0	895.0
Na(WS)	704.0	686.0	694.0	698.00	698.00	688.00	624.00
Na(AS)	312.0	326.0	275.0	268.00	247.00	209.00	198.00
Na(AI)	10.0	21.0	28.0	22.00	21.00	65.00	73.00
Ca(TOTAL)	1428.0	1451.0	1427.8	1463.0	1452.0	1477.0	1389.0
Ca(WS)	14.0	14.0	10.0	8.00	5.00	16.00	14.00
Ca(AS)	1400.0	1375.0	1275.0	1265.00	1110.00	845.00	419.00
Ca(AI)	14.0	62.0	142.8	190.00	337.00	616.00	956.00
Mg(TOTAL)	1008.0	998.0	984.0	1008.0	1002.0	1018.0	957.0
Mg(WS)	8.0	8.0	6.0	6.00	5.00	16.00	10.00
Mg(AS)	1000.0	965.0	865.0	870.00	780.00	542.00	226.00
Mg(AI)	.0	25.0	113.0	132.00	217.00	460.00	721.00
Cl	566.0	557.0	426.0	390.00	377.00	291.00	248.00
SO_4 (WS)	212.0	210.0	166.0	174.00	138.00	67.00	33.00
	COAL	CALCULATED PER 100 MG OF INITIAL MASS					
Na(TOTAL)	350.0	356.3	353.8	346.2	334.9	334.3	322.8	319.6
Na(WS)	233.0	244.4	234.9	241.0	236.6	241.5	230.9	222.9
Na(AS)	109.0	108.3	111.6	95.5	90.8	85.5	70.1	70.7
Na(AI)	8.0	3.5	7.2	9.7	7.5	7.3	21.8	26.1
Ca(TOTAL)	503.0	495.8	496.9	495.8	495.9	502.4	495.6	496.1
Ca(WS)	7.0	4.9	4.8	3.5	2.7	1.7	5.4	5.0
Ca(AS)	489.0	486.1	470.9	442.7	428.8	384.1	283.6	149.6
Ca(AI)	7.0	4.9	21.2	49.6	64.4	116.6	206.7	341.4
Mg(TOTAL)	347.0	350.0	341.8	341.7	341.7	346.7	341.6	341.8
Mg(WS)	3.0	2.8	2.7	2.1	2.0	1.7	5.4	3.6
Mg(AS)	339.0	347.2	330.5	300.3	294.9	269.9	181.9	80.7
Mg(AI)	5.0	.0	8.6	39.2	44.7	75.1	154.4	257.5
Cl	219.0	196.5	190.8	147.9	132.2	130.4	97.7	88.6
SO_4 (WS)	.0	73.6	71.9	57.6	59.0	47.8	22.5	11.8
		PERCENT LOSS OF INORGANICS					
Na	.0	-1.8	-1.1	1.1	4.3	4.5	7.8	8.7
Ca	.0	1.4	1.2	1.4	1.4	.1	1.5	1.4
Mg	.0	-.9	1.5	1.5	1.5	.1	1.6	1.5
Cl	.0	10.3	12.9	32.5	39.6	40.4	55.4	59.6

CARBONISATION TEST, T=830 C, D = 7.5 mm

		PRODUCT PARTICLES						
MAS		301.00	281.00	293.00	302.00	310.00	305.00	292.00
WT LOSS		29.60	44.80	57.00	61.90	68.70	78.40	78.60
TIME,sec		10.0	20.0	30.0	40.00	60.00	90.00	120.00
Na(TOTAL)		1092.0	980.0	976.0	990.0	1021.0	945.0	859.0
Na(WS)		726.0	652.0	662.0	686.00	690.00	688.00	634.00
Na(AS)		354.0	310.0	302.0	282.00	307.00	205.00	147.00
Na(AI)		12.0	18.0	12.0	22.00	24.00	52.00	78.00
Ca(TOTAL)		1493.0	1393.0	1452.0	1501.0	1542.0	1513.0	1447.0
Ca(WS)		15.0	11.0	6.0	5.00	5.00	17.00	8.00
Ca(AS)		1415.0	1305.0	1225.0	1125.00	1145.00	387.00	42.00
Ca(AI)		63.0	77.0	221.0	371.00	392.00	1109.00	1397.00
Mg(TOTAL)		1029.0	960.0	1000.0	1036.0	1059.0	1043.0	998.0
Mg(WS)		12.0	8.0	6.0	5.00	5.00	20.00	6.00
Mg(AS)		990.0	915.0	885.0	795.00	770.00	219.00	21.00
Mg(AI)		27.0	37.0	109.0	236.00	284.00	804.00	971.00
Cl		617.0	497.0	458.0	414.00	369.00	249.00	212.00
SO_4 (WS)		294.0	192.0	198.0	154.00	116.00	143.00	87.00
	COAL	CALCULATED PER 100 mg OF INITIAL MASS						
Na(TOTAL)	350.0	362.8	348.8	333.1	327.8	329.4	309.8	294.2
Na(WS)	233.0	241.2	232.0	225.9	227.2	222.6	225.6	217.1
Na(AS)	109.0	117.6	110.3	103.1	93.4	99.0	67.2	50.3
Na(AI)	8.0	4.0	6.4	4.1	7.3	7.7	17.0	26.7
Ca(TOTAL)	503.0	496.0	495.7	495.6	497.0	497.4	496.1	495.5
Ca(WS)	7.0	5.0	3.9	2.0	1.7	1.6	5.6	2.7
Ca(AS)	489.0	470.1	464.4	418.1	372.5	369.4	126.9	14.4
Ca(AI)	7.0	20.9	27.4	75.4	122.8	126.5	363.6	478.4
Mg(TOTAL)	347.0	341.9	341.6	341.3	343.0	341.6	342.0	341.8
Mg(WS)	3.0	4.0	2.8	2.0	1.7	1.6	6.6	2.1
Mg(AS)	339.0	328.9	325.6	302.0	263.2	248.4	71.8	7.2
Mg(AI)	5.0	9.0	13.2	37.2	78.1	91.6	263.6	332.5
Cl	219.0	205.0	176.9	156.3	137.1	119.0	81.6	72.6
SO_4 (WS)	.0	97.7	68.3	67.6	51.0	37.4	46.9	29.8
		PERCENT LOSS OF INORGANICS						
Na	.0	-3.7	.4	4.8	6.3	5.9	11.5	15.9
Ca	.0	1.4	1.4	1.5	1.2	1.1	1.4	1.5
Mg	.0	1.5	1.5	1.6	1.1	1.6	1.5	1.5
Cl	.0	6.4	19.2	28.6	37.4	45.6	62.7	66.8

Appendix C

CHEMICAL ANALYSIS OF SOLID PRODUCTS FLUID BED COMBUSTION EXPERIMENTS

In this appendix, the results of the analyses of coal, bed material and cyclone ash are presented. The analyses comprises of the following:

- chemical analysis of inorganic constituents (AS 1038. 14.1 - 1981). These analyses are recalculated on a silica-free basis;
- moisture and ash analysis of coal (AS 2434.1 - 1981 and AS 1038.3 - 1979 respectively);
- chemical analysis of the inorganic matter using extraction method (Subsection 3.5.1). For coal, the results are presented as a percentage of dry coal. For bed material, the results are given as a percentage of total inorganic matter (where the total inorganic matter is calculated as oxides);
- size analysis of bed material.

RUN 1, LOCHIEL COAL (HIGH MINERAL), 850 C

SAMPLE No	HOUR	Fe_2O_3	Al_2O_3	SiO_2	MgO	CaO	K_2O	Na_2O	SO_3	TiO_2	Cl
TR4.C	.00	3.00	18.15	34.00	9.01	8.27	.42	9.22	15.85	.90	
TR12.C	3.00	2.95	17.26	31.00	9.42	8.92	.40	9.80	18.13	.88	
TR14.C	9.00	3.84	17.44	35.40	8.46	7.95	.48	9.02	14.99	.97	
TR15.C	12.00	1.84	16.90	26.70	9.45	8.96	.35	11.70	21.31	.81	
TR17.C	18.00	1.92	16.13	29.25	9.08	8.63	.39	11.30	20.99	.75	
TR18.C	21.00	2.06	17.20	29.25	9.13	8.80	.48	10.78	20.00	.71	
AVERAGE		2.60	17.18	30.93	9.09	8.59		10.30	18.55		
Si free basis											
TR4.C	.00	4.63	28.00		13.90	12.76		14.22	24.45		
TR12.C	3.00	4.36	25.48		13.91	13.17		14.47	26.77		
TR14.C	9.00	6.08	27.62		13.40	12.59		14.28	23.74		
TR15.C	12.00	2.58	23.70		13.25	12.56		16.40	29.88		
TR17.C	18.00	2.77	23.31		13.12	12.47		16.33	30.34		
TR17.C	18.00	2.98	24.87		13.20	12.72		15.59	28.92		
AVERAGE		3.90	25.50		13.46	12.71		15.22	27.35		
		BED MATERIAL									
TR1.1	3.00	.62	1.79	94.00	.40	.42	.10	.81	.87	.15	.04
TR4.1A	6.00	.68	3.19	75.05	2.74	2.27	.15	5.51	9.29	.16	.04
TR4.1L	6.00	1.62	3.48	72.70	2.81	2.34	.17	5.91	9.10	.18	.02
TR4.1L	6.00	1.34	3.78	73.10	2.78	2.33	.21	5.59	8.67	.14	.02
TR4.1S	6.00	2.33	4.83	70.98	3.40	3.02	.17	5.74	8.63	.21	.02
TR12.1	3.00	.66	2.12	84.70	1.58	1.48	.13	3.32	5.77	.15	
TR13.1	6.00	.76	3.14	76.50	2.52	2.16	.17	5.12	8.70	.22	
TR14.1	9.00	1.38	3.62	72.80	3.11	2.54	.20	6.20	11.03	.24	
TR15.1	12.00	1.10	4.79	63.55	4.05	3.28	.26	8.10	12.77	.27	
TR16.1	15.00	1.88	6.10	58.35	4.88	3.80	.24	9.05	14.69	.35	
TR17.1	18.00	1.60	5.92	54.45	5.66	4.31	.25	10.20	17.08	.28	
TR18.1	21.00	2.48	6.83	49.00	6.00	4.62	.28	10.65	18.20	.35	
Si free basis											
TR12.1	3.00	4.34	13.94		10.39	9.73		21.83	37.94		
TR13.1	6.00	3.33	13.78		11.06	9.48		22.47	38.17		
TR14.1	9.00	4.87	12.78		10.98	8.97		21.89	38.95		
TR15.1	12.00	3.18	13.84		11.70	9.47		23.40	36.89		
TR16.1	15.00	4.59	14.88		11.91	9.27		22.08	35.84		
TR17.1	18.00	3.53	13.07		12.49	9.51		22.52	37.70		
TR18.1	21.00	5.02	13.82		12.14	9.35		21.55	36.83		
AVERAGE		4.12	13.73		11.52	9.40		22.25	37.47		

RUN 1, LOCHIEL COAL (HIGH MINERAL), 850 C (Cont.)

SAMPLE No	HOUR	Fe_2O_3	Al_2O_3	SiO_2	MgO	CaO	K_2O	Na_2O	SO_3	TiO_2	Cl
		CYCLONE ASH									
TR1.2	3.00	3.58	19.55	42.90	9.73	9.73	.19	8.87	2.59	.80	
TR12.2	3.00	2.73	21.88	42.90	10.11	9.42	.25	8.22	3.07	.95	.11
TR13.2	6.00	2.63	23.35	37.10	11.40	10.72	.25	8.90	3.44	.91	.13
TR14.2	9.00	2.82	23.45	36.10	11.50	10.97	.25	9.18	3.86	.88	.13
TR15.2	12.00	2.65	22.17	33.20	12.32	12.01	.24	9.65	4.71	.86	.08
TR16.2	15.00	2.72	23.28	30.90	13.41	13.06	.21	9.60	4.47	.77	.08
TR17.2	18.00	2.51	22.26	35.75	11.98	11.66	.22	9.45	4.29	.76	.08
TR18.2	21.00	2.90	23.71	33.10	12.86	12.88	.22	9.97	2.75	.82	.05
AVERAGE		2.71	22.87	35.58	11.94	11.53		9.28	3.80		
Si free basis											
TR12.2	3.00	4.82	38.64		17.85	16.63		14.52	5.42		
TR13.2	6.00	4.27	37.91		18.51	17.40		14.45	5.58		
TR14.2	9.00	4.48	37.28		18.28	17.44		14.59	6.14		
TR15.2	12.00	4.10	34.31		19.07	18.59		14.94	7.29		
TR16.2	15.00	4.03	34.48		19.86	19.34		14.22	6.62		
TR17.2	18.00	3.98	35.26		18.98	18.47		14.97	6.80		
TR18.2	21.00	4.38	35.84		19.44	19.47		15.07	4.16		
AVERAGE		4.29	36.24		18.85	18.19		14.68	6.00		

PROXIMATE ANALYSIS OF COAL

		H2O	Ash(db)	Vol.(db)	F.C.(db)
TR4.C	3.00	15.20	13.88		
TR12.C	3.00	17.21	12.98		
TR14.C	9.00	17.62	13.98		
TR15.C	12.00				
TR17.C	18.00				
TR18.C	21.00	17.17	13.66	46.37	39.97

RUN 1, LOCHIEL COAL (HIGH MINERAL), 850 C (Cont.)

COAL ANALYSES (EXTRACTION METHOD), % db

TR4.C		Fe	Al	SiO_2	Mg	Ca	K	Na	SO_3	Cl
	WS	<.01	<.01	.03	.01	.02	.01	.79	0	.47
	AS	.24	.61	.36	.69	.74	.01	.25	0	0
	AI	.08	.90	4.23	.01	<.01	<.01	<.01	3.20	0

BED MATERIAL ANALYSES (EXTRACTION METHOD), %

TR18.1		Fe	Al	SiO_2	Mg	Ca	K	Na	SO_3	Cl
	WS	<.01	<.01	.03	.05	2	.17	7.57	17.80	
	AS	.84	1.51	1.86	2.58	.98	.05	.49	.30	
	AI	.99	2.06	46.27	1.04	.20	.02	.15	0	

BED MATERIAL SIZE DISTRIBUTION

		>1.4	1.18-1.4	1.18-1.0	1.0-.85	.85-.71	MEAN DIA.
SAND	0 hr	0	0	0	100	0	.93
TR12	3 hr	0	0	55	45	0	1.02
TR13	6 hr	4	9	58	28	0	1.07
TR14	9 hr	11	15	55	17	0	1.12
TR15	12 hr	27	28	37	8	0	1.24
TR16	15 hr	37	35	23	5	0	1.30
TR17	18 hr	46	37	14	3	0	1.35
TR18	21 hr	58	34	7	1	0	1.39

RUN 2: LOCHIEL COAL (LOW MINERAL), 850 C

SAMPLE No	HR	Fe_2O_3	Al_2O_3	SiO_2	MgO	CaO	K_2O	Na_2O	SO_3	TiO_2	Cl
TR29.C	3.00	4.26	7.93	4.04	13.80	16.95	.25	11.53	38.55	.10	
Si free basis											
TR29.C		4.55	8.50		14.78	18.15		12.34	41.28		
		BED MATERIAL									
TR29.1	3.00	.79	1.73	75.60	3.42	3.83	.04	3.44	10.04	.10	
TR30.1	3.50	1.01	1.97	73.85	3.88	4.32	.05	3.92	11.07	.13	.02
Si free basis											
TR29.1	3.00	3.38	7.40		14.62	16.37		14.71	42.92		
TR30.1	3.50	3.83	7.48		14.72	16.39		14.88	42.01		
AVERAGE		3.61	7.44		14.67	16.38		14.79	42.47		
		CYCLONE ASH									
TR29.2	3.00	4.00	14.69	15.25	20.84	23.71	.18	5.82	12.77	.36	.92
TR30.2	3.50	5.05	12.98	11.25	20.54	25.05	.18	5.84	17.01	.35	.88
AVERAGE		4.53	13.84	13.25	20.69	24.38		5.83	14.89		
Si free basis											
TR29.2	3.00	4.86	17.83		25.30	28.78		7.07	15.50		
TR30.2	3.50	5.80	14.92		23.61	28.79		6.71	19.55		
AVERAGE		5.33	16.38		24.45	28.79		6.89	17.53		

PROXIMATE ANALYSIS OF COAL

		H2O	Ash(db)	vol.(db)	F.C.(db)
BULK	.00	63.05	9.16	48.27	
TR29.C	3.00	25.56	10.13	48.66	

COAL ANALYSES (EXTRACTION METHOD), % db

		Fe	Al	SiO_2	Mg	Ca	K	Na	SO_3	Cl
BULK										
	WS	<.01	<.01	<.01	.03	.04	.01	.58	0	.89
	AS	.02	.33	<.01	.80	1.10	.01	.34	0	0
	AI	.08	.04	.20	.01	<.01	<.01	<.01	3.40	0

BED MATERIAL ANALYSES (EXTRACTION METHOD), %

		Fe	Al	SiO_2	Mg	Ca	K	Na	SO_3	Cl
TR30.1										
	WS	<.01	<.01	<.05	.02	.77	.04	3.14	7.22	
	AS	.52	.25	.33	1.91	2.27	0	.07	4.04	
	AI	.13	.78	71.70	.37	.04	<.01	.01	0	

RUN 2: LOCHIEL COAL (LOW MINERAL), 850 C (Cont'd.)

		BED MATERIAL SIZE DISTRIBUTION (SIZE IN mm)					
		>1.4	1.18-1.4	1.18-1.0	1.0-.85	.85-.71	MEAN DIA.
SAND	0 hr	0	0	0	100	0	.93
TR29	3 hr	1	3	77	19	0	1.07

RUN 3: LOCHIEL COAL (LOW MINERAL), 800 C

SAMPLE No	HR	Fe_2O_3	Al_2O_3	SiO_2	MgO	CaO	K_2O	Na_2O	SO_3	TiO_2	Cl
TR32.C	6.00	2.98	8.25	4.66	14.67	17.56	.33	10.49	38.02	.10	
Si free basis											
TR32.C	6.00	3.23	8.93		15.88	19.00		11.35	41.15		
		BED MATERIAL ANALYSES									
TR31.1	3.00	.71	1.41	75.30	2.86	3.42	.45	4.03	10.77	.10	
TR32.1	6.00	1.38	2.43	59.85	4.77	5.63	.16	7.11	17.63	.10	
TR33.1	9.00	1.63	2.91	48.90	5.95	6.97	.10	9.11	22.62	.12	.02
Si free basis											
TR31.1	3.00	3.04	6.04		12.25	14.65		17.26	46.12		
TR32.1	6.00	3.51	6.19		12.15	14.34		18.11	44.89		
TR33.1	9.00	3.30	5.89		12.04	14.11		18.44	45.78		
AVERAGE		3.28	6.04		12.15	14.36		17.93	45.60		
		CYCLONE ASH ANALYSES									
TR31.2	3.00	5.38	13.57	10.90	21.98	26.31	.15	4.58	14.41	.33	.88
TR32.2	6.00	4.32	13.49	8.30	22.93	28.16	.15	4.45	15.47	.38	.86
TR33.2	9.00	4.48	13.35	8.90	22.00	27.67	.15	4.55	16.00	.42	.92
AVERAGE		4.73	13.47	9.37	22.30	27.38		4.53	15.29		
Si free basis											
TR31.2	3.00	6.20	15.65		25.35	30.34		5.28	16.62		
TR32.2	6.00	4.83	15.10		25.66	31.52		4.98	17.31		
TR33.2	9.00	5.06	15.06		24.83	31.22		5.13	18.05		
AVERAGE		5.36	15.27		25.28	31.03		5.13	17.33		

PROXIMATE ANALYSIS OF COAL

		H2O	Ash(db)	Vol.(db)	F.C(db)
TR32.C	6.00	17.11	10.03	49.22	40.75

COAL ANALYSES (EXTRACTION METHOD), %db

BULK		Fe	Al	SiO_2	Mg	Ca	K	Na	SO_3	Cl
	WS	<.01	<.01	<.01	.03	.04	.01	.58	0	.57
	AS	.02	.33	<.01	.80	1.10	.01	.34	0	0
	AI	.08	.04	.20	.01	<.01	<.01	<.01	3.40	0

RUN 3: LOCHIEL COAL (LOW MINERAL), 800 C (Cont'd.)

BED MATERIAL ANALYSES (EXTRACTION METHOD), %

TR33.1		Fe	Al	SiO_2	Mg	Ca	K	Na
	WS	<.01	<.01	.06	.04	1.01	.09	6.98
	AS	.86	.36	.22	3.02	3.91	0	.10
	AI	.58	1.11	48.46	.52	.04	<.01	.01

BED MATERIAL SIZE DISTRIBUTION (mm)

		>1.4	1.18-1.4	1.18-1.0	1.0-.85	.85-.71	MEAN DIA.
SAND	0 hr	0	0	0	100	0	.93
TR31	3 hr	1	7	76	17	0	1.09
TR32	6 hr	8	60	31	1	0	1.24
TR33	9 hr	19	75	5	1	0	1.32

RUN 4, LOCHIEL COAL (LOW MINERAL, WATER LEACHED), 800 C

SAMPLE No	HR	Fe_2O_3	Al_2O_3	SiO_2	MgO	CaO	K_2O	Na_2O	SO_3	TiO_2	Cl
TR48.C	3.00	3.56	8.38	4.13	16.30	19.58	.19	5.19	41.37	.48	
TR50.C	9.00	2.57	8.05	4.43	16.64	19.88	.20	5.31	41.08	.45	
AVERAGE		3.07	8.22	4.28	16.47	19.73	.20	5.25	41.23	.47	
Si free basis											
TR51.C	3.00	3.75	8.82		17.15	20.60		5.46	43.52		
TR53.C	6.00	2.73	8.57		17.71	21.16		5.65	43.72		
AVERAGE		3.24	8.69		17.43	20.88		5.56	43.62		
		BED MATERIAL ANALYSES									
TR48.1	3.00	.42	1.19	84.45	1.92	2.53	.04	1.77	5.85	.15	
TR49.1	6.00	.72	1.58	73.25	3.05	4.26	.06	2.74	12.16	.16	
TR50.1	9.00	.67	1.88	71.20	3.23	5.03	.10	3.24	12.04	.18	
Si free basis											
TR48.1	3.00	3.02	8.55		13.79	18.18		12.72	42.03		
TR49.1	6.00	2.91	6.38		12.31	17.20		11.06	49.09		
TR50.1	9.00	2.53	7.10		12.20	19.00		12.24	45.47		
AVERAGE		2.82	7.34		12.77	18.12		12.00	45.53		
		CYCLONE ASH ANALYSES									
TR48.2	3.00	4.10	11.07	11.45	22.77	27.10	.14	3.87	15.63	.96	.38
TR49.2	6.00	3.50	11.46	8.65	23.35	27.24	.15	4.41	18.28	.83	.20
TR50.2	9.00	3.43	10.83	7.35	22.37	25.40	.18	5.23	21.60	.77	.10
AVERAGE		3.68	11.12	9.15	22.83	26.58	.16	4.50	18.50	.85	.23
Si free basis											
TR48.2	3.00	4.77	12.87		26.47	31.50		4.50	18.17		
TR49.2	6.00	3.91	12.82		26.11	30.46		4.93	20.44		
TR50.2	9.00	3.81	12.05		24.88	28.25		5.82	24.02		
AVERAGE		4.17	12.58		25.82	30.07		5.08	20.88		

COAL PROXIMATE ANALYSIS

		H2O	Ash(db)	Vol.(db)	F.C.(db)
TR48.C	3.00	17.83	8.07		
TR50.C	9.00	17.45	7.93		

RUN 4, LOCHIEL COAL (LOW MINERAL, WATER LEACHED), 800 C (Cont'd.)

COAL ANALYSES (EXTRACTION METHOD), %db

TR48.C		Fe	Al	SiO_2	Mg	Ca	K	Na	SO_3	Cl
	WS	<.01	<.01	<.01	<.01	<.01	<.01	.16	0	.34
	AS	.04	.29	<.01	.78	1.12	<.01	.18	0	0
	AI	.21	.06	.36	<.01	.01	<.01	<.01	3.50	0

BED MATERIAL ANALYSES (EXTRACTION METHOD), %

TR50.1		Fe	Al	SiO_2	Mg	Ca	K	Na	SO_3	Cl
	WS	<.01	.03	.08	.13	1.53	.07	2.30	7.58	
	AS	.18	.15	.22	1.53	2.20	<.01	.04	4.46	
	AI	.31	.79	71.85	.38	.04	<.01	.01	0	

BED MATERIAL SIZE DISTRIBUTION

		>1.4	1.18-1.4	1.18-1.0	1.0-.85	.85-.71	MEAN DIA.
SAND	0 hr	0	0	0	100	0	.93
TR48	3 hr	0	1	63	36	0	1.03
TR49	6 hr	0	5	86	9	0	1.09
TR50	9 hr	0	16	79	5	0	1.11

RUN 5, LOCHIEL COAL (LOW MINERAL, ACID LEACHED), 800 C

SAMPLE No	HR	Fe_2O_3	Al_2O_3	SiO_2	MgO	CaO	K_2O	Na_2O	SO_3	TiO_2	Cl
TR51.C	3.00	2.75	9.26	4.30	16.95	21.52	.13	3.11	41.66	.36	
TR53.C	9.00	3.09	9.11	5.15	16.55	21.05	.15	3.06	41.02	.47	
AVERAGE		2.92	9.19	4.73	16.75	21.29	.14	3.09	41.34	.42	
Si free basis											
TR51.C	3.00	2.87	9.67		17.70	22.48		3.25	43.51		
TR53.C	6.00	3.27	9.64		17.51	22.28		3.24	43.41		
AVERAGE		3.07	9.66		17.61	22.38		3.24	43.46		
		BED MATERIAL ANALYSES									
TR51.1	3.00	.41	.81	88.50	1.38	1.83	.03	1.01	4.10	.15	
TR52.1	6.00	.70	1.26	81.60	2.20	3.18	.05	1.48	7.13	.16	
TR53.1	9.00	.75	1.76	77.00	2.76	4.21	.06	1.91	9.16	.18	
Si free basis											
TR51.1	3.00	4.20	8.29		14.12	18.73		10.34	41.97		
TR52.1	6.00	4.32	7.78		13.58	19.63		9.14	44.01		
TR53.1	9.00	3.67	8.61		13.51	20.61		9.35	44.84		
AVERAGE		4.06	8.23		13.74	19.66		9.61	43.60		
		CYCLONE ASH ANALYSES									
TR51.2	3.00	3.96	11.94	10.65	23.50	29.40	.11	2.33	14.87	1.04	.09
TR52.2	6.00	3.63	12.25	10.05	24.12	30.37	.11	2.17	15.07	1.07	.07
TR53.2	9.00	4.23	11.80	10.00	23.02	29.17	.13	2.66	15.97	1.03	.06
AVERAGE		3.94	12.00	10.23	23.55	29.65	.12	2.39	15.30	1.05	.07
Si free basis											
TR51.2	3.00	4.55	13.72		27.00	33.78		2.68	17.08		
TR52.2	6.00	4.09	13.79		27.14	34.18		2.44	16.96		
TR53.2	9.00	4.80	13.40		26.14	33.13		3.02	18.14		
AVERAGE		4.48	13.63		26.76	33.69		2.71	17.39		

		COAL PROXIMATE ANALYSIS			
		H2O	Ash(db)	Vol.(db)	F.C.(db)
TR51.C	3.00	19.77	7.46		
TR53.C	9.00	19.68	7.72		

RUN 5, LOCHIEL COAL (LOW MINERAL, ACID LEACHED), 800 C (Cont'd.)

COAL ANALYSES (EXTRACTION METHOD), %db

TR51.C	Fe	Al	SiO_2	Mg	Ca	K	Na	SO_3	Cl
WS	<.01	<.01	<.01	<.01	<.01	<.01	.12	0	.01
AS	.04	.29	.01	.80	1.12	<.01	.06	0	0
AI	.09	.06	.33	<.01	.01	<.01	<.01	3.60	0

BED MATERIAL ANALYSES (EXTRACTION METHOD), %

TR53.1	Fe	Al	SiO_2	Mg	Ca	K	Na	SO_3	Cl
WS	<.01	<.01	.13	.13	1.68	.05	1.41	6.29	
AS	.23	.16	.27	1.26	1.48	<.01	.03	2.87	
AI	.42	.72	77.50	.34	.02	<.01	<.01	0	

BED MATERIAL SIZE DISTRIBUTION (mm)

		>1.4	1.18-1.4	1.18-1.0	1.0-.85	.85-.71	MEAN DIA.
SAND	0 hr	0	0	0	100	0	.93
TR51	3 hr	0	0	26	74	0	.97
TR52	6 hr	0	2	65	33	0	1.04
TR53	9 hr	0	4	76	20	0	1.07

RUN 6, LOCHIEL COAL (LOW MINERAL, NaCl ADDED, BATCH 1), T=800 C

SAMPLE No	HR	Fe_2O_3	Al_2O_3	SiO_2	MgO	CaO	K_2O	Na_2O	SO_3	TiO_2	Cl
TR45.C	3.00	3.02	7.44	3.98	12.80	16.38	.14	14.32	35.35	.35	4.30
TR46.C	6.00	2.60	7.92	5.26	13.22	16.60	.13	14.04	35.32	.79	4.41
AVERAGE		2.81	7.68	4.62	13.01	16.49	.14	14.18	35.34	.57	
Si free basis											
TR45.C	3.00	3.21	7.90		13.60	17.40		15.21	37.55		
TR46.C	6.00	2.74	8.33		13.91	17.47		14.77	37.17		
AVERAGE		2.97	8.12		13.75	17.43		14.99	37.36		
		BED MATERIAL ANALYSES									
TR45.1	3.00	.64	2.05	70.50	3.36	4.20	.04	4.94	12.04	.15	
TR46.1	6.00	.96	2.66	56.10	5.01	6.33	.04	7.97	19.40	.16	
TR47.1	9.00	1.57	3.77	39.95	7.31	8.40	.06	11.30	24.69	.18	
Si free basis											
TR45.1	3.00	2.33	7.45		12.22	15.27		17.96	43.78		
TR46.1	6.00	2.26	6.25		11.77	14.87		18.72	45.57		
TR47.1	9.00	2.74	6.58		12.76	14.66		19.72	43.09		
AVERAGE		2.44	6.76		12.25	14.93		18.80	44.15		
		CYCLONE ASH ANALYSES									
TR45.2	3.00	4.39	12.15	11.75	20.97	26.30	.16	5.39	15.05	.94	1.92
TR46.2	6.00	4.08	12.48	10.85	21.16	26.80	.13	5.67	14.23	.86	1.95
TR47.2	9.00	4.16	11.07	11.15	18.68	24.08	.19	7.29	18.97	.63	1.98
AVERAGE		4.21	11.90	11.25	20.27	25.73	.16	6.12	16.08	.81	1.95
Si free basis											
TR45.2	3.00	5.03	13.93		24.04	30.15		6.18	17.25		
TR46.2	6.00	4.67	14.29		24.23	30.68		6.49	16.29		
TR47.2	9.00	4.78	12.72		21.46	27.66		8.37	21.79		
AVERAGE		4.83	13.64		23.24	29.50		7.02	18.45		

		COAL PROXIMATE ANALYSIS			
		H2O	Ash(db)	Vol.(db)	F.C.(db)
TR45.C	3.00	21.91	9.45		
TR53.C	6.00	20.11	9.31		

RUN 6, LOCHIEL COAL (LOW MINERAL, NaCl ADDED, BATCH 1), T=800 C (Cont'd.)

COAL ANALYSES (EXTRACTION METHOD),%db

TR45.C		Fe	Al	SiO_2	Mg	Ca	K	Na	SO_3	Cl
	WS	<.01	<.01	<.01	.01	.01	<.01	.80	0	.87
	AS	.04	.29	.01	.67	1.03	<.01	.40	0	0
	AI	.16	.06	.36	<.01	<.01	<.01	<.01	-	0

BED MATERIAL ANALYSES (EXTRACTION METHOD),%

TR47.1		Fe	Al	SiO_2	Mg	Ca	K	Na	SO_3	Cl
	WS	<.01	.03	.08	.02	2.19	.06	7.96	17.91	o.5
	AS	.48	.32	.49	3.43	3.69	<.01	.06	6.78	0
	AI	.43	1.51	41.90	.72	.09	<.01	.02	0	0

BED MATERIAL SIZE DISTRIBUTION (mm)

		>1.4	1.18-1.4	1.18-1.0	1.0-.85	.85-.71	MEAN DIA.
SAND	0 hr	0	0	0	100	0	.93
TR45	3 hr	.40	5	73	22	0	1.07
TR46	6 hr	9.50	64	26	.50	0	1.26
TR47	9 hr	23	61	15	0	0	1.30

RUN 7, LOCHIEL COAL (LOW MINERAL NaCl ADDED, BATCH 2), 800 C

SAMPLE No	HR	Fe_2O_3	Al_2O_3	SiO_2	MgO	CaO	K_2O	Na_2O	SO_3	TiO_2	Cl
TR60.C	.50	3.38	7.71	4.32	12.25	15.61	.10	15.88	32.36	.30	7.51
Si free basis											
TR60.C	.50	3.55	8.11		12.88	16.41		16.70	34.03		
		BED MATERIAL ANALYSES									
TR59.1	.50	.41	1.47	85.30	2.22	2.39	.05	2.27	4.44	.15	
TR60.1	.50	.42	1.16	84.35	1.68	2.11	.06	2.56	5.68	.16	
TR68.1	.50	.67	3.52	61.50	5.75	6.58	.04	5.62	12.10	.18	2.05
Si free basis											
TR59.1	.50	3.05	10.93		16.51	17.77		16.88	33.01		
TR60.1	.50	3.03	8.36		12.11	15.21		18.46	40.95		
TR68.1	.50	1.83	9.64		15.74	18.01		15.38	33.12		
AVERAGE		2.64	9.64		14.79	17.00		16.91	35.70		
		CYCLONE ASH ANALYSES									
TR60.2	.50	5.93	10.39	15.55	15.40	20.36	.19	8.61	19.06	.70	1.67
TR68.2	.50	6.64	7.62	13.05	11.63	17.46	.16	13.69	24.24	.93	2.26
AVERAGE		6.29	9.01	14.30	13.52	18.91	.18	11.15	21.65	.82	1.97
Si free basis											
TR60.2	.50	7.20	12.62		18.71	24.74		10.46	23.16		
TR68.2	.50	7.85	9.00		13.74	20.63		16.18	28.64		
AVERAGE		7.53	10.81		16.23	22.68		13.32	25.90		

COAL PROXIMATE ANALYSIS

		H2O	Ash(db)	Vol.(db)
TR60.C	.50	20.88	10.40	

COAL ANALYSES (EXTRACTION METHOD), % db

TR60.C	Fe	Al	SiO_2	Mg	Ca	K	Na	SO_3	Cl
WS	<.01	<.01	<.01	.01	.01	<.01	1.09	0	1.09
AS	.06	.31	.01	.69	1.08	.01	.43	0	0
AI	.17	.08	.43	<.01	.02	<.01	<.01	-	0

RUN 7, LOCHIEL COAL (LOW MINERAL NaCl ADDED, BATCH 2), 800½C

TR68.1

BED MATERIAL ANALYSES (EXTRACTION METHOD),%

	Fe	Al	SiO_2	Mg	Ca	K	Na	SO_3	Cl
WS	<.01	.66	.02	.01	1.96	.05	4.14	7.86	2.05
AS	.38	1.03	1.14	3.28	2.78	<.01	.12	4.24	0
AI	.11	.11	60.60	.07	.06	<.01	.01	0	0

BED MATERIAL SIZE DISTRIBUTION (COULD NOT BE DETERMINED)

RUN 8, LOCHIEL COAL (MINERAL FREE), 750½C (Cont'd.)

COAL PROXIMATE ANALYSIS

		H2O	Ash(db)	Vol.(db)	F.C.(db)
TR34.C	3.00	36.41	10.08	49.45	40.47
TR36.C	9.00	37.89	9.69	47.83	42.48

COAL ANALYSES (EXTRACTION METHOD),%db

	Fe	Al	SiO_2	Mg	Ca	K	Na
WS	<.01	<.01	<.01	.03	.04	.01	.58
AS	.02	.33	<.01	.80	1.10	.01	.34
AI	.08	.04	.20	.01	<.01	<.01	<.01

BED MATERIAL (EXTRACTION METHOD),%

	Fe	Al	SiO_2	Mg	Ca	K	Na
WS	<.01	<.01	<.05	.02	.95	.12	7.70
AS	.65	.55	.23	2.95	3.43	.01	.08
AI	.57	.81	47.69	.36	.42	<.01	.01

BED MATERIAL SIZE DISTRIBUTION (mm)

		>1.4	1.18-1.4	1.18-1.0	1.0-.85	.85-.71	MEAN DIA.
SAND	0 hr	0	0	0	100	0	.93
TR34	3 hr	0	1	55	44	0	1.02
TR35	6 hr	0	19	72	9	0	1.11
TR36	9 hr	0	60	39	1	0	1.21
TR37	12 hr	1	92	7	0	0	1.28

RUN 8, LOCHIEL COAL (MINERAL FREE), 750 C

SAMPLE No	HR	Fe_2O_3	Al_2O_3	SiO_2	MgO	CaO	K_2O	Na_2O	SO_3	TiO_2	Cl
TR34.C	3.00	2.45	8.51	4.40	13.45	17.02	.35	11.89	38.96	.10	
TR36.C	9.00	4.02	7.56	3.70	13.70	17.06	.34	11.92	38.97	.10	
AVERAGE		3.24	8.04	4.05	13.58	17.04		11.91	38.97		
Si free basis											
TR34.C	3.00	2.64	9.18		14.50	18.35		12.82	42.01		
TR36.C	9.00	4.29	8.07		14.63	18.21		12.73	41.60		
AVERAGE		3.47	3.47		3.47	3.47		3.47	3.47		
		BED MATERIAL ANALYSES									
TR34.1	3.00	.39	1.16	81.03	2.01	2.60	.03	3.38	7.88	.22	
TR35.1	6.00	1.18	1.88	68.10	3.36	4.28	.13	6.06	13.83	.10	
TR36.1	9.00	1.49	2.30	56.47	4.48	5.82	.09	8.56	18.82	.15	
TR37.1	12.00	1.79	2.75	47.23	5.47	6.91	.12	10.72	23.17	.14	.03
Si free basis											
TR34.1	3.00	2.21	6.56		11.38	14.71		19.13	44.60		
TR35.1	6.00	3.83	6.10		10.90	13.89		19.66	44.87		
TR36.1	9.00	3.57	5.51		10.74	13.95		20.52	45.12		
TR37.1	12.00	3.50	5.38		10.71	13.53		20.99	45.37		
AVERAGE		3.28	5.89		10.93	14.02		20.08	44.99		
		CYCLONE ASH ANALYSES									
TR34.2	3.00	5.26	12.81	8.50	21.72	26.20	.20	5.25	16.93	.46	1.00
TR35.2	6.00	5.38	13.50	7.50	22.75	26.51	.15	4.76	16.47	.34	1.00
TR36.2	9.00	4.95	13.95	7.12	23.02	26.81	.14	4.58	16.64	.27	1.12
TR37.2	12.00	5.58	13.91	7.12	23.04	26.64	.15	4.78	16.30	.29	1.03
AVERAGE		5.29	13.54	7.56	22.63	26.54		4.84	16.59		
Si free basis											
TR34.2	3.00	5.92	14.42		24.45	29.49		5.91	19.06		
TR35.2	6.00	5.99	15.02		25.32	29.50		5.30	18.33		
TR36.2	9.00	5.48	15.44		25.48	29.67		5.07	18.42		
TR37.2	12.00	6.15	15.34		25.41	29.37		5.27	17.97		
AVERAGE		5.88	15.06		25.16	29.51		5.39	18.44		

RUN 9, LOCHIEL COAL (LOW MINERAL), 700 C

SAMPLE No	HR	Fe2O3	Al2O3	SiO2	MgO	CaO	K2O	Na2O	SO3	TiO2	Cl
TR39.C	6.00	3.59	8.00	4.24	13.97	17.15	.28	11.82	37.89	.10	
TR41.C	12.00	9.02	7.63	3.86	13.05	15.80	.25	10.91	38.02	.10	
AVERAGE		6.31	7.82	4.05	13.51	16.48		11.37	37.96		
Si free basis											
TR39.C	6.00	3.87	8.62		15.05	18.48		12.74	40.83		
TR41.C	12.00	9.52	8.05		13.77	16.67		11.51	40.11		
AVERAGE		6.69	8.34		14.41	17.58		12.12	40.47		
		BED MATERIAL ANALYSES									
TR38.1	3.00	.48	1.07	79.17	2.14	2.71	.04	3.55	8.34	.10	
TR39.1	6.00	.72	1.87	65.90	3.79	4.62	.07	6.46	14.91	.10	
TR40.1	9.00	1.11	2.27	54.95	5.04	6.10	.11	8.81	20.29	.14	
TR41.1	12.00	1.52	2.90	45.30	5.99	7.37	.14	11.00	24.18	.10	.07
Si free basis											
TR38.1	3.00	2.52	5.61		11.23	14.22		18.63	43.76		
TR39.1	6.00	2.21	5.74		11.63	14.18		19.82	45.75		
TR40.1	9.00	2.53	5.17		11.49	13.90		20.08	46.25		
TR41.1	12.00	2.86	5.45		11.26	13.85		20.68	45.45		
AVERAGE		2.53	5.49		11.40	14.04		19.80	45.30		
		CYCLONE ASH ANALYSES									
TR38.2	3.00	6.20	12.85	6.77	21.78	25.48	.17	5.87	18.40	.27	1.24
TR39.2	6.00	4.73	13.13	5.86	22.46	26.49	.18	5.71	18.58	.29	1.34
TR40.2	9.00	6.99	12.81	8.00	21.00	24.75	.16	5.59	17.96	.29	1.30
TR41.2	12.00	4.72	12.98	6.36	22.48	26.34	.17	5.60	18.27	.35	1.21
AVERAGE		5.66	12.94	6.75	21.93	25.77		5.69	18.30		
Si free basis											
TR38.2	3.00	6.81	14.12		23.93	27.99		6.45	20.22		
TR39.2	6.00	5.19	14.40		24.64	29.06		6.26	20.38		
TR40.2	9.00	7.81	14.30		23.45	27.64		6.24	20.06		
TR41.2	12.00	5.19	14.28		24.73	28.97		6.16	20.10		
AVERAGE		6.25	14.28		24.19	28.42		6.28	20.19		

RUN 9, LOCHIEL COAL (LOW MINERAL), 700 C (Cont'd.)

COAL PROXIMATE ANALYSIS

		H2O	Ash(db)	Vol.(db)	F.C.(db)
TR39.C	6.00	36.11	9.31	49.92	40.77
TR41.C	12.00	35.21	10.19	49.27	40.54

COAL ANALYSES (EXTRACTION METHOD),%db

		Fe	Al	SiO2	Mg	Ca	K	Na	SO3	Cl
BULK										
	WS	<.01	<.01	<.01	.03	.04	.01	.58	0	.56
	AS	.02	.33	<.01	.80	1.10	.01	.34	0	0
	AI	.08	.04	.20	.01	<.01	<.01	<.01	-	0

BED MATERIAL ANALYSES (EXTRACTION METHOD),%

TR41.1									
	WS	<.01	<.01	.07	.02	.84	.12	7.93	15.64
	AS	.57	.90	.12	3.30	3.71	.01	.03	7.90
	AI	.41	.47	45.93	.19	.45	<.01	.01	0

BED MATERIAL SIZE DISTRIBUTION (mm)

		>1.4	1.18-1.4	1.18-1.0	1.0-.85	.85-.71	MEAN DIA.
SAND	0 hr	0	0	0	100	0	.93
TR38	3 hr	0	1	39	60	0	.99
TR39	6 hr	0	25	67	8	0	1.13
TR40	9 hr	0	65	34	1	0	1.22
TR41	12 hr	1	90	10	0	0	1.29

RUN 10 LOCHIEL COAL LOW MINERAL, FINER BED MATERIAL

SAMPLE No	HR	Fe_2O_3	Al_2O_3	SiO_2	MgO	CaO	K_2O	Na_2O	SO_3	TiO_2	Cl
TR41.C	12.00	9.02	7.63	3.86	13.05	15.80	.25	10.91	38.02	.10	
Si free basis											
TR41.C	12.00	9.52	8.05		13.77	16.67		11.51	40.11		
		BED MATERIAL ANALYSES									
TR42.1	3.00	.60	1.35	75.90	2.56	3.16	.05	4.24	10.13	.10	
TR43.1	6.00	1.19	2.14	59.80	4.17	5.30	.09	7.21	17.22	.10	
TR44.1	9.00	1.68	2.74	49.85	5.49	6.62	.12	9.38	22.00	.10	
Si free basis											
TR42.1	3.00	2.69	6.06		11.48	14.18		19.02	45.45		
TR43.1	6.00	3.17	5.70		11.11	14.13		19.22	45.90		
TR44.1	9.00	3.48	5.68		11.38	13.73		19.45	45.61		
AVERAGE		3.12	5.81		11.33	14.01		19.23	45.65		
		CYCLONE ANALYSES									
TR42.2	3.00	5.48	12.78	8.90	20.95	25.07	.17	5.50	17.61	.44	1.22
TR43.2	6.00	5.31	13.08	8.20	21.55	25.80	.15	5.22	16.81	.43	1.07
TR44.2	9.00	4.18	13.03	6.80	22.53	26.75	.14	4.80	17.62	.38	1.05
AVERAGE		4.99	12.96	7.97	21.68	25.87		5.17	17.35		
Si free basis											
TR42.2	3.00	6.14	14.32		23.48	28.10		6.16	19.74		
TR43.2	6.00	5.94	14.63		24.10	28.85		5.84	18.80		
TR44.2	9.00	4.62	14.40		24.90	29.56		5.31	19.47		
AVERAGE		5.57	14.45		24.16	28.84		5.77	19.34		

COAL PROXIMATE ANALYSIS

		H2O	Ash(db)	Vol.(db)	F.C.(db)
TR42.C	3.00	36.41	10.08	49.45	40.47

RUN 10 LOCHIEL COAL LOW MINERAL, FINER BED MATERIAL (Cont'd.)

COAL ANALYSES (EXTRACTION METHOD), %db

	Fe	Al	SiO_2	Mg	Ca	K	Na	SO_3	Cl
WS	<.01	<.01	<.01	.03	.04	.01	.58	0	.57
AS	.02	.33	<.01	.80	1.10	.01	.34	0	0
AI	.08	.04	.20	.01	<.01	<.01	<.01	-	0

BED MATERIAL SIZE DISTRIBUTION (mm)

		>1.4	1.18-1.4	1.18-1.0	1.0-.85	.85-.71	MEAN DIA.
SAND	0 hr	0	0	0	0	100	.78
TR42	3 hr	0	0	0	62	38	.87
TR43	6 hr	1	7	34	51	7	1.00
TR44	9 hr	3	17	60	19	1	1.10

RUN 11, LOCHIEL COAL LOW MINERAL, DOLOMITE BED

DOLOMITE ANALYSES

SAMPLE No	HR	Fe_2O_3	Al_2O_3	SiO_2	MgO	CaO	K_2O	Na_2O	SO_3	TiO_2	Cl
DOLOMITE	.00	2.00	6.67	52.50	16.30	15.67	2.33	1.06	.43	.22	.02

BED MATERIAL ANALYSES

TR55.1	3.00	6.23	4.72	34.25	13.53	13.13	1.01	5.67	18.45	.34	
TR56.1	6.00	2.36	5.93	30.95	12.65	13.25	.94	8.26	23.31	.26	
TR57.1	9.00	2.26	5.87	27.65	11.36	12.12	.76	10.37	27.88	.30	
TR58.1	12.00	2.37	5.48	20.20	12.35	13.49	.58	12.18	31.78	.20	
Si free basis											
TR55.1	3.00	9.88	7.48		21.45	20.81		8.99	29.25		
TR56.1	6.00	3.52	8.86		18.89	19.79		12.34	34.81		
TR57.1	9.00	3.19	8.28		16.02	17.09		14.62	39.31		
TR58.1	12.00	3.02	6.99		15.75	17.20		15.53	40.52		
AVERAGE		4.90	7.90		18.03	18.72		12.87	35.97		

CYCLONE ASH ANALYSES

TR55.2	3.00	3.87	11.58	11.20	21.94	26.36	.25	4.96	15.73	.79	.89
TR56.2	6.00	3.59	11.81	10.45	21.80	25.70	.24	5.20	16.27	.78	.95
TR57.2	9.00	3.60	11.78	10.25	21.71	26.34	.20	5.22	16.63	.71	.85
TR58.2	12.00	4.48	11.58	10.60	21.85	26.72	.18	5.47	16.44	.81	.70
AVERAGE		3.89	11.69	10.63	21.83	26.28	.22	5.21	16.27	.77	.85
Si free basis											
TR55.2	3.00	4.48	13.41		25.40	30.52		5.74	18.21		
TR56.2	6.00	4.15	13.65		25.20	29.70		6.01	18.80		
TR57.2	9.00	4.14	13.53		24.94	30.26		6.00	19.11		
TR58.2	12.00	5.08	13.12		24.76	30.28		6.20	18.63		
AVERAGE		4.46	13.43		25.08	30.19		5.99	18.69		

COAL PROXIMATE ANALYSIS

H2O	ASH(db)
20.20	10.10

RUN 11, LOCHIEL COAL LOW MINERAL, DOLOMITE BED (Cont'd.)

		BED MATERIAL SIZE DISTRIBUTION (mm)					
		>1.4	1.18-1.4	1.18-1.0	1.0-.85	.85-.71	MEAN DIA.
SAND	0 hr	0	0	0	100	0	.93
TR55	3 hr	0	0	52	48	0	1.01
TR56	6 hr	0	20	75	5	0	1.12
TR57	9 hr	2	70	27	1	0	1.24
TR58	9 hr	7	90	3	0	0	1.30

RUN 12, LOCHIEL COAL LOW MINERAL, 12% OXYGEN

BED MATERIAL ANALYSES

SAMPLE No	HR	Fe_2O_3	Al_2O_3	SiO_2	MgO	CaO	K_2O	Na_2O	SO_3	TiO_2	Cl
TR65.1	2.25	.59	1.59	73.00	3.27	3.85	.05	4.38	11.07	.20	
Si free basis											
TR65.1	2.25	2.36	6.36		13.08	15.40		17.52	44.28		

CYCLONE ASH ANALYSES

TR65.2	2.25	4.60	11.42	10.15	21.21	26.10	.14	4.65	16.75	.08	1.24
Si free basis											
TR66.2	3.00	5.29	13.14		24.40	30.03		5.35	19.27		

PROXIMATE ANALYSIS

H2O	ASH(db)
19.70	9.70

RUN 13, LOCHIEL COAL LOW MINERAL, 5% OXYGEN

BED MATERIAL ANALYSES

SAMPLE No	HR	Fe_2O_3	Al_2O_3	SiO_2	MgO	CaO	K_2O	Na_2O	SO_3	TiO_2	Cl
TR66.1	3.00	.21	1.61	75.40	3.47	3.86	.03	3.83	9.86	.22	
Si free basis											
TR66.1	3.00	.91	6.97		15.03	16.72		16.59	42.70		

CYCLONE ASH ANALYSES

TR66.2	3.00	5.62	9.05	9.95	15.83	19.53	.27	7.38	27.91	.52	.91
Si free basis											
TR66.2	3.00	6.46	10.40		18.19	22.44		8.48	32.07		

COAL PROXIMATE ANALYSIS

H2O	ASH(db)
21.00	9.80

BED MATERIAL ANALYSES (EXTRACTION METHOD),%

TR66.1	Fe	Al	SiO2	Mg	Ca	K	Na	SO3	Cl
WS	<.01	.13	.05	.01	1.47	.02	2.78	7.23	
AS	.10	.41	.42	1.92	1.46	<.01	.02	2.63	
AI	.06	.41	74.80	.16	.04	.02	.02		

Appendix D

CORRELATION BETWEEN COATING THICKNESS AND OPERATING TIME

The mass of the bed inventory (M) can be related to the number of bed particles (N_b), radius of particles (r) and density of particles (ρ_p):

$$M = N_b \frac{4\pi r^3}{3} \rho_p \qquad (D.1)$$

Re-arranging Equation D.1 :

$$N_b = \frac{3M}{4\pi r^3 \rho_p} \qquad (D.2)$$

Assuming the density of the coating is the same as that of the parent bed material, the mass of coating deposited on a single bed particle (m_c) can be expressed in terms of the initial radius of the bed particles (r) and coating thickness (δ):

$$m_c = \frac{4\pi}{3} \rho_p [(r+\delta)^3 - r^3] \qquad (D.3)$$

The mass of coating on a single bed particle can also be related to the rate of deposition of coating (R_d), operating time (t) and number of bed particles:

$$m_c = \frac{R_d t}{N_b} \qquad (D.4)$$

Combining Equations D.2, D.3 and D.4 and inserting the following data, the coating thickness can be expressed in terms of rate of deposition of coating and operating time:

M = 100 g

ρ_p = 2.5 g/cm^3

For r = 0.0462 cm (bed material of 0.85 to 1.0 mm size range):

$$\delta = (-2.31 + \sqrt{5.34 + 0.0711 R_d t}) x 10 \qquad (D.5)$$

For r = 0.039 cm (bed material of 0.71 to 0.85 mm size range):

$$\delta = (-1.95 + \sqrt{3.8 + 0.0507 R_d t}) x 10 \qquad (D.5)$$

where δ is given in micron, R_d in g/h and t in hour.

In deriving Equations D.5 and D.6, δ^3 term is ignored due to the relatively small values of δ

By replacing Equations D.5 and D.6 into Equations 7.30 and 7.31, one can express the rate of agglomeration and the onset of defluidisation as a function of operating time.

Calculation of the rate of agglomeration versus coating thickness

The extent of agglomeration determined, periodically, from size distribution of the bed material (Subsection 3.4.3) is given in the following table:

Table D.1: Extent of Agglomeration (percent bed material agglomerated)

Operating time h		0	3	6	9	12	15	18	21	24
Run	1	0	0	0	0	3.75	9.8	19.4	33.8	48.8
	3	0	0	3.9	17.5					
	4	0	0	0	0					
	5	0	0	0	0					
	6	0	0.3	9.3	30.3					
	8	0	0	0	0.5	3.0				
	9	0	0	0	0	0				
	10	0	0	4.5	20.1					
	11	0	0	0	3.0	7.0				

Note: Runs 2 and 7 defluidised
Runs 12 1nd 13 were carried out for 3 hours only.
The results for Run 11 is not accurate due to the breakage of the bed particles in the furnace

The rate of agglomeration (% bed material agglomerated per hour) was then estimated for each period:

Table D.2: ***Rate of Agglomeration (percent/hour)***

Period h		0-3	3-6	6-9	9-12	12-15	15-18	18-21	21-24
Run	1	0.0	0.0	0.0	1.2	2.0	3.2	4.8	5.0
	3	0.0	1.3	4.5					
	4	0.0	0.0	0.0					
	5	0.0	0.0	0.0					
	6	0.1	3.0	7.0					
	8	0.0	0.0	0.2	0.8				
	9	0.0	0.0	0.0	0.0				
	10	0.0	1.5	5.2					

The average coating thickness in each period can be estimated from Equations D.5 and D.6:

Table D.3: ***Average Coating Thickness (micron).***

Period h		0-3	3-6	6-9	9-12	12-15	15-18	18-21	21-24
Run	1	10.5	30.0	48.0	65.5	82.0	97.6	112.5	126.8
	3	21.5	61.0	96.5					
	4	9.0	27.0	44.5					
	5	5.5	16.5	27.5					
	6	24.0	68.5	107.5					
	8	16.5	48.5	79.0	105.59				
	9	15.5	40.0	72.0	7.0				
	10	16.5	54.0	84.5					

By combining Table D.2 and D.3, the agglomeration rate can be presented as a function of coating thickness:

Period h		0-3		3-6		6-9		9-12		12-15		15-18		18-21		21-24	
		A	C	A	C	A	C	A	C	A	C	A	C	A	C	A	C
Run	1	0.0	10.5	0.0	30.0	0.0	48.0	1.2	65.5	2.0	82.0	3.2	97.6	4.8	112.5	5.0	126.8
	3	0.0	21.5	1.3	61.0	4.5	96.5										
	4	0.0	9.0	0.0	27.0	0.0	44.5										
	5	0.0	5.5	0.0	16.5	0.0	27.5										
	6	0.1	24.0	3.0	68.5	7.0	107.5	0.8									
	8	0.0	16.5	0.0	48.5	0.2	79.0	0.0	105.5								
	9	0.0	15.5	0.0	40.0	0.0	72.0		97.0								
	10	0.0	16.5	1.5	54.0	5.2	84.5										

A = Agglomeration rate (percent per hour)

C = Coating thickness (micron)

Note: The results presented in Table D.4 are shown in Figures 6.12 and 6.14.

Table D.4: ***Agglomeration Rate (percent per hour) versus Coating Thickness.***

BIBLIOGRAPHY

Allan, R.J., "Sodium removal from Wakefield Coal" AMDEL Report 1408, July (1981).

Allan, R.J., "Sodium removal from Wakefield Coal": Stage II" AMDEL Report 1435 (1981).

Atakul, H. and Ekinci, E., "Agglomeration of Turkish lignites in fluidised-bed combustion", J. Inst. Energy, 56 (1989).

Atogi, A.M., Altenkirch, R.A. and Midkiff, K.C., "Distribution of sulphur in one dimensional P.C. flames." Fuel, 65, 1663 (1986).

Attar, A., "Sulphur groups in coal and their determinations", Analytical Methods for Coal and Coal Products, Vol. 4, Academic Press (1980).

Basu, P., "A study of agglomeration of coal-ash in fluidised beds", Can J. Chem. Eng., 60, 791 (1982).

Beisswenger, H., Darling, S., Hampton, J., Kaupp, F.O., Koch, W., "CFB combustion of typical waste materials from pulp and paper mill operations" Pulping Conference, 351 (1985).

Boow, J., "Sodium/ash reactions in the formation of fireside deposits in pulverised-fuel-fired boilers." Fuel, 51, 170 (1972).

Brinsmead, K.H. and Kear, R.W., "Behaviour of sodium chloride during the combustion of carbon". Fuel, 35, 84 (1956).

Brockway, D.J. and Chalmers, D.P., "Chemical assessment of coal for power generation." Chemistry in Australia, 192 (1986).

Bryers, R.W. and Walchuck, O.R., "Operating experience with a pilot scale combustion facility used for studying slagging and fouling characteristics of coal. Part II - Experimental results." Third Eng. Conf. on Slagging and Fouling Due to Impurities in Combustion Gases, Colarado, 253 (1984).

Casswell, S.A., "Distribution of water-soluble chlorine in coals using stains and acetate peels." Fuel, 60, 1164 (1981).

Daybell, G.N., "The relationship between sodium and chlorine in some British coals". J. Inst. Fuel, 40, 312 (1967).

Daybell, G.N. and Pringle, W.J.S., "The mode of occurrence of chlorine in coal." Fuel, 37, 283 (1958).

Dean, J.A., Ed. Lange's Handbook of Chemistry 13th Edition, McGraw Hill Book Co. (1985).

Domazetis, G., "The chemistry of formation of ash during the combustion of brown coal - Part I." State Electricity Commission of Victoria, Research and Development Department, Brown Coal Research Division, Report No. SO/85/91, Project No. 262 (1985).

Durie, R.A., "The inorganic constituents in Australian coals III. Morwell and Yallourn brown coals." Fuel, 40, 407 (1961).

Durie, R.A. and Swaine, D.J., "Inorganic constituents in coal." Coal Research in CSIRO, 45, 9 (1971).

Edgecombe, L.J., "Stage of combination of chlorine in coal I - Extraction of coal with water." Fuel, 35, 8 (1956).

Energy Resources Co. "Low rank coal study-national needs for resource development.", prepared for U.S. Dept. of Energy. Contract No. DE-AC18-79FC10066, Nov. (1980).

Ergun, S., "Fluid flow through packed columns", Chem. Eng. Prog., 48, 89 (1952).

Falcone, S.K. and Schobert, H.H., "Mineral transformations during ashing of selected low rank coals.", ACS Symposium Series 301, American Chemical Society, Washington D. C. (1986).

Fowkes, W.W., "Separation and identification of minerals from lignites", Analytical Methods for Coal and Coal Products, Vol. 2 (Karr. C. Ed.) Academic Press, (1978).

Frenkel, J.J., "Viscous flow of crystalline bodies under the action of surface tension." J. Physics, Moscow, 9, 385 (1945).

Gibb, W.H., "The nature of chlorine in coal and its behaviour during combustion", Corrosion Resistant Materials for Coal Conversion Systems, Applied Science Publishers (1983).

Gluskoter, H.J. and Rees, O.H., "Chlorine in Illinois coals." Illinois Geological Survey Circ. 372, (1964).

Gluskoter, H.J. and Ruch, R.R., "Chlorine and sodium in Illinois coals as determined by neutron activation analyses." Fuel, 50, 65 (1971).

Gluckman, M.J., Yerushalmi, J. and Squires, A.M., "Defluidization characteristics of sticky or agglomerating beds", Proc. of the Int. Fluidization Conf., California, U.S.A., 395 (1976)

Goblirsch, G.M., Benson, S.A., Karner, F.R., Rindt, D.K. and Hajicek, D.R., "AFBC bed material performance with low-rank coals", 12th Biennial Lignite Symposium, N.D. USA, (1983).

Goblirsch, G.M., Vander Molen, K.H., Wilson, K. and Hajicek, D., "Atmospheric fluidized bed testing of North Dakota lignite", 6th Int. Conf. on Fluidized Bed Combustion, 850 (1980).

Godel, A.A., Rev. Gen. Therm., 5, 349 (1966)

Goldberger, W.M., "Collection of fly ash in a self-agglomerating fluidized-bed coal burner", ASME Winter Annual Meeting and Energy systems Exposition, (1967).

Hajicek, D.R., Zobeck, B.J., Mann, M.D., Miller, B.G., Ellman, R.C., Benson, S.A., Goblirsch, G.M., Cooper, J.L., Guillory, J.L. and Eklund, A.G., "Performance of low-rank coal in atmospheric fluidized bed combustion", US Deparment of Energy Contract, No. DE-FC21-83FF60181, (1985).

Hale, G.L., Levasseur, A.A., Tyler, A.L. and Hensel, R.R. "The Akali metals in coal: A study of their nature and their impact on ash fouling". Coal Technology '80 3rd Int. Coal Utilization Exhibition and Conference, Houston, Texas, Nov. (1980).

Halstead, W.D. and Raask, E. "The behaviour of sulphur and chlorine compounds in pulverised-coal-fired boilers." J. Inst. Fuel, 344 (1969).

Hodges, N.J., Ladner, W.R. and Martin, T.G., "Chlorine in coal: A review of its origin and mode of occurrence." J. Inst. Energy, 158 (1983).

Howard, J.R., "Fluidized bed technology", Adam Higer Publication, (1989)

Hsieh, C.R. and Roberts, P.T., "A laboratory study of agglomeration in coal gasification, Am. Chem. Society, 30 (3), 468 (1985)

Huang, C.S., Arastoopour, H. and Weil, S.A., " Fundementals of fluidization of sticky particles", Draft Final Report, Gas Research Institute, (1982)

Huffman, G.P., Huggins, F.E. and Dunmyre, G.R. "Investigations of the high-temperature behaviour of coal ash in reducing and oxidising atmospheres", Fuel, 60, 585 (1981)

Jackson, P.J., "From mineral matter to deposits in PF-fired boilers Part I: The behaviour of mineral matter in the flame. Part II: The basic physics and chemistry of deposit formation and high temperature corrosion." Conf. Pulverised Coal Firing - The Effect of Mineral Matter, University of Newcastle, Paper L10, 1 (1979).

Jacquier, L., Langcharbon, L. and Van de Putte, G., J. Inst. Fuel 33, 584 (1960)

Jen, C.O. and Tsao, K.C., "Coal-ash agglomeration mechanism and its application in high temperature cyclones", Separation Science and Technology, 15(3), 263 (1980)

Jenkins, R.G. and Walker, P.L., "Analysis of mineral matter in coal", Chapter 26, 265 (1978).

Karner, F.R., Schobert, H.H., Falcone, S.K. and Benson, S.A., "Elemental distribution and association with inorganic and organic components in the North Dakota lignites.", in Mineral Matter and ash in Coal, Vorres K.S. Ed., A.C.S. Symposium Series 301, American Chemical Society, Washington D.C. (1986).

Kemezys, M. and Taylor, G.H., "Occurrence and distribution of minerals in some Australian coals.", J. Inst. Fuel, 37, 389 (1964).

Kiss, L.T. and King, T.N., "Reporting of low-rank coal analysis - The distinction between minerals and inorganics.", Fuel, 58, 547 (1979).

Kube, W.R., Schobert, H.H., Benson, S.A. and Karner, F.R., "The structure and reactions of Northern Great Plains lignites.", The Chemistry of Low Rank Coals, Schobert H.H. Ed., A.C.S. Symposium Series 264, American Chemical Society, Washington D.C. (1984).

Langston, B.G. and Stephens, F.M, "Self-agglomerating fluidized-bed reduction", J. Metals, 312, (1960)

Levin, E.M., Robbins, C.R. and McMurdie, M.F., Phase Diagrams For Ceramists. The American Chemical Society, Ohio U.S.A. 4th Edition (1979).

Lindner, E., "A study of sodium-ash reactions during the combustion of pulverised coal", PhD Thesis, University of New Castle, (1988)

Lisner, A. and Goebel, W., "Investigations in the determination of the ash content organically bound metals and mineral content of brown coals.", Freiberger Forschung-shefte, 19, A 373, (1965).

Lyon, R.K. and Freund, H., "The sulphur retention of calcium-containing coal during fuel rich combustion", Paper presented at Fall Meeting, Western States Section of the Com-bustion Institute, (1980).

Matulevicius, E.S. and Golan, L.P., "Review of ash agglomeration in fluidised bed gasifiers", U.S. Department of Energy, Contract No. DE-AC21-82MC19265, (1984).

Merry, J.M., Chen, J.L. and Keairns, D.L., "Fluidization technology" Mc Graw-Hill, 3, 423 (1975)

Miller, R.M. and Given, P.H., "Variations in organic constituents of some low rank coals.", International Conf. on Ash Deposits and Corrosion from Impurities in Combustion Gases. Eng. Foundation, 39 (1977).

Mitchell, R.S. and Gluskoter, H.J., "Mineralogy of ash of some American coals: Variations with temperature and source.", Fuel, 55, 90 (1976).

Morgan, M.E. and Jenkins R.G., "Role of exchangeable cations in the rapid pyrolysis of lignites.", American Chemical Society, 213 (1984).

Moza, A.K., "Characterisation of slag deposit formation from the analysis of several thousand individual ash particles.", Proceedings of the Eng. Foundation Conference on Fouling and Slagging Resulting from Impurities in Combustion Gases, New Hampshire 281 (1981).

Murray, J.B., "The state of combination of the inorganic ash-forming constituents of Yallourn brown coal." State Electricity Commission of Victoria, Planning and Investigations Department, Scientific Division, Miscellaneous Report No. Mr-145 (1968).

Murray, J.B., "The state of combination of the major inorganic ash-forming constituents in coal samples form the Loy Yang field." State Electricity Commission of Victoria, Report No. 233, June (1971).

Murray, J.B., "The state of combination of the major inorganic ash-forming constituents in Morwell coal.", State Electricity Commission of Victoria, Report No. 203, April (1970).

Murray, J.B., "The state of combination of the major inorganic ash-forming constituents in Yallourn North Extension brown coal.", State Electricity Commission of Victoria, Report No. 224, Feb. (1971).

Murray, J.B. and Bonafede, G., "The state of combination of the major inorganic ash-forming constituents in additional coal samples from the Loy Yang Field.", State Electricity Commission of Victoria, Report, No. 249, Jan. (1972).

Murray, J.B. and Ledger, R.C., "The changes in functional group contents of natural and ion substitution Morwell brown coals during carbonisation.", State Electricity Commission of Victoria, Planning and Investigations Dept. Scientific Div. Report No. 255, (1982).

Neville, M., "Formation of Inorganic Submicron Particles Under Simulated Pulverised Coal Combustion Conditions.", D. Sc. Thesis, Dept. Chem. Eng., Mass. Inst. of Technology, August (1982).

O'Gorman, J.V. and Walker, P.L., "Thermal behaviour of mineral fractions separated from selected American coals.", Fuel, 52, 71 (1973).

Padia, A.S., The Behaviour of Ash in Pulverised Coal Under Simulated Combustion Conditions, D. Sc. Thesis, Dept. Chem. Eng., Mass. Inst. of Technology, Jan. (1976).

Padia, S.P., Sarofim, A.F. and Howard, J.B., "The behaviour of ash in pulverised coal under simulated combustion conditions.", Combustion Institute's Central States Section, Spring Meeting, April (1977).

Patel, J.G., Oil and Gas Journal, 51, August (1977)

Quann, R.J., Ash Vaporisation Under Simulated Pulverised Coal Combustion Conditions, D. Sc. Thesis, Dept. Chem. Eng., Mass. Inst. of Technology, Jan. (1982).

Quann, R.J. and Sarofim, A.F., "A scanning electron microscopy study of the transformations of organically bound metals during lignite combustion.", Fuel, 65, 40 (1986).

Raask, E., "Slag/coal interface phenomena", Trans. ASME for power, 40 (1966)

Raask, E., Mineral Impurities in Coal Combustion. Hemisphere Publishing Corp. (1985).

Raven, M.D. and Self, P.G., "XPLOT-USER MANUAL Manupulation of powder X-ray diffraction data", CSIRO Division of Soils, Tech. Mem. No. 30, (1988)

Readett, D.J., "Benefication of Wakefield lignite: With particular reference to the reduction of the sodium content.", South Australian Institute of Technology, February, (1983).

Readett, D.J., "Benefication of Wakefield lignite: With particular reference to the reduction of the sodium content. Stage 2, Parts 1", South Australian Institute of Technology, March/July (1984).

Readett, D.J. and Quast, K., "Minerals and inorganics associated with South Australian lignites - Stage 1.", South Australian Institute of Technology, Report to S.E.N.R.A.C. December (1986).

Readett, D.J. and Quast, K., "Mechanical dewatering of South Australian brown coals: Applications in inorganics characterisation.", Coal Science Conference, Adelaide, (1988).

Rehmat, A. and Saxena, S.C., "Agglomeration of ash in fluidised-bed gasification of coal by steam-oxygen (or air) mixture", Ind. Eng. Chem. Proc. Des. Dev., 19, 223 (1980)

Sandstrom, W.A., Vora, M.K., Rehmat, A.G., "Recent developments in high-temperature fluidization at the ash-agglomeration pilot plant", AICHE 72nd Annual Meeting, Nov. (1979).

Saunders, K.G., "Microstructural studies of chlorine in some British coals.", J. Inst. Energy, 53, 109 (1980).

Schafer, A.N.S., "Pyrolysis of brown coals. 1 Decomposition of acid groups in coals containing carboxyl groups in the acid and cation forms.", Fuel, 58, 667 (1979).

Self, P.G., "Pc-PW1710-USER MANUAL PC based system for the control of a Phillips PW1710 X-ray diffraction system", CSIRO Division of Soils, Tech. Mem. No. 41, (1988).

Shibaoka, M. and Ramsden, A.R., "Microscopic investigation of the behaviour of inorganic material in coal during combustion.", Int. Conference on Ash deposits and Corrosion from Impurities in Combustion Gases, New England College, (1977).

Solomon, P.R. and Kersten, A.S., "The evolution of pollutants during the rapid devolatilisation of coal", United Technologies Research Centre, United Technologies Connecticut, Report R76- 952588-2 (1977).

Sondreal, E.A., Gronhovd, H., Tufte, P.H. and Beckering, W., "Ash Fouling Studies of low-rank Western U.S. Coals.", Int. Conference on Ash Deposits and Corrosion from Impurities in Combustion Gases, New England College (1977).

Squires, A.M., Scientific America, 227, (1972)

Srinivasachar, S. and Boni, A.A., "A kinetic model for pyrite transformations in a combustion environment, Fuel, 68, 829 (1989).

Stallman, J.J. and Neavel, R.C., "Technique for measuring the temperature of agglomeration of coal ash, Fuel, 59, 584 (1980)

Suuberg, E.M., Peters, W.A. and Howard, J.B., "Product composition and kinetics of lignite pyrolysis.", Ind. Eng. Chem. Proc. Des. Dev., 71, 37 (1978).

Turnbull, A.G., "A general computer program for the calculation of chemical equilibria and heat balances.", CALPHAD 7, (2) 137 (1983).

Turnbull, A. and Wadsley, M., Themodata Service, CSIRO Division of Mineral Chemistry, P.O. Box 124, Port Melbourne, 3207, private communication (1987).

Turnbull, A.G. and Wadsley, M.W., The CSIRO-SGTE Thermodata System, Version IV.", CSIRO Division of Mineral Chemistry Inst. Energy and Earth Resources (1985).

Wall, T.F., Lowe, A., Wibberley, L.J. and Stewart, I. McC., "Mineral matter in coal and the thermal performance of large boilers.," Prog. Energy Combust. Sci., 5 (1979).

Warne, S.St.J., "Introduction to minerals in coal", Lecture Notes, Department of Geology, University of Newcastle (1983).

Warne, S.St.J., "Coal Mineral Reactions", Lecture Notes, Department of Geology, University of Newcastle (1983).

Wen C.Y. and Yu Y.H. "A generalised method for predicting the minimum fluidisation veocity", AICHE J, 12, 610 (1966).

Wildegger-Gaissmaier, A.E., "Fluidised Bed Utilisation of South Australian Coal", PhD Thesis, Chem. Eng. Department, the University of Adelaide, (1989).

Yerushalmi, J., Gluckman, M.J. and Graff, R.A., Fluidization Technology, Mc Graw-Hill, 2, 437 (1976).